

HIGH SPEED ELECTRICAL BREAKDOWN MECHANISMS
IN GASEOUS, LIQUID AND SOLID DIELECTRIC MATERIALS

by

BAHMAN FARAZMAND

Awarded degree of M. Sc. *the degree of Doctor of Philosophy*

October 1969

Electrical Engineering Department,
University of Aston in Birmingham,
Gosta Green,
Birmingham 4.

131115

(i)

SUMMARY

Far-reaching similarities between the mechanism of electrical breakdown in the three insulating media - gaseous, liquid and solid - have been found. In all media, discharge channels of a similar type, generally referred to as streamers, are formed which differ for each electrode configuration.

In a divergent field of a point-plane electrode system, streamers are generated in the vicinity of the point-electrode. They are subsequently promoted by direct ionization and photo-electric ionization processes in the direction of the plane-electrode.

The charge carriers remaining behind in the streamer tail, due to their ionized state and space charge, affect the subsequent processes.

A model for streamer propagation in gaseous dielectrics is presented and its relationship to the characteristics of discharge growth is discussed. The initiation phase is considered first, leading to primary, secondary and return streamers, and finally to possible transition to arc-over. It is suggested that the same pattern of events applies to electrical breakdown of liquids and solids based on the many points of similarity observed in the growth of discharge in the three media.

Acknowledgements

The author wishes to express his gratitude to Professor F. M. Page for his advice and to Professor J. E. Flood for providing the facilities that made the findings in this thesis possible.

The author also wishes to acknowledge the encouragement given to him by Professor E. J. Davies and the co-operation of the Technical Staff of the Electrical Engineering Department.

TABLE OF CONTENTS

Summary

Acknowledgements

Table of Contents

Nomenclature

List of Figures

List of Tables

1. INTRODUCTION

2. GASEOUS DIELECTRICS

2.1 Introduction

2.2 Literature Survey

2.2.1 Fundamental processes

2.2.1.1 Introduction

2.2.1.1.1 Inelastic collision

2.2.1.1.1.1 Excitation

2.2.1.1.1.2 Ionization

2.2.1.1.1.2.1 Ionization by photons

2.2.1.1.1.2.2 Ionization by electrons

2.2.1.1.1.2.3 Ionization by heavy particles

2.2.1.1.1.3 Deionization

2.2.1.1.1.3.1 Attachment

2.2.1.1.1.3.2 Recombination

2.2.2 Electron avalanches

2.2.2.1 Determination of first ionization coefficient, α

2.2.2.2 Charge carrier drift velocities

2.2.2.3 Space charge effect on avalanche growth

2.2.3 Avalanches with successors

2.2.3.1 Determination of second ionization coefficient,

2.2.3.1.1 δ_p - mechanism2.2.3.1.2 δ_i - mechanism

2.2.3.1.3	γ_m - mechanism
2.2.3.2	Townsend generalised equation
2.2.4	Breakdown
2.2.4.1	Introduction
2.2.4.2	Townsend or generation criterion
2.2.4.3	Streamer (or Kanal) mechanism
2.2.4.3.1	Anode directed negative streamer
2.2.4.3.2	Cathode directed positive streamer
2.2.5	Time lags
2.2.5.1	Origin and importance of time lag
2.2.5.2	Statistical time lag
2.2.5.3	Formative time lag
2.3	Instrumentation
2.3.1	Supply voltage
2.3.1.1	The microsecond range system
2.3.1.1.1	The control circuit
2.3.1.1.2	The push-button pulse forming circuit
2.3.1.1.3	The delay unit
2.3.1.1.4	The high voltage thyratrons
2.3.1.1.5	The impulse generator
2.3.1.1.6	The test gap protection circuit
2.3.1.1.7	The test cell
2.3.1.1.8	The power packs
2.3.1.2	The nano-second range system
2.3.1.2.1	Power supply
2.3.1.2.2	Synchronous pulse generator
2.3.1.2.3	High voltage pulse generator
2.3.2	Measurement techniques
2.3.2.1	Methods employed by other investigators
2.3.2.1.1	Cloud chamber method
2.3.2.1.2	Electrical method - current measurement
2.3.2.1.3	Optical methods
2.3.2.1.3.1	Photomultiplier

- 2.3.2.1.3.2 Direct photography
- 2.3.2.2 Methods employed by author
- 2.3.2.2.1 Streamer track recording transverse to
and along the main field axis methods
- 2.4 Experimental results
 - 2.4.1 Spatial build-up of discharges
 - 2.4.1.1 Primary streamers
 - 2.4.1.2 Secondary streamers
 - 2.4.1.3 Return streamers
 - 2.4.2 Primary streamer parameters
 - 2.4.2.1 Streamer number
 - 2.4.2.2 Streamer spread
 - 2.4.2.3 Streamer spatial progress
 - 2.4.2.4 Streamer spatial-time characteristics
 - 2.4.2.5 Streamer velocity
- 2.5 Theoretical analysis
 - 2.5.1 Electrostatic field analysis of point-
plane or point-point geometry
 - 2.5.1.1 Field about a charged sphere in
spherical co-ordinates
 - 2.5.1.2 Field about a charged paraboloid in
parabolic co-ordinates
 - 2.5.1.3 Field about a charged sphere in bi-
spherical co-ordinates
 - 2.5.1.4 Field about a charged hyperboloid in
prolate spheroidal co-ordinates
 - 2.5.2 Positive primary streamer threshold
 - 2.5.3 Theory of positive primary streamer
propagation
 - 2.5.3.1 Introduction
 - 2.5.3.2 Propagation criterion
 - 2.5.4 Theory of positive secondary streamer
propagation
 - 2.5.4.1 Introduction
 - 2.5.4.2 Propagation criterion

- 2.6 Discussion
- 2.7 Bibliography
- 3. LIQUID DIELECTRICS
 - 3.1 Introduction
 - 3.2 Literature survey
 - 3.2.1 Introduction
 - 3.2.2 Pre-breakdown condition
 - 3.2.2.1 Low field conduction
 - 3.2.2.2 High field conduction
 - 3.2.3 Electrode effect
 - 3.2.4 Impurities effect
 - 3.2.5 Temperature effect
 - 3.2.6 Pressure effect
 - 3.2.7 Density effect
 - 3.2.8 Time effect
 - 3.2.9 Mechanism of breakdown
 - 3.3 Instrumentation
 - 3.4 Experimental results
 - 3.4.1 Streamer range at voltages below breakdown
 - 3.4.2 Streamer spatial-temporal build-up
 - 3.4.3 Streamer velocity
 - 3.4.4 Time integrated streamer pattern
 - 3.5 Discussion
 - 3.6 Bibliography
- 4. SOLID DIELECTRICS
 - 4.1 Introduction
 - 4.2 Literature survey
 - 4.2.1 Introduction
 - 4.2.2 Electrode effect
 - 4.2.3 Immersion medium effect
 - 4.2.4 Temperature effect

- 4.2.4.1 Crystalline solids
 - 4.2.4.1.1 Polar
 - 4.2.4.1.2 Non-polar
- 4.2.4.2 Amorphous and partially crystalline solids
- 4.2.5 Intrinsic or electronic breakdown
 - 4.2.5.1 Introduction
 - 4.2.5.2 Boltzmann's transport equation
 - 4.2.5.3 Collective breakdown theory
 - 4.2.5.4 Avalanche theory
 - 4.2.5.5 Field emission theory - Zener effect
- 4.2.6 Thermal breakdown
- 4.2.7 Gas-discharge breakdown
- 4.2.8 Electrochemical breakdown
- 4.2.9 Electromechanical breakdown
- 4.2.10 Highly divergent field breakdown - treeing
- 4.3 Instrumentation
 - 4.3.1 Test sample design
- 4.4 Experimental results
 - 4.4.1 Streamer inception and breakdown voltage
 - 4.4.2 Streamer propagation
 - 4.4.3 Spatial build-up of streamers
- 4.5 Discussion
- 4.6 Bibliography
- 5. CONCLUSION
- 6. SUGGESTIONS FOR FURTHER STUDIES
- 7. APPENDICES
 - 7.1 Electric field in a point-plane electrode system
 - 7.2 Coefficient of diffusion
 - 7.3 Diffusion equation - error function solution
 - 7.4 Secondary streamer tail parameters
 - 7.5 Electrical potential and field strength of the secondary streamers

- 7.6 Gas ionization and photon production
- 7.7 Ions and electrons movement
- 7.8 Electric field strength ahead of the secondary streamer
- 7.9 Electric field strength inside the secondary streamer tip
- 7.10 Polymethylmethacrylate

Nomenclature

C	=	Radius of curvature of a point-electrode; streamer capacitance per unit length; velocity of E-M wave in free space
D	=	Diffusion coefficient
E	=	Electric field strength
E_{av}	=	Average electric field strength
E_m	=	Maximum electric field strength
e	=	Electron
G	=	Electrode gap length
H	=	Energy
h	=	Planck's constant
I	=	Threshold energy
i	=	current
k	=	Boltzmann's constant
L	=	Streamer axial length
l	=	Distance between point-electrode and film
m	=	Mass of electron
m_i	=	Mass of particle.
N	=	Number of incident point on the film
n_e	=	Number of electrons
n_i	=	Number of ions
n_s	=	Number of secondary electrons
P	=	Probability
p	=	Pressure
q	=	Electron charge

R	=	Streamer resistance per unit length
r	=	Radius
r_d	=	Diffusion radius
r_s	=	Streamer radius
S	=	Spread of streamer on the film
T_e	=	Electron temperature
T_k	=	Formative time lag
t	=	Time
t_p	=	Pulse duration
U	=	Velocity
U_e	=	Electron drift velocity
V	=	Velocity; voltage
V_b	=	Breakdown voltage
V_e	=	Electron drift velocity
V_i	=	Ionization potential
V_s	=	Streamer inception voltage
v_-	=	Electron drift velocity
v_a	=	Attachment frequency
W	=	Energy
W_e	=	Electron energy
W_i	=	Ionization energy
W_p	=	Particle energy
X	=	Neutral atom
X^*	=	Excited atom
X^m	=	Metastable atom

X^{\pm}	=	Positive or negative ion
Y	=	Young's modulus
XY	=	Molecule
α	=	First ionization coefficient
β	=	Attachment coefficient
γ	=	Second ionization coefficient; photon
η	=	Number of ions per centimetre length
θ	=	Temperature
θ_b	=	Boiling point
θ_0	=	Ambient temperature
λ	=	Wave length; electron mean free path
μ	=	Absorption coefficient for photo-ionization
μ_e	=	Electron mobility
μ	=	Mean mobility
ν	=	Frequency
τ	=	Time
τ_e	=	Interval between succeeding avalanches
τ_s	=	Statistical time lag
ϕ	=	Work function
ψ	=	Rate of electron production
$h\nu$	=	Photon

List of Figures

Fig. No.	Page	Description
2.1	15	Ionization efficiency as a function of electron energy
2.2	17	Ionization yield from excited and non-excited atoms
2.3	19	Multiplication ratio as a function of electrode separation
2.4	21	Recombination coefficient in air
2.5	24	Ionization coefficient $\frac{\alpha}{p}$ as a function of $\frac{E}{p}$
2.6	26	Multiplication ratio as a function of electrode separation for nitrogen
2.7	27	Ionization coefficient $\frac{\alpha}{p}$ as a function of $\frac{E}{p}$ in different gases.
2.8	29	Ionization coefficient $\frac{\alpha}{p}$ as a function of $\frac{E}{p}$ in nitrogen
2.9	31	Drift velocity of electrons in air as a function of $\frac{E}{p}$
2.10	32	Drift velocity of positive ions in air as a function of $\frac{E}{p}$
2.11	33	Effect of space charge of an avalanche of high amplification
2.12	38	Secondary emission coefficient as a function of $\frac{E}{p}$ for hydrogen and nitrogen
2.13	40	Electron current as a function of time
2.14	42	Idealised current as a function of time
2.15	42	Current due to avalanches with successors in oxygen
2.16	44	Multiplication factor in air
2.17	52	Schematic representation of anode-directed negative streamer
2.18	53	Schematic representation of cathode-directed positive streamer
2.19	57	Plot of $\frac{N_0}{N_t}$ as a function of time
2.20	60	Dependence of probability P on overvoltage
2.21	62	Current build-up for various overvoltages
2.22	63	Formative time lag as a function of overvoltage
2.23	65	Duration of streamer development in ether
2.24	66	Duration of streamer development
2.25	68	Laue plots of time lag
2.26	69	Formative time lag for point-anode
2.27	70	Formative time lag for Hermstein glow

Fig. No.	Page	Description
2.28	73	Block diagram of electrical circuit
2.29	75	Pulse forming network
2.30	77	Delay unit
2.31	79	High voltage hydrogen thyratron
2.32	80	500 kV impulse generator
2.33	82	Impulse generator gap length controller
2.34	83	100 kV charging generator
2.35	84	Test gap protection circuit
2.36	86	Test circuit
2.37	86	7 kV power unit
2.38	88	High voltage power supply
2.39	89	Synchronous pulse generator
2.40	91	High voltage pulse generator
2.41	94	Streamer track recording
2.42	97	Primary positive streamer pattern in air
2.43	97	Primary positive streamer pattern in air
2.44	98	Primary positive streamer pattern in air
2.45	98	Primary positive streamer pattern in air
2.46	99	Primary positive streamer pattern in air
2.47	100	Primary and secondary positive streamer pattern in air
2.48	101	Primary and secondary streamer pattern in air
2.49	103	Single-frame, time-integrated photograph of a secondary positive streamer in air
2.50	103	Single-frame, time-integrated photograph of a secondary positive streamer in air
2.51	104	Secondary positive streamer tips and negative return streamers in air
2.52	106	Schematic representation of streamer pattern
2.53	108	Number of primary streamers in air
2.54	109	Number of primary streamers in air
2.55	111	Spatial progress of primary streamers in air
2.56	114	Spread of primary streamers in air
2.57	116	Average values of primary streamer parameters in air
2.58	118	Primary streamer spatial-time characteristic in air
2.59	120	Primary streamer velocity in air
2.60	125	Parabolic co-ordinates
2.61	128	Bi-spherical co-ordinates
2.62	132	Prolate spheroidal co-ordinates
2.63	137	Computer flow diagram of electric field strength
2.64	140	Charge generation in the proximity of the point-electrode in air
2.65	146	Some parameters of a positive secondary streamer
2.66	148	Voltage-streamer range characteristics

Fig. No.	Page	Description
3.1	169	Drift mobility of electrons in hexane
3.2	170	Conduction current in n-hexane under d. c. and pulse
3.3	172	Dependence of conduction current density on voltage in n-hexane
3.4	175	Influence of electrode oxidation on breakdown of liquid argon
3.5	177	Conditioning effect on the electric strength of liquid argon
3.6	180	Electric strength-temperature variation of n-paraffins
3.7	181	Electric strength-temperature variation of n-paraffins
3.8	184	Electric strength-dependence of organic liquids on pressure
3.9	186	Variation of electric strength of some liquids with density
3.10	188	Electric strength-time variation of liquids
3.11	190	Time dependence of electric breakdown in liquid hydrocarbons
3.12	191	Time lag, gap length and electric strength relationship
3.13	197	Electric strength as a function of molecular structure for liquid alkanes
3.14	199	Test cell
3.15	202	Secondary streamer range as a function of voltage in oil
3.16	203	Secondary streamer range as a function of voltage in oil
3.17	205	Secondary negative streamer range as a function of pulse duration in oil
3.18	207	Secondary positive streamer range as a function of pulse duration in oil.
3.19	209	Secondary streamer range as a function of pulse duration in oil
3.20	211	Secondary streamer velocity in oil
3.21	212	Time-integrated patterns of secondary negative streamers in oil
3.22	212	Time-integrated patterns of secondary positive streamers in oil
4.1	228	Influence of annealing and thickness of potassium bromide on electric strength
4.2	231	Types of specimens of solid dielectrics
4.3	232	Electric strength of potassium bromide
4.4	234	Electric strength of muscovite ruby clear mica
4.5	235	Electric strength of borosilicate
4.6	236	Electric strength of polymers

Fig. No.	Page	Description
4.7	237	Electric strength of polyethylene as a function of temperature
4.8	241	Rates of gain and loss of energy to crystal lattice
4.9	243	Rates of gain and loss of energy to crystal lattice in optical mode
4.10	246	Rates of gain and loss of energy to crystal lattice in optical and acoustical modes
4.11	248	Rates of energy gain and loss as a function of electron temperature
4.12	250	Electric strength of polyethylene against temperature
4.13a	256)	Critical field strength for thermal breakdown
4.13b	257)	
4.14	258	Effect of temperature on insulation resistance of various glasses
4.15	259	Ionic conduction of sodium chloride-cadmium chloride mixed crystals
4.16	263	Electric strength of polyethylene and polyisobutylene
4.17	265	Variation of average electric strength of polythene with temperature
4.18	266	Variation of divergent field electric strength with radius of curvature of the point
4.19a	268	Test sample mould design
4.19b	269	Test sample mould design
4.20a	270	Test sample mould design
4.20b	271	Test sample mould design
4.21	275	Streamer inception and breakdown in PMMA
4.22	277)	Streamer range in PMMA as a function of voltage
4.23	279)	
4.24	281	Streamer range in PMMA as a function of voltage
4.25	282	Average streamer range in PMMA as a function of voltage
4.26	284	Positive streamer pattern in PMMA
4.27	284	Negative streamer pattern in PMMA
5.1	299	Sequence of events leading to breakdown in air
5.2	299	Sequence of events leading to corona in air
A1	307	Computer flow diagram for per unit values of electric field strength
A2	308	Specimen digital program for electric field strength

List of Tables

No.	Page	Description
2.1	10	Fundamental processes in gas discharge
2.2	12	Ionization potential of atoms or molecules
2.3	28	Constants in equation $\frac{\alpha}{p} = A \exp \left[- B \left(\frac{p}{E} \right) \right]$
2.4	45	Values of coefficients in Townsend's generalised equation
2.5	107	Number of primary streamers in air
2.6	110	Primary streamer spatial progress in air
2.7	113	Primary streamer spread in air
2.8	115	Primary streamer average parameters in air
2.9	117	Primary streamer spatial - time characteristic in air
2.10	119	Primary streamer velocity in air
2.11	138	Calculated values of electric field strength along the main field axis
2.12	139	Charge generation near the point electrode
2.13	144	Calculated primary streamer parameters for air
3.1	201	Variation in streamer range with voltage in oil
3.2	204	Secondary negative streamer range in oil
3.3	206	Secondary positive streamer range in oil
3.4	210	Secondary streamer velocity in oil
4.1	226	Theories of breakdown of solids
4.2	274	Streamer inception and breakdown voltage in PMMA
4.3	276	Streamer range variation in PMMA in 1.0 mm gap
4.4	278	Streamer range variation in PMMA in 3.0 mm gap
4.5	280	Streamer range variation in PMMA in 5.0 mm gap

CHAPTER 1

INTRODUCTION

1. Introduction

The transition from the non-conducting state of a dielectric to a transient or continuing arc of high conductivity may be achieved in two ways.

The first is the classical mechanism in which conventional ionization and heating by current flow gradually build up the conducting state. The fastest growth occurs on a time scale of multiples of electron transit time across the gap. This growth rate is limited by the velocity of the ionizing electrons.

The second mechanism involves one very rapid luminous pulse of ionization called a streamer or, more often, a succession of pulses, that have been recorded at speeds ranging from 10^5 to 10^8 m/s.

The streamers have been observed to occur in a wide diversity of phenomena in almost all gases at pressures ranging from 10^{-2} to 760 torr and above. They unquestionably appear in the very fast breakdown of liquids and solids.

The phenomenon of electrical breakdown is familiar enough in its occurrence, but is extremely complex in its nature. To understand it requires a systematic examination of the three states of matter - gas, liquid and solid. The major aspects of the subject that need to be so studied and understood include the classical theories of the mechanisms of breakdown, the significance of time effects, the influence of variables (such as density, electrode spacing and cathode composition), and the relation of breakdown to the nature of dielectric itself, principally electron behaviour and molecular structure.

The subject is well developed within the framework of breakdown in gases, beginning with the historic work of Townsend in establishing the breakdown theory that bears his name, as the basic concepts of breakdown are most thoroughly understood in

gases. The elucidation is then applied to the consideration of breakdown in liquids and solids.

The main interest throughout the study is in the transition from an insulating state of gases, liquids and solids to a conducting state of a plasma. The major concern has been with those aspects of electrical discharge which include photo-ionization as a significant process in their maintenance.

The electrode geometry selected for all three media is of point-plane form producing an extreme mode of electric field non-uniformity.

The investigation of electrical discharges using asymmetrical electrode arrangements offers exceptional opportunities for the study of breakdown phenomena. The reason for this lies in the high field concentration at one electrode resulting in extension over a considerable voltage range of the phenomena leading to breakdown. Asymmetrical electrode systems represent most of the engineering electrode arrangements in high-voltage technology.

The method employed in discovering the build-up of the streamers in gaseous and liquid dielectrics is to bring an electro-magnetic radiation sensitive plate into the electrode-gap space. This is achieved in two ways, viz. plate transverse to the electric field or parallel to the field axis.

If the plate is at transverse to the field axis, given sufficiently high impulse voltage, outgoing streamers from the point electrode strike it and produce a number of tracks, resulting in a Lichtenberg figure. If the distance between the point electrode and the electro-magnetic radiation sensitive place is varied for a definite voltage wave and electrode gap, or if the impulse duration is varied with a definite distance between the plates, one can trace out the streamers' growth with time and also the range of the forward rushing photo-electric radiation, and thus the spatial spreading

of the streamers can be established. Similar information can be obtained by placing the electro-magnetic radiation sensitive layer along the main field axis.

The absence of the phenomenon of dielectric recovery in the breakdown of solids presents numerous problems in the engineering field. The detailed studies of non-conducting to conducting transition state of solid dielectrics are greatly hampered by this phenomenon. A large number of samples is required with the same physical properties free from voids and imperfections. This is achieved by injection moulding of materials in specially designed mould accepting metal electrodes.

The permanent destructive nature of breakdown in solid dielectrics is put to good use by employing transparent materials where the appearance and extension of discharge channels can be studied in detail.

A theory of the propagation of positive streamer in non-electro-negative gaseous dielectric is presented. Formulae are derived which enable speeds of propagation, electron densities and streamer radii to be predicted as a function of applied voltage and fundamental atomic cross-sections. The experimental results are in reasonable accord with the hypotheses expounded.

A clear understanding of fundamental mechanism leading to breakdown of dielectrics can be employed as a basis for the improved design for electrical insulation arrangements and equipment.

CHAPTER 2

GASEOUS DIELECTRICS

2.1 Introduction

Although the nature of the breakdown of a gas at moderate electrode spacing and low gas pressure is now well understood^(30, 67, 132) in terms of normal Townsend multiplication, in association with secondary electron emission processes, the understanding of breakdown at large electrode separations and high gas pressures is still far from complete.

The streamer mechanism of breakdown in the high pressure regions was independently proposed by Meek⁸⁹ and Raether¹¹⁰. They tentatively put forward a semi-empirical hypothesis for streamer advance which neglected the important role of photo-ionization in the gas and was fundamentally incomplete.

Loeb⁷² indicated that the basic form of all breakdown equations must bear a formal analogy to the original breakdown criterion of Townsend which is valid at low pressure.

The complementary relationship between the Townsend and streamer mechanisms of ionization growth in uniform-field gap breakdown has been stressed by many writers and adequately demonstrated by Raether and co-workers¹¹⁶.

In all considerations of the mechanism of the streamer breakdown, it has been recognised^{35, 37} that both positive and negative streamer processes depend on a photo-electric ionization of the gas ahead of the streamer tip for their advance. However, for many reasons, most investigators^{89, 78, 112, 113} have emphasised the role of the space charge accumulations at the avalanche head as the critical factor. The single attempt⁸¹ at a complete quantitative formulation, both of discharge threshold and streamer advance, has taken account of the photo-ionization in the gas. This has resulted in furnishing the regenerative counterpart of α of the Townsend criterion in satisfying the self-sustaining threshold condition.

The study of the spark breakdown phenomena has taken

advantage of widely different techniques for specific purposes, such as cloud chamber track, oscillographic current measurements, and optical light recording by photomultiplier. Each of these methods of investigation is restricted by special circumstances and each provides only limited information about the processes involved in breakdown.

The knowledge of the potential and field distribution across the electrode gap, achieved with computational aids, has led the author to two important deductions:

(a) the evaluation of the first Townsend coefficient, α , as a function of distance from the point-electrode surface, and
 (b) the presence of "zero" or low field region across the gap a short distance away from the point-electrode. The case (a) would allow the quantitative study of streamer onset conditions and the case (b) would give support to the criterion for primary streamer propagation. Case (b) also shows the lack of disturbance in electric field pattern when introducing an electromagnetic radiation-sensitive plate into the electrode gap space.

The introduction of the Lichtenberg figure technique originally by von Hippel and in modified form by Nasser⁹⁹ has led to a new method for studying streamer propagation in gaps undistorted by ionic space charge.

By employing measurement techniques, which are a modification and improvement of Nasser's Lichtenberg methods, the author has been able to take photographs of traces of the positive and negative streamer tips in air. The streamer propagations are deflected by the photographic film, and continue in the gas close to the surface leaving time-integrated traces behind.

The studies in point-to-plane geometry establish the

presence of streamers in a large range of impulse potential below that value for which the streamer crosses the gap with a sufficient tip potential to produce a spark. An increase in the applied potential results in the streamers moving further into the gap and showing a strong radial branching in their progress.

The number of streamer branches and the radial spread of the discharge as a function of distance from the point-electrode are measured and the spatial build-up of streamer discharge resolved.

A hypothesis for electrical breakdown of gaseous dielectrics, based on appearance of primary streamers followed by secondary and return streamers, is put forward and supported by experimental results.

2.2 Literature Survey

2.2.1 Fundamental Processes

2.2.1.1 Introduction

The molecules of a gas interact only weakly as compared with those of liquids and solids. For the greater part of their existence they are subject to a uniform, linear motion, but one particle may, from time to time, approach sufficiently close to another, or several others, for their orientations, velocities and even their internal characteristics to be altered. These encounters are called collisions. Despite their rarity, it is collisions which dominate gas theories because of their immediate and important consequences. These are (a) the setting up of thermodynamic equilibrium or a steady state, (b) the nature and intensity of radiation emitted by a gas, and (c) the state and distribution of the particles present.

The presence of electrons and ions in the gas under investigation alters the situation considerably. Firstly, charged particles are influenced by electro-magnetic forces which have no effect on the neutral atoms or molecules, and secondly, the particles themselves produce an electric field with a large range of influence. The result is that, with the same density of particles, the interactions between particles are more important and their effects more long-lasting.

The low density of gases results in most collisions being of a binary nature; however, there can also be tertiary collisions. A differentiation should be made between elastic and inelastic collisions. The first only modifies the magnitude and direction of the velocities, while the second can also give rise to changes in the internal energy or in the nature of the particles present; the total kinetic energy being altered in such a way as to conserve the total energy.

Basic ionization processes in electrical breakdown of gaseous dielectrics are a) those involving the collisions of electrons, ions and photons with gas molecules or atoms, and b) electrode processes which take place at the electrode boundaries.

2.2.1.1.1 Inelastic Collisions

An inelastic collision is one in which the internal energy of the particles, as well as the kinetic energy, changes. Photons can take part in such collisions. The number and diversity of the possible reactions increases with the complexity of the particles involved.

The probability of an inelastic reaction depends essentially on the time, t , for which the distance between the particles is of the order of the radius of action, a , of the atomic forces, i. e. of the order of one Angström. The time t is of the order of $\frac{a}{V_r}$, where V_r is the relative velocity of the two particles. The time for an atomic transition of energy, ΔW , according to quantum theory is:

$$\tau = \frac{h}{\Delta W} \quad (2.1)$$

which is of the order of 10^{-15} sec. where h is Planck's constant.

If $t \gg \tau$, the atomic structure will be progressively transformed to take account of the presence of the incident particle by means of an adiabatic change in the course of which the quantum state remains unaltered.

If $t = \tau$, an instantaneous transition to another level will take place. The increase in V_r diminished the duration of the interaction and with it the probability of the transition. The maximum for the effective excitation cross-section, σ_e , should therefore occur at

$$V_r = \frac{a}{\tau} \quad (2.2)$$

which is of the order of 10^7 cm/sec. While for electrons this velocity corresponds to some eV, for ions it corresponds to some keV.

Table 2.1 shows the main types of inelastic collisions. These

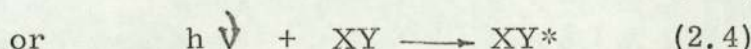
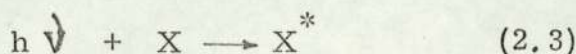
are excitation, ionization, charge transfer, attachment, recombination, detachment and dissociation.

2.2.1.1.1.1 Excitation

An excited atom or molecule is one which has absorbed a sufficient amount of energy for one of its electrons to pass to a higher energy level. The internal energy of the atom or molecule increases by the difference, ΔW , between the energies of the final and initial state. The initial energy level of the excited particles is not necessarily that corresponding to the ground state. If inelastic collisions lead to excitation of bound energy levels in the particle, this would allow the probability of excitation to be defined.

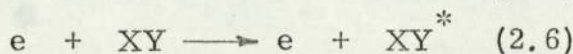
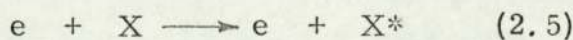
The probability of excitation has been measured by many investigators^{82, 126}. Schulz and Fox¹²⁶ measured the excitation cross-sections in relation to structure of target atom. One of the most dramatic results of studying electronic excitations is the development of gas lasers.

Excitation by photons can be represented by



The reaction is only possible if $h\nu \geq \Delta W$, but even if this condition is satisfied, the selection rule may forbid the reaction taking place. The cumulative excitation by photons with an energy lower than ionization energy, W_i , may lead to ionization of an atom or a molecule.

The basic reaction of excitation by an electron is:

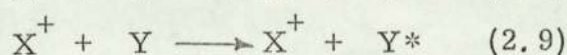
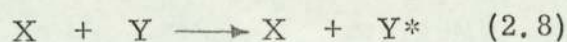


With the target assumed at rest and the incident electron having a kinetic energy W_e , the reaction threshold is:

$$W_e = \Delta W \quad (2.7)$$

However, the probability of excitation close to the threshold energy remains very low, since it is difficult to fulfil the condition of conservation of angular momentum.

The excitation by atoms or ions may be represented by:



If the target particle, assumed at rest, and the incident particle with a kinetic energy, W_p , have masses m_1 and m_2 respectively, the reaction threshold is

$$W_p = \frac{m_1 + m_2}{m_1} \cdot \Delta W \quad (2.10)$$

2.2.1.1.1.2 Ionization

When an atom or a molecule has absorbed a sufficient amount of energy for one of its electrons to escape, it is said to have been ionized, and its internal energy increased by the ionization energy

$$W_i = \Delta W \quad (2.11)$$

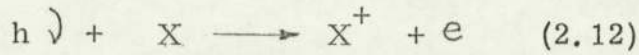
Table 2.2 shows the ionization potential, V_i for single ionization of various atoms or molecules.

TABLE 2.2 : Ionization Potentials of Atoms and Molecules

Element	V_i	Molecule	V_i
H	13.6	H ₂	15.4
N	14.5	N ₂	15.5
O	13.5	O ₂	12.1
Cl	13	Cl ₂	11.5
F	17.4	F ₂	16.5
C	11.3	NO	9.2
He	24.5	NO ₂	11
A	15.7	H ₂ O	13

2.2.1.1.1.2.1 Ionization by Photons

The basic reaction representing photo-ionization is:



and it can take place when $h\nu \gg W_i$.

This condition limits the photoelectric effect to the ultra-violet or x-ray region of the spectrum due to the wavelength given by:

$$\lambda = \frac{hc}{qVes} \quad (2.13)$$

Putting values for Planck's constant, h , electron charge, q , and the velocity of E-M wave, C , the wave length will be given by:

$$\lambda = \frac{12400}{V} \quad (2.14)$$

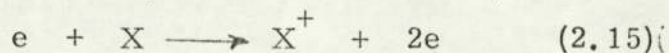
It is convenient to discriminate between two cases of photo-ionization when the energy $h\nu$ of the quanta absorbed is (a) of the order of the ionization energy W_i , or (b) of much greater value compared with W_i .

Case (a): $h\nu \gg W_i$. The radiation required lies in the ultraviolet or soft x-ray range. A photon ionizes the gas atom or molecule with a maximum probability at a critical wavelength or energy which is of the order of 0.1 - 1.0 eV above the minimum energy. The emitted electron is the one least firmly bound to the atom or molecule.

Case (b): $h\nu \gg W_i$. The radiation, being in the x-ray region, acts preferably on an electron of the inner shell. This may lead to 'Auger effect' resulting in the production of a large number of ion pairs.

2.2.1.1.1.3 Ionization by Electrons

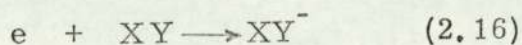
The ionization by electrons can be represented by:



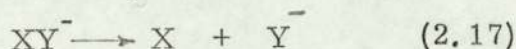
If the target is at rest and the incident electron has a kinetic energy, W_e , the reaction can only take place if $W_e > W_i$.

The effective cross-section increases rapidly once the threshold energy has been passed^{29, 30, 104} as the conservation conditions are easily satisfied due to the ejected electrons. This results in a similar increase in the ionization efficiency, Q_i , given as the number of ion pairs produced per centimetre of the incident electron's path in the target gas at pressure p (see Fig. 2.1). Reed¹¹⁷ summarises the basic gas ionization by electron impact as follows:-

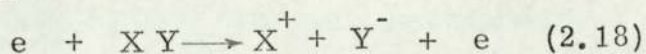
The process that occurs at the lowest electron energy is usually that of electron addition - by electron resonance capture - to give a negative ion:



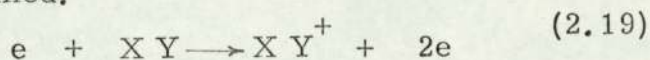
This ion may dissociate to give a neutral atom and a negative ion:



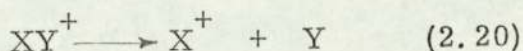
At higher energy, the production of ions may occur, thus



and at still higher levels the positive molecular ion is formed:



which may dissociate to give a positive ion together with a radical or atom



2.2.1.1.1.2.3 Ionization by Heavy Particles

Ionization by ions, atoms or molecules can be represented by:

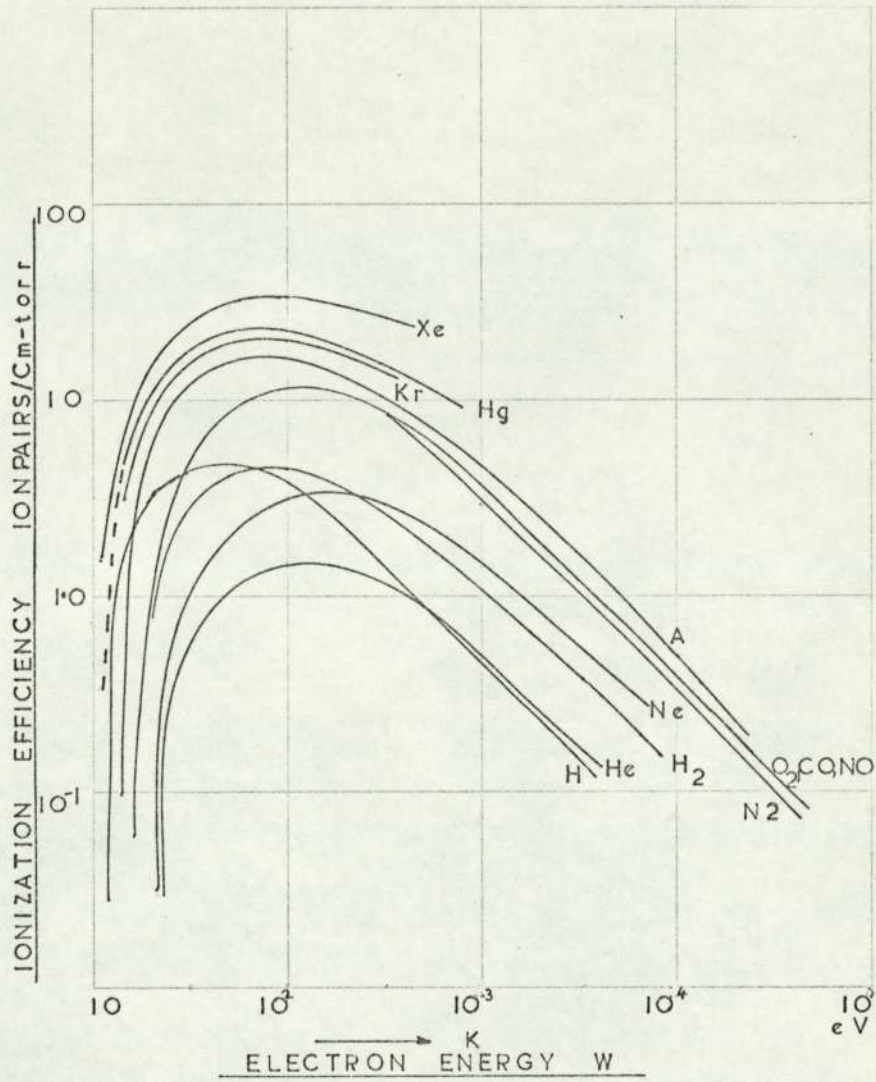
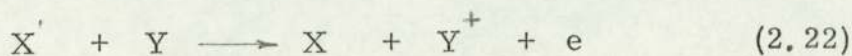
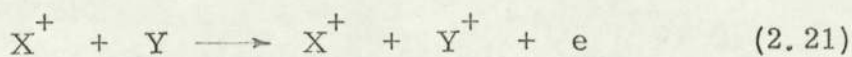


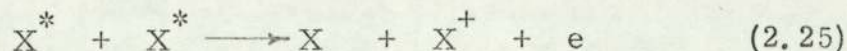
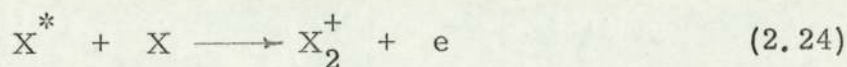
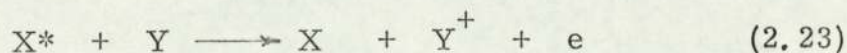
Fig. 2.1 IONIZATION EFFICIENCY AS A FUNCTION OF THE ELECTRON ENERGY FOR VARIOUS GASES AT 1 TORR AND 0° C.

(After von Engel 30)



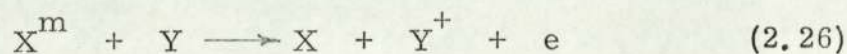
The maximum effective cross-sections correspond to very high kinetic energies.

Excited atoms can be ionized more easily than neutral atoms due to reduction in ionization threshold and increase in the effective cross-section (see Fig. 2.2). Some of the reactions can be represented by:

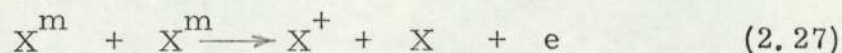


The second reaction has a high probability especially where, in low-energy electron swarm, more X^* than X^+ are created.

Penning effect is a special case of a collision of the second kind, which can be of great importance in the conduction of electricity through gases. This is represented by a collision of a metastable and a neutral particle



Ionization by metastable interaction,



first discovered by Biondi^{8, 10}, causes ionization to appear long after excitation, since X^m generated in large numbers, has a long life, and diffuses slowly in clean gas.

2.2.1.1.1.3 De-ionization

De-ionization can take place through the action of processes of attachment, recombination, diffusion and drift. The processes of attachment and recombination are by far the most important ones on phenomena of short duration breakdown. Impurity

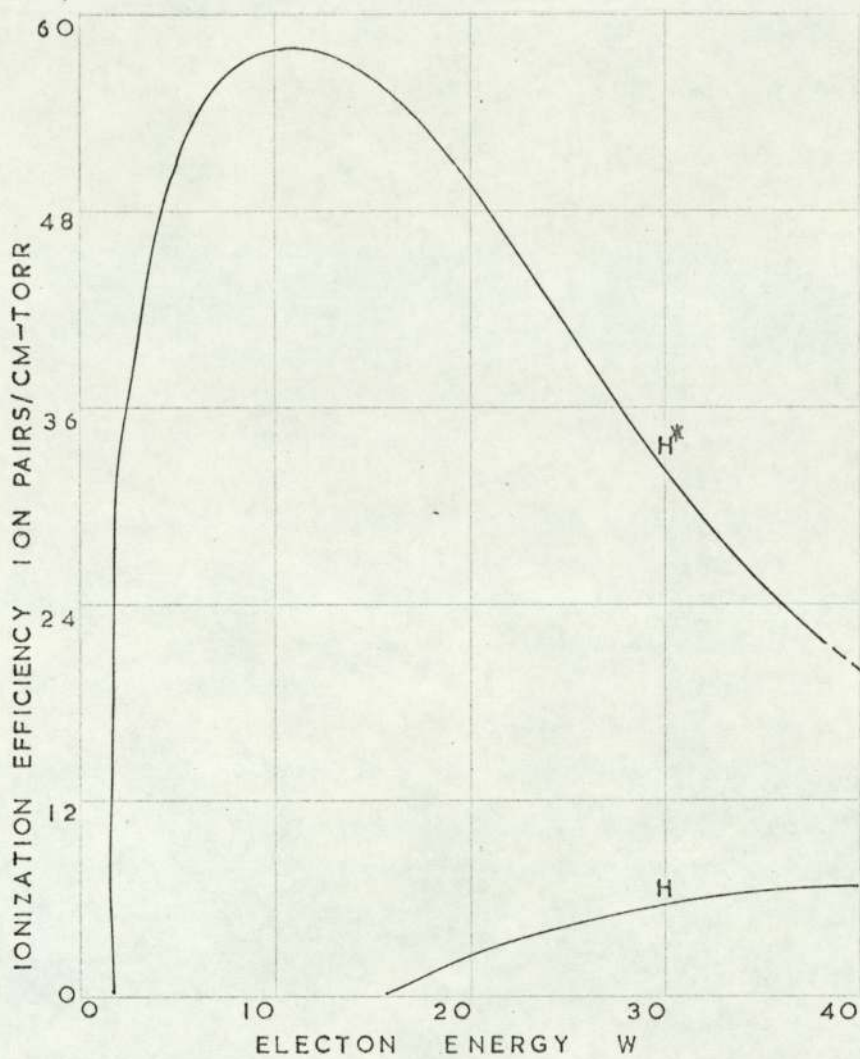


Fig. 2.2 COMPARISON OF YIELDS FROM EXCITED AND NON-EXCITED HYDROGEN ATOMS IONIZED BY ELECTRONS AT 1 TORR AND 0°C (After Mandl 85)

particles normally enhance the de-ionization processes.

2.2.1.1.1.3.1 Attachment

Electron attachment to a neutral atom can be most easily accomplished for those neutral atoms whose outer electronic shells are nearly filled. A measure of the ease with which this can be accomplished is given by the electron affinity energy which varies from 4 volts for electro-negative gases to negative values for rare gases. The probability of attachment per centimetre of travel, β , is given by:

$$\beta = \frac{\mathcal{V}_a}{\mathcal{V}_e} \quad (2.28)$$

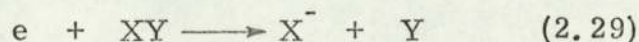
where \mathcal{V}_a is the attachment frequency and $\mathcal{V}_e = \mu E$ is the drift velocity of electron.

Measurements of attachment coefficient have been successfully carried out^{6, 15} by making careful measurement of the first ionization coefficient, α . If electron multiplication alone takes place, the log current versus electrode separation curves should be linear (see Fig. 2.3). Departures from linearity can be related to the electron-attachment phenomenon, as had been successfully shown by Harrison and Geballe^{43, 45}.

Collision processes that lead to electron attachment are controlled to a large extent by the conservation of energy which must account for all the energy involved in the collision.

A number of different attachment mechanisms are possible.

(a) Dissociative collision of electron with a molecule^{14, 42} represented by



normally leads to the transition to the repulsive state. Gases showing this kind of electron attachment have very marked energy thresholds and the attachment coefficient increases with $\frac{E}{P}$.

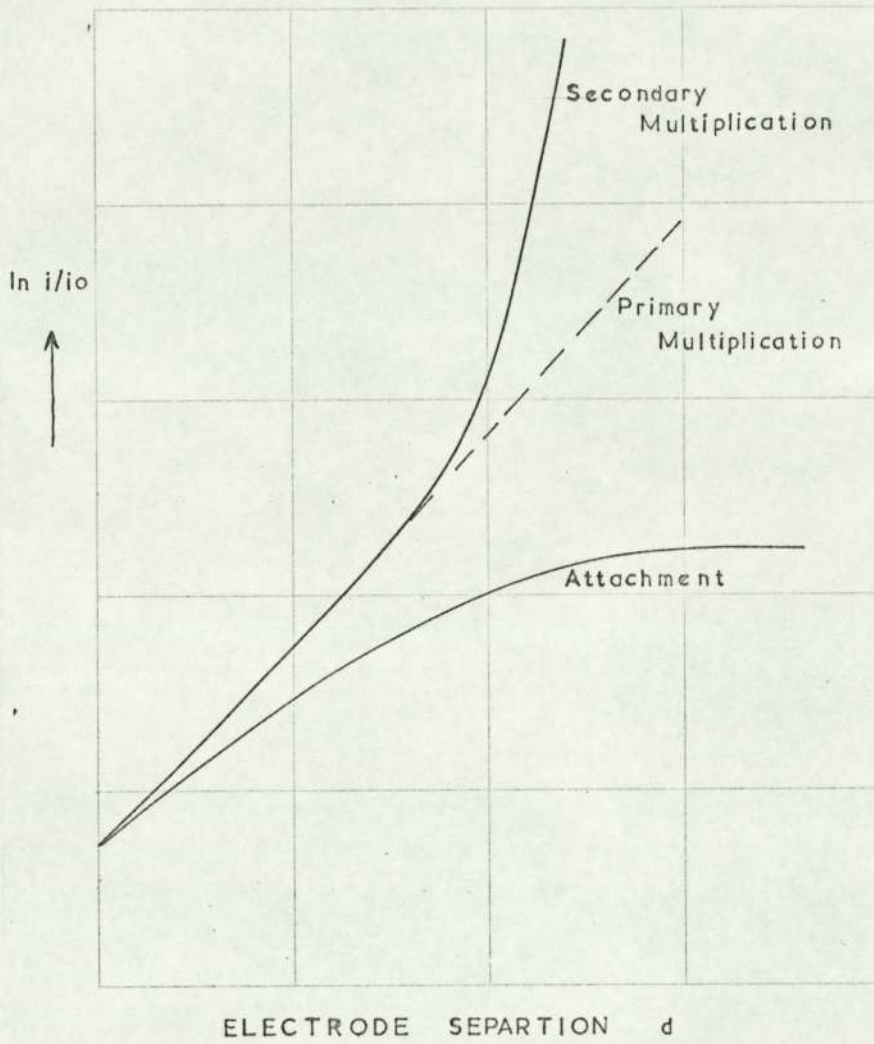
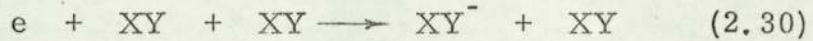


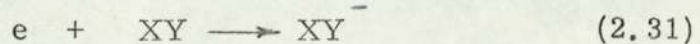
Fig. 2.3 THE MULTIPLICATION RATIO, $\frac{i}{i_0}$, AS A FUNCTION OF ELECTRODE SEPARATION, d , FOR CONSTANT REDUCED FIELD $\frac{E}{P}$ WHEN A SECONDARY EFFECT OR ATTACHMENT OCCURS.

(b) A third body attachment can take place when an electron is captured in the presence of a third body¹⁴ which can take up the excess energy.



This type of attachment phenomenon is pressure dependent.

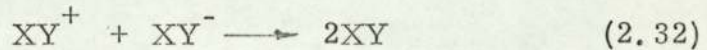
(c) Electron attachment by a molecule is possible leading to vibrational excitation of the molecule.



Subsequently, the molecule settles down to the ionic ground state¹².

2.2.1.1.3.2. Recombination

(a) A very common loss mechanism for ions is the recombination of negative ions with positive ions.



The loss of ions due to this effect is proportional to the ion concentration so that

$$\frac{d n_{i+}}{dt} = \frac{d n_{i-}}{dt} = -\zeta n_{i+} n_{i-} \quad (2.33)$$

where ζ is the recombination coefficient given by the high-pressure theory introduced by Langevin⁶⁰ as

$$\zeta = 4\pi q^2 (\mu_{i+} + \mu_{i-}) \quad (2.34)$$

where q is the electron charge and μ_{i+} and μ_{i-} are the mobility of positive and negative ions respectively.

The low-pressure theory based on works of Thomson¹³⁰ considers motion of the ions to be thermal and the recombination coefficient directly proportional to pressure (see Fig. 2.4).

(b) Electron-ion recombination studies have experienced difficulties due to the sensitivity of the phenomenon to impurities.

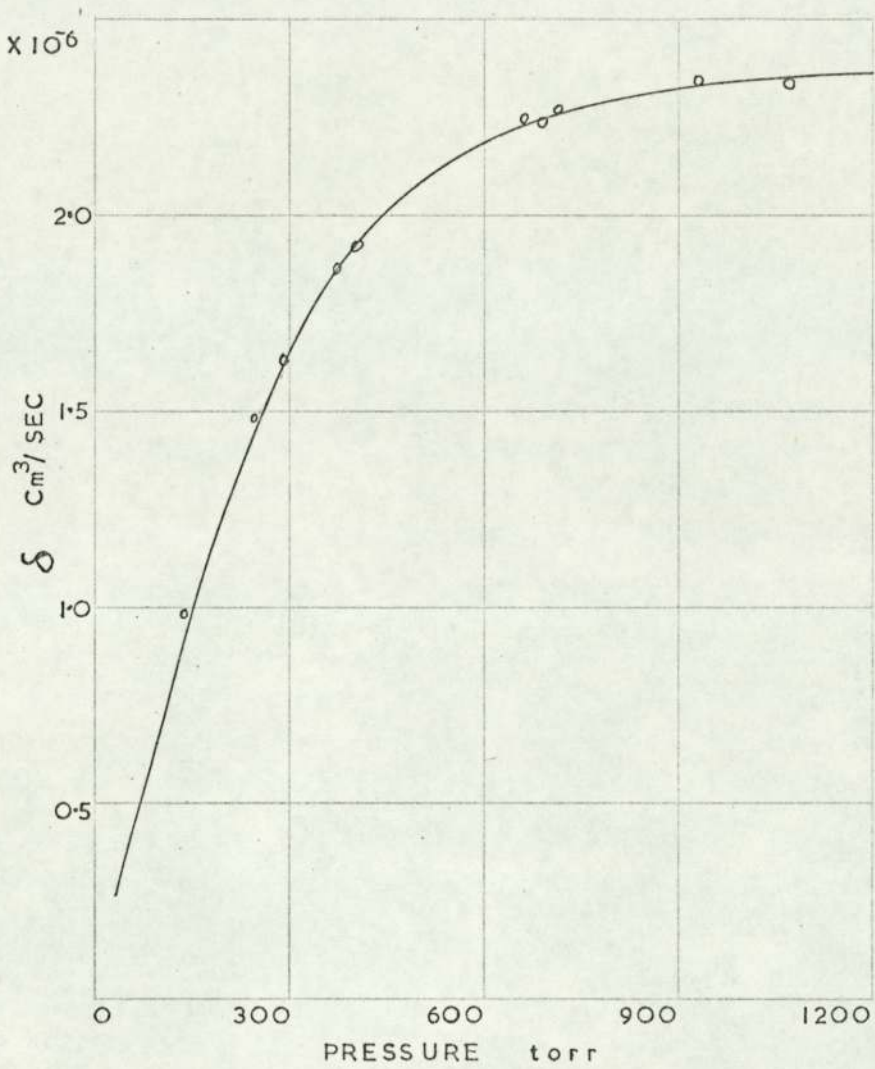
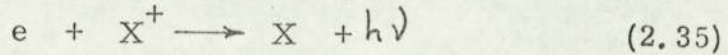
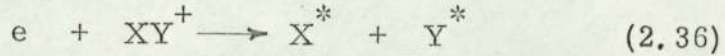


Fig. 2.4 RECOMBINATION COEFFICIENT, δ , IN AIR.
(After Brown 13)

A common type of electron-ion recombination is called radiative, typified by



Dissociative recombination is the result of electron positive molecule recombination⁹. This may be represented by



A third form of electron-ion recombination can occur by a three-body recombination with electrons removing the necessary momentum and energy.



The studies of Makin and Keck⁸³ have shown the importance of this mechanism at high electron density and low temperature when radiative recombination is unimportant.

2.2.2 Electron Avalanche

Impact ionization by electrons is probably the most important process in the breakdown of gases, but, as will be shown later, this process alone is not sufficient to produce breakdown. An electron in sufficiently high electric field ionizes gas molecules or atoms by collision such that, on drifting a distance X cm in a uniform field electrode system, it will create a mean number of electrons given by:

$$n_e = \exp(\alpha X) \quad (2.38)$$

α , the first Townsend coefficient¹³¹⁻¹³⁴, for ionization by electron impact, represents the mean number of ionizing collisions by one electron per centimetre of drift across the electrode gap. $\frac{1}{\alpha}$ is therefore the average ionizing free path.

An initial current, i_0 , at the cathode produced by, for

example U-V or cosmic radiation given by

$$i_0 = \gamma_0 q \quad (2.39)$$

where q is the electron charge, will have created a current, i , on arrival at the anode, at a distance d , given by

$$i = \gamma q$$

where $i = i_0 \exp(\alpha d)$ (2.40)

One electron and its progeny $\exp(\alpha d)$ electrons on arrival at the anode constitute an "electron avalanche".

The ionization process is characterised by a cross-section for ionization, which can be considered as a product of two terms, a physical cross-section for collision and a probability for ionization which depends on electron energies.

The coefficient α is found to obey a relation

$$\frac{\alpha}{p} = f\left(\frac{E}{p}\right) \quad (2.41)$$

characteristic of each gas (see Fig. 2.5), where p is the gas pressure and E is the electric field strength. The rise can be fitted into an exponential of the form

$$\frac{\alpha}{p} = A_1 \exp\left(\frac{B_1 E}{p}\right) \quad (2.42)$$

The next section can be fitted by a relation

$$\frac{\alpha}{p} = A_2 \left(\frac{E}{p} - B_2\right)^2 \quad (2.43)$$

There is a linear section at the point of inflexion. The upper portion is given by

$$\left(\frac{\alpha}{p} + B_3\right)^2 = \frac{A_3 E}{p} \quad (2.44)$$

Townsend¹³² derived an equation of the form

$$\frac{\alpha}{p} = A \exp\left(-\frac{Bp}{E}\right) \quad (2.45)$$

which can be fitted to any section of the curve with some accuracy.

The point of inflexion in Fig. 2.5 marks the region of $\frac{E}{p}$

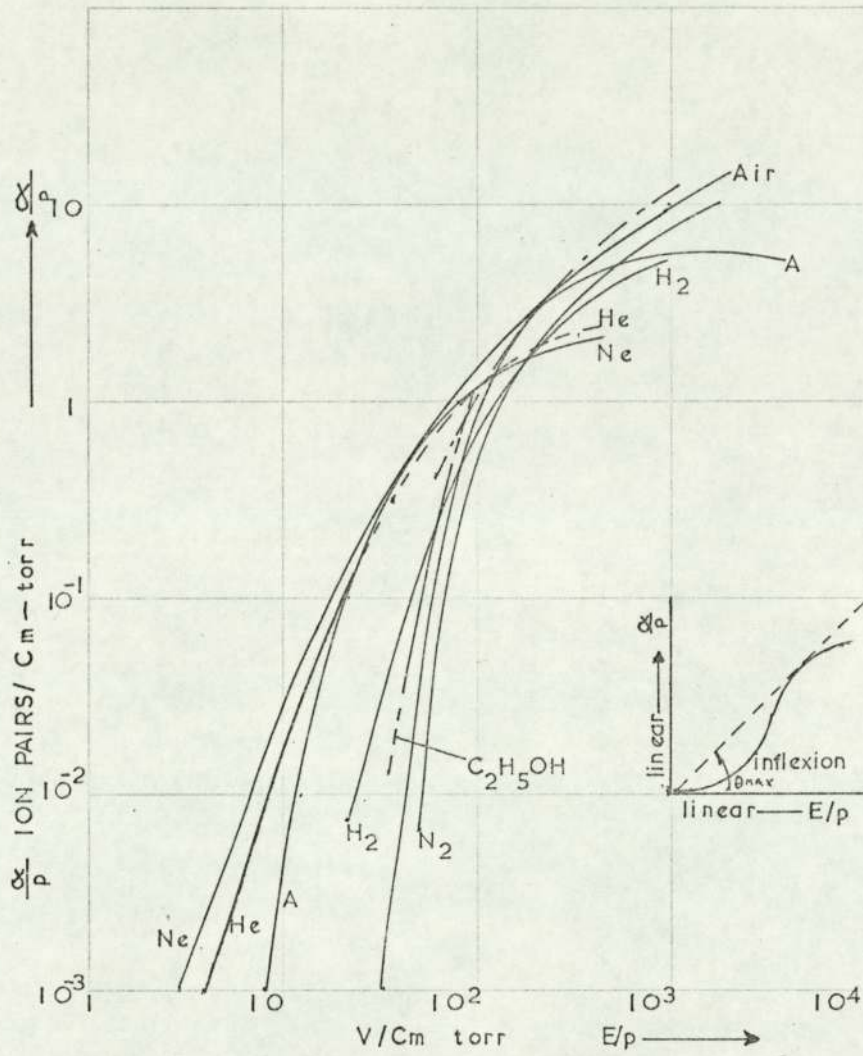


Fig. 2.5 IONIZATION COEFFICIENT $\frac{\alpha}{p}$ AS A FUNCTION OF THE FIELD $\frac{E}{p}$ FOR DIFFERENT GASES.

(After von Engel 30)

values - The Morton-Johnson⁵² regime - in which charge accumulation in a uniform field gap ceases to aid charge multiplication.

2.2.2.1 Determination of First Ionization Coefficient

One of the most important data of elementary processes is the Townsend First Ionization Coefficient, α , which can be measured by a variety of techniques, the first and the most widely used one being the Townsend (or stationary) method^{67, 74, 88, 132}. In this method $\log \left(\frac{I}{I_0} \right)$ is observed as a function of gap distance, d , with $\frac{E}{p}$ as a parameter (see Fig. 2.6).

Employing this technique, von Engel and Steenbeck³¹ provide typical values for constant A and B of Eqn. 2.45 which can be fitted empirically over fairly wide ranges of $\frac{E}{p}$ for a large number of gases (see Table 2.3).

Fromhold's³⁹ studies on the distribution of the pulse heights of single avalanches as a function of the carrier number has led Schlumbohm¹¹⁹ to measure α in different vapours (see Fig. 2.7 and Table 2.3).

A determination of α is possible by measuring the time constant, τ_e , of the growth of an avalanche which is given by

$$\tau_e = \frac{1}{\alpha v_e} \quad (2.46)$$

where v_e is the drift velocity of electrons.

Fig. 2.8 shows values of α in nitrogen obtained by the time constant method⁴⁰ compared with Townsend's method^{24, 50, 87}

2.2.2.2 Charge Carriers Drift Velocity

The observation of the avalanche process allows

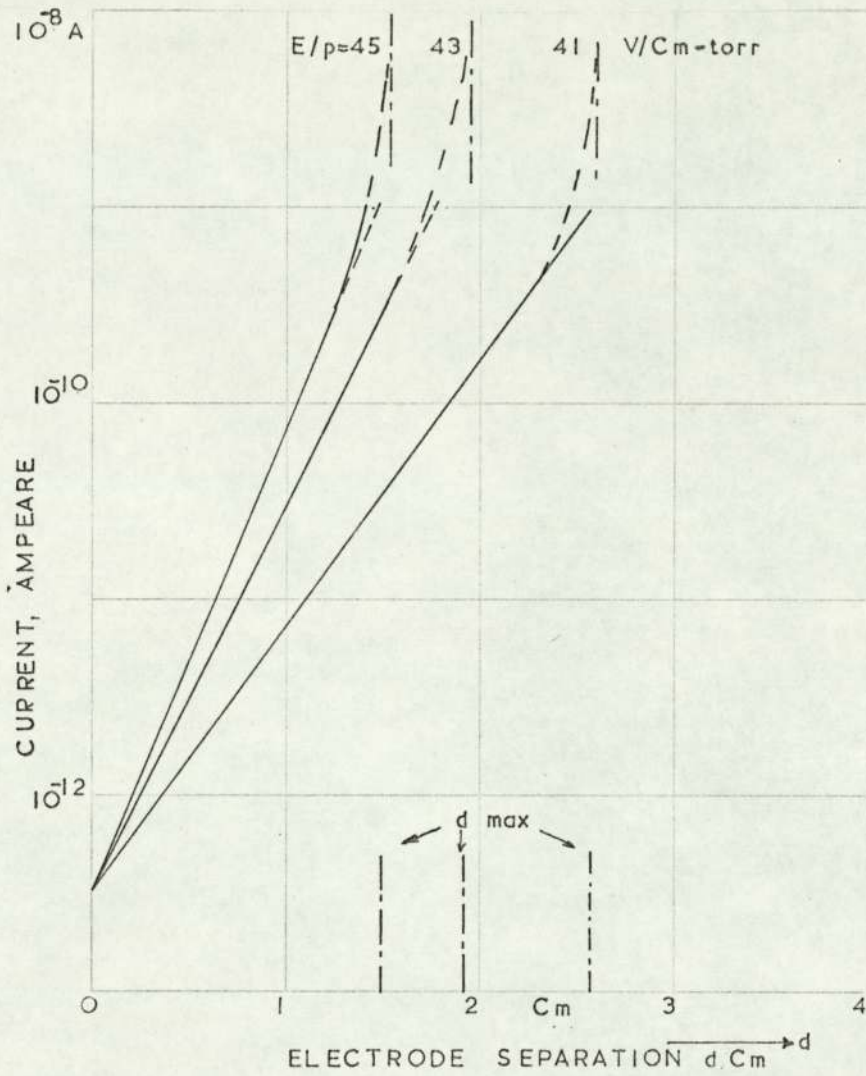


Fig. 2.6 MULTIPLICATION RATIO $\frac{i}{i_0}$ AS A FUNCTION OF THE ELECTRODE SEPARATION FOR DIFFERENT FIELD $\frac{E}{p}$ FOR NITROGEN AT 300 TORR WITH Ni ELECTRODES.

(After Dutton, et al 24)

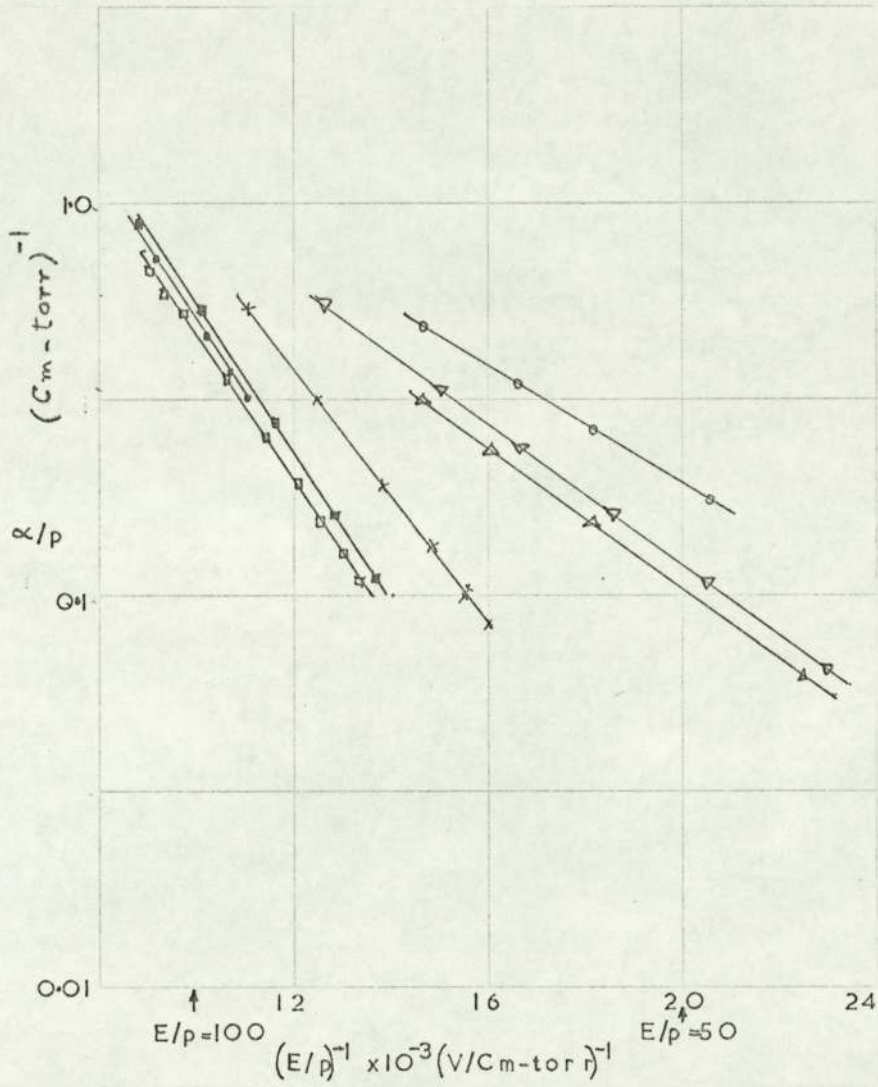


Fig. 2.7 IONIZATION COEFFICIENT $\frac{\alpha}{p}$ AS A FUNCTION OF $\frac{E}{p}$
 IN DIFFERENT GASES AT 20°C.
 (After Schlumbohm 119)

Details in TABLE 2.3

TABLE 2.3 Values of A and B in $\frac{\alpha}{p} = A \exp \left[-B \left(\frac{p}{E} \right) \right]$

After Schlumbohm 119.

Gas	Fig. 7 marking	A (cm-torr) ⁻¹	B V/cm-torr	$\frac{E}{p}$ V/cm-torr
Methane	▽	6.99	192.1	40-80
Carbon dioxide	△	4.75	182.5	44-70
Methyl alcohol	○	6.77	173.5	48-68
Diethylether	■	24.5	388.8	72-116
Acetone	□	14.3	360.8	74-110
Methylal	x	29.7	360.8	60-90
Cyclohexane	●	26.4	400.0	89-108

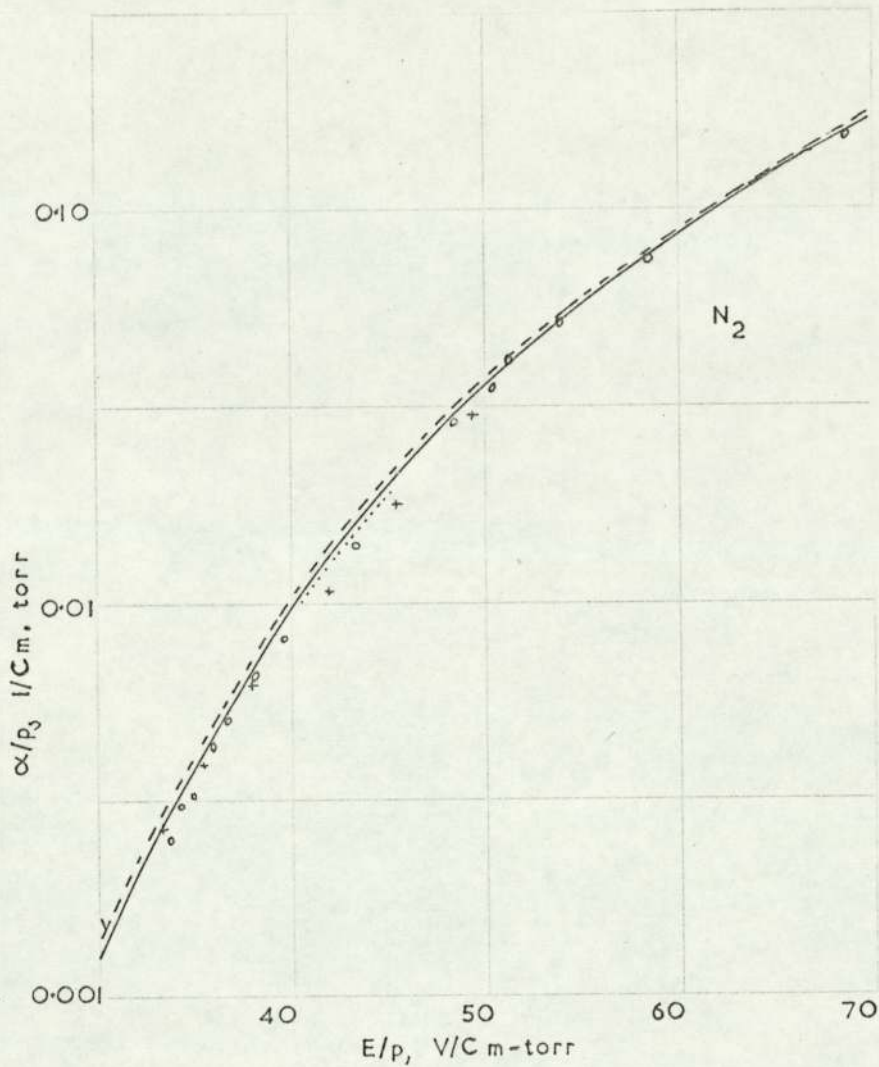


Fig. 2.8 IONIZATION COEFFICIENT $\frac{\alpha}{p}$ AS A FUNCTION OF $\frac{E}{p}$
IN N_2 AT $20^{\circ}C$.

- o Frommhold 40 - Time constant method (electron current)
- + Frommhold 40 - Time constant method (ion current)
- Masch 87 - Townsend method
- - - Dutton, et.al.24 - Townsend method
- Heylen 50 - Townsend method

deduction of the drift velocity of charge carriers. Different methods of measurements of drift velocity are described in detail by von Engel³⁰, Loeb⁷⁴ and Raether¹¹⁶. These include electrical, optical, magnetic deflection and shutter methods.

The values of drift velocity of charge carriers obtained by these methods in air are shown in Fig. 2.9 for electrons and in Fig. 2.10 for positive ions. The difficulties in measuring electron drift velocity, V_e , in air, is due to the presence of additional processes besides the normal behaviour of electron component, characterised by the exponential growth of current with time^{40, 122, 125, 137}.

2.2.2.3 Space Charge Effect on Avalanche Growth

The growth of the charge carriers in an avalanche in a homogeneous field $E_0 = \frac{V}{d}$ is described by Townsend equation

$$n = n_0 \exp(\alpha d)$$

This is valid as long as the electric field of the space charge of electrons and ions can be neglected compared to E_0 .

The electrical field around an avalanche according to Raether¹¹³ is shown in Fig. 2.11. The electric field ahead and behind the head of the avalanche is increased by the space charge and reduced between the electrons and ions cloud compared with the electrostatic field E_0 . An approximate value of this space charge field can be deduced as the charge lies nearly in a sphere of radius r_D ; then the field of this charged sphere at its surface is:

$$E_r = \frac{q}{4\pi\epsilon_0 r_D^2} \exp(\alpha d) \quad (2.47)$$

The field distortion produces, for example at $\frac{E}{p} = 40$ in nitrogen, a change of α of about 5%, a remarkable result¹¹⁶.

Observations on avalanches in the cloud chamber¹¹⁰

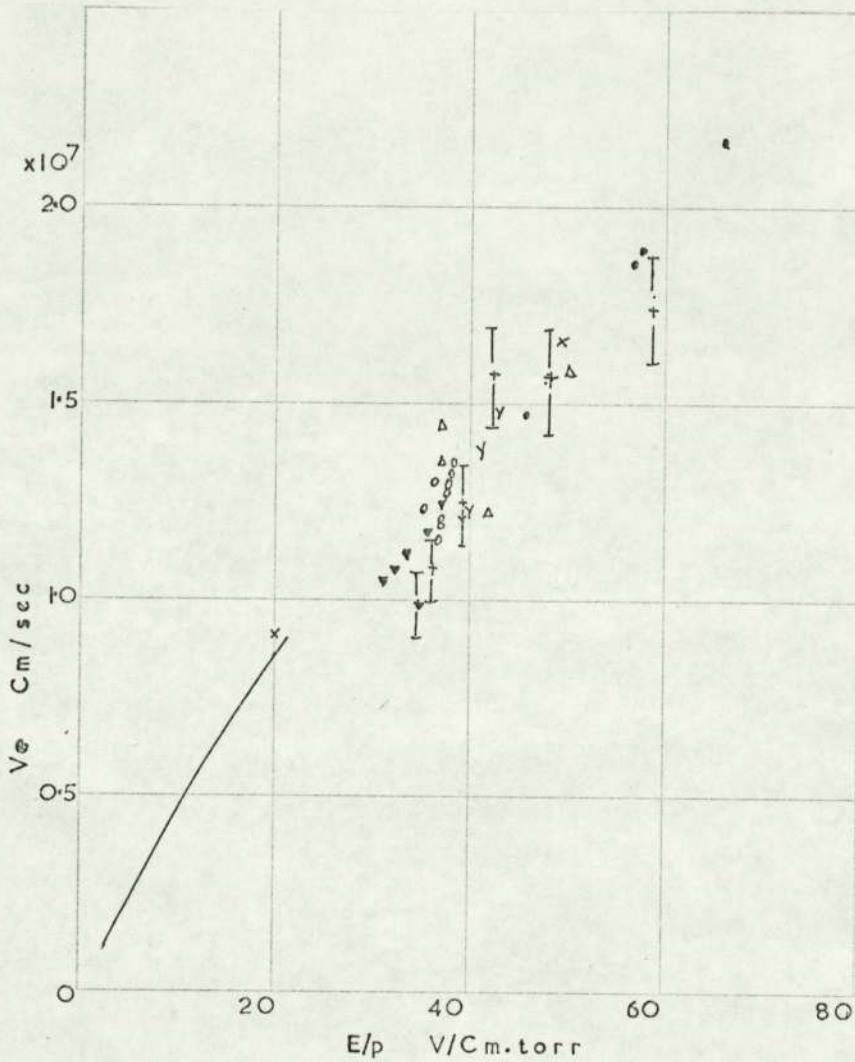


Fig. 2.9 DRIFT VELOCITY OF ELECTRONS IN AIR, AS A FUNCTION OF $\frac{E}{P}$

- x Townsend 132 - Deflection method
- Nielsen and Bradbury 102 - Shutter method
- Y Frommhold 41 - Electrical method (1-6 torr of water vapour)
- + Frommhold 41 - Electrical method
- Raether 116 - Optical method
- Δ Raether 113 - Cloud chamber method
- ▼ Allen and Phillip - Cloud chamber method
- o Schröder 125 - Optical method

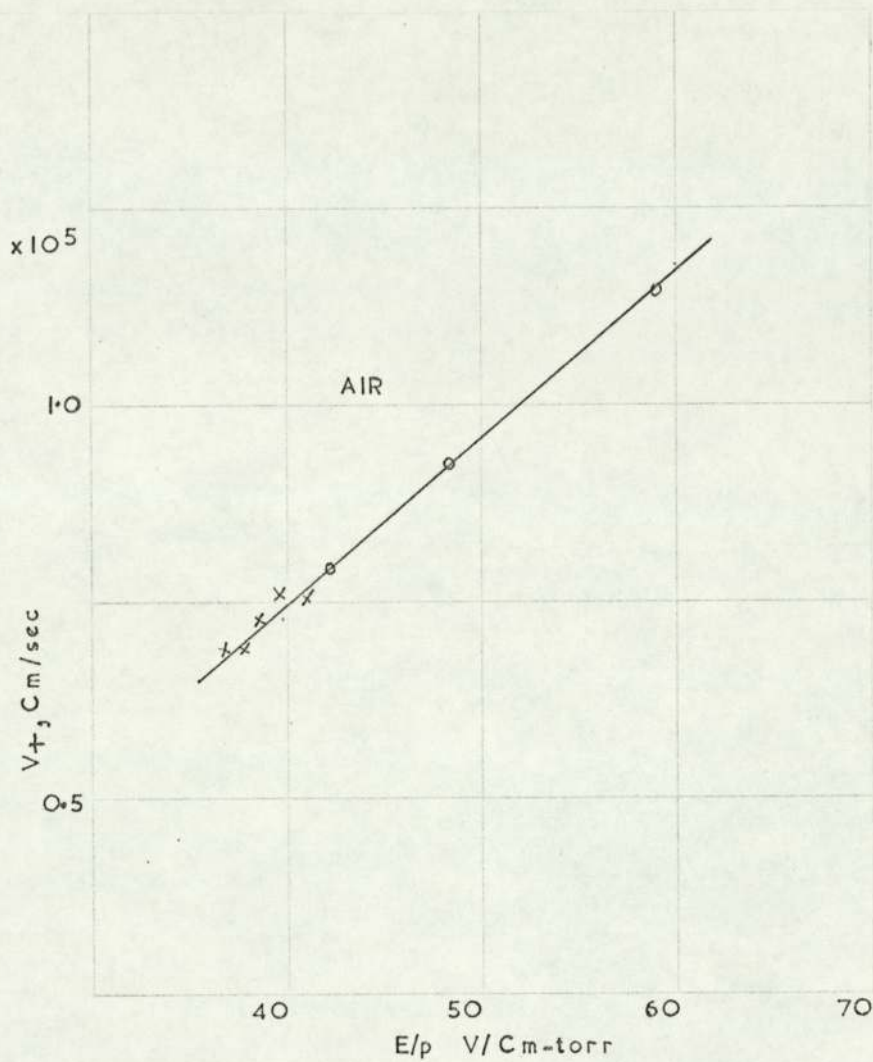


Fig. 2.10 DRIFT VELOCITY OF POSITIVE IONS IN AIR AS A FUNCTION OF $\frac{E}{P}$

- o Frommhold 40 - Transit time method
- x Raether 116 - Transit time method

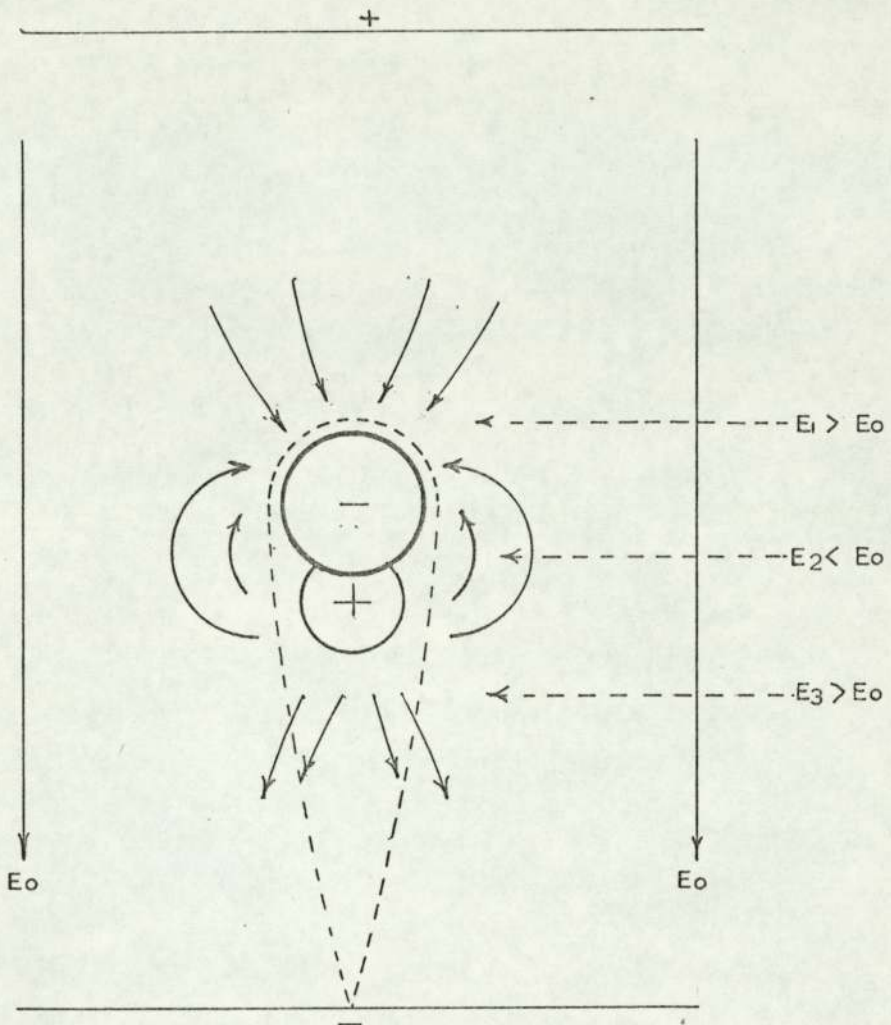


Fig. 2.11 THE EFFECT OF SPACE CHARGES OF AN AVALANCHE OF HIGH AMPLIFICATION ON THE ELECTRIC FIELD.

(After Raether 113)

show a strong enlargement of the head of the avalanche, exceeding the normal diameter due to thermal diffusion, if the amplification approaches values of 10^8 . Raether¹¹⁰ and Petropoulos¹⁰⁶ suggest the reasons for this enlargement to be (a) the effect of the gas ionizing radiation, which produces ion pairs in the environment of the avalanche, especially of the avalanche head, and (b) an electrostatic expansion of the electron cloud of the avalanche head.

The electric field, E_r , acts on the electron at the surface of the sphere containing $\exp(\alpha d)$ electrons and accelerates them into outer direction such that:

$$\frac{dr}{dt} = \mu_e E_r \quad (2.48)$$

where μ_e is the mobility of the electrons.

The radius of the expanded sphere is given by

$$r^3 = A \exp(\alpha n) - \exp(\alpha x_D) + r_D^3 \quad (2.49)$$

The equation 2.49 suggests that, up to a certain $x = x_D$ value, the avalanche diameter as a function of x can be described by the thermal diffusion. At higher amplifications

$$\exp(\alpha x) > 10^6$$

r grows much more rapidly with x than the thermal diffusion radius.

It is suggested^{116, 125} that, at values of $pd \gg 5000$ torr-cm, the positive ion space charge due to the ionization resulting from even a single initiating electron can strongly affect the initiation of breakdown in air. On the other hand, Dutton and Morris²⁷ show that the maximum pre-breakdown ionization current of the order of $0.5 \mu A$ is not influenced by space charge up to $pd = 10,000$ torr-cm.

2.2.3 Avalanches with Successors

One of the most important experiments in the elucidation of the mechanism of gaseous conduction results from varying the voltage applied to the gap, and changing the electrode spacing d , keeping α constant. A plot of the logarithm of the observed current against d should give a straight line with slope α . It is expected that from relationship

$$\frac{\alpha}{p} = f\left(\frac{E}{p}\right)$$

if pressure of the gas and the electric field strength are kept constant, then α should remain constant. Figure 2.6 shows such a plot for several applied fields. Except at high fields and with large gaps, the results are as expected. From these data, a curve for α as a function of $\frac{E}{p}$ can be constructed (see Fig. 2.7), and in all cases a similar functional dependence has been observed.

From the discussion so far, it is expected that the current will fall to zero if the source of cathode illumination is removed. Townsend, however, discovered that at a sufficiently large gap this is not true, and that above a certain sparking distance the current is independent of the external illumination. The key to this behaviour lies in the departure of the curves in Fig. 2.6 from linearity. It is clear that some additional mechanism must be operative in the production of charged species in the region. These mechanisms which all have in common the characteristic of producing additional electrons at the cathode can be explained as follows:

- 1) While ions cannot gain enough kinetic energy to ionise molecules, they do have sufficient potential energy to cause the ejection of electrons upon striking the cathode. The probability of this process increases with increasing kinetic energy of the ions.

2. The importance of electronic excitation in hindering the development of an avalanche has already been noted, as has also the fact that the absorbed energy may reappear as radiation of light as a result of the excited molecular electron falling back to its normal energy level. This radiation may fall upon the cathode to produce photo-emission of electrons which may then start avalanches of their own.

3. Occasionally, some of the electronically excited molecules may collide with neutral molecules to lose a small fraction of their energy.

A new excited state is now produced from which the molecules cannot lose the remainder of their energy by radiation. These so-called metastable molecules may diffuse back to the cathode and cause electron emission on striking it.

These three processes are described quantitatively by a coefficient γ , called Townsend's second ionization coefficient, which is defined as the number of secondary electrons produced at the cathode per electron produced in the gap by primary collisional ionization.

These secondary electrons, the mean number of which is

$$n_s = \gamma \left[\exp(\alpha d) - 1 \right] \quad (2.50)$$

per avalanche, produce new avalanches in the next generation. If the primary generation begins with n_0 electrons, then the second generation follows with $n_s n_0$ electrons.

The various γ processes are often distinguished by a subscript - γ_i for positive ions, γ_p for photons, and γ_m for metastables. Although the magnitude of γ may be small, (e.g. 10^{-4}), its overall effect may be large since these secondary electrons are produced at the cathode and each will be multiplied by the factor $\exp(\alpha d)$ by the time it crosses the gap.

Unlike α , the secondary coefficient γ is not proportional to the pressure. This is reasonable when one notes that secondary electrons are produced at the cathode surface rather than by collision of the active species with molecules. The coefficient γ , however, is determined by the energy of the primary electrons, and is accordingly a function of $\frac{E}{p}$.

2.2.3.1 Determination of Second Ionization Coefficient, γ

Townsend's second ionization coefficient increases with increase in $\frac{E}{p}$ (see Fig. 2.12) but it is subject to alteration by pre-discharges.

As the three components of γ contain different time scales, their significance becomes dependent on the duration of the applied field. With microseconds pulse duration only γ_p can be active. However, if the time scale exceeds $10 \mu\text{sec}$, γ_i may be involved and, if it is in the range $0.1 - 1.0 \text{ m. sec}$, one may also expect metastable action γ_m to be involved.

The photons active in γ_p must usually be of a kind that do not experience delay and dissipation by resonance absorption. The secondary mechanism which involves γ_p may suffer a delay per generation of the order of $3\tau_e$ in air and nitrogen⁷⁶ where τ_e is the electron transit time.

Increase in electrode work function, ϕ , reduces γ_i and γ_m . In contrast, γ_p depending on photo-electric effect, is not so sensitive to changes in surface conditions. Oxide layers generally reduce γ_i and γ_m but do not alter γ_p as radically.

2.2.3.1.1 Secondary Electron Liberated by Photon Radiation on the Cathode

Some excited states will radiate photons of energy

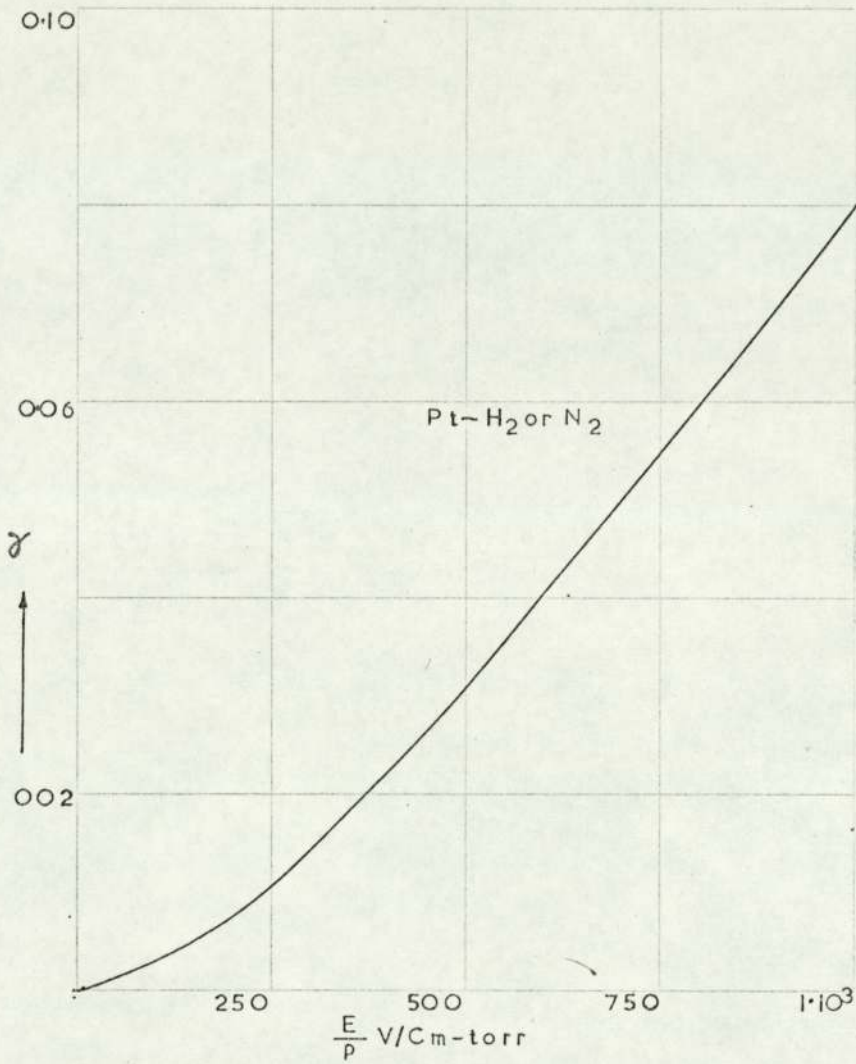


Fig. 2.12 THE SECONDARY EMISSION COEFFICIENT γ FOR N₂ & H₂ AS A FUNCTION OF $\frac{E}{p}$. Pt-ELECTRODES.

(After Llewellyn - Jones 65)

$h\nu$ which will be directed back to the cathode. Absorption of these photons en route will reduce their number. A fraction of these arriving at the cathode with sufficiently large values of $h\nu$ will succeed in liberating further electrons.

The generation interval, after which the succeeding avalanche starts, is given by

$$\tau_c = \frac{d}{v_e} \quad (2.51)$$

It is possible to observe the oscillatory character of the electron component of the current, which comes from the succeeding avalanches¹¹⁶. This is illustrated in Fig. 2.13 which shows the electron current as a function of time, when $n_s = 1$. The broken line shows the ideal case which assumes that the whole radiation producing the photo-effect at the cathode is produced at the moment the electrons enter the anode. In fact, however, the radiation intensity is proportional to $\exp(-\alpha v_e t)$, and secondary electrons are liberated from the cathode during the transit time of the avalanche electrons, resulting in the full line in Fig. 2.13.

2.2.3.1.2 Secondary Electron Liberation by Ion Impact on the Cathode

Ions with energies higher than 2ϕ , where ϕ is the work function for a metal surface, will, on impact with the surface, yield secondary electrons. The probability that these ions liberate electrons on impact is designated by χ_i . The values of χ_i depend on the type of ions, gas pressure, and $\frac{E}{p}$ and have a range of 0.01 - 0.25 for singly charged ions.

Ions with energies lower than 2ϕ will also liberate secondary electrons if their kinetic energy is sufficiently

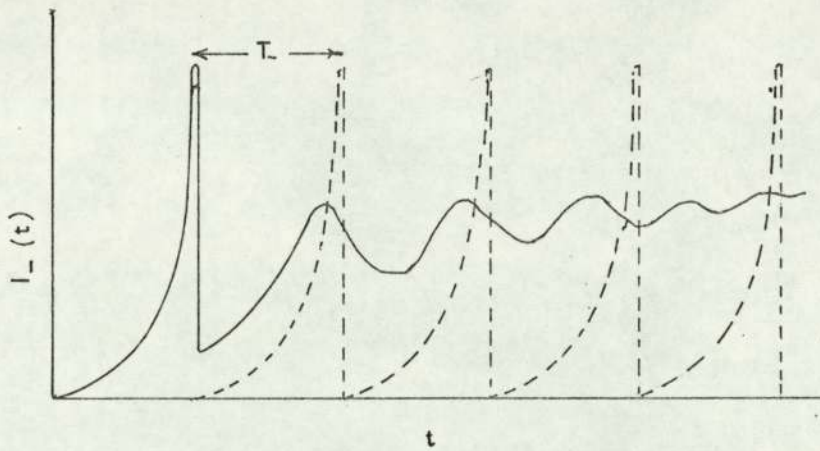


Fig. 2.13 ELECTRON CURRENT AS A FUNCTION OF TIME. SUCCEEDING AVALANCHES ARE PRODUCED BY PHOTO EFFECT AT THE CATHODE, γ p.

(After Schlumbohm 120 and Kluckow 56)

high (> 150 v). The value of γ_i is about 10^{-6} at 150 volts and may reach 10^{-2} at 1-kv. Emission of secondary electrons by this kinetic process may be quite large on dirty or negative ion-coated metal surfaces.

If the succeeding avalanches are only produced by positive ions reaching the cathode, the generation time, τ_t , can be represented in the ideal case by Fig. 2.14. This can be realised¹³⁶ by using gases in which the avalanches reach a very high αd value, so that the positive ions are concentrated practically at the anode. Schmidt-Tiedemann¹²³ gives the transit time in oxygen, with the production of secondary electrons by γ_i process, as about 5μ sec (see Fig. 2.15).

2.2.3.1.3 Secondary Electrons Liberation by Metastable Impact on the Cathode

Metastable atoms with $W_m > \phi$ will liberate secondary electrons on reaching the metal surface with a coefficient γ_m which has a longer time scale than γ_p and γ_i in that order. γ_m is operative only in very pure rare gases.

Secondary electrons are readily emitted from metal surfaces when slow metastable atoms impinge upon them. Large yields have been found for rare gas metastables^{23, 29}. The yield seems to depend more on the surface layer than on the nature of the substance and it usually increases with gas contamination. Green⁴⁴ suggests that the energy in excess of the work function of the surface is transferred to the ejected electrons.

2.2.3.2 Townsend's Generalised Equation

A number of investigators^{22, 27, 45, 67} in recent

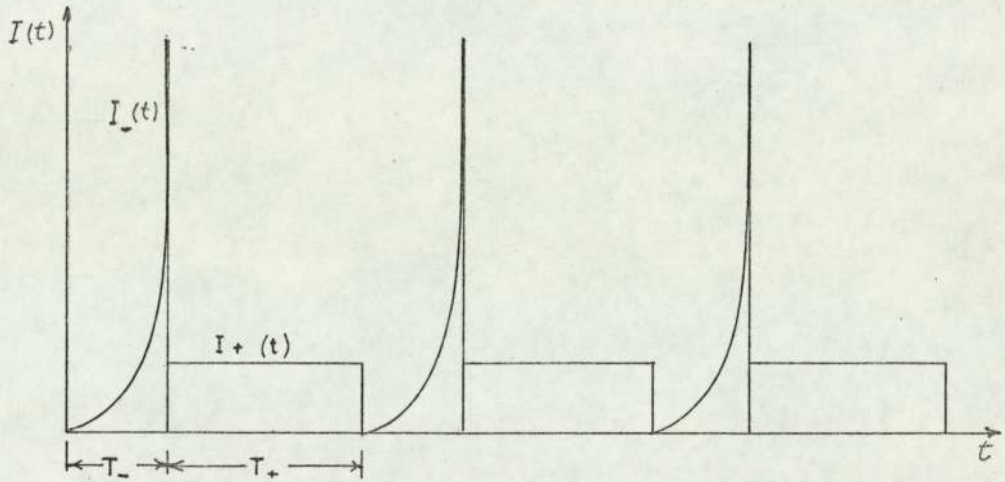


Fig. 2.14 IDEALIZED CURRENT AS A FUNCTION OF TIME.
SUCCEEDING AVALANCHES ARE PRODUCED BY POSITIVE IONS AT THE
CATHODE, γ_i .

(After Raether 116)

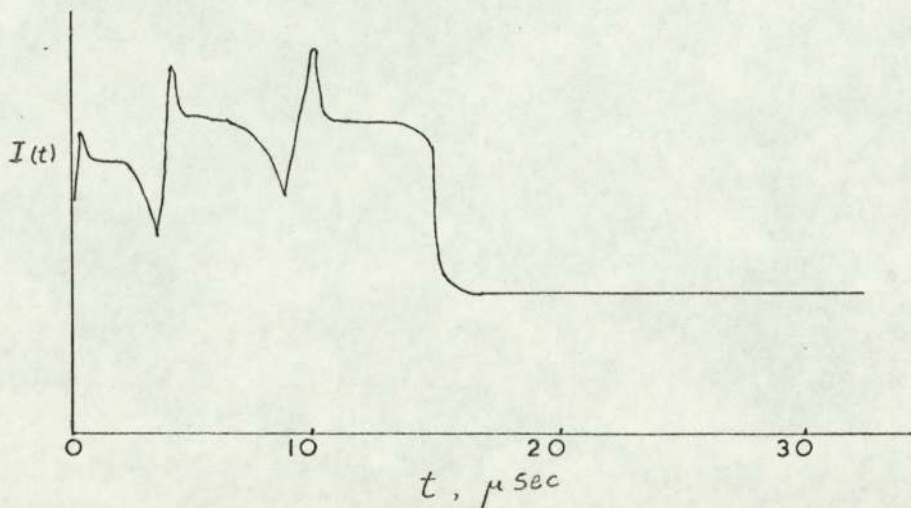


Fig. 2.15 OSCILLOGRAM OF A SERIES OF AVALANCHES WITH SUCCESSORS
IN O_2 PRODUCED BY IONS AT THE CATHODE.

(After Schmidt-Tiedmann 123)

pd = 60 torr-cm, d = 0.5 cm

years have elaborated on Townsend's original criterion to account for different secondary electron emissions from electrodes and the de-ionization processes, mainly attachment and recombination. This has led to the generalised Townsend relationship of the form:

$$\frac{i}{i_0} = \frac{C [(\alpha - \lambda) / (\alpha' - \lambda)] \exp(\alpha' d)}{1 - (\omega/\alpha') [\exp(\alpha' d) - 1]} \quad (2.52)$$

where α' and ω/α' are the apparent primary and secondary ionization coefficients respectively and

$$\alpha' = \frac{1}{2} \left\{ (\alpha - \beta - \delta) + [(\alpha - \beta - \delta)^2 + 4\alpha\delta]^{1/2} \right\} \quad (2.53)$$

$$= \frac{1}{2} \left\{ (\alpha - \beta - \delta) - [(\alpha - \beta - \delta)^2 + 4\alpha\delta]^{1/2} \right\} \quad (2.54)$$

where α , β and δ are the true ionization, attachment and recombination coefficients respectively.

Measurements of pre-breakdown current by Dutton and Morris²⁷ in dry air at pressures of about two atmospheres are in good agreement with the Townsend generalised equation (see Fig. 2.16). In analysing the curves of Fig. 2.16 by the use of the expression given by Schlumbohm¹²¹, they give a value of attachment coefficient, β , in the same order as the true primary ionization coefficient, α , and a value of recombination coefficient δ between one and two order of magnitude smaller than α .

2.2.4 Breakdown

2.2.4.1 Introduction

A high conductivity between electrodes in an electric field may result in a short time such that the gap capacity cannot be reloaded quickly and the breakdown of voltage across

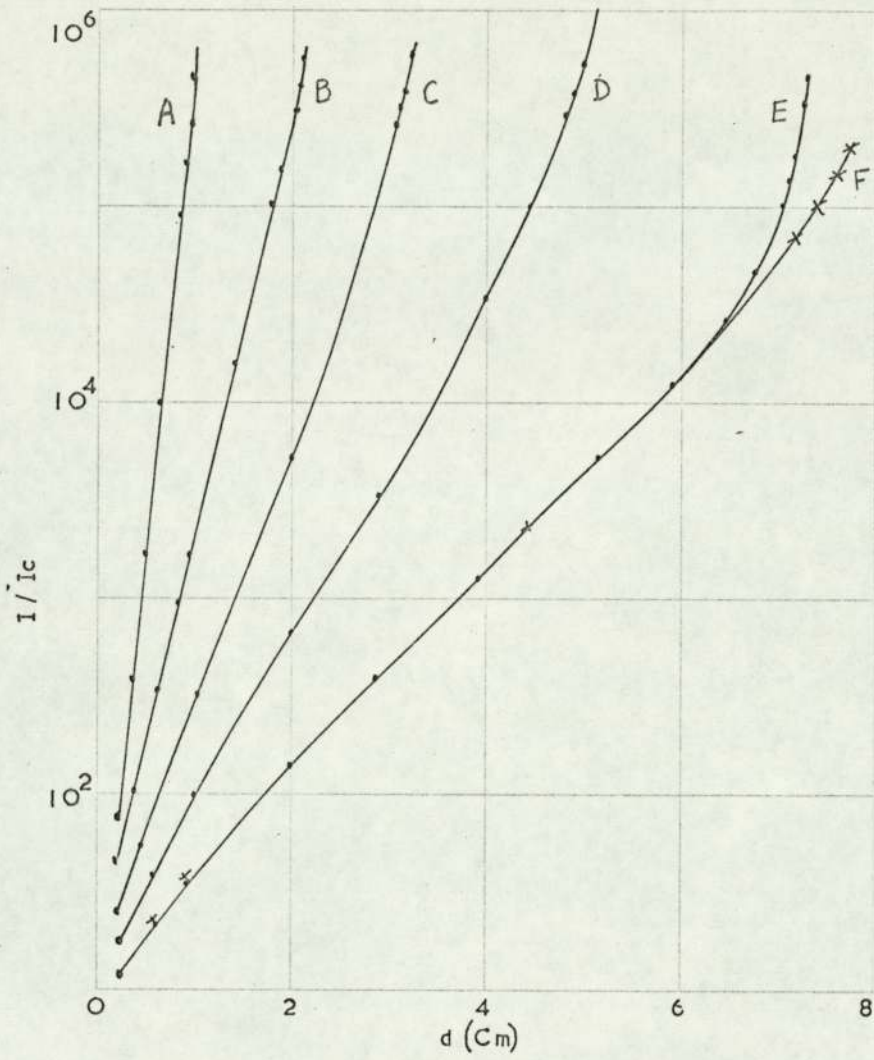


Fig. 2.16 THE MULTIPLICATION RATIO $\frac{i}{i_0}$ IN AIR USING SILVER ELECTRODE AS A FUNCTION OF ELECTRODE SEPARATION. DETAILS IN TABLE 24.

(After Dutton and Morris 27)

TABLE 2.4 Values of Coefficients in Townsend's Generalised Equation. After Dutton and Morris²⁷

Curve	E/p_{20} ($\text{vcm}^{-1} \text{ torr}^{-1}$)	p_{20} (torr)	α' (cm^{-1})	(ω/α') $\times 10^6$	$\frac{C(\alpha' - \lambda)}{\alpha' - \lambda}$	Cathode condition
A	36	1611	8.44 ± 0.05	6.6 ± 0.8	5.7 ± 0.2	Polished 1 month
B	35	1611	5.22 ± 0.02	6.4 ± 0.6	8.1 ± 0.2	previously; sparked several times during interval between polishing and these measurements
C	34	1636	2.96 ± 0.05	28 ± 5	14.1 ± 1.4	Polished previous day; not sparked
D	33.5	1636	1.91 ± 0.02	48 ± 6	16.0 ± 1.2	Curve obtained 1 day after C; not sparked
E	33	1652	1.15 ± 0.02	190 ± 24	16.0 ± 1.5	Curve obtained 1 day after sparking once only
F	33	1636	1.14 ± 0.01	91 ± 12	16.7 ± 1.0	Curve obtained 2 days after D; not sparked

the gap is the consequence. The main problem of gas discharge studies is concerned with the way this high conductivity builds up by fundamental processes. At present, two mechanisms are known.

(a) A 'slow' mechanism - Townsend or generation - requiring a large number of avalanches¹⁰² to produce breakdown^{24-27, 65-70, 131-134}.

(b) A 'rapid' mechanism - streamer or kanal - which develops the first avalanche directly to breakdown^{2, 78-81, 89-91, 109-116, 127, 128}.

Other variations^{38, 57, 58, 107, 108} are suggested which can be understood as transitions between these types.

The space charge produces in both cases the decisive current growth which leads to the voltage drop. In mechanism (a), it is the space charge of the slow positive ions produced by the rapidly succeeding avalanches which favours in general the ionization conditions of the electrons and produces a rapid current growth. In mechanism (b), it is the effect of the space charge of the avalanche on its own development which transforms it into a plasma streamer of a high conductivity.

2.2.4.2 Townsend or Generation Criterion for Breakdown

The field intensified ionization current in the external circuit of a uniform field gap is given by

$$i = \frac{i_0 \exp(\alpha d)}{1 - \gamma [\exp(\alpha d) - 1]} \quad (2.55)$$

As breakdown approaches $\exp(\alpha d) \gg 1$ and the field intensified current becomes

$$i = \frac{i_0 \exp(\alpha d)}{1 - \gamma \exp(\alpha d)} \quad (2.56)$$

Increase in potential results in increase in $\exp(\alpha d)$ and $\gamma \exp(\alpha d)$. As $\gamma \exp(\alpha d)$ approaches unity, the avalanches will be sustained independent of the initial current, i_0 . The current, i , will increase and be limited only by the impedance of the external circuit and the conducting gas. This condition referred to as Townsend criterion for spark breakdown is expressed quantitatively by the relation

$$\gamma \exp(\alpha d) = \gamma \exp(\eta V) = 1 \quad (2.57)$$

where η represents the number of new ions per centimetre path per unit field strength.

The fulfilment of Eqn. 2.57 does not depend upon the value of i_0 , provided of course there are sufficient electrons to start the sequence of the avalanche leading to breakdown. This is not a very stringent requirement since cosmic radiation and radiation from radio-active impurities are easily able to produce these initiating electrons.

The fulfilment of the breakdown criterion for a given gap spacing depends on the values of α and γ . For a given gap spacing and gas pressure, the value of potential V , which gives values of α and γ satisfying the Eqn. 2.57 is the spark breakdown voltage. Since γ is the number of secondary electrons generated per primary electron in the gap, the Townsend criterion guarantees that, for each electron avalanche, one secondary electron will be generated at the cathode to initiate another avalanche, and the discharge becomes self-sustaining.

γ is a probability for which an average value is obtained by observing some 10^7 or so simultaneous avalanches. Again, $\exp(\alpha d)$ is governed by chance, since in most discharges $9 < \alpha d < 18$.

The probable fluctuation of αd can be between -3 and $+4$ in a single avalanche. This can produce a large variation in $\exp(\alpha d)$. It is shown by Wijsman¹⁴⁰ that, by setting

$$M = \gamma \exp(\alpha d) \quad (2.58)$$

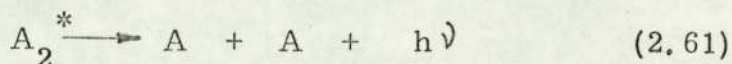
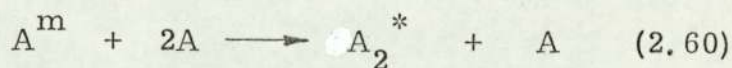
then the breakdown probability P_o is

$$P_o = 1 - \frac{1}{M} \quad (2.59)$$

This makes the breakdown probability zero at threshold, for any sub-average avalanche can break off the sequence. As the amplification factor M exceeds unity, the chance of breakdown increases. In any event, sustained current is not always ensured, since sooner or later an avalanche sequence can interrupt the discharge.

However, other factors influence this statistical consequence. Delayed carriers ensure re-ignition when an interruption occurs. With many triggering electrons, the chance of continuity is much increased^{35, 62, 63}.

In some gases, photons experience delay by dissipation and resonance absorption. In such cases there may be a delay in creating the state to produce γ_p . Thus, in the inert gases, notably in argon, the photons yielding γ_p are created by the reactions



These are pressure dependent and suffer a delay in the order of 3μ sec in their generation from A^m in collision with two A atoms. This action sets the threshold for a γ_p breakdown at near atmospheric pressure.

At some tens of torrs pressure, breakdown proceeds largely by the γ_i mechanism since triple impact of A^m with $2A$ atoms becomes infrequent.

Electron emission of electrode in the fields of the order of 10^5 V/cm has been studied by Llewellyn Jones and De La Perelle⁶⁸. The emission rate was found to be as high as $10^5 - 10^6$ electron/sec with steel and copper cathodes. The emission is dependent on the cathode material, its history, and the presence or absence of surface layers of tarnish or dust.

Studies of Dutton and co-workers²⁴⁻²⁷ show that the Fowler-Nordheim equation on the dependence of rate of emission on the applied field leads to too small a value of work function and emitting area. Llewellyn-Jones and Morgan⁶⁹ suggest a different mechanism due to positive ions piling up on thin tarnish films at the cathode and creating a strong field across the tarnish film to cause field emission.

Lewis⁶⁴ considers the nature of the surface barrier and presents an explanation based on field dependent thermionic emission, which leads to a reasonable emitting area. The field emission rate obtained by Feldt and Raether³⁵ is in the range $10^6 - 10^8$ electrons/sec.

Llewellyn-Jones and co-workers^{25, 67, 70} have shown that the physical significance of the Townsend criterion is that the sparking potential, v_s , becomes independent of initial current, i_0 , up to the levels of current of 10^{-11} A and that a finite current, i , can flow at zero initial current.

Dutton and co-workers^{19, 24-27} have found experimentally good agreement with the Townsend breakdown criterion in uniform fields at voltages up to 400 -kV and pd values in excess of 12000 torr-cm (see Fig. 2.16). Similar results, within the experimental parameters are obtained by Schröder¹²⁵ and Boyd et al.¹¹

The fulfilment of the breakdown criterion for a particular

gap width depends on the values of γ and α . These variables may depend on $\frac{E}{p}$, gas pressure, cathode composition, and the nature of the gas.

2.2.4.3 Streamer (kanal) Mechanism

There exists a development of the avalanche into a spark which progresses in a very short time - about one electron transit time - when high voltages above the static threshold are applied to a uniform field gap. Rogowski¹¹⁸ applied a sharply peaked impulse to a gap in air and found that the voltage collapsed in a range of time of 0.1 - 1.0 μ sec. This result introduced considerable difficulties in the explanation of the spark on the Townsend theory of static breakdown, involving some method of feedback generating electrons at the cathode.

It also became difficult to envisage a Townsend mechanism of non-uniform gap breakdown under pulse voltages. The branched, filamentary, irregular channel of discharge in long gaps was also difficult to reconcile with the Townsend theory.

As a consequence, and following much experimental work on spark development, including those utilising the cloud chamber technique, the streamer or kanal theory of breakdown was proposed by Meek⁸⁹ and Loeb⁷⁸ for positive streamers, and independently by Raether¹⁰⁹⁻¹¹² for negative streamers. The comparatively narrow luminous tracks occurring at spark breakdown at high pressure were called streamers.

2.2.4.3.1. Anode Directed - Negative Streamers

Raether¹⁰⁹⁻¹¹³ postulated that streamers would develop when the initiating avalanche mechanism produced a sufficient number of electrons, $\exp(\alpha x)$, resulting in an electric field due to space charge comparable to the applied field. His criterion for streamer development was:

$$E_{S.C.} = \frac{q}{4 \pi r_D^2 \epsilon_0} \exp(\alpha x) \approx E \quad (2.62)$$

where E is the applied field and r_D is the avalanche radius.

The total enhanced field due to space charge and applied field promotes secondary anode-directed electron-avalanches ahead of the negative streamer which has formed. These avalanches are initiated by electrons formed by photo-ionization in the gas space ahead of the streamer or by faster electrons from the streamer tip (see Fig. 2.17).

The avalanche multiplication factor satisfying Raether's criterion would lead to streamer development which corresponds to a value of

$$\alpha d = 20 \quad (2.63)$$

resulting in an average number of electrons on the avalanche head given by

$$n_e = 5 \times 10^8 \quad (2.64)$$

2.2.4.3.2 Cathode Directed - Positive Streamer

The positive streamer from the anode as explained by Loeb and Meek⁷⁸ has certain similarities to the Raether¹⁰⁹⁻¹¹³ Theory. In this case, the field enhancement is thought to be due to a positive space charge left behind by the faster electrons drawn into the anode (see Fig. 2.18). The positive ions are assumed to be within a sphere, which becomes a hemispherically ended column as the streamer develops. The field enhancement at a distance r from the centre of the positive ion space charge is given by

$$E_{S.C.} = \frac{4 q r_s \alpha}{r^2} \exp(\alpha d) \quad (2.65)$$

where r_s is the streamer radius.

The avalanche radius is calculated from the velocity of

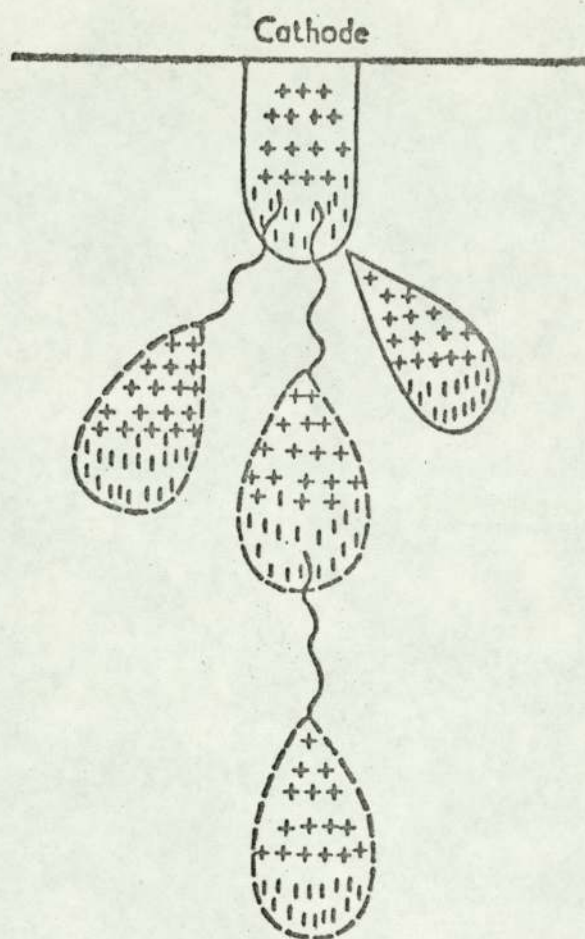


Fig. 2.17 SCHEMATIC REPRESENTATION OF ANODE-DIRECTED
NEGATIVE-STREAMER MECHANISM

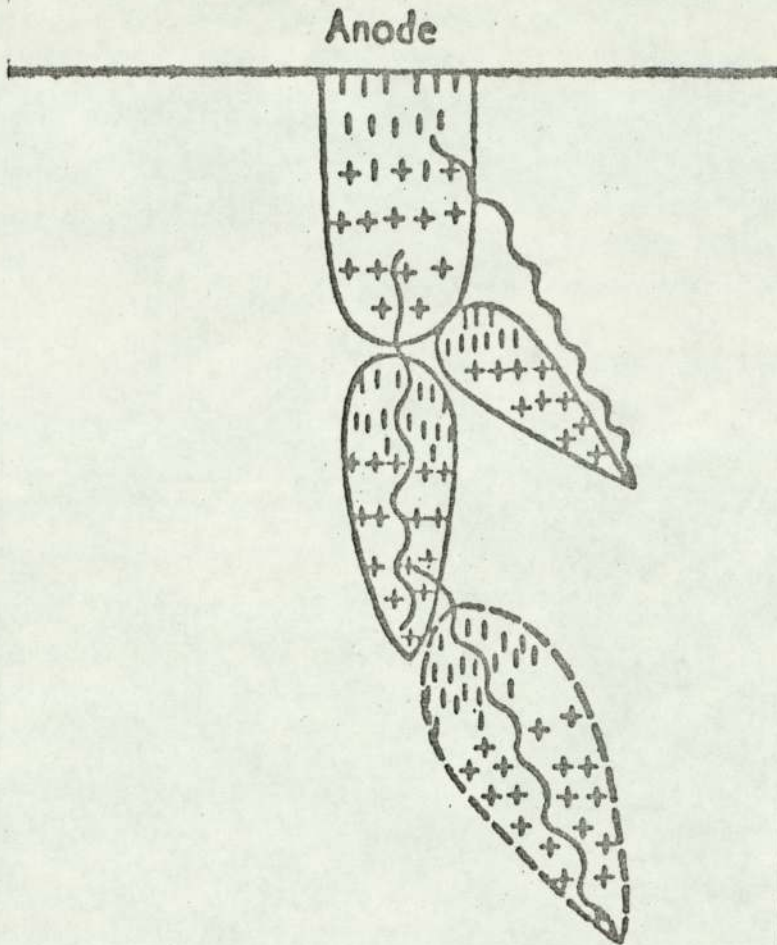


Fig. 2.18 SCHEMATIC REPRESENTATION OF CATHODE-DIRECTED
POSITIVE-STREAMER MECHANISM

of advance of the avalanche and the radial diffusion of the charge. Inserting this value in the above equation gives the following relation of the electric field at the surface of the avalanche head

$$E_r = 5.3 \times 10^7 \left(\frac{x}{p}\right)^{-\frac{1}{2}} \exp(\alpha x) \quad (2.66)$$

The streamer is assumed to propagate continuously across the gap when

$$E_r = k E \quad (2.67)$$

where E is the applied electric field at the critical breakdown condition. The ratio k was originally⁸⁹ assumed to be about 0.1 but later⁹⁰ was considered to be nearly equal to unity, as in Raether's criterion.

Loeb⁷² has elaborated on the original theory, which assumed that only the photo-ionization was adequate for propagating the streamer. This includes the ratio of positive ions to effective photons f , the absorption coefficients for photo-ionization μ , and the distance x , from the streamer tip needed to produce secondary avalanches feeding into the tip. The critical condition for streamer advance is postulated to be the formation of these secondary avalanches at the streamer tip given by the relation

$$\frac{\omega}{3\pi} r_s \propto f \exp(-\mu x_1) \exp(\alpha d) = 1 \quad (2.68)$$

where ω is the solid angle in which the photons are effective.

2.2.5 Time Lags

2.2.5.1 Origin and Importance of Time Lags

It has so far been assumed that the time of application of voltage plays no part in determining the pre-breakdown currents or the breakdown threshold. Actually, this may not always be true. When a field sufficiently large to cause breakdown is applied to a system of electrodes, there are two

reasons why sparkover does not occur immediately:—

- (1) time is required for one or more initial electrons to appear in a favourable position in the gap to lead to the necessary avalanches, and
- (2) the development of these avalanches and build-up of current to a value corresponding to breakdown requires time because of the finite mobilities of the particles.

Thus, there is a time delay before breakdown which is the sum of these two periods, the first being called the statistical time lag, and the second the formative time lag.

With an unirradiated gap in which cosmic rays and radioactive impurities are the sole source of electrons, the time lag will be largely statistical. In a gap purposely irradiated, the statistical time lag may be sufficiently reduced so that the principle contribution to total lag comes from the formative part. These time lags are of considerable practical as well as theoretical interest, since, if the duration of the applied voltage pulse approaches the time lag, appreciable increase in breakdown voltage may be observed.

2.2.5.2 Statistical Time Lag

If ψ is the rate at which electrons are produced in the gap by external radiation, P_1 the probability of an electron appearing in a region of the gap where it can lead to a spark, and P_2 the probability that such an electron will lead to a spark, then the average statistical time lag is given by

$$\tau_s = \frac{1}{\psi P_1 P_2} \quad (2.69)$$

Also, if a gap has survived breakdown for a time, t , then the probability that it will break down in the next interval of time, dt , is $\psi P_1 P_2 dt$. This will be independent of t if $\psi P_1 P_2$ is independent of t .

If time to breakdown in N_0 experiments is measured and

after a time t , N_t of them have not broken down, then in the next interval, dt , the number breaking down will be dN_t where

$$dN_t = - \psi P_1 P_2 N_t dt \quad (2.70)$$

Integration gives

$$\ln \left(\frac{N_t}{N_0} \right) = - \int_0^t \psi P_1 P_2 dt \quad (2.71)$$

or, if ψ , P_1 and P_2 are constant over the time range of interest,

$$N_t = N_0 \exp(-\psi P_1 P_2 t) = N_0 \exp\left(-\frac{t}{\tau_s}\right) \quad (2.72)$$

This relates the fraction of breaks, $\frac{N_t}{N_0}$, occurring after time t , to the average statistical time lag. A plot of $\ln \left(\frac{N_0}{N_t} \right)$ versus time should give a straight line⁶⁸ whose slope is $\frac{1}{\tau_s}$, provided that $\psi P_1 P_2$ is constant (see Fig. 2.19).

If the level of irradiation is increased, ψ increases and therefore τ_s decreases; hence the slopes of the lines shown in this plot will increase. With cathodes of higher work function, ψ will be smaller for a given level of illumination. This is evidenced by the larger time lags for tungsten compared with nickel. The work function of the cathode will be influenced strongly by the presence of surface films. These usually raise the work function and so would be expected to increase the average time lag. However, experiments have shown that positive ions produced in the gas by collision ionization may collect on very thin insulating films to produce high local fields at the underlying cathode, and hence field emission of electrons. If this is the case, then the time lag is reduced as shown in Fig. 2.19. This phenomenon which may result in an apparent decrease in sparking potential, is known as the Paetou¹⁰³ or Malter⁸⁴ effect. Statistical time lag becomes field dependent

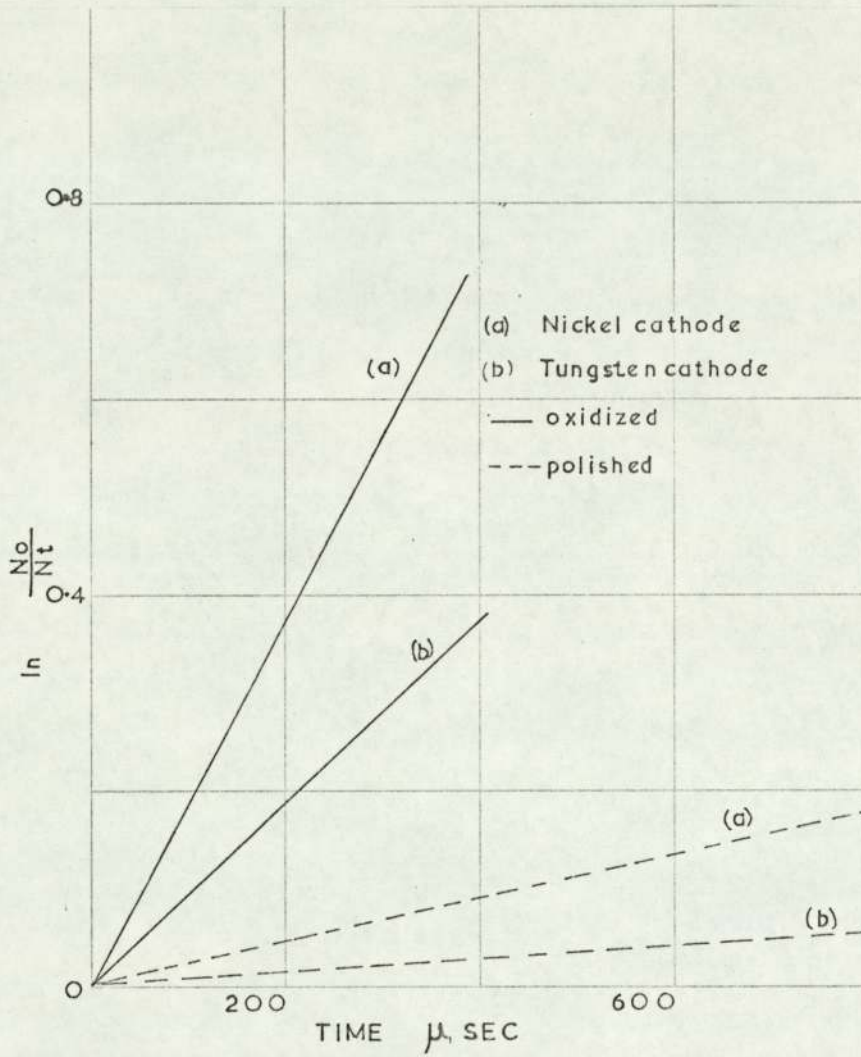


Fig. 2.19 PLOTS OF $\frac{N_0}{N_t}$ AS A FUNCTION OF TIME AT A FIELD STRENGTH

OF 10^5 V/cm

(After Llewellyn - Jones and De La Perrelle 68)

if the initiating electrons are by cathode field emission. It is also realised that β may be affected by gap geometry, since for short gaps it may be more difficult to irradiate the cathode.

Presence of initiating or triggering electrons in the gap to start the primary multiplication is essential⁷⁹. It has become important in studies of gaseous discharge to ensure adequate initiating electrons to trigger the discharge and thus facilitate ascertaining the correct threshold values⁷⁷.

With uniform field gaps, except for very short gaps, the initial triggering presents no serious problem for breakdown under steady potential where time lags are not sought for. This is not the case either with time-dependent and alternating potential studies in uniform gaps, or, in particular, in non-uniform gaps. To achieve a successful triggering and reduce the statistical time radiation or the gap or the electrode by u. v. illumination or radioactive materials has been tried by many workers^{31, 33, 55, 95}.

The type of irradiation used will be an important factor controlling P_1 , i. e. the probability of an electron appearing in a favourable position to produce breakdown. The most favourable position is, of course, near the cathode. In the case of closely-spaced spheres, the area under a stress sufficiently large to cause breakdown will vary with electrode spacing and with overvoltage, so that these will be important variables in determining P_1 . Overvoltage is defined here as the increase in voltage required to ensure breakdown within a fixed time interval over that which would be required if infinite time were available.

The factors which will cause changes in statistical time lag through changes in P_2 can now be considered. The fulfilment of the Townsend breakdown criterion,

$\gamma[\exp(\alpha d) - 1] = 1$, does not guarantee that breakdown will be initiated by a single electron starting from the cathode. This criterion was derived on the basis of the average behaviour of a large number of electrons, and a single electron may or may not liberate the necessary secondary electron as it avalanches toward the anode.

However, if the gap is overvolted and $\gamma[\exp(\alpha d) - 1] > 1$, then the probability, P , that a single electron will be multiplied into a steady current rapidly increases. The relationship between P and overvoltage may be calculated using statistical methods, and a typical curve is shown in Fig. 2.20. To construct such a curve for any gas and electrode system requires a knowledge of the dependence of $\frac{\alpha}{p}$ and γ on $\frac{E}{p}$. As it is to be expected, with increasing overvoltage the average statistical time lag approaches $\frac{1}{\psi p_1}$.

Very long statistical time lags have been obtained by Narbut, et al.¹⁰¹ with sulphur hexafluoride which is attributed to the attachment of the initiating electrons.

2.2.5.3 Formative Time Lags

It can now be assumed that an amount of time equal to the statistical time lag has elapsed and an electron has become available. Consequently, this electron will eventually lead to a breakdown. An additional amount of time will be required for this electron to cause a breakdown for two reasons: i) electrons, positive ions, metastable atoms, etc., all require a certain amount of time to cross the breakdown gap. ii) since the Townsend breakdown criterion requires an infinitely large current for breakdown, many such transits must occur before the initial currents are amplified to a spark-over level. This requirement of an infinite current at breakdown is really a formal one, since the generation of sufficient

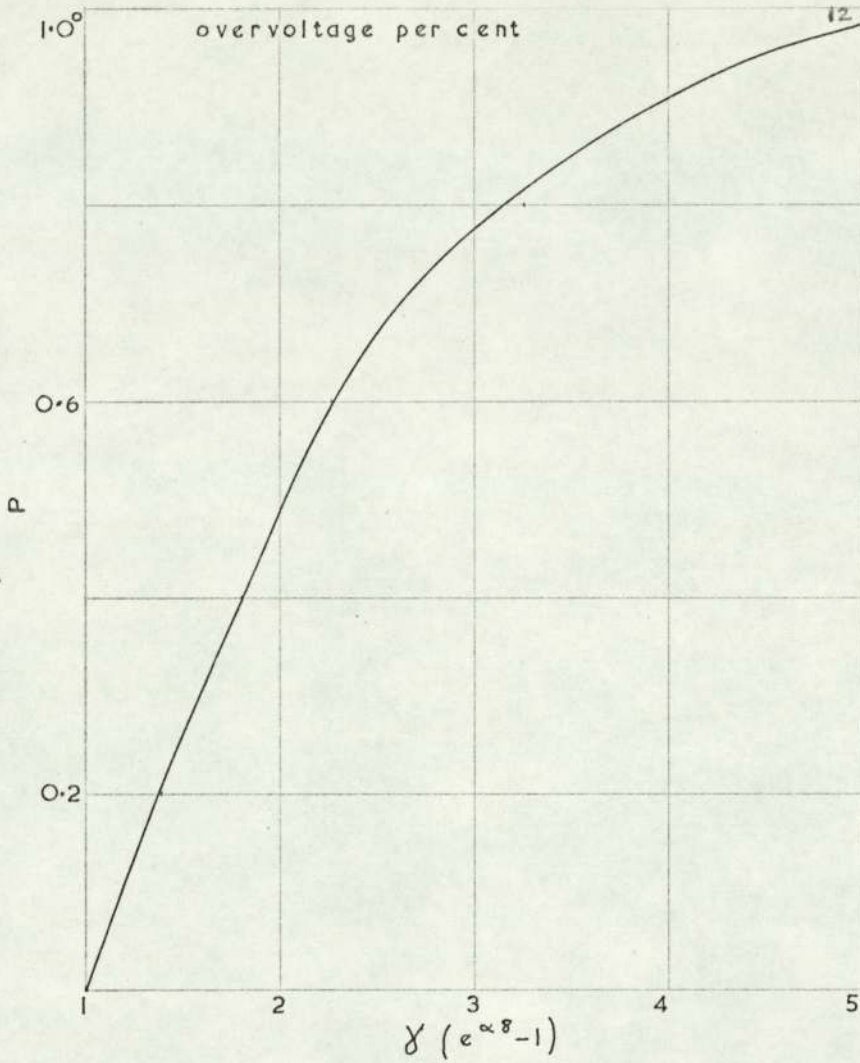


Fig. 2.20 DEPENDANCE ON OVERVOLTAGE OF PROBABILITY, P , THAT A SINGLE STARTING ELECTRON WILL BE MULTIPLIED INTO A STEADY CURRENT.

(After Devin and Sharbough 21)

space charge causes finite currents to lead to breakdown.

The temporal build-up of these currents has been calculated and measured experimentally²¹ and a few typical results are shown in Fig. 2.21 for different levels of over-voltage. Since photons, positive ions, and metastable molecules have greatly differing mobilities (decreasing in this order), a comparison between calculated and measured curves helps to identify the particular secondary mechanism which is dominant.

It has been shown theoretically that a linear growth of current with time - the straight line of Fig. 2.21 - occurs when the applied field is such that the Townsend criterion is just satisfied. For lower fields, the current levels off at some finite value of current, while for fields higher than breakdown the current grows rapidly to large values. The precise value of current at which the space charge distortion leads to breakdown may not be known. The interrupted line in Fig. 2.21 indicates the value of current, i_{c1} , at which space charge becomes important and causes breakdown. However, if a large value, i_{c2} , has been chosen, it is clear that the observed formative time would be changed only slightly, since the curves are very steep in this region. In Fig. 2.21 the formative time is the time which elapses as the current builds up to i_c and, as the over-voltage is increased, the time lag decreases. Although it is desirable to observe the complete temporal development of current to breakdown more often, only the time to sparking has been observed.

Fig. 2.22 shows some typical observed formative time lags as a function of overvoltage, ΔV . Curves (a) and (b) are calculated curves^{36, 37} for $i_c = 10^{-1}$ and 10^{-9} A/cm² respectively, where it is assumed that all the secondary electrons are produced by photon mechanism. The curve (c) is computed for an

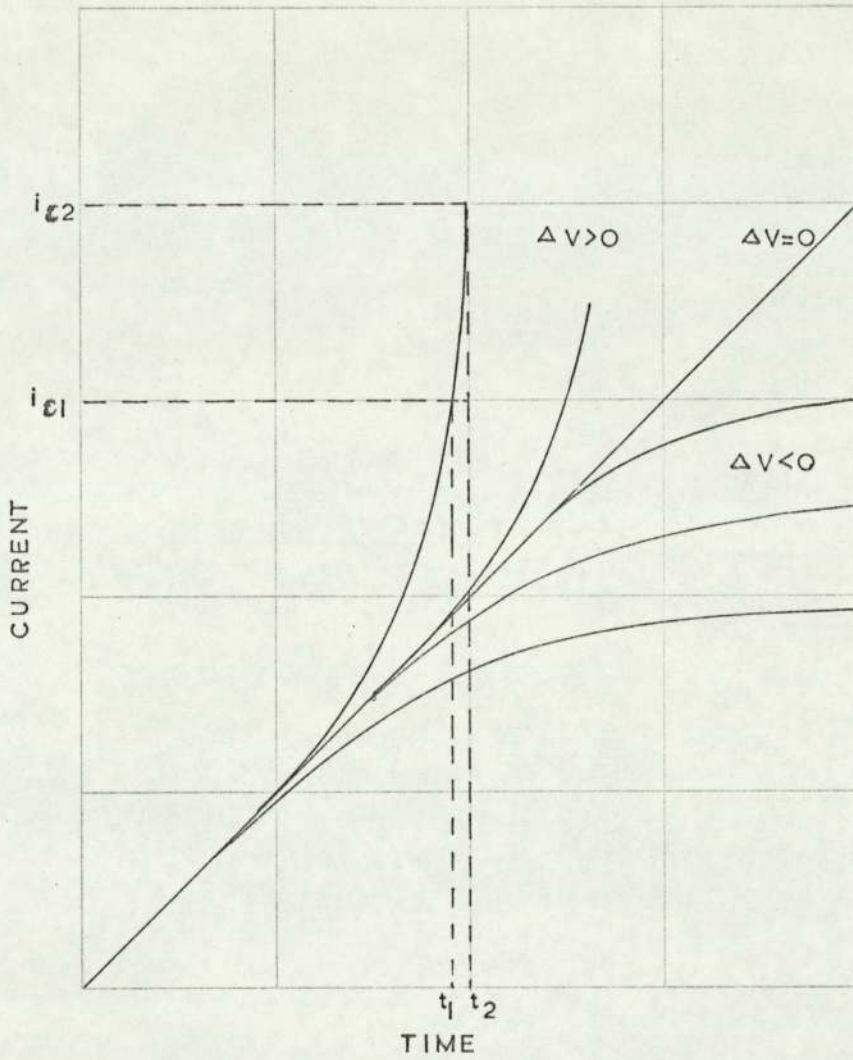


Fig. 2.21 THE TEMPORAL BUILD-UP OF CURRENT FOR VARIOUS OVERVOLTAGES ΔV
 (After Devin and Sharbough 21)

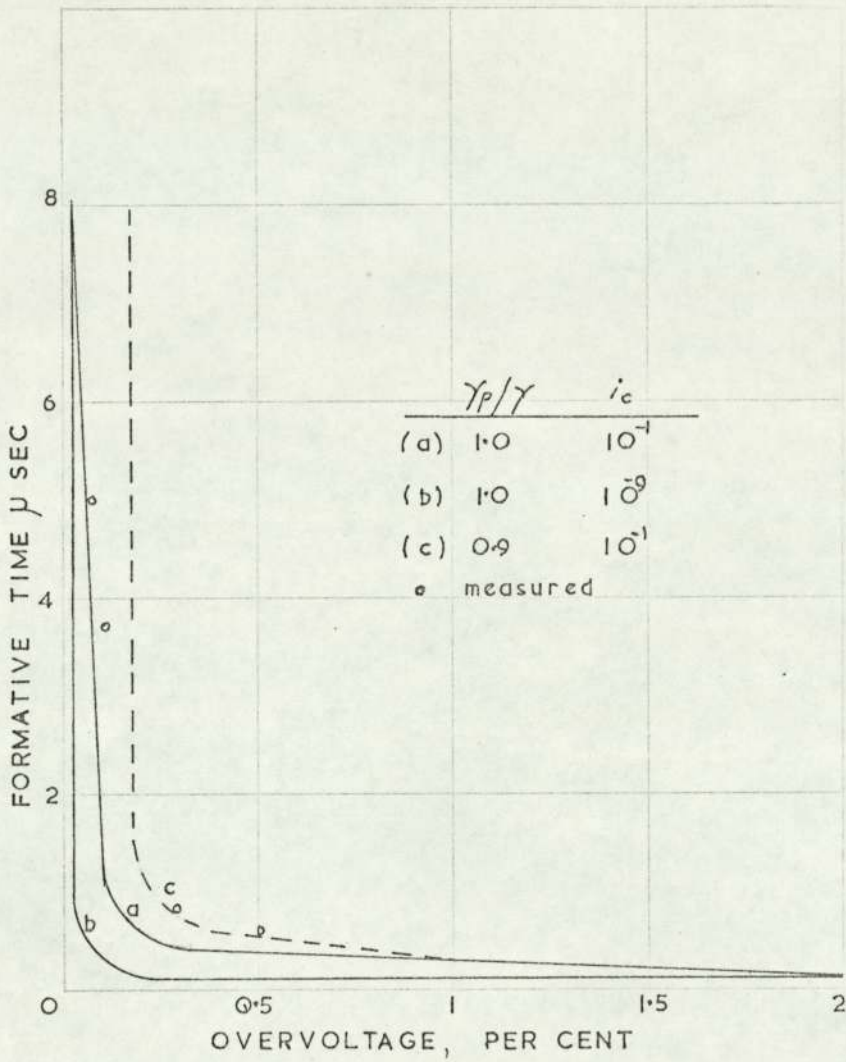


Fig. 2.22 FORMATIVE TIME LAGS AS A FUNCTION OF OVERVOLTAGE

—) Haydon and Llewellyn - Jones 47 - Theoretical
 - - -)

o Fisher and Bederson 36 - measurements

i_c of 10^{-1} A/cm², assuming that 10 per cent of the secondary electrons are produced by γ_i process and 90 per cent by γ_p process. It is apparent that, by further selection of the value of i_c and the ratio $\frac{\gamma_i}{\gamma_p}$, the experimental points could be fitted. In this way, the nature of the previous secondary processes are elucidated.

Fisher and Bederson³⁶ undertook a study of formative time lags in uniform field geometry in air at atmospheric pressure. Adequate triggering photo-electrons were released by u. v. light from the cathode. They discovered that, as potential was lowered from some percentage of overvoltage towards the breakdown threshold, the formative portion of the time lag increased from some 10^{-7} to a value as great as 10^{-5} sec.

The appearance of a breakdown very near threshold taking 10^{-5} or more second signifies that the streamer breakdown is preceded by the slower conventional Townsend breakdown of the gap as a whole^{36, 73, 76}.

Raether^{113, 116} defines the formative time lag in uniform field breakdown as the time, T_k , which must elapse until the streamer development sets in from the first avalanche. T_k as a function of the number of carriers of individual avalanches, n , is given by Pfaue and Raether¹⁰⁸ to be in the range 15-100 n. sec (see Fig. 2.23). Similar results are obtained by Schlumbohm¹¹⁹⁻¹²² in a detailed study (see Fig. 2.24) showing that:

- 1) T_k depends on the carrier number in an exponential form.
- 2) T_k is reduced by overvoltage.
- 3) T_k shows little dependence on the pressure.
- 4) T_k increases with the gap distance.

Larger values of T_k for gases with appreciable attachment coefficient, η , are given by many investigators^{36, 57, 58, 125}.

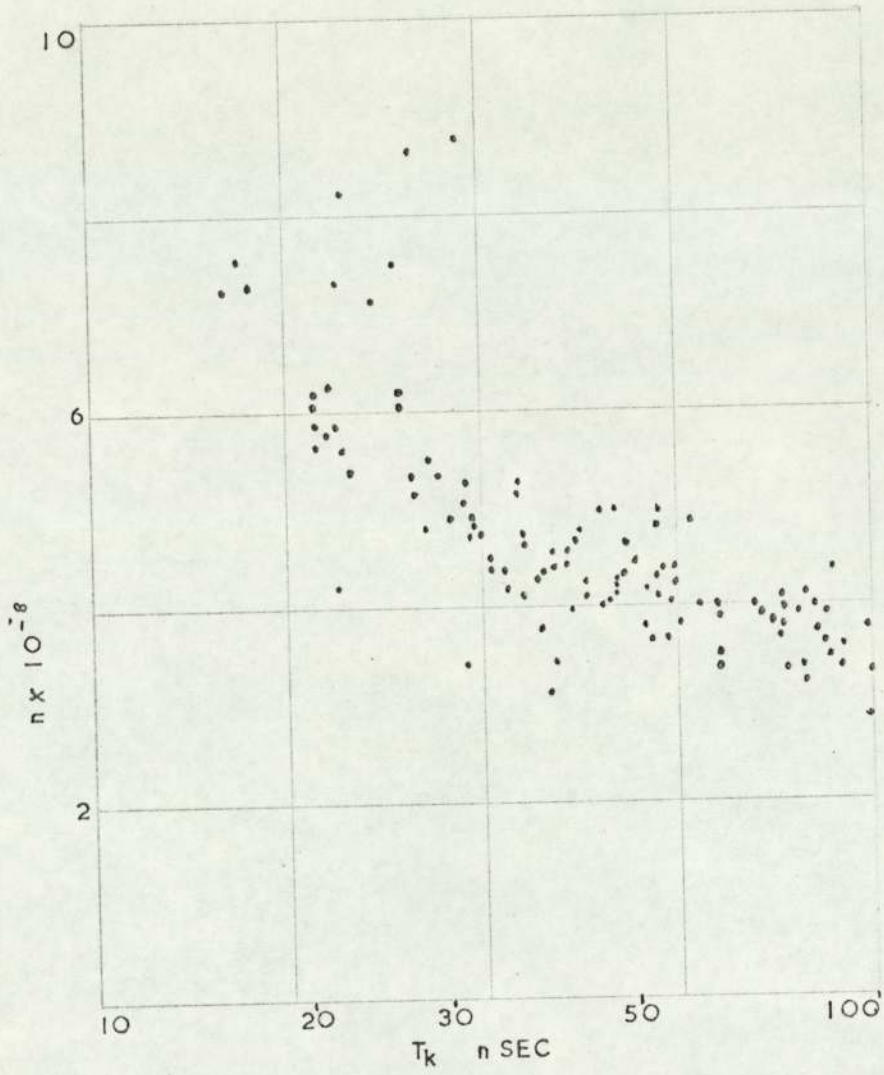


Fig. 2.23 STREAMER DEVELOPMENT TIME, T_k , IN ETHER, AS A FUNCTION OF NUMBER OF CARRIERS, n .

(After Raether 116)

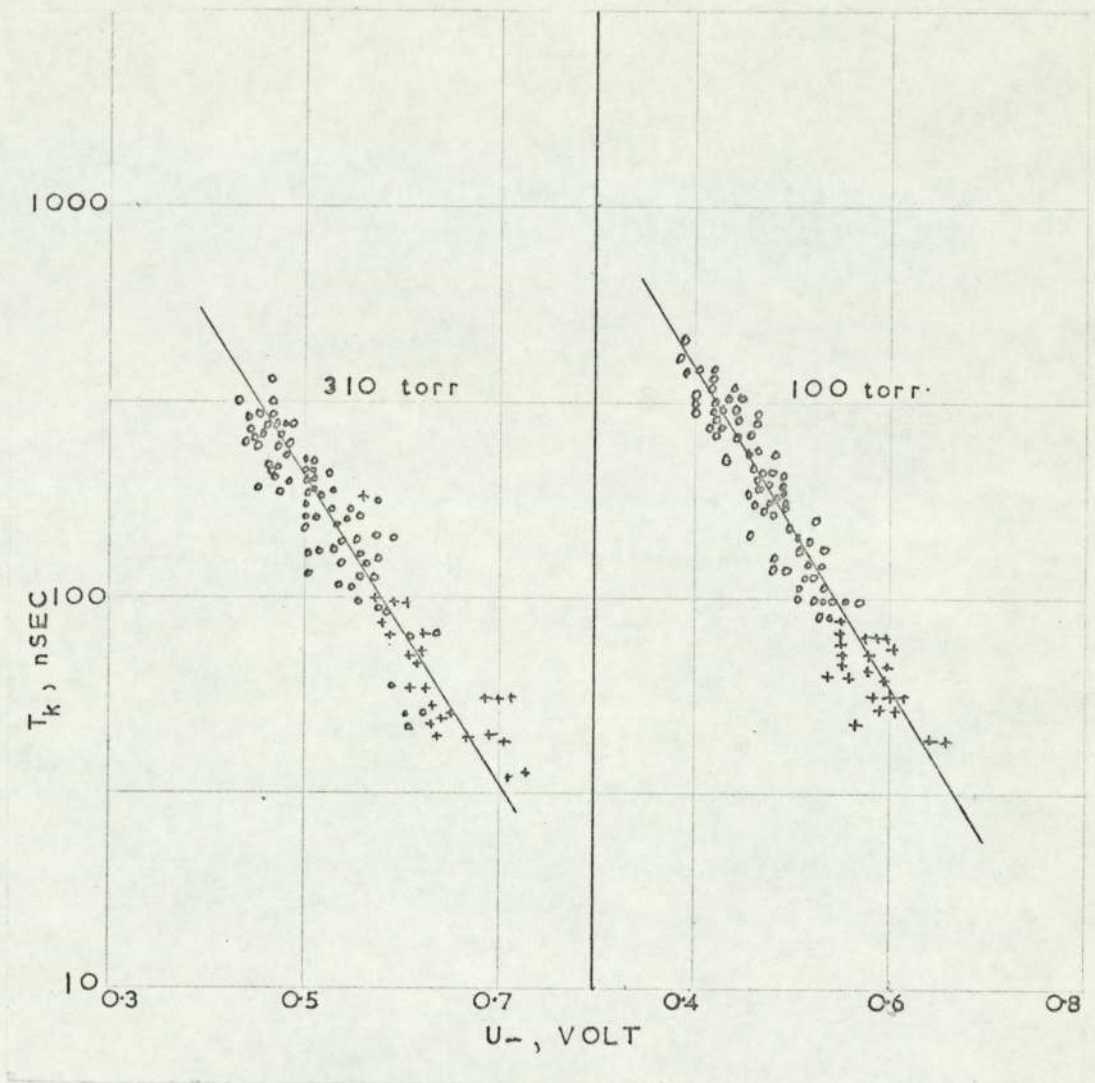


Fig. 2.24 THE DEPENDANCE OF STREAMER DEVELOPMENT TIME, T_k , ON THE CARRIER NUMBER IN AN AVALANCHE, MEASURED BY ITS PLATEAU HEIGHT, U_- , IN METHANE.

(After Schlumbohm 122)

o, V_{dc} ; +, 1% overvoltage

Schröder's¹²⁵ study on air at atmospheric pressure provides a value for T_k in about $50 \mu \text{ sec.}$ The time rapidly diminishes with increasing overvoltage, dropping to 250 nsec at 1% overvoltage.

Extensive studies of time lag in positive-point breakdown has been carried out by Menes and Fisher⁹³. The time lag measurements show much scatter which decreases with increasing photocurrent emission by u.v. radiation and with increasing voltage. Figure 2.25 shows a Laue diagram of the number of lags exceeding t , relative to the time lag in $\mu \text{ sec.}$ for three different u.v. illuminations. The intersect corresponds to a time lag of $0.15 \mu \text{ sec.}$ at 0.18% overvoltage, for a point of 0.3 mm radius at 200 torrs pressure. Menes and Fisher⁹³ give the initiating probability for electrons from the cathode as starting about 0.7% at threshold and increasing to 7% at 3% overvoltage.

Figure 2.26 shows the formative time lag for the positive point discharge⁹³ of radius 0.3 mm at 1.5 cm gap setting for the whole pressure range from 30-700 torr, at 0-4% overvoltage. At low pressure the lags appear to approximate to a microsecond, which may indicate an increased diffusion and raises the question as to whether the streamers are the active mechanisms. For a uniform field gap³⁶ at 0.5% overvoltage, there is an increase of 10 - 100 fold in the time lag over the non-uniform gap.

Miyoshi^{76, 97, 98} has made extensive measurements of formative time lag for the threshold of positive-point streamer corona in air and obtained reproducible results. These results, displayed as time lag in $\mu \text{ sec.}$ against the relative voltage

$$\Delta = \frac{\Delta V + V}{V_s} \quad \text{applied at a } \Delta < 1 \text{ or } \Delta > 1 \quad \text{are shown in}$$

Fig. 2.27.

Values of $\Delta > 1$ correspond to tests run with an overvoltage. The data represent the transition from streamer pulse to a spark for a 1 cm gap with point radius $r = 0.7 \text{ mm}$ at 100 torr. The circles give the transition time from pre-onset streamers to

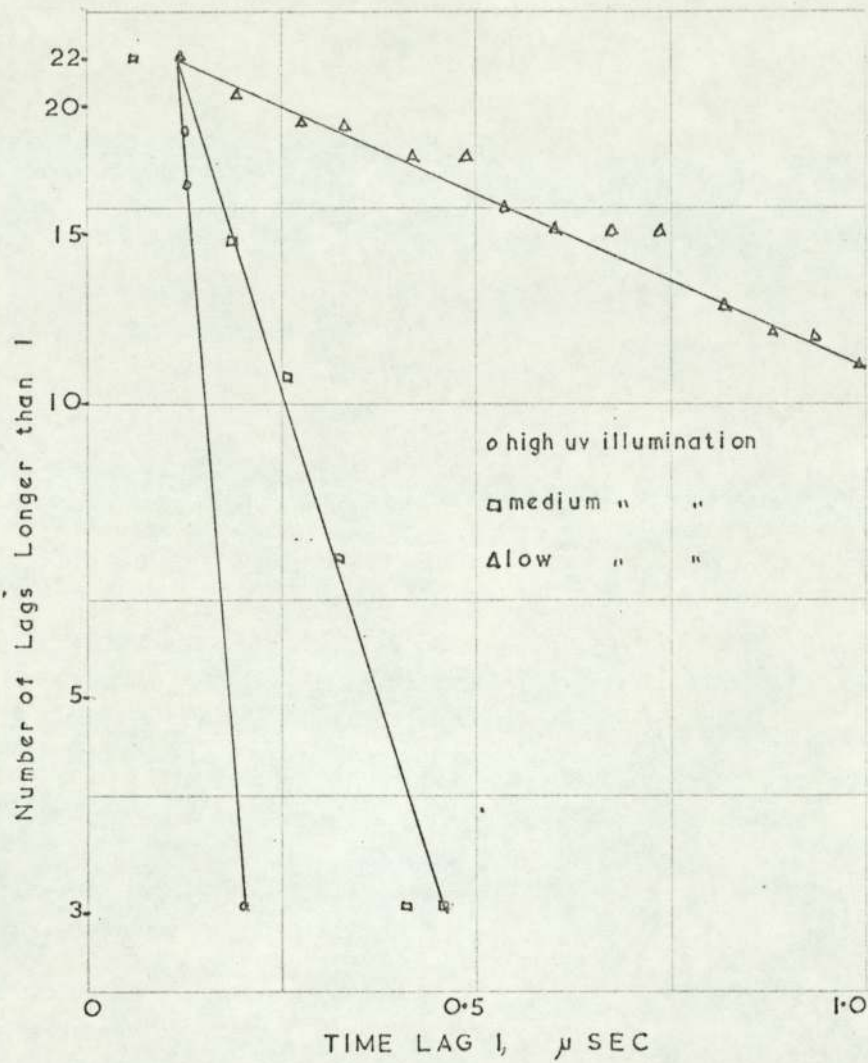


Fig. 2.25 LAUE PLOTS OF TIME LAGS FOR THREE INTENSITIES OF U-V TRIGGERING ILLUMINATION OF THE CATHODE.

(After Loeb 76)

Point radius, 0.3 mm; gap length, 1.0 cm; Pressure, 200 torr; overvoltage, 0.18%.

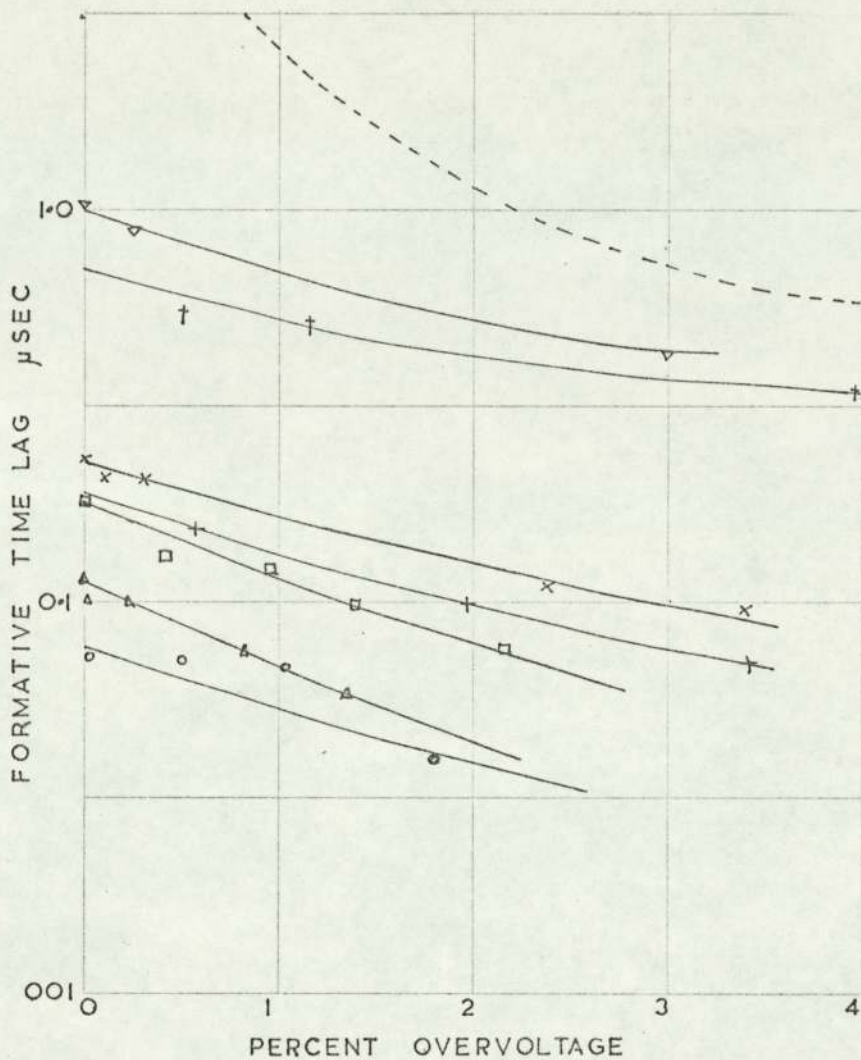


Fig. 2.26 FORMATIVE TIME LAG FOR POINT-ANODE AS A FUNCTION OF PERCENT OVERVOLTAGE AND A RANGE OF PRESSURE.

(After Menes 92)

Point radius, 0.3 mm; gap length, 1.5 cm.

- = 700 mm
- △ = 500 mm
- = 300 mm
- + = 200 mm
- × = 100 mm
- † = 50 mm
- ▽ = 30 mm

----- Fisher and Bederson 36 - uniform field, 1 cm gap.

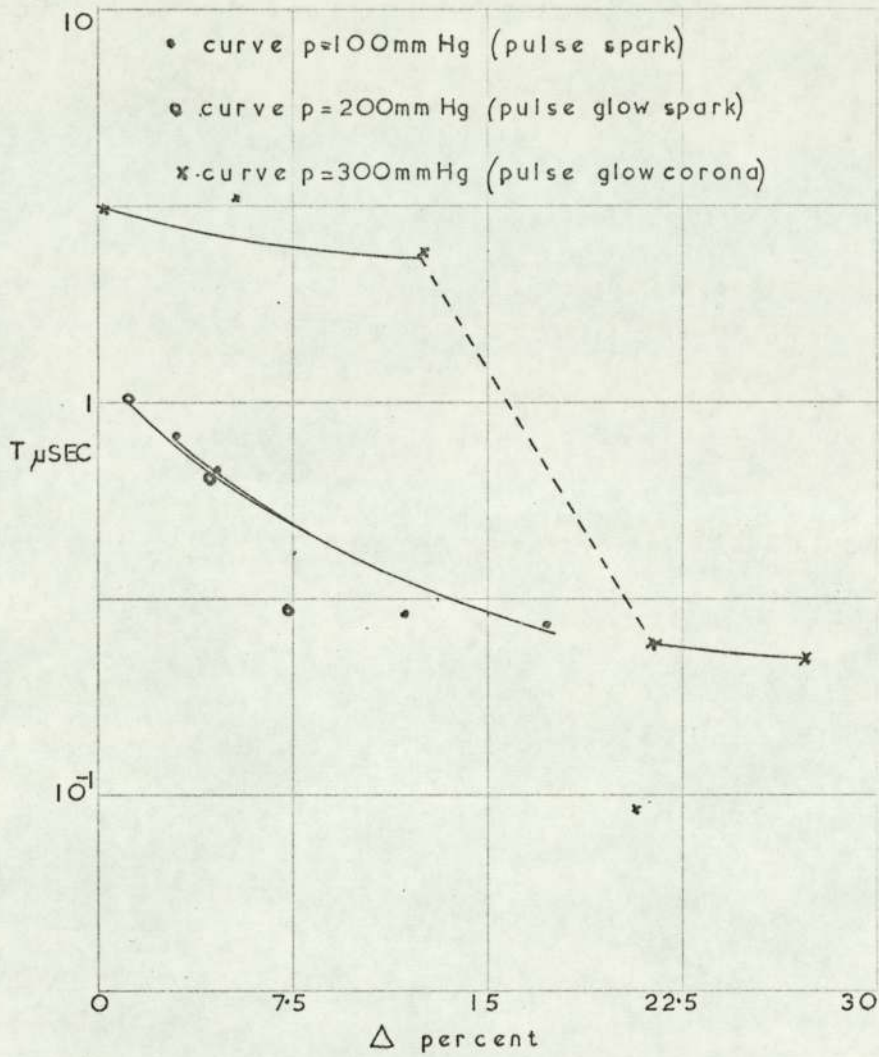


Fig. 2.27 FORMATIVE TIME LAG FOR HERMSTEIN GLOW TO A SPARK TRANSITION AS A FUNCTION OF RELATIVE VOLTAGE Δ
 (After Loeb 76)

spark through the Hermstein^{48, 49} glow corona region at 200 torr. The crosses give the the time for transition from pre-onset streamers pulse corona to a Hermstein glow corona at 300 torr.

The transitions to sparks from the time of appearance of streamer pulses, either pre-breakdown or pre-onset, appear to be about the same and of the order of 1μ sec. The time decreases to about 0.3μ sec. as Δ reaches the threshold for sparking. Miyoshi suggests that these findings are in keeping with Hudsons'⁵¹ photomultiplier observations as well as with Menes and Fisher's⁹³ data.

A great deal of effort has gone into attempts to obtain time lags for negative point breakdown^{76, 97-98, 135} without reasonable success. The difficulties have been attributed to the meaningless nature of negative point time lags that are governed by conditioning of the point surface.

There is an enormous range of formative time lags for the Trichel^{74, 135} pulse, the glow and the spark breakdown. As an example of the sort of fluctuations that are observed, one may cite Miyoshi's⁹⁷⁻⁹⁸ results. These show the time lag for Trichel Pulse corona as a function of gap length, l , from 2 to 25 mm, for a tungsten point electrode of radius 0.7 mm in dry air at 760 torr, with an overvoltage of 6% above theshold. These lags range from 2-150 μ sec. at $l = 2$ mm, and rise to a range of 30-500 μ sec. for $l = 10$ and $l = 15$ mm.

2.3 Instrumentation

2.3.1 Supply Voltage

2.3.1.1 The Microsecond Range System

The experimental equipment was set up in the new high-voltage laboratory at the University of Aston in Birmingham. The plan of the laboratory has been to make basic apparatus so adaptable that it could easily be applied to different lines of research with the minimum of alteration.

The main equipment is the impulse generator which can produce a variety of impulse waves and which, in conjunction with a triggered chopping gap, can produce a rectangular pulse of different duration.

The impulse generator is designed to give a very short rise time and a long delay time of the output voltage. Consequently the rectangular pulse is obtained by chopping the voltage at a predetermined short time from its initiation. Initiation and chopping are performed by trigatron units. This is a method by which the charging voltage is limited to a value just below the spontaneous breakdown of the first gap. The gap is then triggered with the aid of a pilot electrode which stresses the gap to within 1% of its natural breakdown voltage.

2.3.1.1.1 The Control Circuit

The electronics control system governs the duration of the high voltage pulses and through the protection circuit it minimises the damage to the electrodes and the dielectrics after each breakdown. The control circuit also contains facilities enabling it to produce triggering pulses, delayed a definite time with respect to the generated high voltage impulse.

Fig. 2.28 shows a block diagram of the electrical circuit. A positive pulse from a remote push-button pulser is applied to a single shot multivibrator producing a rectangular pulse. This

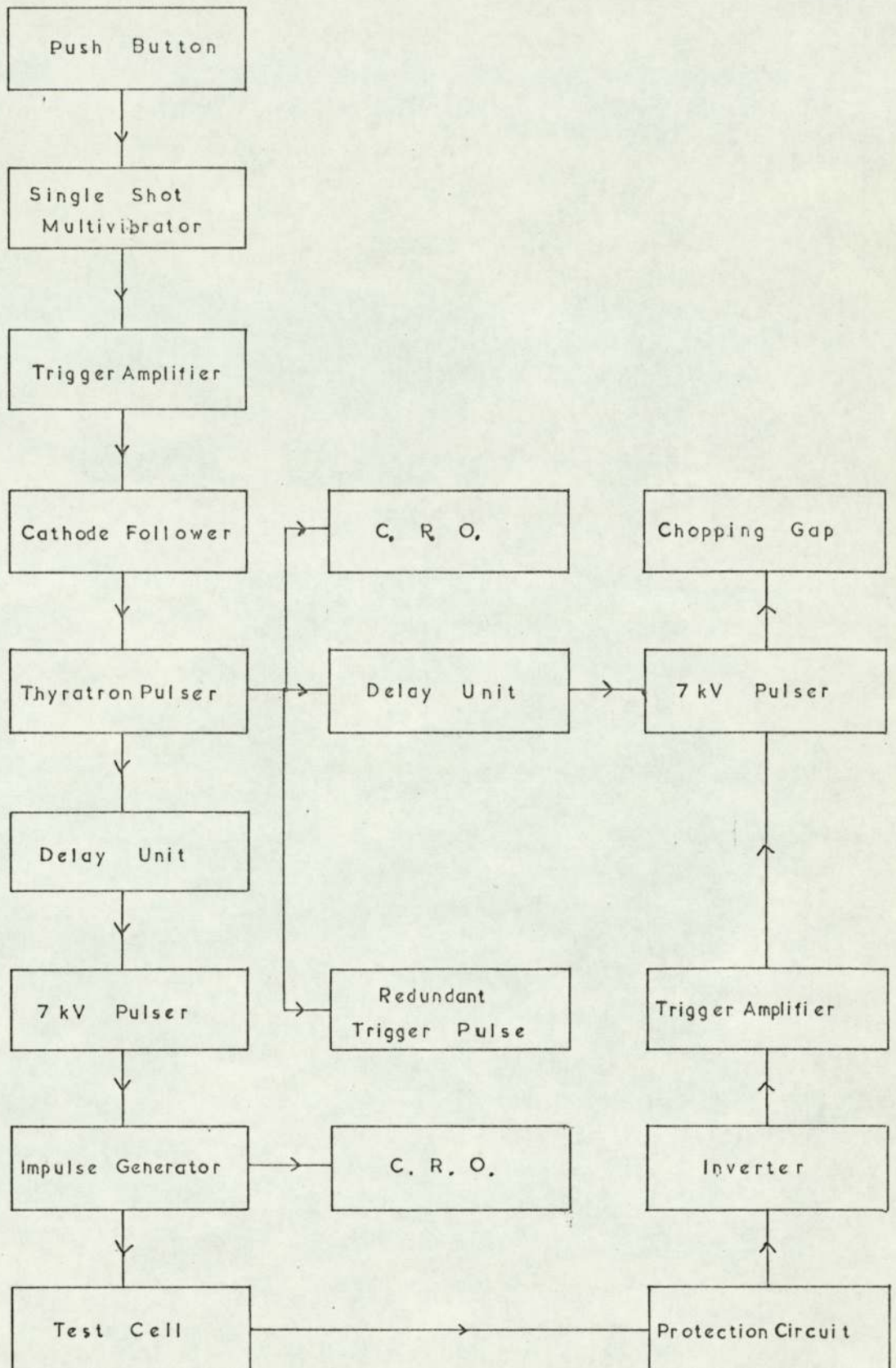


FIG 2.28 BLOCK DIAGRAM OF ELECTRICAL CIRCUIT
FOR MICROSECOND RANGE SYSTEM

pulse is applied to a cathode follower through a differentiating network and a trigger amplifier.

The pulse from the cathode follower triggers the first stage of a soft valve delay unit which has a twofold purpose. It starts the time base of a cathode ray oscilloscope and, after a fixed delay, it triggers its second stage producing three pulse signals.

The first signal triggers a 7 kV hydrogen thyratron whose output fires a five-stage Marx-Goodlet impulse generator.

The second signal through a variable soft valve delay unit triggers a 7 kV hydrogen thyratron which in turns fires the chopping gap of the impulse generator. This will determine the duration of the impulse wave applied to the test sample.

The third signal is redundant but can be made available to trigger any high voltage circuit or measuring device.

When a dielectric breakdown occurs, a signal is generated which, through the 7 kV thyratron, fires the chopping gap thus terminating the applied voltage.

Co-axial cables are used in all the terminal connections. The electronic control panels are screened against E-M radiation.

2.3.1.1.2 The Push-Button Pulse Forming Circuit

The circuit diagram of the pulse forming network is shown in Fig. 2.29. A remote push-button in conjunction with a simple R-C network and a 120 volts dry battery produces a long decay positive pulse. This pulse is applied to the grid of the first triode of the single shot multivibrator V1. A square pulse from the anode of the second triode is differentiated by the coupling network and applied to the trigger amplifier V2.

The multivibrator once fired returns to its stable state after a fixed delay determined by the time constant of the coupling.

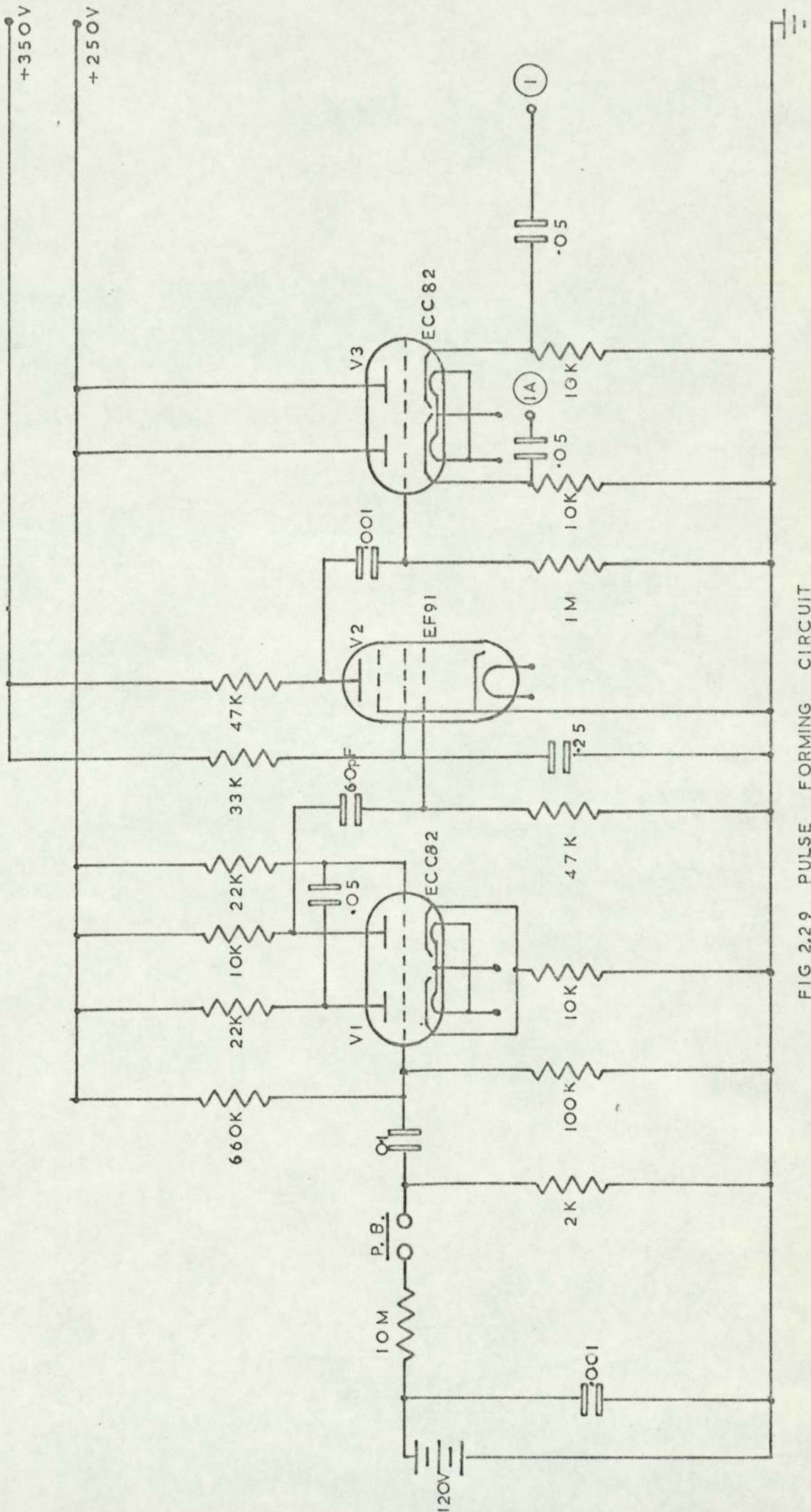


FIG 2.2.9 PULSE FORMING CIRCUIT

A negative and a positive pulse appears at the anode of amplifier V2. The negative pulse is ignored by the circuitry. The cathode follower V3 reduces its negative edge and the following diode V4 eliminates it.

The positive pulse entering the valve V3 produces two identical positive pulses at terminals (1) and (1a).

The output of the first delay unit is applied through terminal (4) to the impulse wave duration delay timer and through terminal (3) to a 7 kV thyatron which in turn fires the impulse generator.

The second delay unit is identical to the first one except that the resistance arm of the R-C integrating network is variable. This enables an output pulse to be available at terminal (5) at a varied time delay with respect to the impulse generator trigger pulse.

At the input of each delay unit, a diode clipper, V4 or V7, is used which ensures that only a positive voltage pulse will appear as the input signal.

2.3.1.1.3 The Delay Unit

Figure 2.30 shows two soft valve delay units connected in series so that the output of the first delay unit triggers the second one. Each unit contains two thyatrons with a firing time of less than 50 nanoseconds.

The one microfarad capacitor on the anode of thyatron V5 is normally charged. The positive pulse passed by diode V4 fires valve V5 discharging the anode capacitor to the extinction level of the thyatron and producing a slow decaying positive pulse at its cathode. A fraction of this pulse at terminal (2) starts the time base of a high-speed oscilloscope.

The full output pulse, delayed for about 5 μ sec by a fixed

network, fires the thyatron V6. This also discharges the anode capacitor to below the extinction level.

2.3.1.1.4 The High-Voltage Thyratrons

The trigatrons on the impulse generator and the chopping unit are designed to operate with a 6 kV pulse. These pulses are produced by the high voltage hydrogen thyatron shown in Fig. 2.31.

The incoming positive pulse from terminal (3) fires the thyatron V10, discharging the $0.001 \mu\text{F}$ anode capacitor and producing a 6 kV negative pulse at terminal (6). The thyratrons V11 and V12 operate in the same way as V10.

2.3.1.1.5 The Impulse Generator

The high voltage supply is generated by a 500 kV five stage Marx-Goodlet impulse generator (British Patent No. 344862) shown in Fig. 2.32. This is built from 0.1 microfarad condensers, capable of withstanding a charging voltage of 100 kV, in a double column mounting. Cylindrical R.B.P.P. insulations rated at over 100 kV provide the necessary mechanical connections between the stages. Wave-tail control resistances which also perform the function of charging resistances are $1.5 \text{ k}\Omega$ made of low inductance Silko ribbon. The output resistance controlling the wave front is of a similar nature. For a nominal $1/50$ microsecond wave, the output resistance is selected as $1.8 \text{ k}\Omega$. The maximum discharge energy available is 2.5 kJ.

The spark gaps are equally and simultaneously varied by a d.c. motor driving a tube carrying the five normally earthed spheres. The motor speed and its forward and reverse movements are directed from the remote control panel. The angular rotation of the spark gap spheres is indicated by a mag slip unit.

The apparatus for controlling and measuring the impulse

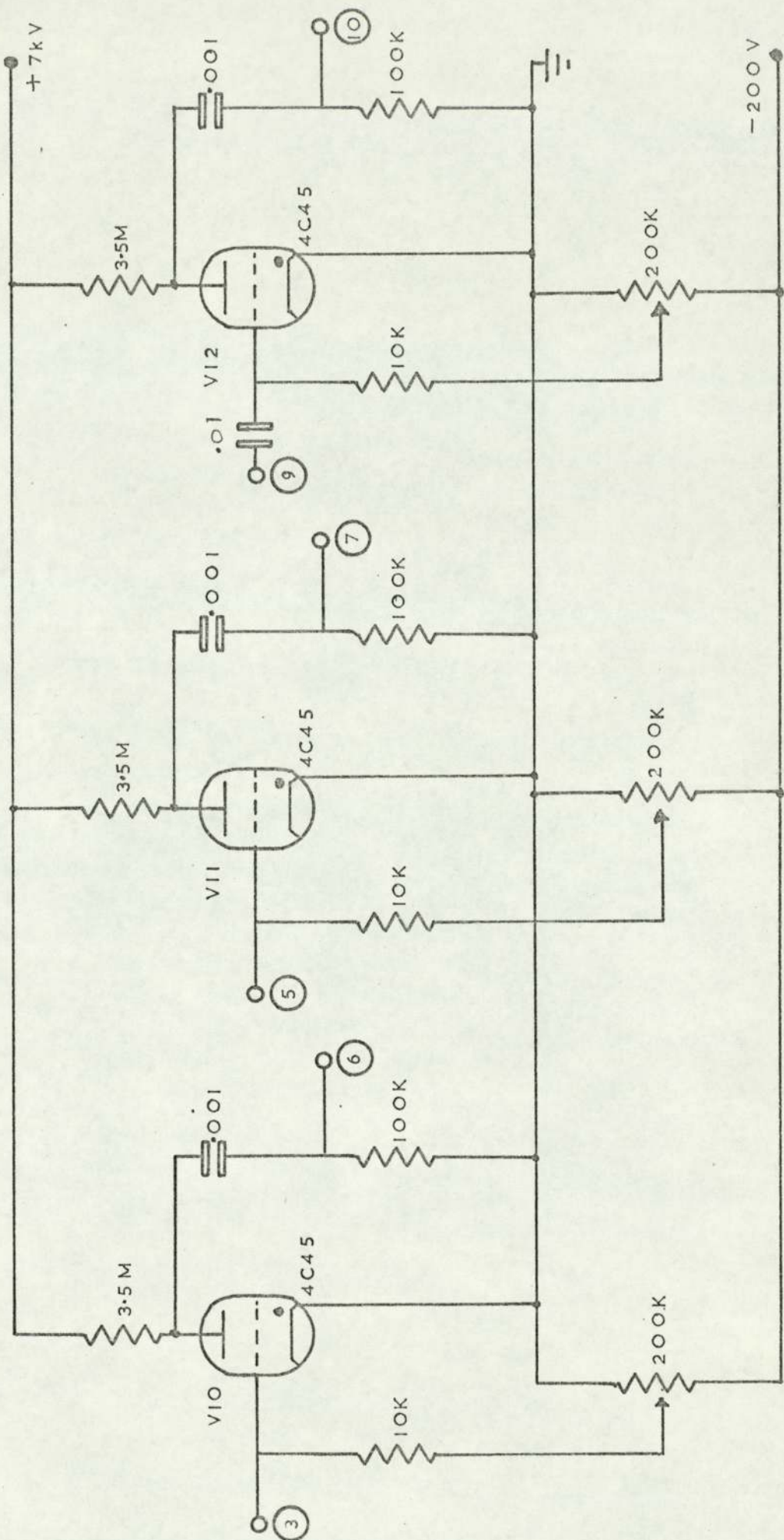


FIG 2-31 THE HIGH VOLTAGE HYDROGEN THYRATRONS

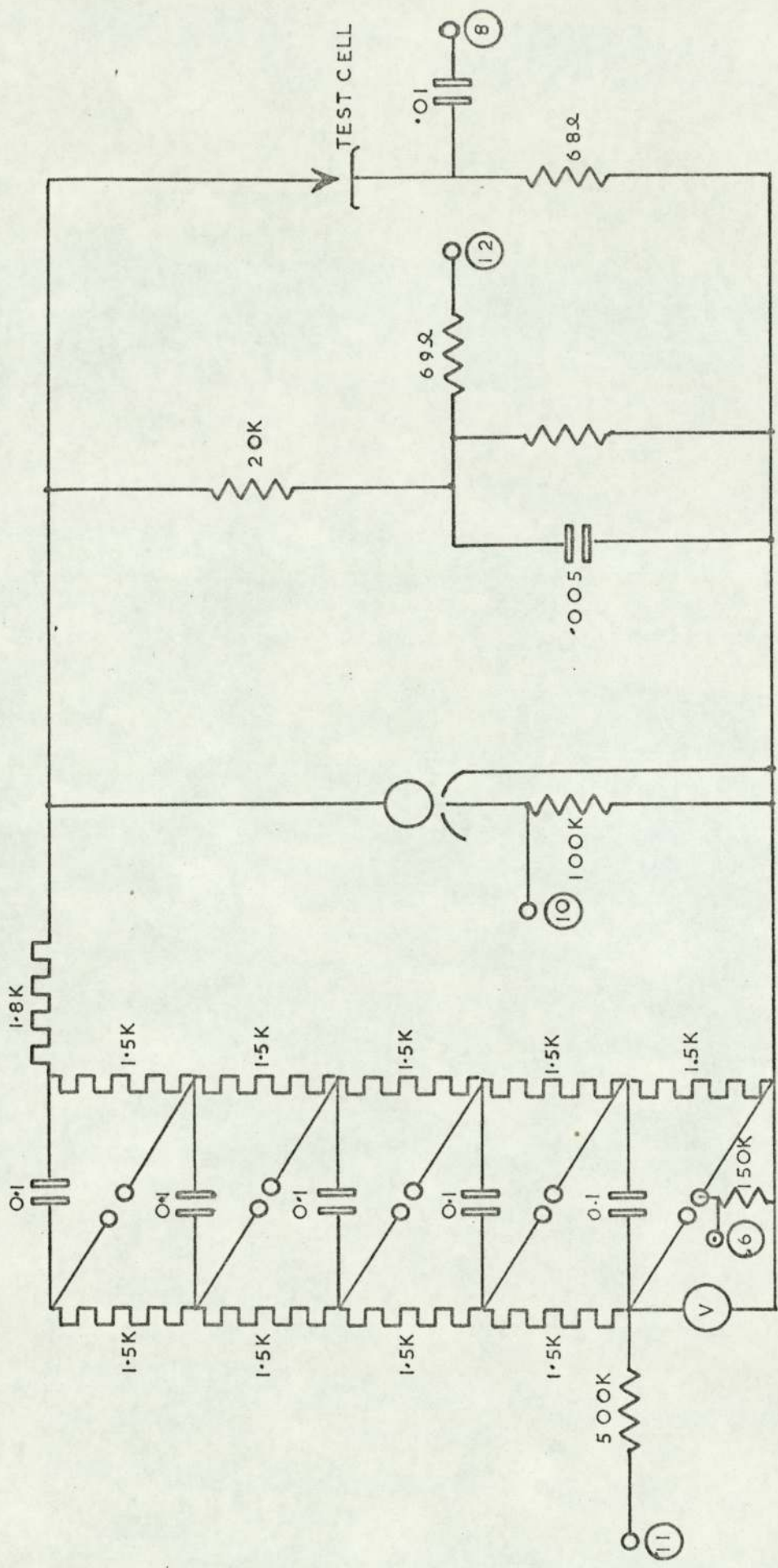


FIG 2.32 500kV FIVE STAGE IMPULSE GENERATOR

generator sphere gap length is shown in Fig. 2.33. The drive is provided by a 7 volts d.c. motor incorporating reduction gears to obtain the low speed of rotation of moving spheres. The receiver magstrip is connected through a step-up gear to the shaft carrying the movable spheres. The receiver magstrip is mounted on the control panel and a pointer on its shaft indicates the position of the transmitter on a disc of 4 inches diameter.

The magnitude of the impulse voltage is obtained by measuring the stage charging voltage of the impulse generator with a 100 kV electrostatic voltmeter, which is multiplied by the number of stages. The measurements are checked by the sphere-gap measurements using 50 cm spheres in accordance with B.Sc. 358:1939. The waveshape and pulse duration are examined by an oscilloscope.

To reduce the oscillations due to breakdown across the chopping gap, a disc of non-linear resistor is connected in series with the gap and short connecting leads used to minimise the self inductance.

The impulse generator is charged from a 100 kV d.c. generator consisting of selenium rectifiers fed from a Cockroft-Walton voltage multiplier (see Fig. 2.34). Alternative polarities can be selected by means of a swinging link and voltage can be measured by means of a resistive potential divider. The input to the low tension side of the main transformer and the push-button contactor with overload protection relay RL/1 are remotely controlled.

The impulse generator charging side is earthed when not in operation by a solenoid driven arm which also interrupts the input to the d.c. charging set.

2.3.1.1.6 The Test Gap Protection Circuit

The test gap protection circuit, together with the high-voltage pulse duration timer, are shown in Fig. 2.35.

The soft valve delay unit incorporating a pair of hydrogen thyratrons V16 and V17 introduces a pre-selected time delay on the

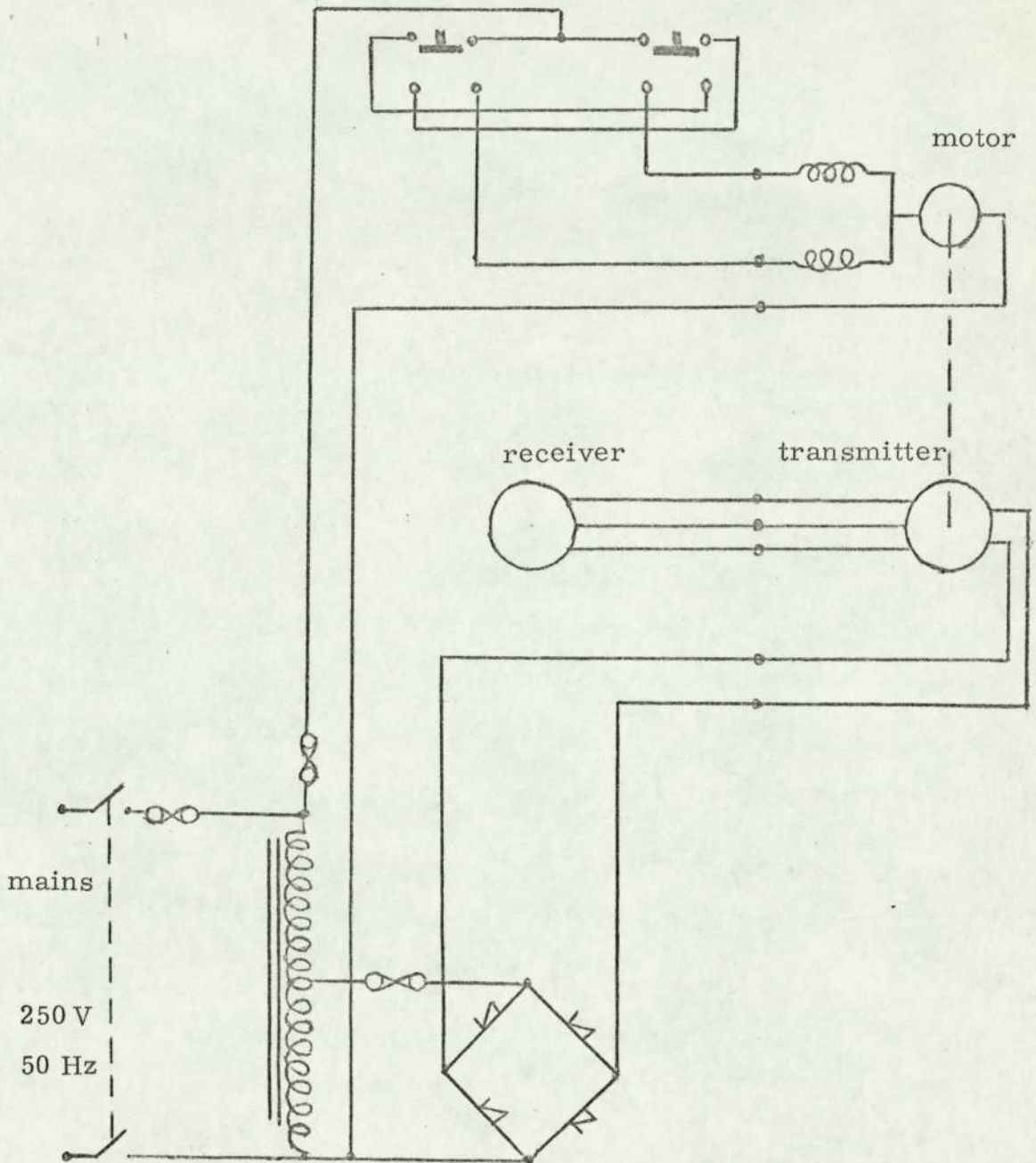


Fig. 2.33 Impulse Generator Gap Length Controller

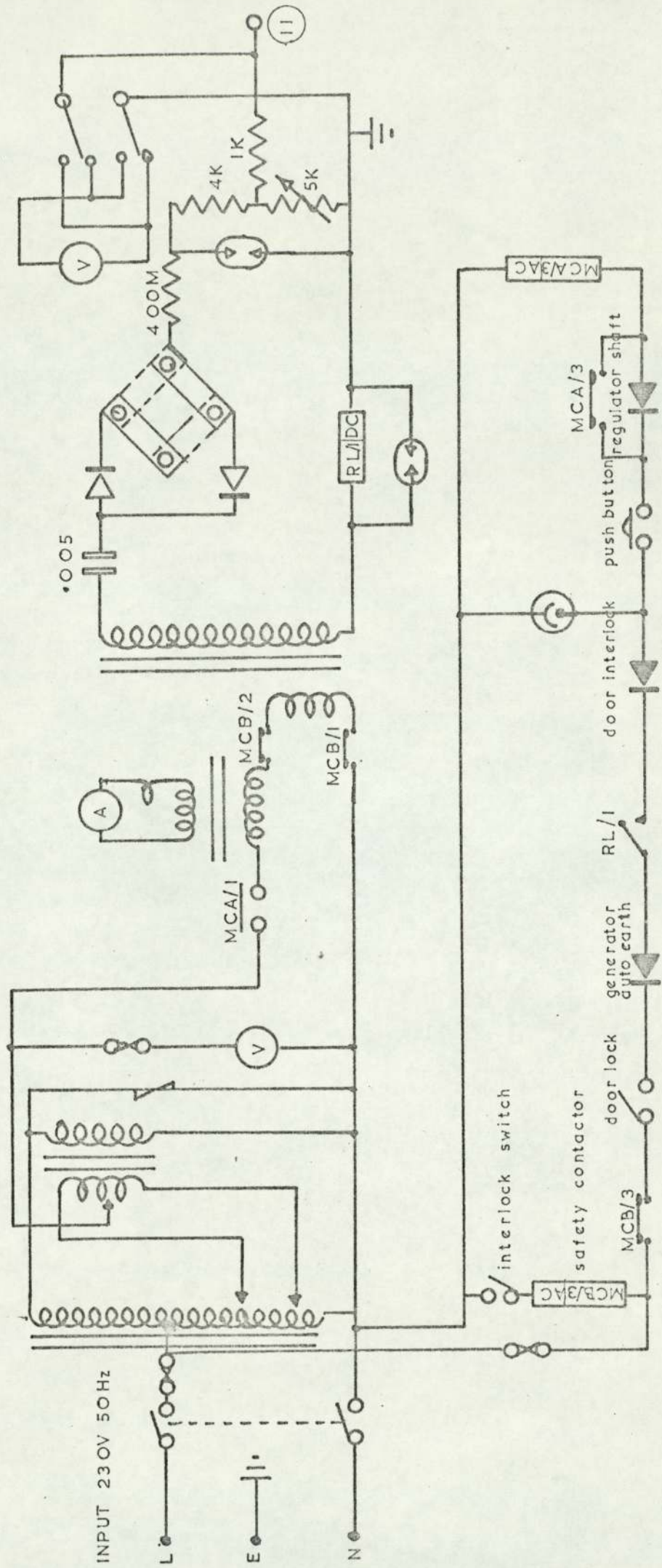


FIG 2.3.4 100kV CHARGING GENERATOR AND CONTROL UNIT

signal entering terminal (4). The output pulse from terminal (9) operates the chopping gap trigatron.

On breakdown of dielectrics in the test cell, a pulse is generated across a low resistance in series with the test gap. This is applied to the inverter V13 at the terminal (8) and, irrespective of its polarity, a negative pulse is selected on the output side of the inverter. The negative pulse applied to the amplifier V14 produces a positive pulse at its anode.

The two thyratrons, V15 and V16, are effectively in parallel. The incoming pulse from V14 fires V15 discharging the $0.01 \mu\text{F}$ anode capacitance to below the extinction level and producing a sharp positive pulse at the terminal (9).

The protection unit, by short circuiting the test gap after a breakdown, reduces the damage to the electrode surface and limits the possible carbonization of the dielectric. The duration of the post-breakdown current through the test gap is reduced to less than one microsecond by the operation of the protection system.

2.3.1.1.7 The Test Circuit

By confining the studies of gaseous discharge to that in air at normal pressure and temperature, a very simple test circuit results (see Fig. 2.36). The point electrode is supported from the high voltage bus-bar. The plane electrode is rounded at the edge to reduce the effect of field concentration. The current detector is enclosed within the plane electrode which acts as a Faraday cage minimising the influence of radiation noise.

The film support is made of PMMA and is free to rotate. This enables the film to be placed transverse or parallel to the main field axis. Film size up to 20 cm can be supported in both single and double emulsion types.

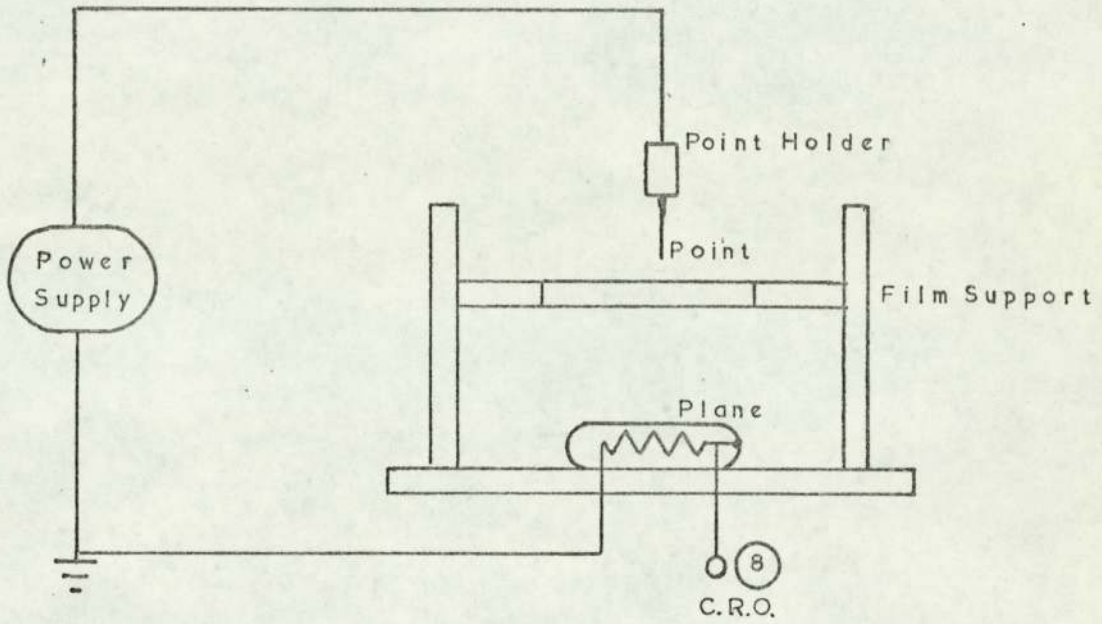


FIG 2.3 6 TEST CIRCUIT

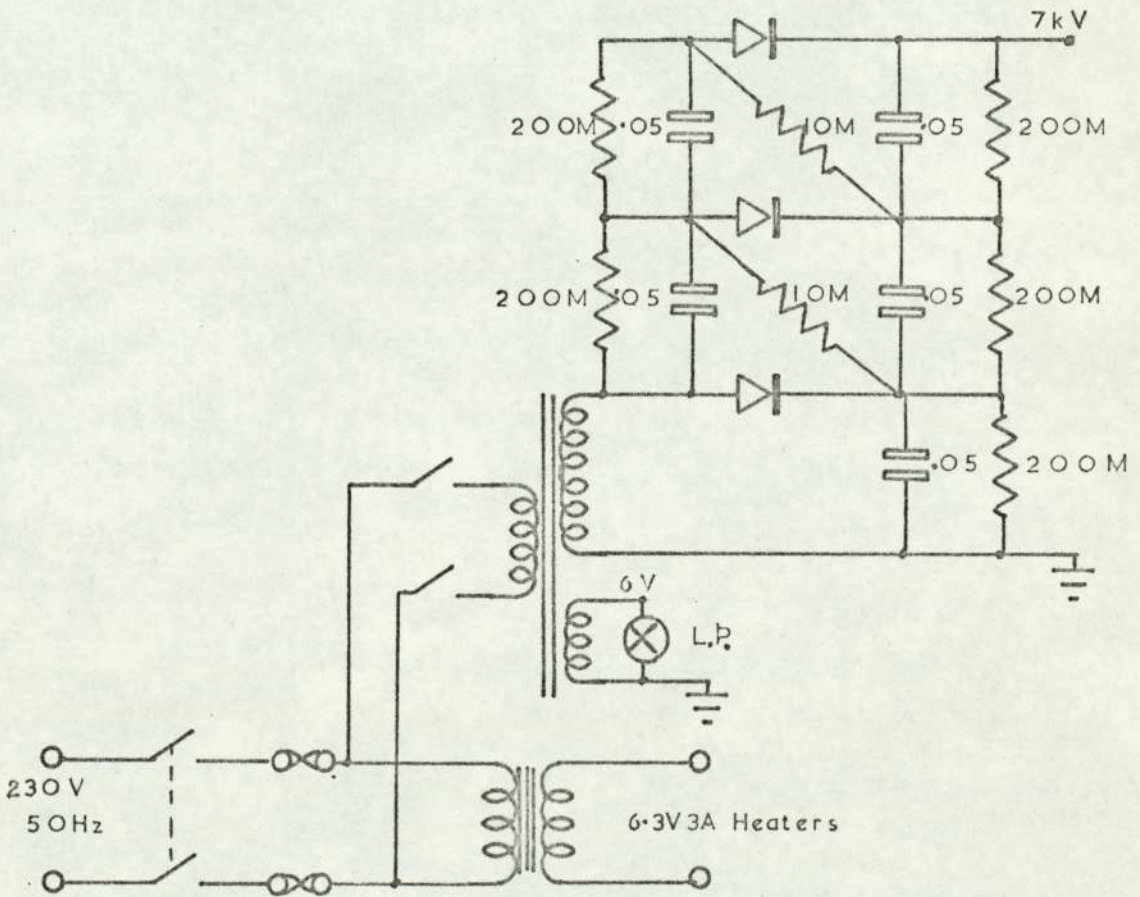


FIG 2,37 7 kV POWER UNIT

2.3.1.1.8 The Power Packs

The anode voltages, the grid bias voltages and the heater element supply voltages are provided from stabilised power packs of standard design.

Figure 2.37 shows the circuit diagram of the high voltage power supply for the hydrogen thyratrons.

2.3.1.2 The Nanosecond Range System

The high voltage pulses in the nanosecond range are generated by a high pressure hydrogen thyratron incorporating a discharge network. The rise time of the high voltage pulse can be kept as low as 5 n. sec at maximum output of 32 kV.

2.3.1.2.1 High Voltage Power Supply

The high voltage power supply (see Fig. 2.38) provides a positive d.c. output adjustable from 0 to 32 kV with a continuous current capability of 1.5 mA. The maximum ripple does not exceed 0.5%.

The high voltage output is equipped with a zero voltage start feature to prevent accidental surging on the high voltage, as well as an overcurrent relay which disables the power. In the event of an overload or a line voltage failure, the unit will automatically be de-energised.

No special cooling is required as the open construction provides natural conventional cooling.

2.3.1.2.2 Synchronous Pulse Generator

The pulse generator (see Fig. 2.39) is designed to accept a low voltage high impedance input pulse and deliver a high voltage low impedance output pulse. The output drives a hydrogen thyratron pulse generator.

The input can vary between 5 - 20 volts providing a 50 - 75 n. sec delay. There is also an internally supplied power frequency signal

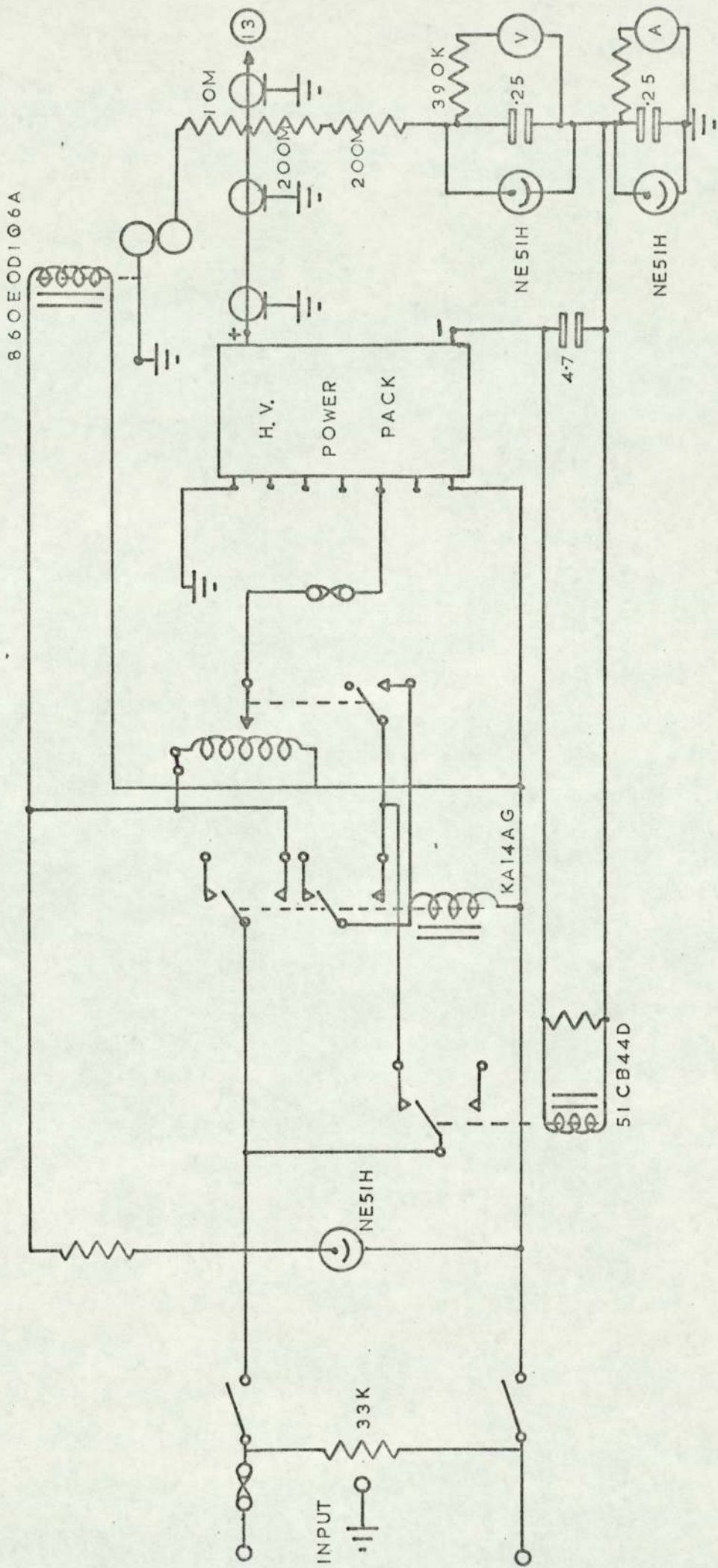


FIG 2-38 HIGH VOLTAGE POWER SUPPLY

for system alignment.

The main output in a single pulse form varies in the range of 0 - 500 volts. The rise time of the output pulse is 20 n. sec. and the pulse width is 0.25 μ sec. There is also an auxiliary output of 500 volts.

2.3.1.2.3 High Voltage Pulse Generator

The high voltage pulse generator provides extremely fast and brief high voltage waveforms. The generator (see Fig. 2.40) utilizes a unipotential cathode, three element, hydrogen filled, high voltage thyratrons in a low inductance coaxial configuration. The unit encloses a corona shielded hydrogen thyatron tube, circuitry for controlling hydrogen pressure to achieve the fastest possible thyatron operation, and a high voltage resistor pad for pulse circuitry. The pulse forming network allows versatility of operation.

2.3.2 Measurement Techniques

2.3.2.1 Methods Employed by Other Investigators

2.3.2.1.1 Cloud Chamber Method

The ions produced by the ionizing collisions of electrons in the discharge act as condensation nuclei in the supersaturated environment of cloud chamber and thus become visible.

This method can only be used in gaseous dielectrics at low pressure. For maximum sensitivity of the system, a high expansion ratio is required.

2.3.2.1.2 Electrical Method - Current Measurement

The drifting electrons and ions of discharge produce an electrical current pulse during their transit time. This current pulse is observed as a voltage pulse across a resistance in series with the test cell and is displayed after sufficient amplification on a cathode-ray oscilloscope.

For a reasonable sensitivity, the signal must appreciably

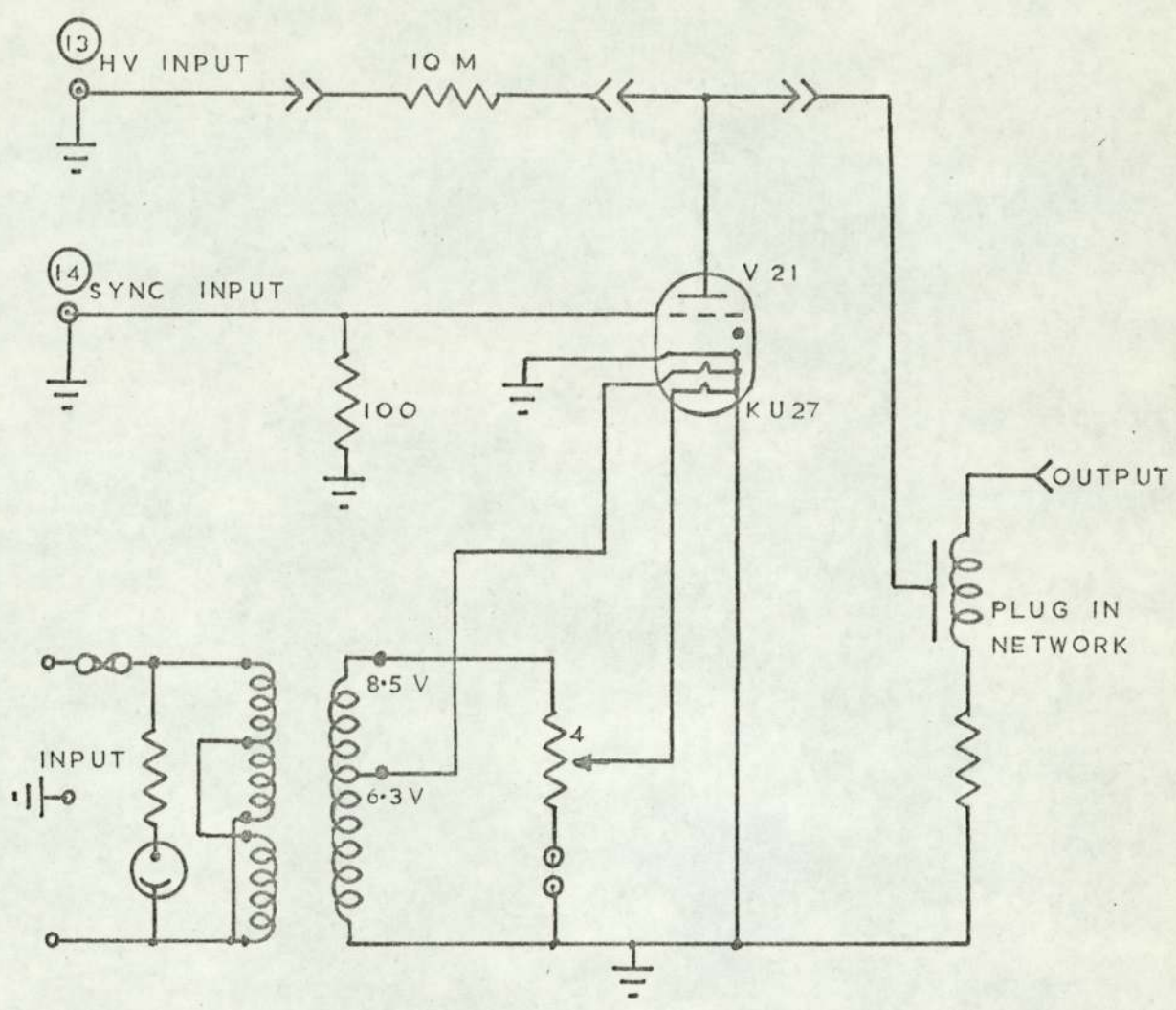


FIG 2.40 HIGH VOLTAGE PULSE GENERATOR

exceed the noise level and form a smooth curve on the c. r. o.

The problems involved in this type of measurement are:

- (a) Input capacitance of the detector
- (b) Time constant of the current shunting resistor
- (c) Amplifier bandwidth
- (d) Noise level due to thermal, grid current and shot noise

2.3.2.1.3 Optical Methods

2.3.2.1.3.1 Photomultiplier

The drifting electrons excite the gas molecules to light emission energy state. These quanta are collected by a photomultiplier and thus transformed to a current pulse, which can be observed on the screen of a c. r. o.

For any detection, at least one photo-electron must be liberated from the cathode of the multiplier. For any reasonable detection, such that thermal noise can be ignored and a measure of time constant of the discharge provided, the number of liberated photo-electrons by the photomultiplier should be much greater than one.

2.3.2.1.3.2 Direct Photography

Direct photography is normally used when the electrical discharge has reached a stage of development where it emits light quanta. There are two different types of this method of photography employed.

(i) Time-integrated Single Frame

This is the simplest and cheapest method of photography. It requires a large number of frames for any statistical analysis of discharge to be made.

Early stages of discharge development, especially those with low light emission recorded by time-integrated single frame technique, are lost due to the superposition of brighter late stages of discharge.

(ii) Ultra High Speed

The ultra high speed cameras employed in single frame, framing or streak modes of photography are of two basic different types:

(a) Mechanical-Optical - These employ either transport mechanism with continuous motion or stationary film and rotating mirror or prism.

(b) Image Converter - The image of radiating discharge resembling cloud chamber results are recorded. The low light-level applications of this device where high effective aperture is essential are an added advantage.

2.3.2.2 Methods Employed by the Author

2.3.2.2.1 Streamer Track Recording

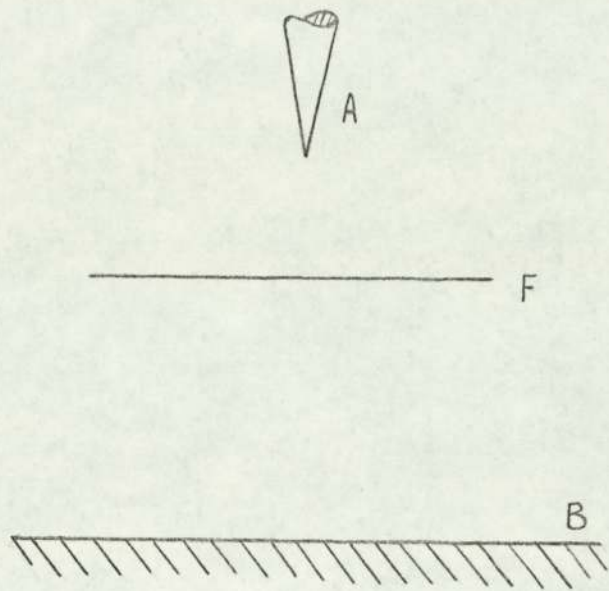
Direct recording of streamer track is possible by means of radiation sensitive layers placed in two positions in the inter-electrode gap.

(a) Normal to main electric field axis and at a different position from the point-electrode as shown in Fig. 2.41a.

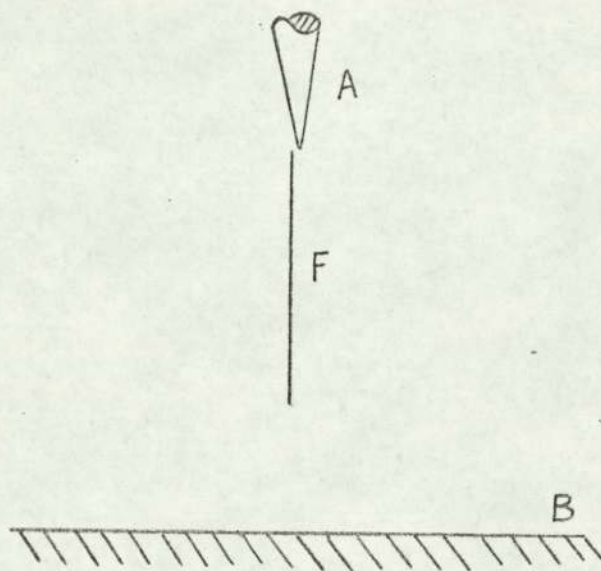
(b) Along the main field axis and in contact with the point-electrode as shown in Fig. 2.41b.

With radiation sensitive film transverse to the field axis, given sufficiently high impulse voltage, discharge channels develop outward from the point-electrode. Every outgoing streamer produces an incident point with its associated branching on the film emulsion.

If the distance between the film and the point-electrode is varied with a definite impulse wave or if the impulse wave is varied with a definite distance between point-electrode and the film, then the following information can be made available:



(a)



(b)

A = Point-electrode
 B = Plane-electrode
 F = Film

Fig. 2.41. Streamer Track Recording Technique

- (a) Radiation sensitive film transverse to the field axis
 (b) Radiation sensitive film parallel to the field axis

- 1 - Forward rushing photon radiation
- 2 - Primary streamer growth
- 3 - Secondary streamer growth
- 4 - Return streamer growth
- 5 - Breakdown

This method of measurement is found to be the most sensitive one available in recording the pre-breakdown phenomena. With a large range of film sensitivity available in single and double emulsion, a detailed study of discharge life cycle can be made.

2.4 Experimental Results

2.4.1 Spatial Build-up of Discharge

2.4.1.1 Primary Streamers

When a film is placed transverse to the electric field and directly against the point-electrode, a streamer pattern similar to a Lichtenberg discharge figure results (see Fig. 2.42). Multi-branched tracks start from the point of incident directly placed against the point-electrode. The pointed ends of the streamer tracks lie approximately in a circle showing that there is no preferred path.

Moving the film away from the point-electrode, several separate incident points, each leading to a branched stem, are recorded indicating multi-branched primary plate-electrode-directed streamers (see Fig. 2.43). With increasing distance between the film and the point-electrode, the number of incident points becomes greater and so does the region enclosed by them (see Fig. 2.44).

With the film placed on the plate (see Fig. 2.45), the presence of a large number of incident points with further outward branching shows that the primary streamers would have bridged the gap in the absence of the film. The presence of this phenomenon is also confirmed by bridging the gap with a film placed parallel to the electric field (see Fig. 2.46). The bridging of the gap by the primary streamers does not necessarily lead to breakdown.

2.4.1.2 Secondary Streamers

At higher applied field strength, primary streamers are followed by secondary streamers which are luminous, highly ionized conducting channels following the main stems of the primary streamers. Figures 2.47 and 2.48 show the secondary streamers superimposed on primary ones for films placed transverse and along

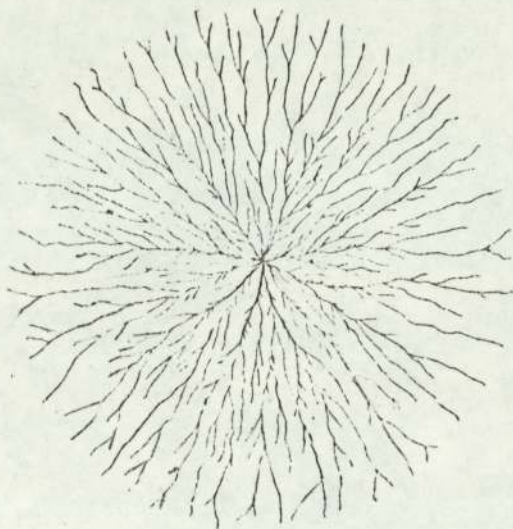


Fig. 2.42 Primary Positive Streamer Pattern when film is placed transverse to the main electric field axis and directly against the point-electrode in air at N. T. P.

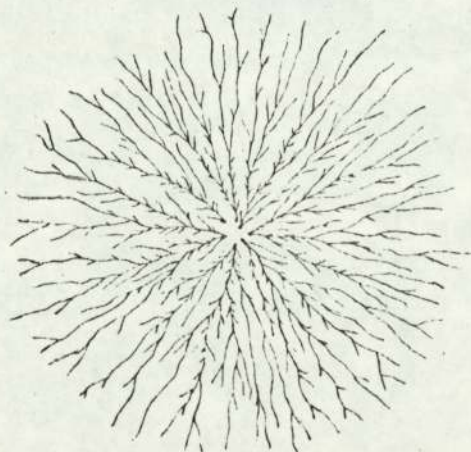


Fig. 2.43 Primary Positive Streamer Pattern when film is placed a distance 1 away from the point-electrode in air at N. T. P.

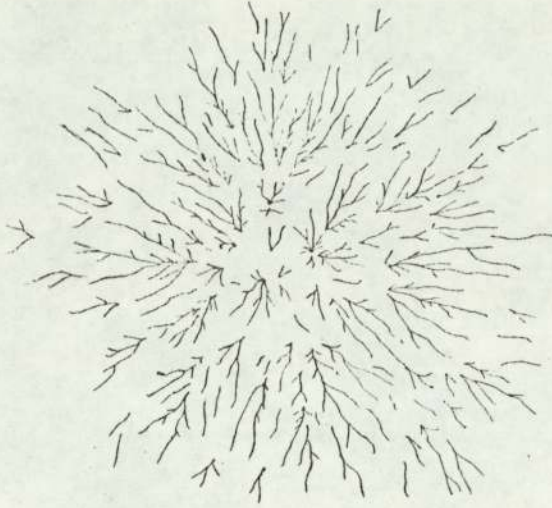


Fig. 2.44 Primary Positive Streamer Pattern when film is placed a distance l' ($l' > l$) away from the point-electrode in air at N.T.P.

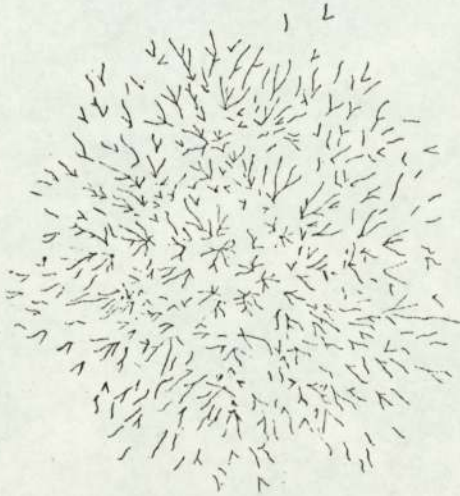


Fig. 2.45 Primary Positive Streamer Pattern when film is placed on the plate-electrode facing the point-electrode in air at N.T.P.

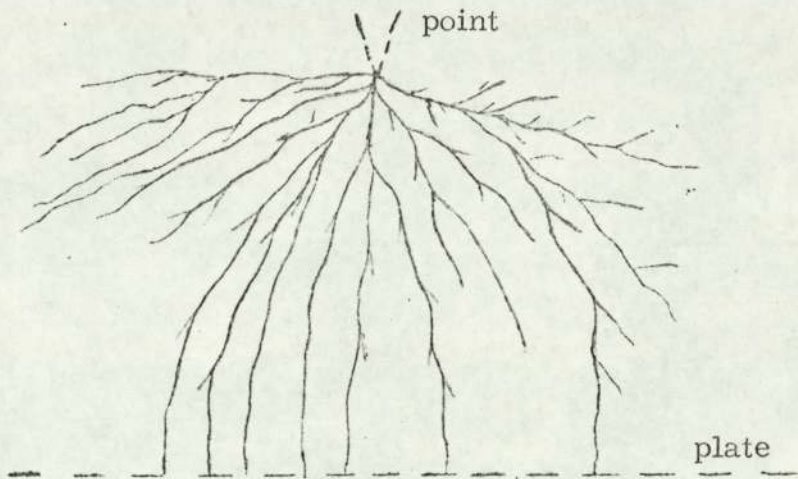


Fig. 2.46 Primary Positive Streamer Pattern when film is bridging the gap in air at N. T. P.

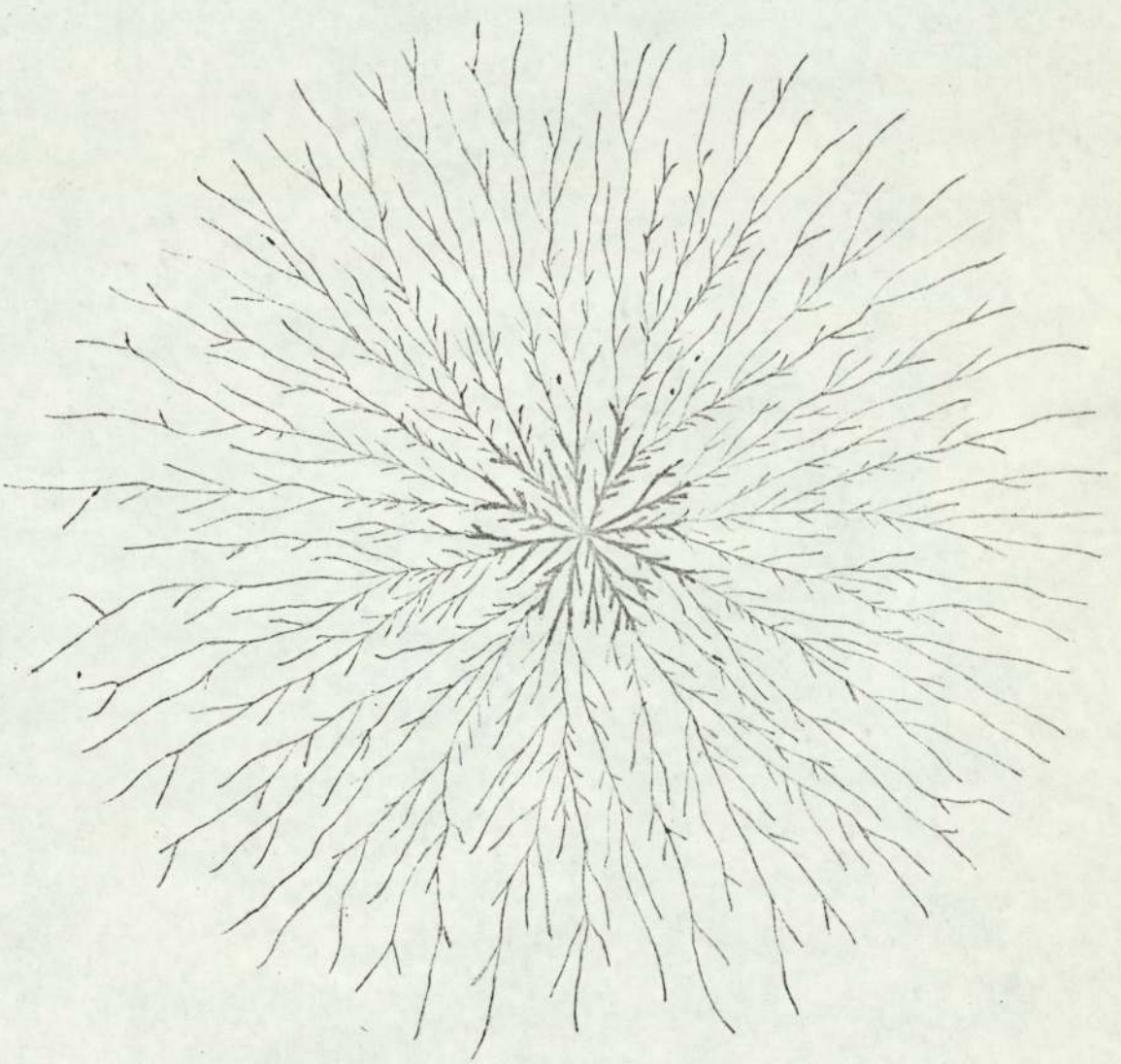


Fig. 2.47 Primary and Secondary Positive Streamer Patterns when film is placed transverse to the main electric field in air at N. T. P.

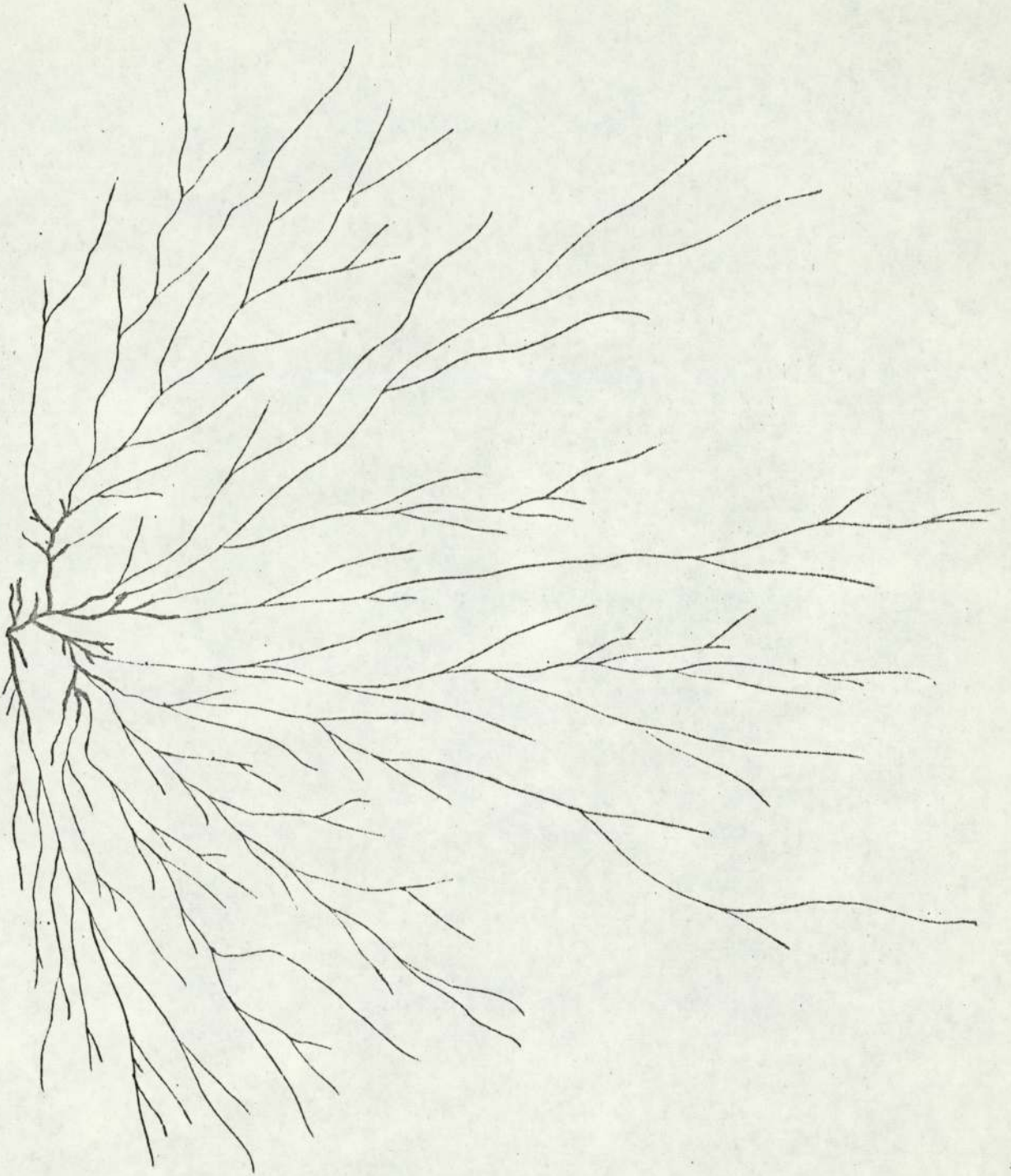


Fig. 2.48 Primary and Secondary Positive Streamer Patterns when film is placed along the electrode gap against the point electrode at N.T.P.

the field axis respectively. The spatial build-up of secondary streamers could extend about half-way across the gap without leading to breakdown. The luminosity of the discharge channel is shown by Figs. 2.49 and 2.50 taken by placing single-frame, time-integrated cameras close to the electrode system.

2.4.1.3 Return Streamers

The extension of the secondary streamers beyond half-way distance across the gap normally leads to breakdown. The breakdown can be suppressed by placing an extensive size film transverse to the field-axis. With the approach of the secondary streamer tips to the plate-electrode, opposite polarity streamers - named return streamers - are generated from the plate electrodes. Figure 2.51 shows positive plate-cathode directed secondary streamer tips, with some branching on one side of a double-emulsion film, and negative return streamer tips with some radial spread on the other side. If the secondary streamers and return streamers are allowed to meet, a highly conductive channel would result connecting the electrodes, and the breakdown is ensured.

2.4.2 Primary Streamer Parameters

When placing the film transverse to the field axis, a stepped movement is carried out away from the point-electrode and towards the plane electrode keeping the impulse wave and electrode gap unchanged. With single-side emulsion film, the emulsion side faces the point electrodes. At potentials near and above breakdown, the double-sided emulsion film is employed to record presence of return streamers.

The following quantities were evaluated for each recording:-
 1 - The number of the incident points, N_p , of the streamer head reaching the film.



Fig. 2.49 A single-frame, time integrated photograph of secondary positive streamer in air at N. T. P.

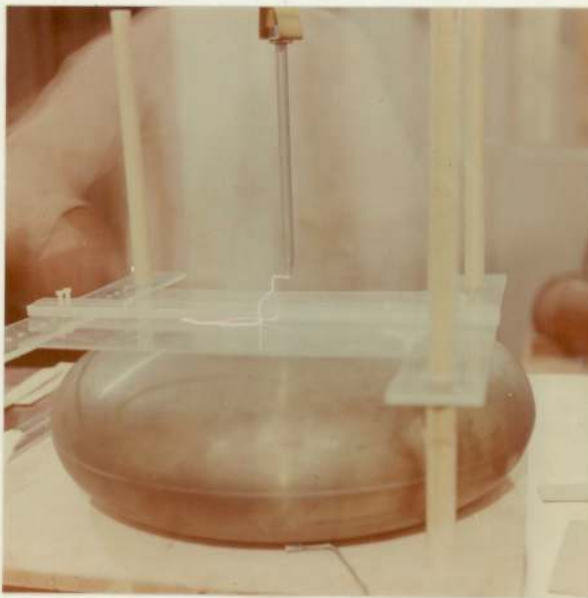


Fig. 2.50 A single-frame, time integrated photograph of secondary positive streamer in air at N. T. P. Electrode assembly is superimposed.

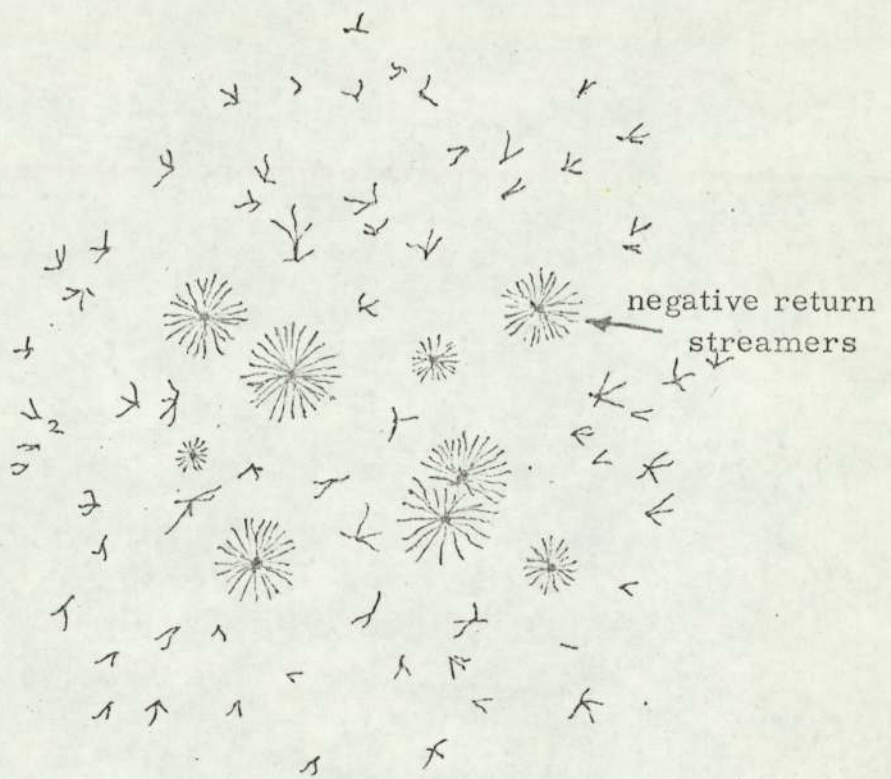


Fig. 2.51 Positive Plate-Cathode directed Secondary Streamer tips with branching on one side of a double emulsion film in air at N. T. P., and negative return streamer tips with some radial spread on the other side.

- 2 - The radius of the circle surrounding the incident point, R , (see Fig. 2.52). This circle shows the streamer spread in the plane of the film.
- 3 - The length of the largest branching of the streamer tracks, S . This represents the extent of the streamer spread in the absence of the film. It may also provide a measure of the streamer head potential.

Due to a certain amount of scatter associated with the measurements of the three parameters, a large number of readings was taken for each position in the field with the same impulse wave and electrode geometry.

2.4.2.1 Number of Primary Streamers

Figure 2.53 shows the relationship between the number of the streamers, N_p , and the distance between the film and the point-electrode, l , at different impulse wave levels. The electrode gap is 2.5 cm and the radius of the curvature of the points is 100 microns. The applied voltage is $1/50 \mu s$ wave according to B.S. 358:1039 and B.S. 923:1940. When the number of primary streamers is drawn to a log-scale (see Fig. 2.54), a linear relationship with the distance from the point-electrode is observed.

2.4.2.2 Spatial Progress of Primary Streamer

The measure of lateral spread of streamers is given by Fig. 2.55. This shows a great lateral development of the streamers only a short distance away from the point-electrode. The spread reaches a maximum near the plane-electrode and then decrease with further propagation. The graphs in Fig. 2.55, if rotated round the axis l , envelop the entire streamer spatial propagation.

2.4.2.3 Spread of Primary Streamers

The extreme extent of streamer branching is shown

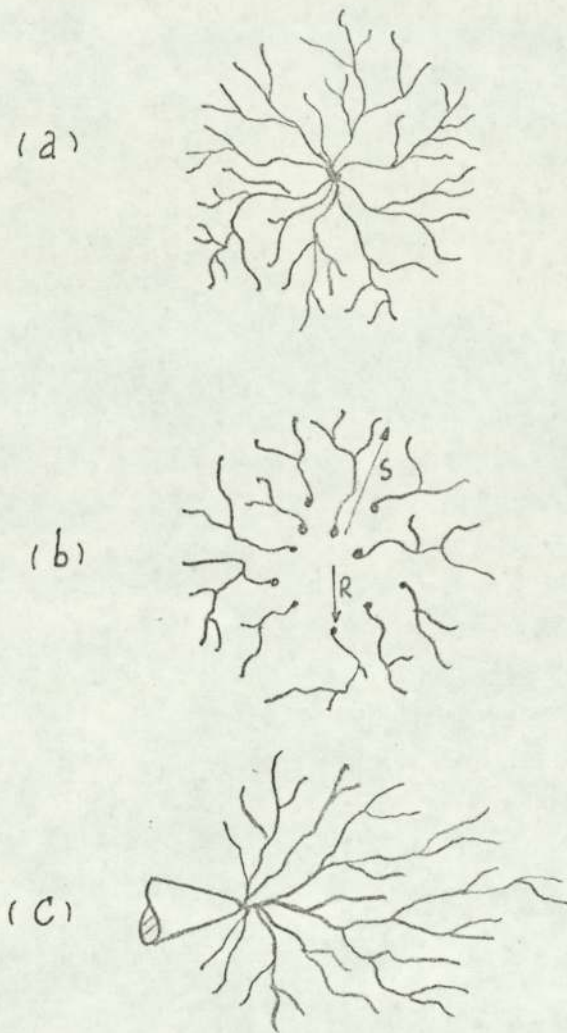


Fig. 2.52 Schematic Representation of Streamer Pattern

- (a) Film transverse to field axis and directly against the point
- (b) Film transverse to field axis and some distance from the point
- (c) Film parallel to field axis and placed in contact with the point

TABLE 2.5. Number of Primary Streamers, N_p , in the Interelectrode Space in Air at N. T. P.

Point-Plane electrodes; point-anode; Gap length, $G = 2.5$ cm;

Radius of Curvature of point, $C = 100$ microns; $1/50 \mu s$ impulse wave.

Impulse Voltage kV	P. S. Number	Point-Film Gap, l mm				
		5	10	15	20	25
15	N_p	11	19	30	40	65
		13	20	31	42	66
		13	20	31	45	66
		13	21	33	48	72
		14	22	35	49	74
		15	22	35	51	75
		15	24	36	51	79
		16	25	38	55	80
20	N_p	12	24	38	63	100
		13	25	38	65	104
		15	25	40	67	106
		15	26	41	67	106
		16	26	42	70	110
		16	27	45	71	110
		17	28	45	73	115
		18	30	48	75	120
25	N_p	15	26	52	87	145
		16	26	53	90	147
		16	27	55	91	148
		16	30	55	93	150
		17	30	57	95	151
		18	31	58	96	155
		18	33	58	96	157
		18	33	60	100	160
30	N_p	16	28	55	99	179
		16	28	55	107	181
		18	29	57	110	187
		18	33	59	111	192
		19	34	60	116	195
		20	35	63	120	195
		20	35	63	121	198
		22	38	71	125	200
35	N_p	16	30	61	127	209
		18	32	64	130	211
		20	35	65	130	218
		20	36	65	131	218
		20	36	67	132	220
		20	38	68	141	220
		21	38	68	146	227
		21	38	70	150	230

FIG. 2.53 Number of Primary Streamers in Air in the Inter-Electrode Space at N.T.P.

Point-Plane Electrodes
 Point - Anode
 $c = 100$ microns
 $g = 2.5$ cm.
 $1/50 \mu s$ Impulse Wave

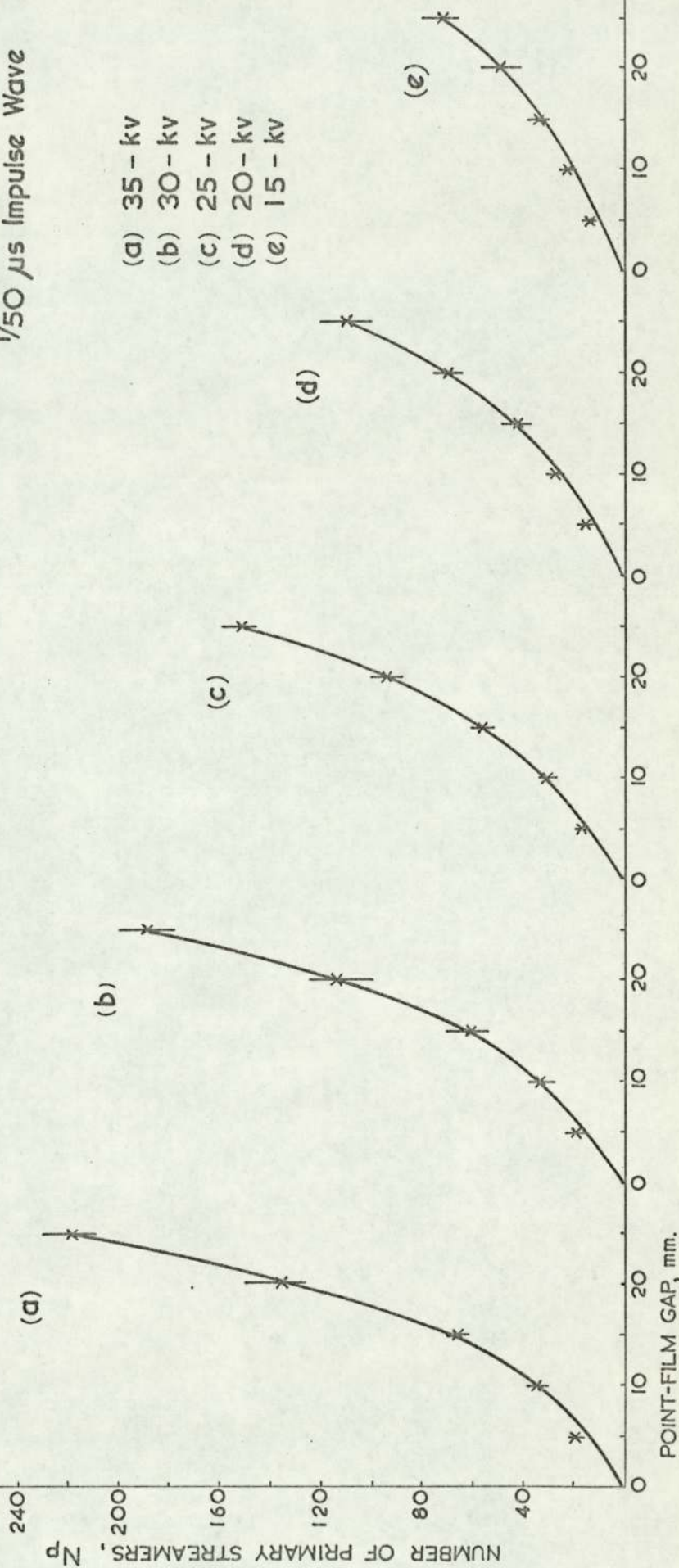


FIG. 2-54 Number of Primary Streamers in Air in the Inter-Electrode Space at N.T.P.:

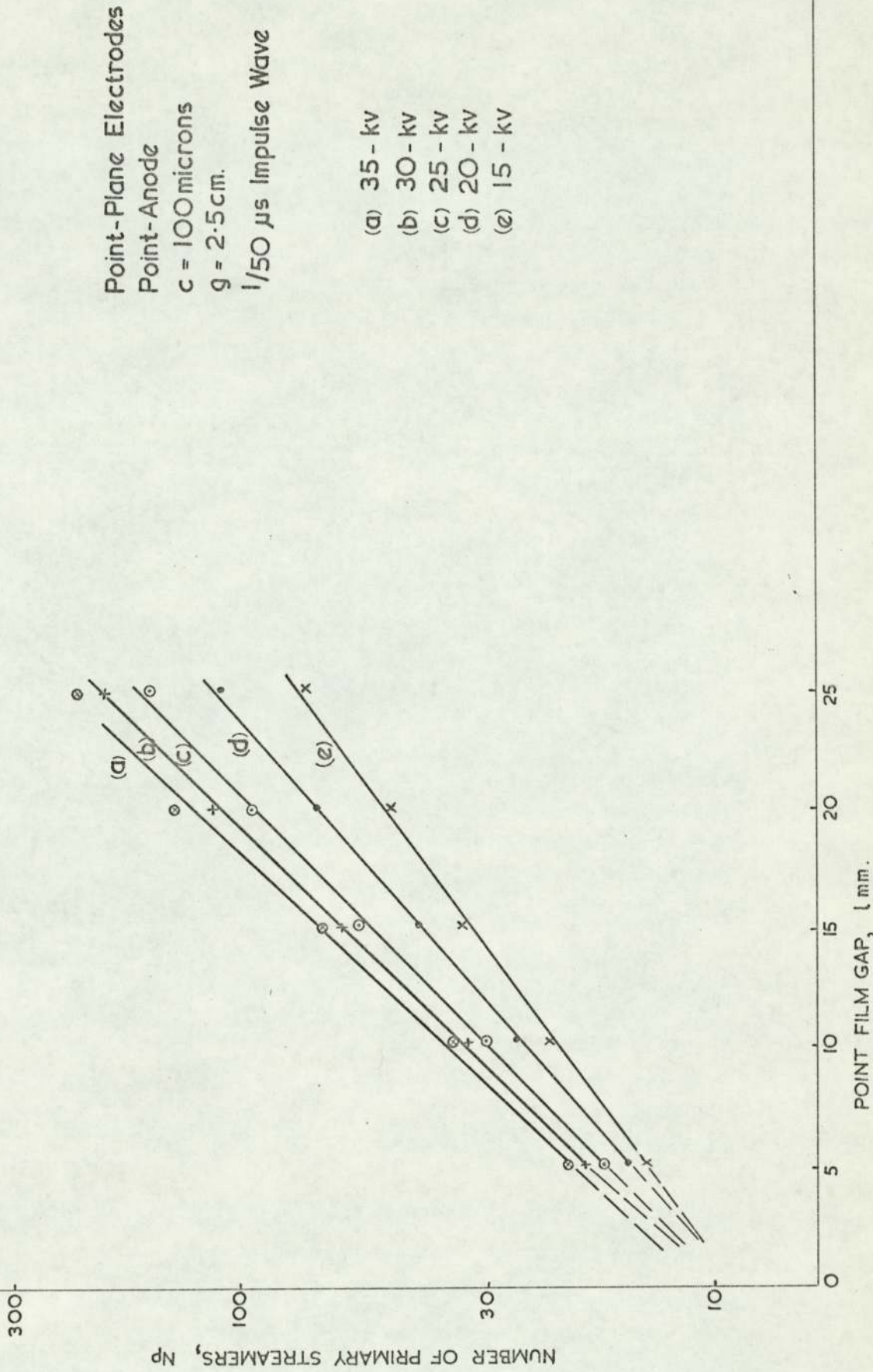


TABLE 2.6. Primary Streamer spatial progress, R, in air at N.T.P.

Point-Plane Electrodes; Point-Anode; Gap length, G = 2.5 cm ;

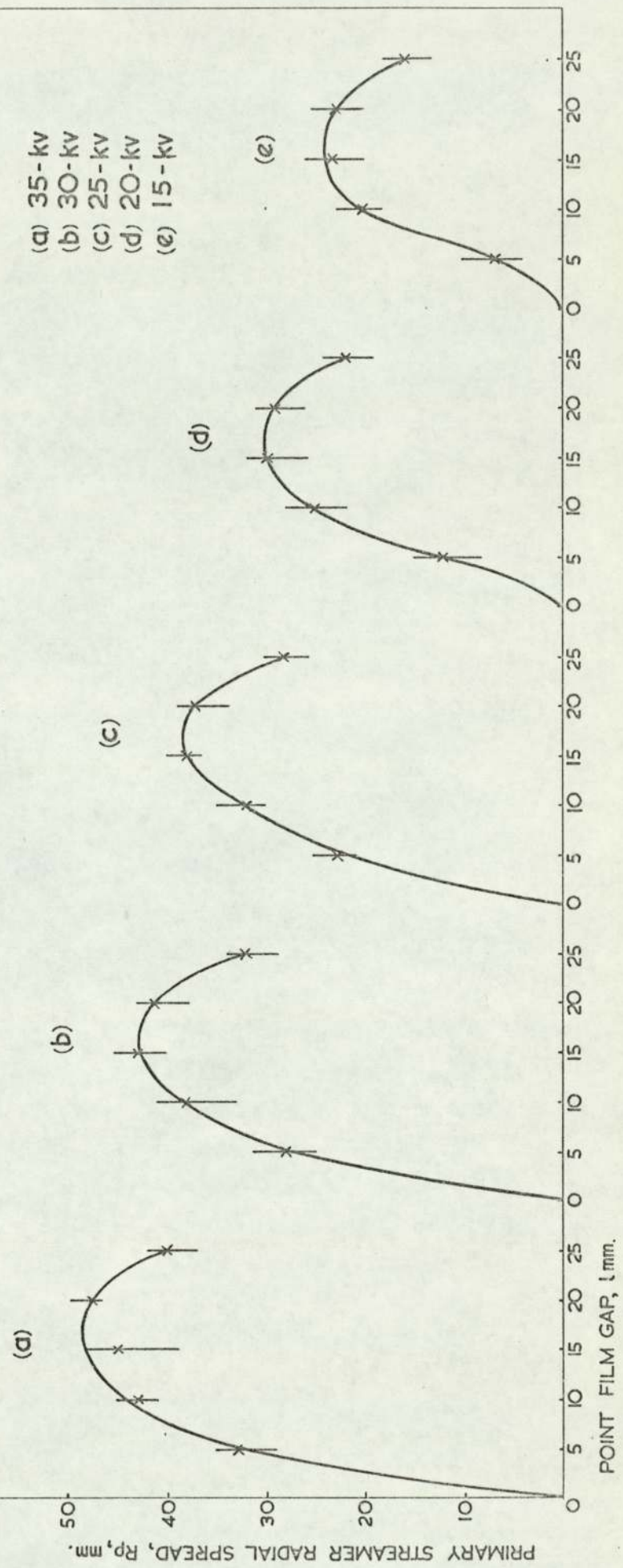
Radius of Curvature of point, C = 100 microns ; 1/50 μ s impulse wave.

Impulse Voltage kV	Spatial Progress mm	Point - Film Gap, l mm				
		5	10	15	20	25
15	R	4	18	20	20	13
		6	19	21	20	15
		7	19	21	22	15
		7	21	23	23	16
		8	21	24	23	16
		8	22	24	24	16
		8	23	24	25	17
		10	23	25	25	18
20	R	8	22	25	26	19
		9	23	27	26	20
		11	23	28	28	20
		12	25	30	29	22
		12	26	31	29	22
		12	26	31	30	23
		13	27	32	30	24
		15	28	32	31	24
25	R	21	30	35	34	26
		22	31	37	34	26
		23	33	37	36	27
		23	33	38	37	27
		24	33	38	37	28
		24	34	38	37	29
		24	35	39	38	29
		25	35	40	39	30
30	R	25	33	40	37	29
		27	35	40	38	29
		27	37	42	41	32
		28	38	43	41	32
		29	38	43	41	32
		29	38	43	42	33
		30	40	45	42	33
		31	41	45	43	34
35	R	29	41	39	47	37
		30	41	41	48	39
		33	43	45	48	40
		33	43	46	48	40
		33	43	46	48	40
		34	44	48	49	41
		34	45	48	49	41
		35	45	48	50	42

FIG. 2.55 Primary Streamers Spatial Progress in Air at N.T.P.

Point-Plane Electrodes
Point-Anode
 $c = 100$ microns
 $g = 2.5$ cm
 $1/50 \mu s$ Impulse Wave

- (a) 35-kv
- (b) 30-kv
- (c) 25-kv
- (d) 20-kv
- (e) 15-kv



POINT FILM GAP, mm.

PRIMARY STREAMER RADIAL SPREAD, R_p , mm.

in Fig. 2. 56. In the vicinity of the point-electrode the branching remains almost constant but it decreases sharply upon approaching the plate.

Point-electrode size makes little difference to streamers once the streamers have travelled a short distance away from the point. This phenomenon seems reasonable from the results of electrostatic field study by computational techniques. It is found that the smaller the point-electrode, the larger is the number of streamers.

The average values of the three main parameters of primary streamers are shown in Fig. 2. 57 for varying applied potential.

2.4.2.4 Spatial-time Characteristics of Primary Streamers

Using a nanosecond pulse generator, a series of tests was carried out exploring the spatial-time characteristics of the primary streamers. By keeping the pulse amplitude constant at 25 kV and varying the pulse duration in the range 6 - 200 nanoseconds, radial spread of the primary streamers was measured for a 2.5 cm gap in air (see Fig. 2. 58). The experiment was repeated for the maximum available pulse amplitude of 35 kV.

2.4.2.5 Velocity of primary streamers

At vary short duration, pulse voltages the progress of the primary streamer terminates in the mid-gap region. The extent of the streamer propagation in the main field axis and the duration of the applied voltage determine the average value of the velocity of the streamer tip. The velocity of the primary streamer and streamer tip position in the electrode gap is shown in Fig. 2. 59.

TABLE 2. 7. Primary Streamer Spread, S, in the interelectrode space in air at N. T. P.

Point-Plane Electrodes; Point-anode Gap length, $G = 2.5$ cm;
 Radius of curvature of point, $C = 100$ microns; $1/50 \mu s$ impulse wave.

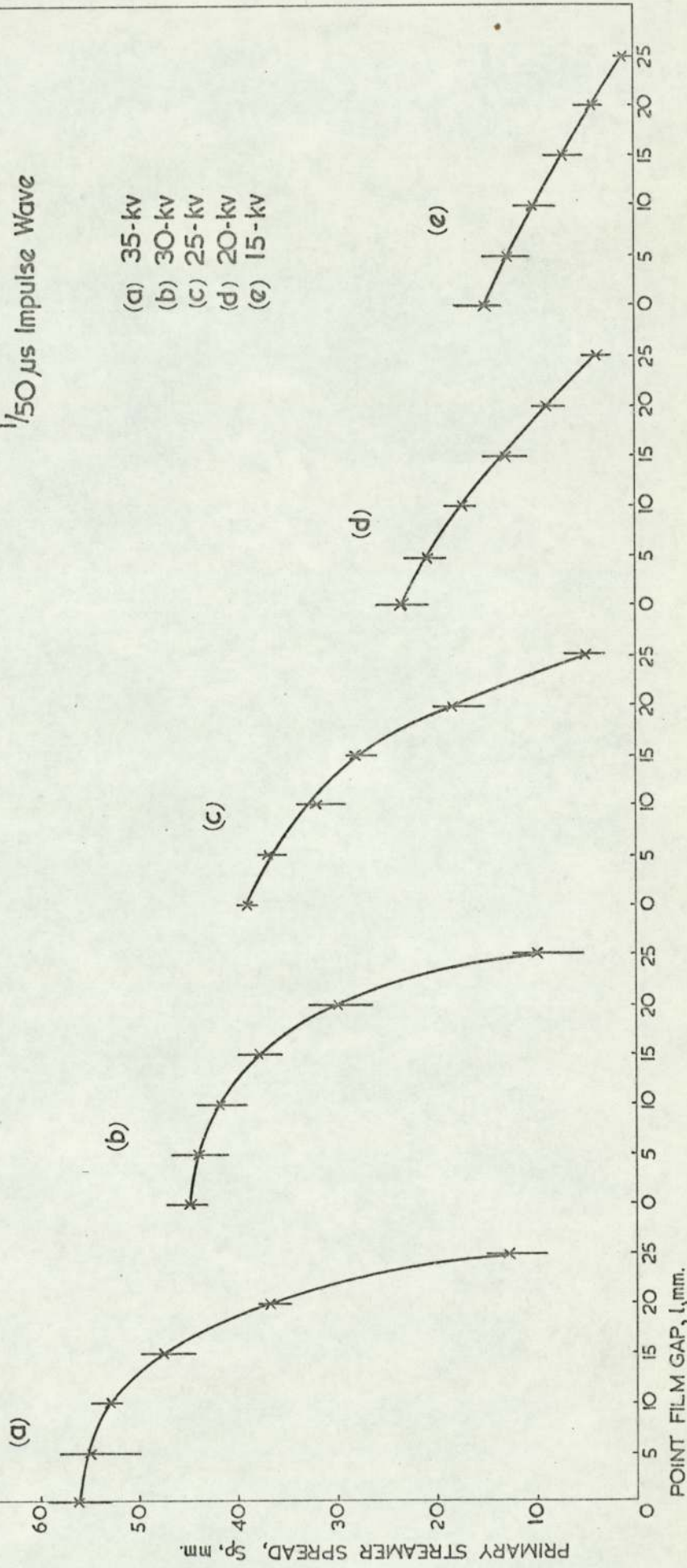
Impulse Voltage kV	P.S. Spread mm	Point-Film Gap, l mm					
		0	5	10	15	20	25 ⁺
15	S	13	10	7	5	3	-
		14	10	8	5	3	-
		14	12	10	7	4	0.5
		15	13	11	7	4	1
		16	13	11	7	4	1
		16	14	11	8	5	1
		16	14	12	8	6	2
		18	15	12	9	6	2
20	S	20	18	16	11	7	2
		21	19	16	12	8	3
		22	20	17	13	8	3
		22	21	17	13	8	4
		23	21	17	13	9	4
		23	21	18	13	9	4
		23	22	18	14	10	5
		26	23	19	15	10	5
25	S	38	35	29	26	15	3
		38	36	30	26	17	4
		39	36	32	27	18	4
		39	36	32	27	18	5
		39	37	33	27	19	5
		39	37	33	28	19	6
		40	38	33	28	20	6
		40	38	34	29	20	7
30	S	43	41	39	35	25	5
		44	42	42	37	30	8
		45	44	42	37	30	10
		45	44	42	37	30	10
		45	45	42	38	31	10
		46	45	43	39	31	11
		47	45	43	39	32	11
		47	47	44	40	33	12
35	S	58	50	52	44	35	9
		53	53	52	46	36	11
		56	55	52	48	36	13
		56	55	53	48	36	13
		56	55	53	48	37	13
		57	55	54	48	37	14
		57	57	55	50	38	15
		59	58	55	50	38	15

⁺ True gap length = 25 - film thickness.

FIG. 2.56 Primary Streamers Spread in the Inter-Electrode Space in Air at N.T.P.

Point-Plane Electrodes
 Point Anode
 $c = 100$ microns
 $g = 2.5$ cm.
 $1/50 \mu s$ Impulse Wave

- (a) 35-kv
- (b) 30-kv
- (c) 25-kv
- (d) 20-kv
- (e) 15-kv



PRIMARY STREAMER SPREAD, S_p , mm.

POINT FILM GAP, l , mm.

TABLE 2.8 Primary Streamer Average Parameters in Air
at N. T. P.

Point-plane electrodes; point anode; gap length,
G, = 2.5 cm; radius of curvature of point, C = 100 microns.
1/50 μ s impulse wave

Impulse voltage	P. S. Parameters	Point-film gap, 1mm					
		0	5	10	15	20	25
15 kv	Sp mm	15	13	10	7	4	1
	Rp mm	-	7	21	23	23	16
	Np	-	14	22	34	48	72
20 kv	Sp mm	23	21	17	13	9	4
	Rp mm	-	12	25	30	29	22
	Np	-	15	26	42	69	109
25 kv	Sp mm	39	37	32	28	18	5
	Rp mm	-	23	32	38	37	28
	Np	-	17	30	56	94	152
30 kv	Sp mm	45	44	42	38	30	10
	Rp mm	-	28	38	43	41	32
	Np	-	19	33	60	114	191
35 kv	Sp mm	56	55	53	48	37	13
	Rp mm	-	33	43	45	48	40
	Np	-	20	35	66	136	219

FIG. 2-57 Average Value of Primary Streamer Parameters in Air at N.T.P.

POINT-PLANE ELECTRODES
 POINT-ANODE
 C = 100 microns
 g = 2.5 cm.
 1/50 μs IMPULSE WAVE

X - 15 kv
 ● - 20 kv
 ○ - 25 kv
 + - 30 kv
 ⊗ - 35 kv

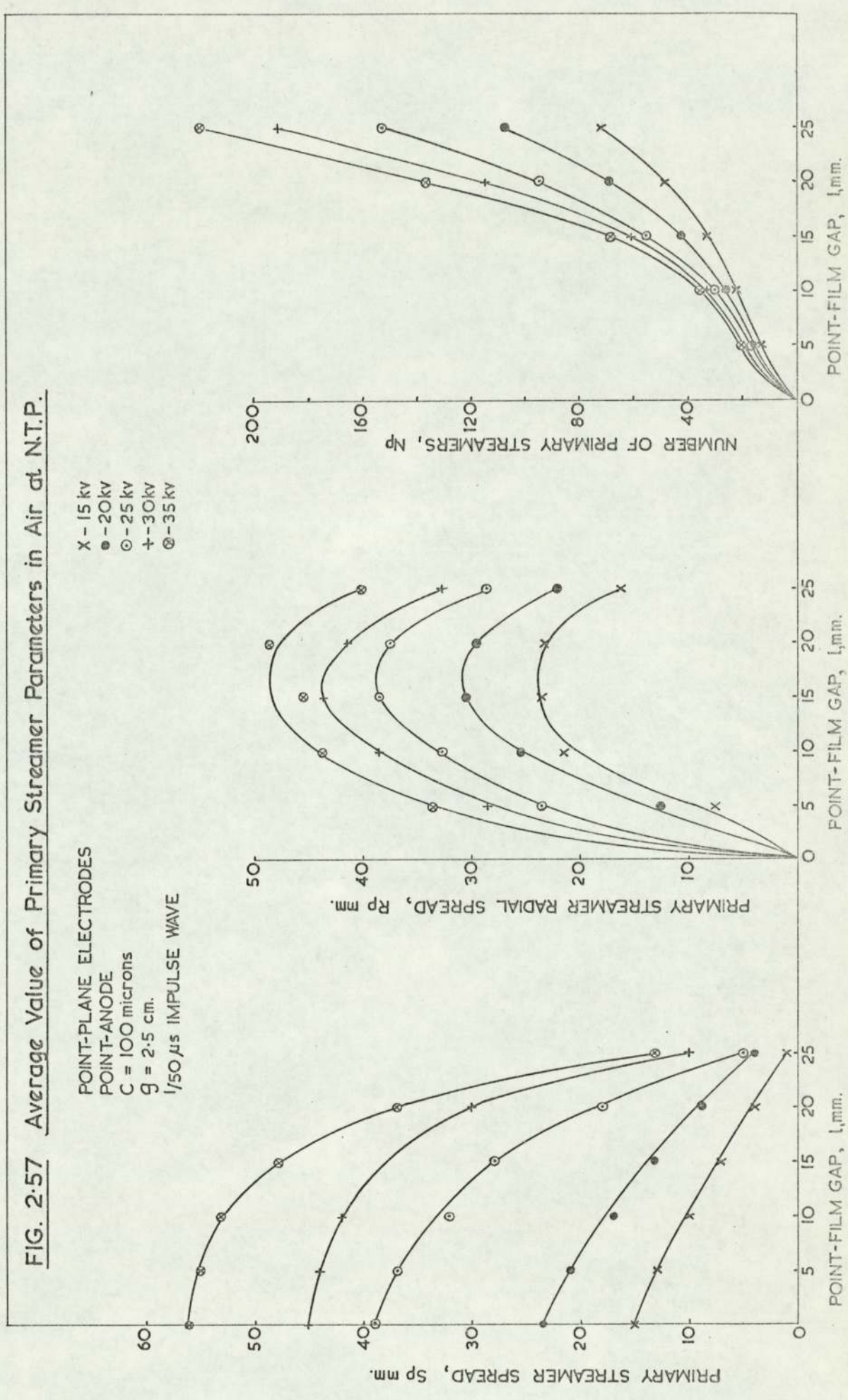


TABLE 2.9 Primary Streamers Spatial-Time Characteristics
in Air at N. T. P.

Point-plane electrodes; point-anode; gap length,
G, = 2.5 cm; radius of curvature of point = 100 microns
rectangular voltage wave.

Pulse height kV	Point -film gap 1mm	Pulse Width											
		6 ns		10 ns		20 ns		50 ns		100 ns		200 ns	
		S mm	R mm	S mm	R mm	S mm	R mm	S mm	R mm	S mm	R mm	S mm	R mm
25	0	10	-	15	-	26	-	27	-	30	-	31	-
	5	3	5	9	7	20	7	22	13	24	14	26	15
	10	-	-	3	7	17	11	18	17	22	23	24	25
	15	-	-	-	-	14	12	16	19	20	24	23	28
	20	-	-	-	-	11	10	13	18	17	24	20	28
	25	-	-	-	-	3	5	3	13	4	19	4	21
35	0	-	-	-	-	-	-	-	-	-	-	-	-
	5	-	4	-	8	-	11	-	12	-	14	-	15
	10	-	3.5	-	13	-	16	-	22	-	28	-	29
	15	-	-	-	13	-	17	-	28	-	33	-	36
	20	-	-	-	7	-	14	-	27	-	34	-	38
	25	-	-	-	-	-	7	-	22	-	26	-	29

FIG. 2.58 Primary Streamers Spatial - Time Characteristics in Air at N.T.P.

Point Plane Electrodes
 Point Anode
 $c = 100$ microns
 $g = 2.5$ cm.
 (a) 35-kv
 (b) 25-kv

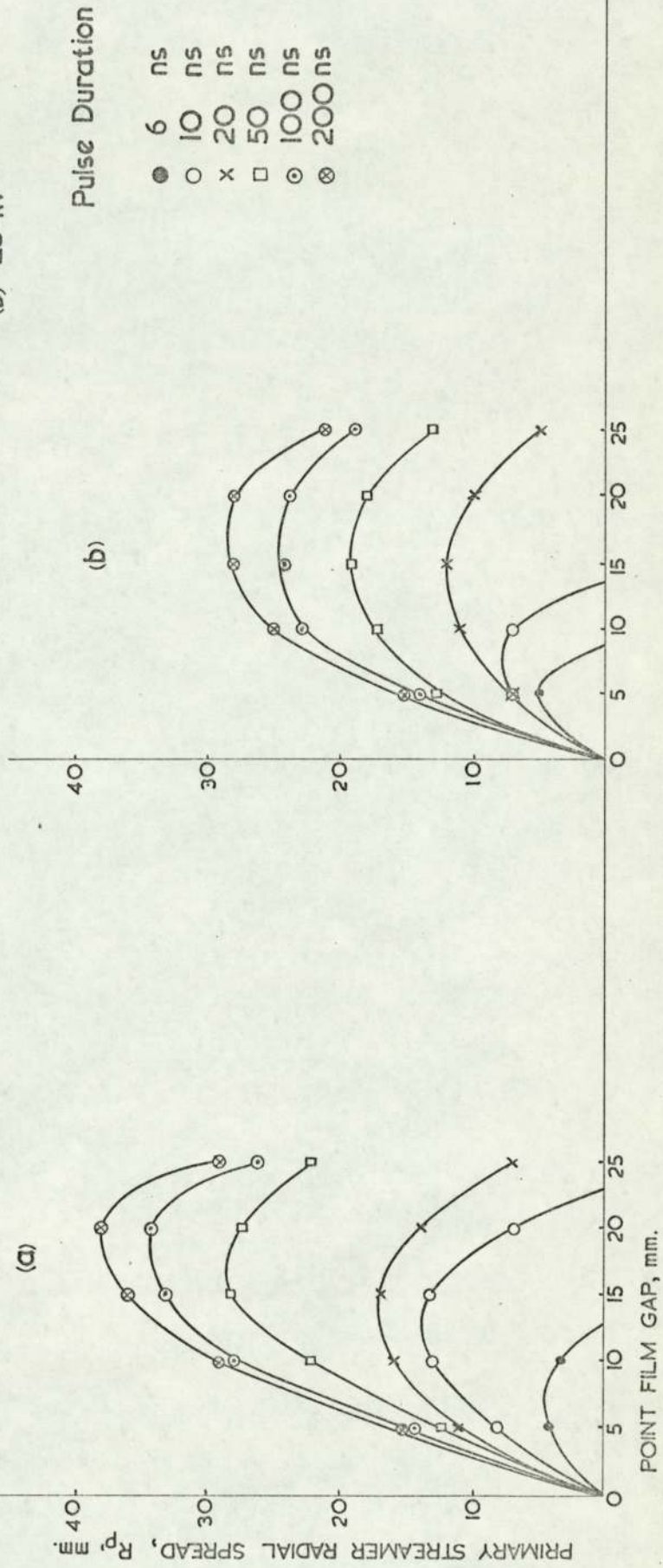


TABLE 2.10 Primary Streamer Velocity in Air at N. T. P.

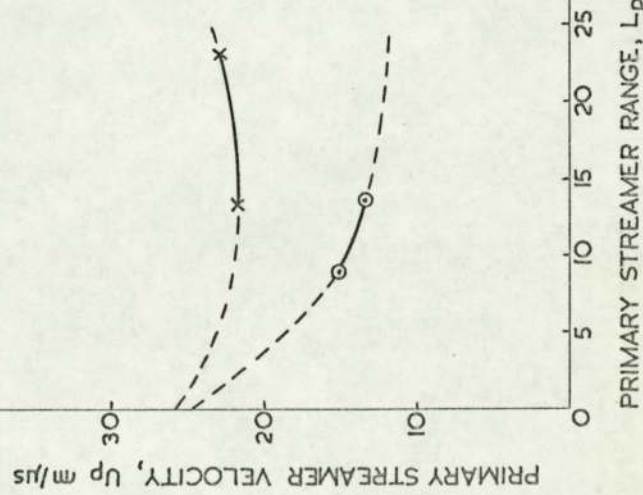
Point-plane electrodes; point-anode; gap length, G , = 2.5 cm; radius of curvature of point, C , = 100 microns; rectangular voltage wave.

Pulse Width ns	Streamer Range L_p mm		Velocity V_p m/ μ s	
	35 kV	25 kV	35 kV	25 kV
6	13	9	2.17	1.5
10	23	13.5	2.3	1.35

FIG. 2-59 Primary Streamers Velocity in Air at N.T.P.

Point-Plane Electrodes
 Point-Anode
 $c = 100$ microns
 $g = 2.5$ cm

x - 35 - kv
 o - 25 - kv



2.5 Theoretical Analysis

2.5.1 Potential and Potential Gradient in Point-Plane Electrode System

There has been diversity of opinion in the past about representing the electrostatic field pattern of point-plane electrode geometry^{28, 34, 37, 55, 130}. The main difficulty has arisen because of the fitting of the boundary condition since there is no co-ordinate system which will degenerate from a point to a plane.

The first contribution was made by Edmund²⁸ who represented the point by a paraboloid of revolution. This study was extended by Fitzsimmons³⁷. The point representation by a small sphere was suggested by Thomson¹³⁰ while more recent studies assume the point to be represented by a hyperbola of revolution.

Different representations of a point electrode in point-plane configuration are analysed and an overall comparison is made.

The potential gradient at any point across the gap is resolved with the computational aid. The first coefficient of ionization, α , is then calculated thus providing a measure of charge density of the primary streamer launcher.

2.5.1.1 Field about a Charged Sphere in Spherical Co-ordinates

Laplace's equation in spherical co-ordinates is:

$$\nabla^2 \phi = \frac{\partial^2 \phi}{\partial r^2} + \frac{2}{r} \frac{\partial \phi}{\partial r} + \frac{1}{r^2} \frac{\partial^2 \phi}{\partial \theta^2} + \frac{\cot \theta}{r^2} \frac{\partial \phi}{\partial \theta} + \frac{1}{r^2 \sin^2 \theta} \frac{\partial^2 \phi}{\partial \varphi^2} = 0 \quad (2.73)$$

Solutions are given in terms of the Legendre functions. The particular solutions are:

$$\phi = r^m P_m^n (\cos \theta) \sin n\psi$$

$$\phi = r^{-m-1} Q_m^n (\cos \theta) \cos \psi \quad (2.74)$$

$$\phi = r^m P_m^n (\cos \theta) \cos n\psi$$

The solution of Laplace's equation is of the form:

$$\begin{aligned} \phi = & \sum_{m=0}^{\infty} B_{m0} \left(\frac{r}{c}\right)^m P_m (\cos \theta) \\ & + \sum_{m=0}^{\infty} \sum_{n=1}^{\infty} \left\{ B_{mn} \left(\frac{r}{c}\right)^m P_m^n (\cos \theta) \cdot \cos n\psi \right. \\ & \left. + A_{mn} \left(\frac{r}{c}\right)^m P_m^n (\cos \theta) \cdot \sin n\psi \right\} \quad (2.75) \end{aligned}$$

where the coefficients are given by

$$B_{m0} = \frac{2m+1}{4\pi} \int_{-1}^{+1} \int_0^{2\pi} \phi_0(\theta, \psi) \cdot P_m(\mu) d\psi d\mu$$

$$B_{mn} = \frac{2n+1}{2\pi} \frac{(n-m)!}{(n+m)!} \int_{-1}^1 \int_0^{2\pi} \phi_0(\theta, \psi) P_n^m(\mu) \cos n\psi d\psi d\mu \quad (2.76)$$

$$A_{mn} = \frac{2n+1}{2\pi} \frac{(n-m)!}{(n+m)!} \int_{-1}^1 \int_0^{2\pi} \phi_0(\theta, \psi) P_n^m(\mu) \sin n\psi d\psi d\mu$$

Consider two concentric conducting spheres separated by a dielectric material. The boundary conditions are:

$$\begin{aligned} r = c & \quad \phi = V \\ r = b & \quad \phi = 0 \end{aligned} \quad (2.77)$$

where $b > c$. As the electric field depends on one space variable only, Laplace's equation simplifies to:

$$\nabla^2 \phi = \frac{d^2 \phi}{dr^2} + \frac{2}{r} \frac{d\phi}{dr} = 0 \quad (2.78)$$

The general solution of this differential equation is:

$$\phi = A + \frac{B}{r} \quad (2.79)$$

Substituting the boundary conditions (Eqn. 2.77), the potential at any point in the dielectric is given as:

$$\phi = \frac{VC}{b-c} \left[\frac{b}{r} - 1 \right] \quad (2.80)$$

The field strength at any point in the dielectric is:-

$$E = -\text{grad } \phi = -\frac{d}{dr} \frac{d\phi}{dr} = \frac{d}{dr} \frac{Vcb}{(b-c)r^2} \quad (2.81)$$

In a point-plane electrode geometry, where C is the radius of curvature of the point and G is the electrode gap, the boundary conditions suggest that the zero potential sphere is tangential to the plane electrode. The approximation is reasonably justified if $C \ll G$.

The potential is given by:

$$\phi = \frac{VC}{G} \left(\frac{C+G}{r} - 1 \right) \quad (2.82)$$

and the field strength is given by:

$$E = \frac{VC(C+G)}{Gr^2} \quad (2.83)$$

The maximum field strength occurring at $r = c$ is given by:

$$E_m = \frac{V(C+G)}{CG} \quad (2.84)$$

The field strength from Eqn. 2.8.3 in per unit value is given as:

$$\frac{E}{E_{av}} = \frac{C}{G} \left(\frac{C}{G} + 1 \right) \left(\frac{r}{G} \right)^{-2} \quad (2.85)$$

where the average field strength $E_{av} = \frac{V}{G}$.

2.5.1.2 Field about a Charged Paraboloid in Parabolic Co-ordinates

Parabolic co-ordinates (see Fig. 2.60) are related to rectangular co-ordinates by the equations:

$$\left. \begin{aligned} x &= \mu v \cos \psi \\ y &= \mu v \sin \psi \\ z &= \frac{1}{2} (\mu^2 - v^2) \end{aligned} \right\} (2.86)$$

The co-ordinate surfaces $v = \text{constant}$ are paraboloids of revolution opening upward:

$$x^2 + y^2 = v^2 (v^2 + 2z) \quad (2.87)$$

Metric coefficients for parabolic co-ordinates are

$$\begin{aligned} g_{11} &= g_{22} = \mu^2 + v^2 \\ g_{33} &= \mu^2 v^2 \end{aligned} \quad (2.88)$$

Laplace's equation is:

$$\begin{aligned} \nabla^2 \phi &= \frac{1}{\mu^2 + v^2} \left[\frac{\partial^2 \phi}{\partial \mu^2} + \frac{1}{\mu} \frac{\partial \phi}{\partial \mu} + \frac{\partial^2 \phi}{\partial v^2} + \frac{1}{v} \frac{\partial \phi}{\partial v} \right] \\ &+ \frac{1}{\mu^2 v^2} \frac{\partial^2 \phi}{\partial \psi^2} = 0 \end{aligned} \quad (2.89)$$

which separates into

$$\begin{aligned} \frac{d^2 M}{d\mu^2} + \frac{1}{\mu} \frac{dM}{d\mu} - \left(q^2 + \frac{p^2}{\mu^2} \right) M &= 0 \\ \frac{d^2 N}{dv^2} + \frac{1}{v} \frac{dN}{dv} - \left(q^2 + \frac{p^2}{v^2} \right) N &= 0 \quad (2.90) \\ \frac{d^2 \Psi}{d\psi^2} + p^2 \Psi &= 0 \end{aligned}$$

The third equation in Eqn. 2.90 gives the usual trigonometric functions. The other two give Bessel functions:

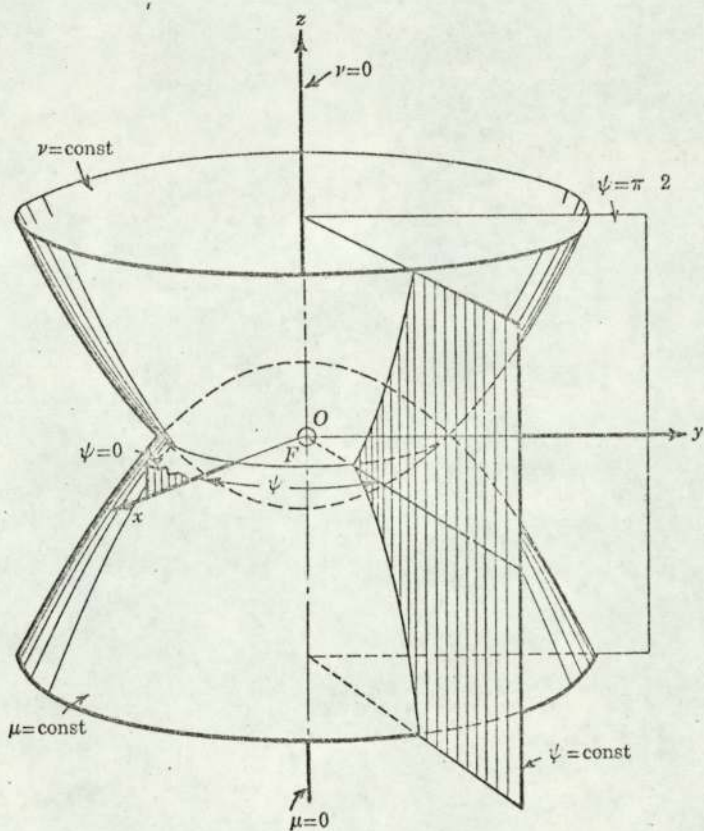


Figure 2.60

Parabolic Co-ordinates. The co-ordinate surfaces are paraboloids of revolution ($\mu = \text{const.}$ and $v = \text{const.}$), and meridian planes ($\psi = \text{const.}$).

$$\left. \begin{aligned} M &= A \mathcal{I} (iq\mu) + B \mathcal{I}_{-p} (iq\mu) \\ N &= A \mathcal{I}_p (qv) + B \mathcal{I}_{-p} (qv) \end{aligned} \right\} (2.91)$$

For ϕ to be a function of v only, the solution of Laplace's equation is:

$$\phi = A + B \ln v \quad (2.92)$$

Constants A and B are evaluated from the boundary conditions:

$$\left. \begin{aligned} v &= a, \quad \phi = V \\ v &= b, \quad \phi = 0 \end{aligned} \right\} (2.93)$$

The potential distribution within the electrode geometry is given by:-

$$\phi = V \frac{\ln \left(\frac{v}{b}\right)}{\ln \left(\frac{a}{b}\right)} \quad (2.94)$$

The field strength is

$$\begin{aligned} E = -\text{grad } \phi &= -d_v (\mu^2 + v^2)^{-\frac{1}{2}} \frac{\partial \phi}{\partial v} \\ &= -\frac{2v (\mu^2 + v^2)^{-\frac{1}{2}}}{v \ln \left(\frac{a}{b}\right)} \end{aligned} \quad (2.95)$$

For the upper surface $v = a$

$$E = -\frac{V (\mu^2 + a^2)^{-\frac{1}{2}}}{a \ln \left(\frac{a}{b}\right)} \quad (2.96)$$

The maximum gradient which occurs at $\mu = 0$ is given by:

$$E_{\max} = -\frac{V}{a^2 \ln \left(\frac{a}{b}\right)} \quad (2.97)$$

The relationship between $v = a$ representing an equipotential of the paraboloids and the radius of the curvature of the 'point' parabola, c , which is equal to the semi-latus rectum is given by:

$$\frac{a^2}{2} = \frac{C}{2} \quad (2.98)$$

The equipotential which just touches the plane $V = b$ is given, by:

$$\frac{b^2}{2} = G + \frac{C}{2} \quad (2.99)$$

where G is the electrode gap.

The field strength from Eqn. 2.95 is given by:

$$E = - \frac{2V(\mu^2 + V^2)^{-\frac{1}{2}}}{\sqrt{\ln\left(\frac{C}{2G + C}\right)}} \quad (2.100)$$

and its per unit value is

$$\frac{E}{E_{av}} = - \frac{2 \left(\frac{\mu^2}{G^2} + \frac{V^2}{G^2} \right)^{-\frac{1}{2}}}{\sqrt{\ln\left(1 + \frac{2G}{C}\right)}} \quad (2.101)$$

The maximum field strength is:

$$E_m = - \frac{2V}{C \sqrt{\ln\left(\frac{C}{2G + C}\right)}} \quad (2.102)$$

If $C \ll G$

$$E_m = - \frac{2V}{C \sqrt{\ln\left(\frac{C}{2G}\right)}} \quad (2.103)$$

The field strength along the main axis (z-axis) is:

$$E = - \frac{2V}{V^2 \sqrt{\ln\left(\frac{C}{2G + C}\right)}} \quad (2.104)$$

2.5.1.3 Field about a Charge Sphere in Bi-spherical Co-ordinates

Taking z-axis as the axis of rotation (see Fig. 2.61) for the bi-spherical co-ordinates (η, θ, ψ) , the following equations result:

$$\begin{aligned} x &= \frac{a \sin \theta \cos \psi}{\cosh \eta - \cos \theta} \\ y &= \frac{a \sin \theta \sin \psi}{\cosh \eta - \cos \theta} \end{aligned} \quad (2.105)$$

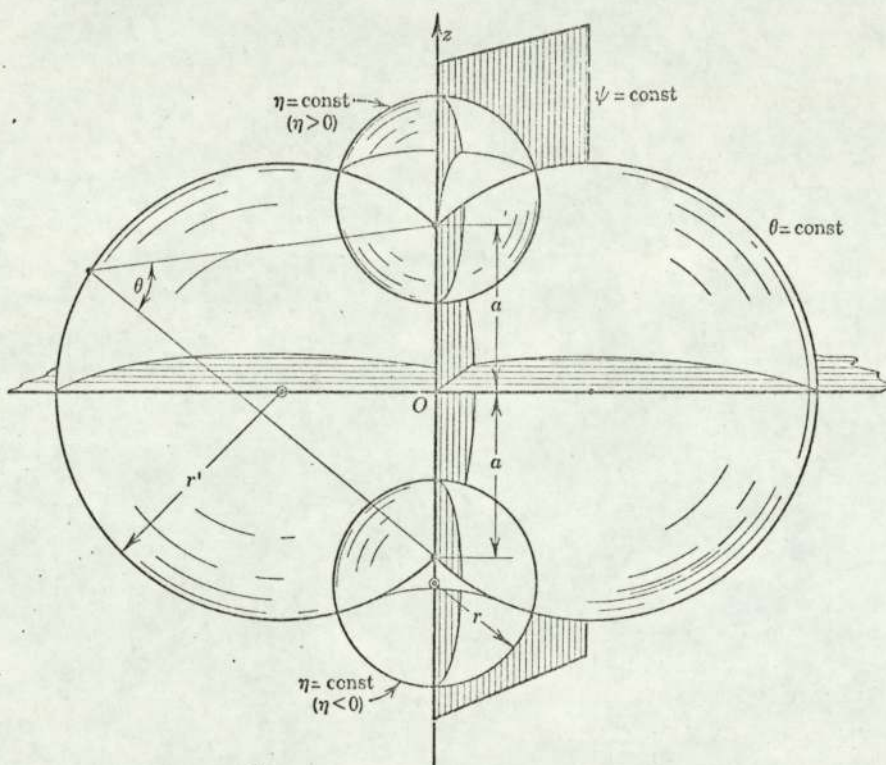


Figure 2.61

Bi-spherical co-ordinates. Surfaces, when η is constant, are spheres with centres on the z -axis.

$$z = \frac{a \sinh \eta}{\cosh \eta - \cos \theta} \quad (2.105)$$

The metric coefficients for the bi-spherical co-ordinates are:

$$\left. \begin{aligned} g_{11} &= g_{22} = \frac{a^2}{(\cosh \eta - \cos \theta)^2} \\ g_{33} &= \frac{a^2 \sin^2 \theta}{(\cosh \eta - \cos \theta)^2} \\ g^{\frac{1}{2}} &= \frac{a^3 \sin \theta}{(\cosh \eta - \cos \theta)^2} \end{aligned} \right\} (2.106)$$

Laplace's equation, being R - separable, may be expressed in bi-spherical co-ordinates as:

$$\left. \begin{aligned} \frac{d^2 H}{d \eta^2} + H \left(-\frac{1}{4} - \alpha_2 \right) &= 0 \\ \frac{1}{\sin \theta} \frac{d}{d \theta} \left(\sin \theta \frac{d \mathbb{H}}{d \theta} \right) + \mathbb{H} \left(\alpha_2 - \frac{\alpha_3}{\sin^2 \theta} \right) &= 0 \end{aligned} \right\} (2.107)$$

$$\frac{d^2 \Psi}{d \psi^2} + \alpha_3 \Psi = 0$$

The particular solutions in the case of axial symmetry with the potential as a function of η and θ only are:

$$\left. \begin{aligned} \phi &= (\cosh \eta - \cos \theta)^{\frac{1}{2}} \exp \left[\pm \left(p + \frac{1}{2} \right) \eta \right] P_p (\cos \theta) \\ \phi &= (\cosh \eta - \cos \theta)^{\frac{1}{2}} \exp \left[\pm \left(p + \frac{1}{2} \right) \eta \right] Q_p (\cos \theta) \end{aligned} \right\} (2.108)$$

The electrostatic field between the two equal spheres is given by the solution:

$$\phi = (\cosh \eta - \cos \theta)^{\frac{1}{2}} \sum_{n=0}^{\infty} A_n \frac{\sinh \left[\left(n + \frac{1}{2} \right) \eta \right]}{\sinh \left[\left(n + \frac{1}{2} \right) \eta \right]} P_n (\cos \theta) \quad (2.109)$$

substituting the boundary condition:

$$\begin{aligned} \phi &= +V & \text{when } \eta &= \eta_0 \\ \phi &= -V & \text{when } \eta &= -\eta_0 \end{aligned} \quad (2.110)$$

gives:

$$\frac{V}{\cosh(\eta_0 - \cos \theta)^{\frac{1}{2}}} = \sum_{n=0}^{\infty} A_n P_n(\cos \theta) \quad (2.111)$$

The left-hand function is expanded in a series of Legendre functions with coefficients of the series given as:

$$A_n = V \left(\frac{2n+1}{2} \right) \int_{-1}^1 \frac{P_n(u)}{(\cosh \eta_0 - u)^{\frac{1}{2}}} du \quad (2.112)$$

where $u = \cos \theta$.

The electric field strength is given by:

$$E = -\text{grad } \phi = -\frac{1}{C} (\cosh \eta - \cos \theta) \left[d_\eta \frac{\partial \phi}{\partial \eta} + d_\theta \frac{\partial \phi}{\partial \theta} \right] \quad (2.113)$$

From Eqns. 2.109 and 2.113:

$$\begin{aligned} E &= -\frac{1}{C} (\cosh \eta - \cos \theta)^{\frac{1}{2}} \left[d_\eta \sum_{n=0}^{\infty} \frac{A_n P_n(\cos \theta)}{\sinh \left[(n + \frac{1}{2}) \eta_0 \right]} \right. \\ &\quad \cdot \left. \frac{1}{2} \left\{ \sinh \eta \sinh \left[(n + \frac{1}{2}) \eta \right] + (n + \frac{1}{2}) (\cosh \eta - \cos \theta) \cosh \left[(n + \frac{1}{2}) \eta \right] \right\} \right. \\ &\quad \left. + d_\theta \sum_{n=0}^{\infty} \frac{A_n \sinh \left[\eta (n + \frac{1}{2}) \right]}{\sinh \left[\eta_0 (n + \frac{1}{2}) \right]} \left\{ \frac{1}{2} \sin \theta \cdot P_n(\cos \theta) + (\cosh \eta - \cos \theta) P_n(\cos \theta) \right\} \right] \end{aligned} \quad (2.114)$$

At the boundaries $\eta = \pm \eta_0$, E is perpendicular to the spherical

surface but, in general, E has both η and θ components. The maximum gradient, E_m , occurs at $\theta = \pi$ and $\eta \rightarrow \eta_0$. Hence

$$E_m = \frac{1}{C} (\cosh \eta_0 + 1)^{\frac{1}{2}} \sum_{n=0}^{\infty} (-1)^n A_n \left\{ \frac{1}{2} \sinh \eta_0 + (n + \frac{1}{2})(\cosh \eta_0 + 1) \coth \left[(n + \frac{1}{2})\eta_0 \right] \right\} \quad (2.115)$$

It can be seen that a one-dimensional solution is not possible in bi-spherical co-ordinates. The boundary condition does not provide equipotentials for surfaces, $\eta = \text{constant}$, of the same family. In general, therefore, a series solution is necessary even in the simplest case.

2.5.1.4 Field about a Charged Hyperboloid in Prolate Spheroidal Co-ordinates

Prolate spheroidal co-ordinates are generated by rotating an orthogonal family of confocal ellipses and hyperbolas about the major axis of the ellipse (see Fig. 2.62).

Prolate spheroidal co-ordinates (η, θ, ψ) are related to rectangular co-ordinates by the equations:

$$\left. \begin{aligned} x &= a \sinh \eta \sin \theta \cos \psi \\ y &= a \sinh \eta \sin \theta \sin \psi \\ z &= a \cosh \eta \cos \theta \end{aligned} \right\} (2.116)$$

The metric coefficients for prolate spheroidal co-ordinates are given as:

$$\left. \begin{aligned} g_{11} &= g_{22} = a^2 (\sinh^2 \eta + \sin^2 \theta) \\ g_{33} &= a^2 \sinh^2 \eta \sin^2 \theta \\ g^{\frac{1}{2}} &= a^3 \sinh \eta \sin \theta (\sinh^2 \eta + \sin^2 \theta) \end{aligned} \right\} (2.117)$$

Laplace's equation in prolate spheroidal co-ordinates is:

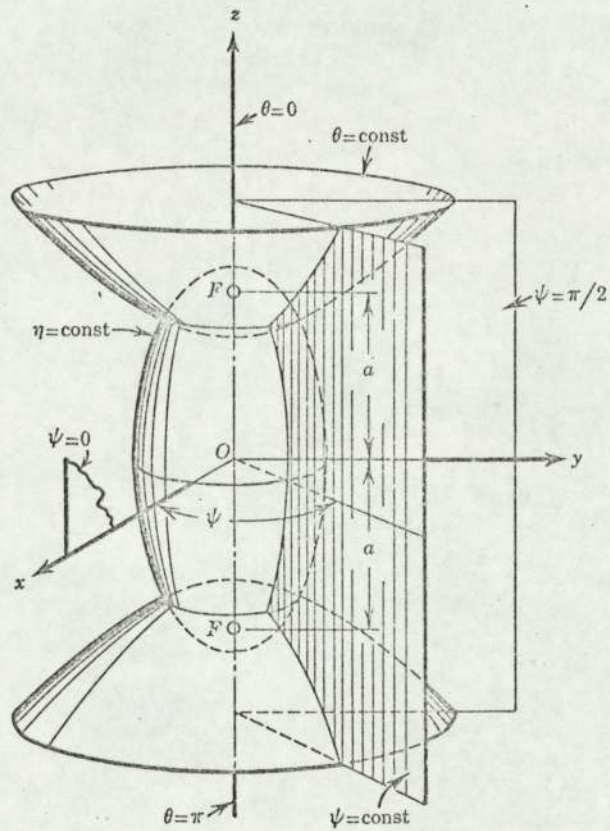


Figure 2.62

Prolate Spheroidal Co-ordinates.

The co-ordinate surfaces are hyperboloid when θ is constant.

$$\nabla^2 \phi = \frac{1}{a^2 (\sinh^2 \eta + \sin^2 \theta)}$$

$$\left\{ \frac{\partial^2 \phi}{\partial \theta^2} + \coth \eta \frac{\partial \phi}{\partial \eta} + \frac{\partial^2 \phi}{\partial \theta^2} + \cot \theta \frac{\partial \phi}{\partial \theta} + \frac{1}{a^2 \sinh^2 \eta \sin^2 \theta} \frac{\partial^2 \phi}{\partial \psi^2} \right\} = 0 \quad (2.118)$$

The elementary solution is:

$$\phi = H(\eta) \cdot \textcircled{H}(\theta) \cdot \Psi(\psi) \quad (2.119)$$

$$\text{where } H = P_p^q(\cosh \eta), \quad \textcircled{H} = Q_p^q(\cosh \eta)$$

$$\textcircled{H} = P_p^q(\cos \theta), \quad \textcircled{H} = Q_p^q(\cos \theta) \quad (2.120)$$

$$\Psi = \frac{\sin}{\cos} (q\psi)$$

If the solution (a) has axial symmetry and is therefore independent of ψ , and (b) depends on single variable, e.g. $\phi = \phi(\theta)$, Laplace's equation becomes:

$$\frac{d^2 \phi}{d\theta^2} + \cot \theta \frac{d\phi}{d\theta} = 0 \quad (2.121)$$

and the solution is:

$$\phi = C \ln \cot \left(\frac{\theta}{2} \right) + D \quad (2.122)$$

The electric field in a system having axial symmetry and single variable solution is give by Eqn. 2.122.

Let the boundary condition be:

$$\begin{aligned} \theta = \theta_0, \quad \phi &= V \\ \theta \rightarrow \frac{\pi}{2}, \quad \phi &= 0 \end{aligned} \quad (2.123)$$

The coefficients C and D become:

$$D = 0$$

$$C = \frac{V}{\ln \cot \left(\frac{\theta_0}{2} \right)} \quad (2.124)$$

The solution therefore becomes:

$$\phi' = V \frac{\ln \cot \left(\frac{\theta}{2} \right)}{\ln \cot \left(\frac{\theta_0}{2} \right)} \quad (2.125)$$

The electric field strength is given by:

$$E = -a_{\theta} \frac{1}{(g_{11})^{\frac{1}{2}}} \frac{d\phi}{d\theta} \quad (2.126)$$

From Eqns. 2.117 and 2.126

$$E = \frac{V (\sinh^2 \eta + \sin^2 \theta)^{-\frac{1}{2}}}{a \left(\ln \cot \frac{\theta_0}{2} \right) \sin \theta} \quad (2.127)$$

The maximum field strength

$$E_m = \frac{V}{a \left(\ln \cot \frac{\theta_0}{2} \right) \sin^2 \theta_0} \quad (2.128)$$

The coefficients a and θ_0 in terms of radius of curvature of the point-electrode, C , and the electrode gap, G , are given as:

$$\theta_0 = \arctan \left(\frac{C}{G} \right)^{-\frac{1}{2}} \quad (2.129)$$

$$a = \frac{G}{\cos \theta_0}$$

The per unit value of field strength from Eqn. 2.127 becomes:

$$\frac{E}{E_{av}} = \frac{\cos \theta_0 (\sinh^2 \eta + \sin^2 \theta)^{-\frac{1}{2}}}{\sin \theta \left(\ln \cot \frac{\theta_0}{2} \right)} \quad (2.130)$$

The simplest solution of different field studies carried out on point-plane electrode geometry is provided by spherical co-ordinates (see Section 2.5.1.1) which also results in the highest value of field strength near the point.

The closest approximation to a point-plane system of the type employed throughout this study is found to be that of a hyperboloid in prolate spheroidal co-ordinates. A general solution for the electric field in per unit value can readily be achieved by computational means.

The result of a computer program (see Appendix 7.1) designed for the University's Elliott 803 shows that the field strength in the electrode gap a short distance away from the point-electrode is sufficiently low to be assumed as "zero" field. There exists no possible ionization process in this region prior to the generation of primary streamers at the point. Introduction of electromagnetic radiation sensitive film, therefore, introduces negligible disturbance in the field pattern in this region.

2.5.2 Positive Primary Streamer Threshold

In a point-plane electrode system, if the point is represented by a charged hyperboloid in a prolate spheroidal co-ordinate, the electric field (see Section 2.5.1.4) is given by:

$$E = \frac{V (\sinh^2 \eta + \sin^2 \theta)^{-\frac{1}{2}}}{a \left(\ln \cot \frac{\theta_0}{2} \right) \sin \theta}$$

In the range of $\theta \leq \theta \leq \frac{\pi}{2}$ (i. e. $0 \leq z \leq G$) along the line $\eta = 0$ (i. e. z-axis) from Eqn. 2.116

$$z = a \cos \theta \quad (2.131)$$

and from Eqn. 2.129

$$z = \frac{G}{\cos \theta_0} \cos \theta \quad (2.132)$$

The per unit value of the distance from the plane-electrode along the main field axis is:

$$M = \frac{z}{G} = \frac{\cos \theta}{\cos \theta_0} \quad (2.133)$$

and the per unit value of the electric field on the same axis is:

$$\frac{E}{E_{av}} = \frac{\cos \theta_0}{\sin^2 \theta \left(\ln \cot \frac{\theta_0}{2} \right)} \quad (2.134)$$

where the average electric field $E_{av} = \frac{V}{G}$

A computer program of electric field strength from Eqn. 2.144 in air at N. T. P. is planned for Digital PDP 9 and its flow diagram is shown in Fig. 2.63. The results with the aid of the collected data of von Engel (see Fig. 2.5) determine the level of charge generation in proximity of the point-electrode (see Fig. 2.64).

The primary streamer inception voltage for a 2.5 cm gap is deduced from the results shown in Fig. 2.56 to be 8 kV. The critical value of αd at this potential level is given by:

$$\alpha d = 20 \quad (2.135)$$

This corresponds to a charge amplification of

$$n = \exp(\alpha d) \approx 5 \times 10^8 \text{ electrons} \quad (2.136)$$

These values are in accord with the results of Raether and co-workers¹¹⁶ in uniform electric field.

2.5.3 Theory of Positive Primary Streamer Propagation

2.5.3.1 Introduction

The propagation of a positive primary streamer in an inhomogeneous field in atmospheric air is represented by a model. This model is based on the behaviour of the streamer tip in the low field region irrespective of the conductivity of the streamer tail.

The effective process of the streamer discharge is localised to one electrode by the utilisation of a non-uniform field of point-plane geometry. In this type of system the applied field is only high near the point-electrode while further away the field strength is negligible. This is verified by the results of electric field study (see Section 2.5.1).

The conductivity of the streamer tail is neglected and the streamer tip is assumed to be isolated from the point-anode. This assumption is verified from the experimental results.

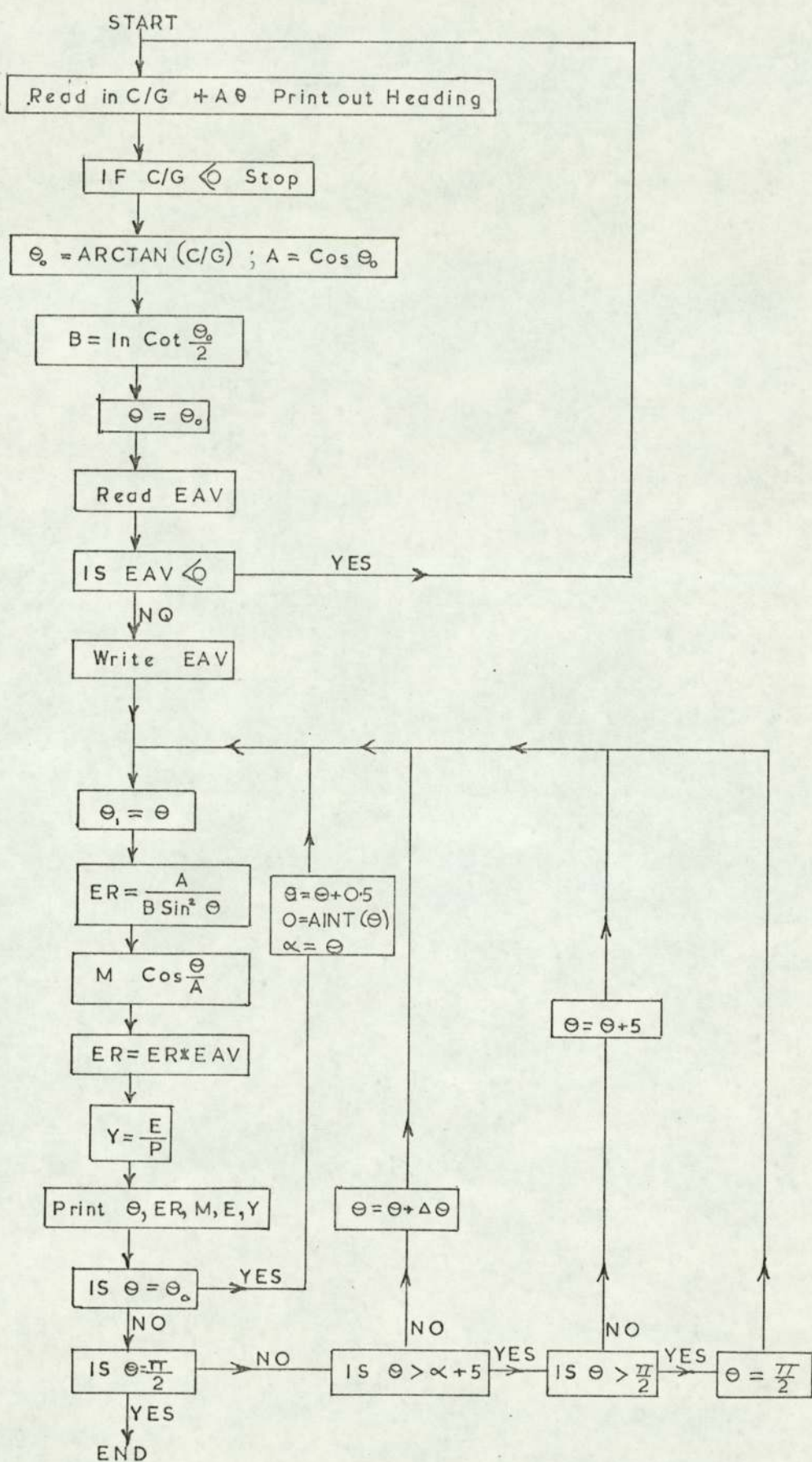


FIG 2.63 Computer flow diagram of electric field strength along the main field axis of point plane electrode

TABLE 2.11.

Calculated values of electric field strength in the electrode gap along the main field axis in air at N. T. P. by computational technique.

Radius of curvature of the point electrode, $C = 100$ micron; gap length, $G = 2.5$ cm; applied voltage, $V = 8$ -kV.

Degrees	E/E_{av}	M	E kV	E/P v/cm. torr
3.62	72.4729	1.0000	231.9	305.1
4.00	59.3697	0.9996	190.0	250.0
4.50	46.9296	0.9989	150.2	197.6
5.00	38.0314	0.9982	121.7	160.1
5.50	31.4476	0.9974	100.6	132.4
6.00	26.4402	0.9965	84.6	111.3
6.50	22.5432	0.9956	72.1	94.9
7.00	19.4511	0.9945	62.2	81.9
7.50	16.9566	0.9934	54.3	71.4
8.00	14.9150	0.9922	47.7	62.8
8.50	13.2230	0.9910	42.3	55.7
9.00	11.8051	0.9897	37.8	49.7
9.50	10.6051	0.9883	33.9	44.7
14.50	4.6082	0.9701	14.7	19.4
19.50	2.5927	0.9445	8.3	10.9
24.50	1.6799	0.9118	5.4	7.1
29.50	1.1914	0.8721	3.8	5.0
34.50	0.9005	0.8258	2.9	3.8
39.50	0.7140	0.7732	2.3	3.0
44.50	0.5880	0.7147	1.9	2.5
49.50	0.4996	0.6507	1.6	2.1
54.50	0.4359	0.5819	1.4	1.8
59.50	0.3891	0.5086	1.2	1.6
64.50	0.3546	0.4314	1.1	1.5
69.50	0.3293	0.3509	1.1	1.4
74.50	0.3111	0.2678	1.0	1.3
79.50	0.2988	0.1826	1.0	1.3
84.50	0.2916	0.0960	0.9	1.2
89.50	0.2889	0.0087	0.9	1.2

TABLE 2.12.

Charge generation near the point electrode along the
main field axis in air at N. T. P.

Radius of curvature of the point $C = 100$ microns; gap
length $G = 2.5$ cm; applied voltage 8 - kV

Distance from the point l , cm microns	$\frac{E}{p}$ V/cm torr	$\frac{\alpha}{p}$ ion pairs/cm	α ion pairs/cm
0	305.1	5.0	3800
10	205.0	4.0	3040
28	197.6	3.5	2660
45	160.1	2.0	1520
65	132.4	1.5	1140
88	111.3	0.9	684
110	94.9	0.55	418
138	81.9	0.5	380
165	71.4	0.4	304
195	62.8	0.1	76
225	55.7	0.07	53
257	49.7	0.055	42
293	44.7	0.015	11
750	19.4	0.0001	0.07

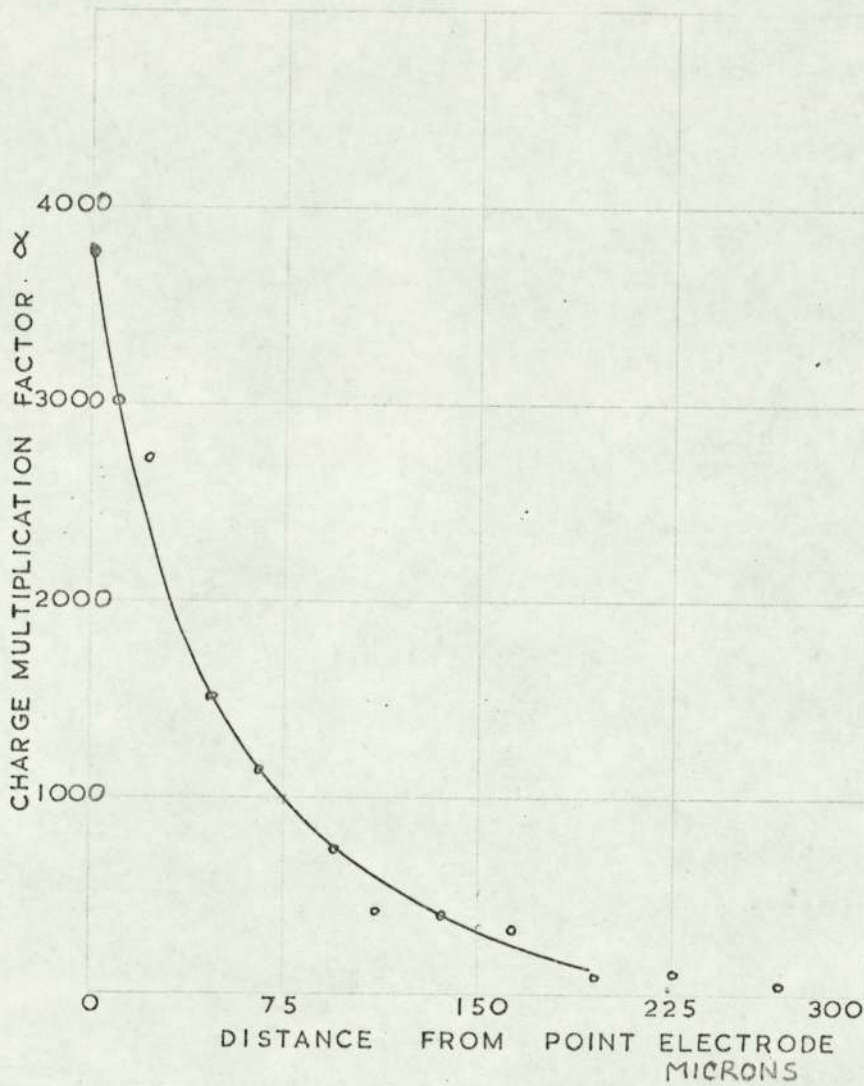


Fig. 2.64 CHARGE GENERATION IN THE PROXIMITY OF THE POINT-ELECTRODE IN AIR AT N.T.P.

$V = 8 - kv$

$C = 100 \text{ microns}$

$G = 2.5 \text{ cm}$

POINT ANODE

2.5.3.2 Propagation Criterion

At a certain potential applied to the point-electrode, called streamer inception voltage, a streamer considered as an isolated region of excitation and ionization extends out from the point. As the potential increases, the streamer travels further into the low field region and may finally reach the plane-cathode. The primary streamers while progressing across the gap leave behind a plasma tail assumed to be almost neutral.

The streamer tip at any instant of time is assumed to consist of a sphere of positive charge with a tail containing a nearly equal number of electrons and positive ions.

The criterion for primary streamer propagation in zero applied electric field is suggested as being the magnitude of charge within the streamer tip reaching a certain level.

It is proposed that the streamer ceases to propagate as the result of diffusion and attachment and energy loss due to formation of ion pairs.

The positive streamer growth is due to the movement of electrons into the positively charged tip. These electrons are produced by photo-ionization in advance of the streamer tip.

If an instant of time is assumed when the streamer tip is a sphere of charge having a radius r_0 and a centre O at the reference point, a single photo-electron is created at a distance r_1 from the centre of the sphere and moves to a point r_2 . This forms an avalanche of multiplication given by:

$$n_e = \exp \left(\int_{r_2}^{r_1} \alpha \, dr \right) \quad (2.137)$$

having a diffusion radius given by (see Appendix 7.2)

$$r_d = \left(6 \int_{r_2}^{r_1} \frac{D}{U_e} \, dr \right)^{\frac{1}{2}} \quad (2.138)$$

where α = Townsend's first ionization coefficient

D = diffusion coefficient

u_e = electron drift velocity.

If sufficient electron multiplication is reached up to the sphere, then the original positive charge is neutralised and a new positive region is created. This charge region is again assumed to be spherical having a radius equal to diffusion radius r_0 and a centre located further away from the point-anode.

The condition for continuous streamer propagation requires that the radius of the two spheres be the same, i.e. each succeeding region of positive charge must be exactly similar to the one preceding it. This model implies that the streamer tip propagates in discrete steps.

The requirements for low-field strength propagation of the primary streamers are:-

- (a) The number of new positive ions created by electron avalanche must be equal to n_0 , the number of ions in the original sphere.
- (b) The diffusion radius of the avalanche head must not become larger than r_0 , the radius of the original sphere.
- (c) The avalanche must reach the required amplification before the two charge regions begin to overlap, i.e. $2r_d \ll r_2$.

The distance r_1 , at which a single photo-electron is created ahead of the streamer tip, is chosen as a value that provides equal probability for ionization and dissociative attachment. This requirement for the limiting value of r_1 occurs (45) in an electric field given by:

$$\frac{E}{p} = 30 \text{ v/cm torr} \quad (2.139)$$

The electric field at a distance r is given by:

$$E = \frac{Q}{4\pi\epsilon_0 r^2} \text{ v/m} \quad (2.140)$$

where charge $Q = n_e q$ coulomb.

The value of r_1 is deduced from Eqns. 2.139 and 2.140 in terms of number of electrons, n_e , in air at N.T.P.

$$r_1 = 2.5 \times 10^{-6} (n_e)^{\frac{1}{2}} \text{ cm} \quad (2.141)$$

The total number of electrons, n_e , can be deduced from Eqn. 2.137 by graphically integrating the curve of α as a function of r between the limits r_1 and r_2 . A value of n_e is first chosen which provides a value of r_1 from Eqn. 2.141. The integration then proceeds with such values of r_2 which will result in the same electron density n_e .

The ratio of diffusion coefficient to electron drift velocity is given⁽³¹⁾ by:

$$\frac{D}{u_e} = \frac{k T_e}{q E} \quad (2.142)$$

where $k = 1.37 \times 10^{-16}$ ergs per $^{\circ}\text{K}$ and the electron temperature, T_e , for air at a value of $\frac{E}{p} = 30$ is given by

$$T_e = 2.32 \times 10^4 \text{ } ^{\circ}\text{K}.$$

$$\therefore \frac{D}{u_e} = 6.6 \times 10^{-3} (E)^{-1} \quad (2.143)$$

where E is in e. s. v/cm.

The diffusion radius, r_d , can be calculated from Eqns. 2.138 and 2.143 for appropriate values of r_1 and r_2 . The calculated results for values of r_1 , r_2 and r_d are summarised in Table 2.13.

The results show that for values of $n_e \leq 10^7$ condition 'c' for primary streamer propagation, i.e. $2r_0 \leq r_2$, is not satisfied. This implies that the avalanche head will reach the edge of the sphere of positive charge before achieving the necessary amplification.

A minimum value of electron density, $n_e = 10^8$, in the streamer head of diameter 60 microns fulfils the necessary

TABLE 2.13

Calculated Primary Streamer Parameters for air at N.T.P.

Number of electrons n_e	E/P v/cm ² torr	length r_1 microns	length r_2 microns	Diffusion radius r_d microns
10^6	30	25	0.8	11
	50	19.4	0.8	10
	100	13.8	0.3	8
10^7	30	79	7.0	19
	50	61.2	7.0	17
	100	43.5	5.0	14
10^8	30	250	65	29
	50	194	65	26
	100	138	56	21
10^9	30	790	300	51
	50	612	300	41
	100	435	265	30
10^{10}	30	2500	1230	82
	50	1940	1230	61
	100	1380	1090	39

requirements. This suggests that a primary streamer tip containing at least 10^8 ion pairs with a radius of 30 microns becomes self-propagating in zero electric field.

2.5.4 Theory of Positive Secondary Streamer Propagation

2.5.4.1 Introduction

A single positive secondary streamer a distance l from the point-anode electrode is considered. The potential v , the electric field E , the electron impact multiplication factor α and the electron and ion densities, n_e and n_i of the streamer are shown in Fig. 2.65.

The high potential gradient at the tip of the streamer results in intense acceleration of advancing electrons leaving behind a relatively static positive space charge. The streamer advances in this fashion ahead of an electrically conducting visible plasma.

2.5.4.2 Propagation Criterion

As the conducting plasma propagates in the main electric field direction, charge must be provided to keep the streamer tip at a potential v . Equations governing potential v and current i along the streamer having a resistance of R ohm per unit length and a capacitance of C farad per unit length are given by:

$$\frac{\partial^2 v}{\partial x^2} = R C \frac{\partial v}{\partial t} \quad (2.144)$$

$$\frac{\partial^2 i}{\partial x^2} = R C \frac{\partial i}{\partial t}$$

These equations are of the forms

$$\nabla^2 J = \mu \sigma \frac{\partial J}{\partial t} \quad (2.145)$$

Called the diffusion equation. Where J is a function of x only and the Laplacian operator reduces to:

$$\nabla^2 = \frac{\partial^2}{\partial x^2}$$

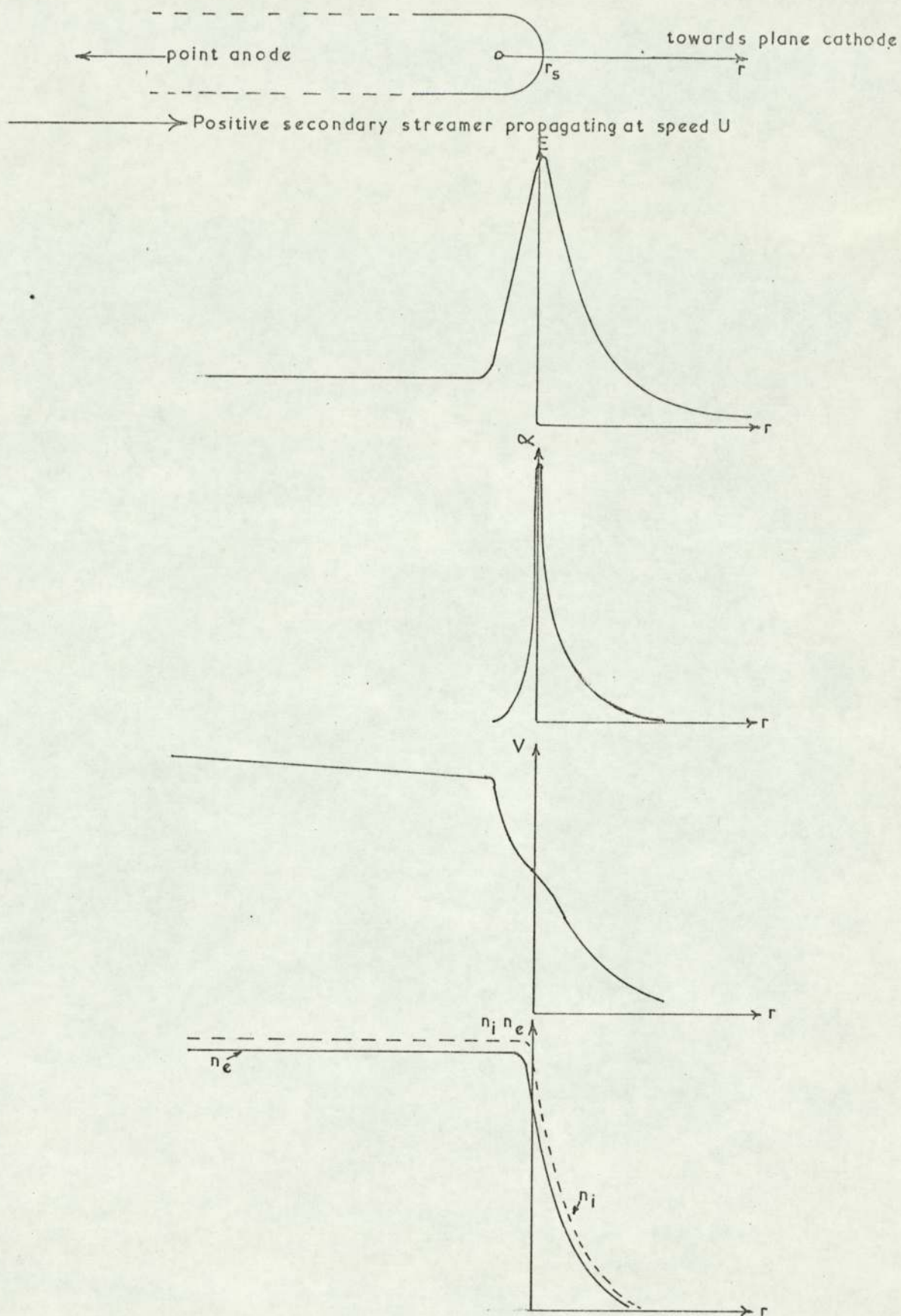


Fig.2.65 SOME PARAMETERS OF A POSITIVE SECONDARY STREAMER

A possible solution for Eqn. 2.144 is given from Appendix 7.3 as:

$$\mathcal{U}(x, t) = V_p \operatorname{erfc} \left[\frac{x}{2} \left(\frac{t}{RC} \right)^{-\frac{1}{2}} \right] \quad (2.146)$$

where V_p = potential of the point-anode, and R and C are given from Appendix 7.4 as:

$$R = \frac{4 n_{es}}{n_{e2} r_s U_r} \quad (2.147)$$

$$C = \frac{1}{2 \ln \left(\frac{r_\infty}{r_s} \right)} \quad (2.148)$$

$$\therefore \mathcal{U}(x, t) = V_p \left[1 - \operatorname{erf} x \left(n_{es} \right)^{\frac{1}{2}} \left(2t n_{e2} r_s U_r \ln \frac{r_\infty}{r_s} \right)^{-\frac{1}{2}} \right] \quad (2.149)$$

where erf is the error function and erfc is the complementary error function given by:

$$\operatorname{erfc} y = 1 - \operatorname{erf} y \quad (2.150)$$

At the streamer tip assuming

$$x = ut$$

and substituting, from Appendix 7.5

$$V_p = E_p r_s \ln \left(\frac{r_\infty}{r_s} \right) \quad (2.151)$$

The potential of streamer tip is therefore given by:

$$\begin{aligned} \mathcal{U}(x, t) &= V_p \left[1 - \operatorname{erf} \left(\frac{1}{2} \frac{U}{U_r} \cdot \frac{n_{es}}{n_{e2}} \cdot \frac{E_p G}{V_p} \cdot \frac{x}{G} \right)^{\frac{1}{2}} \right] \\ &= V_p \left[1 - \operatorname{erf} \left(\frac{1}{2} Q x_{p.u.} \right)^{\frac{1}{2}} \right] \end{aligned} \quad (2.152)$$

$$\text{where } Q = \frac{U}{U_r} \frac{n_{es}}{n_{e2}} \cdot \frac{E_p G}{V_p} \quad (2.153)$$

$$\text{and } x_{p.u.} = \frac{x}{G}$$

The voltage-streamer range characteristics for different values of Q are shown in Fig. 2.66.

The particular case for half voltage at half point across the

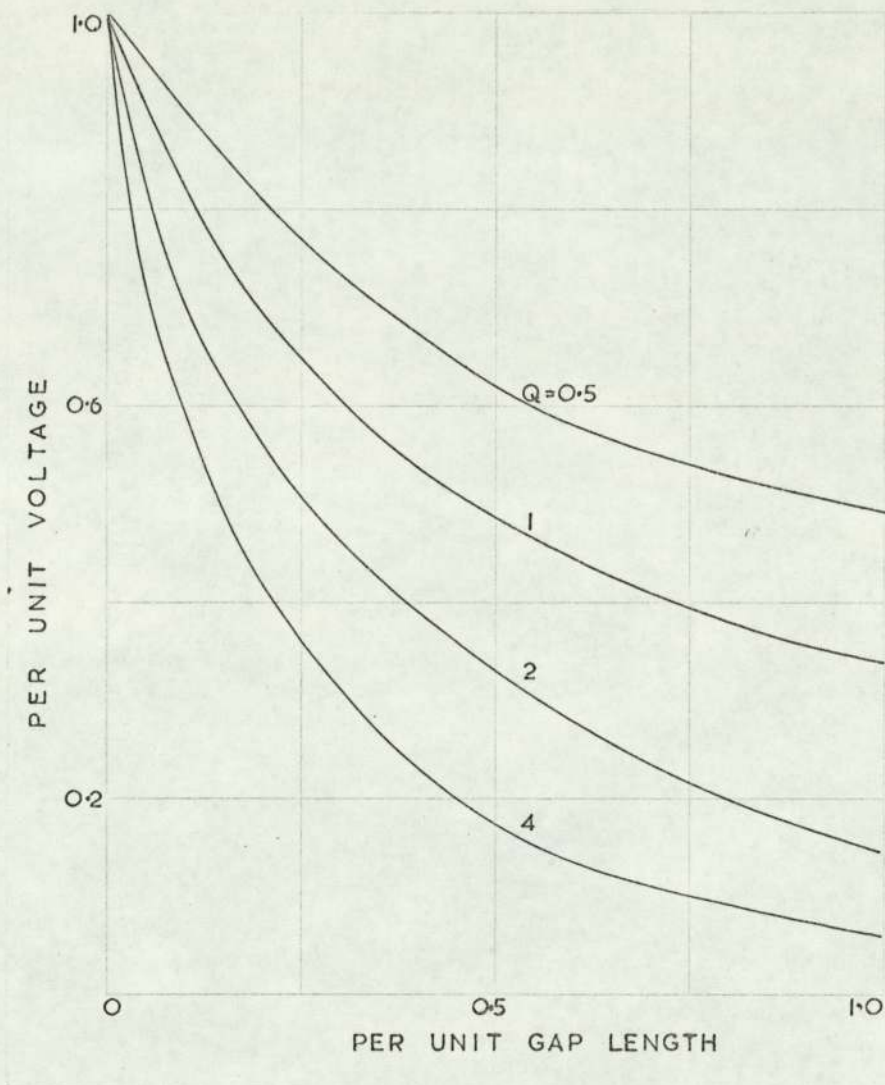


Fig. 2.66 VOLTAGE-STREAMER RANGE FOR DIFFERENT VALUES OF Q.

is taken as the condition for secondary streamer propagation with constant velocity across the gap. This case corresponds to $Q = 1$, i. e.

$$V_p = \frac{U}{U_r} \frac{n_{es}}{n_{e2}} E_p G \quad (2.154)$$

2.6 Discussion

The primary streamer process in a point-to-plane gap indicates the similarity of the positive and negative Lichtenberg figures to the positive and negative streamers. The streamers move through the air above the film but very close to its surface through the inductive attraction of the streamer tip. This permits single streamers, too faint to be photographed directly, to be imprinted on the film surface.

With impulse potentials, streamers start at the streamer threshold and the primary streamers cross the electrode gap at potentials well below the breakdown value.

The electric field studies in the point-to-plane electrode geometry indicate a vertical zero field in the gap a short distance away from the point. The absence, therefore, of any preferred path for the streamer propagation results in extensive branching of the discharge.

In the point-to-plane electrode gap, in contrast to the uniform field gap, where the progress of the streamer is in part dependent on the imposed field, the primary streamer has its energy stored in its tip while in the high potential region. This high energy carries the streamer tip, with some dissipation by branching, ionization, and excitation, across the zero-field regions of the gap. In crossing these regions the streamer leaves behind only a weakly conducting channel.

From these observations, a theory is developed for primary streamer propagation in zero field region. The predicted values of streamer tip diameter, charge per unit length of the advance, and velocity, are confirmed by experimental measurements.

The magnitude of charge on the primary streamer tip of about 10 pico-coulomb is of the same order as suggested by

Raether¹¹⁶ and Loeb and Meek⁷⁸. The radius of the primary streamer tip of about 30 microns agrees with the experimental measurements of the streamer tract on the film.

It is noted from the reported results that, for the potentials at which the positive primary streamers did not advance across the whole gap, the velocities were high near the point-anode and fell in mid-gap toward the cathode. The average speed of propagation with a point of radius of curvature 1.00 mm and a gap of 2.5 cm is about 2×10^8 cm/sec. This observation is in agreement with those obtained by photomultiplier techniques^{20, 51, 59}.

The time resolution using E-M radiation sensitive film technique is superior to other techniques as it indicates the initial decline in velocity of primary streamers that do not approach the cathode.

The extensive branching of the primary streamers in the zero field region of the gap lead to a number of streamer tips reaching the plate. The bridging of the gap by the subsequent secondary streamers and the resultant breakdown, therefore, does not necessarily occur at the shortest gap length.

The secondary positive streamer may start from the point-anode before the arrival of the tip of the first primary streamer at the plane-cathode. The secondary streamer is associated with an increase in current flow in the main stems, fed by currents from the branches and augmented by ionization in the point-anode field.

Owing to its high conductivity, the secondary streamer projects a fraction of the anode potential into the gap at its tip.

A theory suggested for the positive secondary streamer propagation is based on the combined photoelectric-avalanche process. This is shown to account semi-quantitatively for some

of the experimental results.

The experimental methods employed by most investigators suffer from one overall defect in that they are generally sensitive to light-emitted phenomena of relatively late stages of breakdown mechanism. It has not been possible to record the spatial structure and development in time of primary streamers with direct photography.

The main shortcoming of the method employed by the author is that the inclusion of the film in the electrode gap has some influence on the characteristics of the discharge. The film compresses the streamers causing them to move in two dimensions. This results in more crowding of the branches, leading to longer and denser branching than would otherwise exist.

2.7 Bibliography

1. Allen, K. R., and Phillips, K.
J. Electronics and Control, 8, p. 273 (1960)
2. Allibone, T. E., and Meek, J. M.
Proc. Roy. Soc., 166, p. 97 (1938)
3. Amin, M. R.
J. Appl. Phy., 25, p. 358 (1954)
4. Bandle, H. W.
Phys. Rev., 84, p. 92 (1951)
5. Bazelyan, E. M.
Zh. Theo. Fiz., 34, p. 474 (1964)
6. Bhalla, M. S., and Craggs, J. D.
E. R. A. Rept. L/T411, Leatherhead (1961)
7. Biondi, M. A.
Phys. Rev., 77, p. 773 (1950)
8. Biondi, M. A.
Phys. Rev., 83, p. 1078 (1951)
9. Biondi, M. A.
Phys. Rev., 129, p. 1181 (1963)
10. Biondi, M. A., and Brown, S. C.
Phys. Rev., 75, p. 1700 (1949)
11. Boyd, H. A., Bruce, F. M., and Tedford, D. J.
Nature, Lond., 210, p. 719 (1966)
12. Bradbury, N. E., and Tatel, H. E.
J. Chem. Phys., 2, p. 835 (1935)
13. Brown, S. C.
Introduction to Electrical Discharges in Gases
John Wiley, New York (1966)
14. Chanin, L. M., Phelps, A. V., and Biondi, M. A.
Phys. Rev., 128, p. 219 (1962)

15. Cravath, A. M.
Phys.Rev., 33, p.605 (1929)
16. Dakin, T. W., and Berg, D.
Progress in Dielectrics, Vol.4, Heywood, London (1962)
17. Davidson, P. M.
Phys.Rev., 99, p.1072 (1955)
18. Davidson, P. M.
Phys.Rev., 106, p.1 (1957)
19. Davies, W. E. V. J., Dutton, J., Harris, F. M.
and Llewellyn-Jones, F.
Nature, Lond., 205, p.1092 (1965)
20. Dawson, G. A., and Winn, W. P.
Z. Physik, 183, p.159 (1965)
21. Devins, J. C., and Sharbaugh, A. H.
Electro-Tech., 26, p.103 (1961)
22. Devins, J. C., and Wolff, R. J.
Ann.Rept. Conf. on Elec.Ins. (1964)
23. Dorrestein, R.
Physica, 9, p.447 (1942)
24. Dutton, J., Haydon, S. C. and Llewellyn-Jones, F.
Proc.Roy.Soc., A213, p.203 (1952)
25. Dutton, J., Haydon, S. C., Llewellyn-Jones, F., and
Davidson, P. M.
Proc.Roy.Soc., A218, p.206 (1953)
26. Dutton, J., Llewellyn-Jones, F., and Palmer, R. W.
Proc.Phys.Soc.Lond., 78, p569 (1961)
27. Dutton, J., and Morris, W. J.
Brit.J.Appl.Phys., 18, p.1115 (1967)
28. Edmund, P. J.
Phil.Mag., 28, p.234 (1914)

29. von Engel, A.
Handbuck der Physik, Springer-Verlag, Berlin (1956)
30. von Engel, A.
Ionized Gases, Clarendon Press, Oxford (1965)
31. von Engel, A., and Steenbeck, M.
Elektrische Gasentladungen, Springer, Berlin (1932)
32. English, W. N.
Phys. Rev., 71, p. 638 (1947)
33. English, W. N., and Loeb, L. B.
J. Appl. Phys., 20, p. 707 (1949)
34. Eyring, C. F., Mackeown, S. S., and Millikan, R. A.
Phys. Rev., 31, p. 900 (1928)
35. Feldt, W., and Raether, H.
Ann. Phys. Lpz., 18, p. 370 (1956)
36. Fisher, L. H., and Bederson, B.
Phys. Rev., 81, p. 109 (1951)
37. Fitzsimmons, K. E.
Phys. Rev., 61, p. 175 (1942)
38. Franke, W.
Z. Phys., 158, p. 312 (1960)
39. Frommhold, L.
Z. Phys., 144, p. 396 (1956)
40. Frommhold, L.
Z. Phys., 160, p. 554 (1960)
41. Frommhold, L.
Fortschr. Phys., 12, p. 597 (1964)
42. Frost, D. C., and McDowell, C. A.
J. Am. Chem. Soc., 80, p. 6183 (1958)

43. Geballe, R., and Harrison, M. A.
Phys. Rev., 85, p. 372 (1952)
44. Green, D.
Proc. Phys. Soc. Lond., 63, p. 876 (1950)
45. Harrison, M. A., and Geballe, R.
Phys. Rev., 91, p. 1 (1953)
46. Hayashi, M. and Ando, N.
Elect. Engrg. Japan, 86, p. 76 (1966)
47. Haydon, S. C. and Llewellyn-Jones, F.
Brit. J. Appl. Phys., 4, p. 170 (1953)
48. Hermstein, W.
Arch. Elektrotech., 45, p. 209 (1960)
49. Hermstein, W.
Arch. Elektrotech., 45, p. 279 (1960)
50. Heylen, E. A. D.
Nature, London, 183, p. 1545 (1959)
51. Hudson, G. G., and Loeb, L. B.
Phys. Rev., 123, p. 29 (1961)
52. Johnson, G. W.
Phys. Rev., 73, p. 284 (1948)
53. Kachikas, G. A., and Fisher, L. H.
Phys. Rev., 88, p. 878 (1952)
54. Kachikas, G. A., and Fisher, L. H.
Phys. Rev. 91, p. 775 (1953)
55. Kip, A. F.
Phys. Rev., 54, p. 141 (1938)
56. Kluckow, H.
Z. Phys., 161, p. 353 (1961)
57. Kohrman, W.
Z. Angew. Phys., 7, p. 183 (1955)

58. Kohrmann, W., and Raether, H.
Naturwiss, 41, p.400 (1954)
59. Kritzinger, J. J.
Nature, 197, p.1165 (1963)
60. Langevin, P.
Ann.Chim.et Phys., 28, p.433 (1903)
61. von Lane, M.
Ann.Phys.Lpz., 76, p.261 (1925)
62. Legler, W.
Z.Physik, 140, p.221 (1955)
63. Legler, W.
Z. Naturforsch, 16A, p.254 (1961)
64. Lewis, T. J.
Proc. Phys.Soc.Lond., 68B, p.513 (1955)
65. Llewellyn-Jones, F.
Proc.Phys.Soc.Lond., 64B, p.397 (1951)
66. Llewellyn-Jones, F.
Proc.Roy.Soc., A213, p.203 (1952)
67. Llewellyn-Jones, F.
Ionization and Breakdown in Gases, Methuen, London
(1957)
68. Llewellyn-Jones, F., and De La Perelle, E. T.,
Proc. Roy.Soc. A216, p.267 (1953)
69. Llewellyn-Jones, F., and Morgan, C. G.
Proc. Roy.Soc. A218, p.88 (1953)
70. Llewellyn-Jones, F., and Parker, A. B.
Proc. Roy.Soc., A213, p.185 (1952)
71. Loeb, L. B.
Fundamental Processes of Electrical Discharges in
Gases, Wiley, New York (1939)

72. Loeb, L. B.,
Rev. Mod. Phys., 20, p. 151 (1948)
73. Loeb, L. B.,
Phys. Rev., 81, p. 287 (1951)
74. Loeb, L. B.,
Basic Processes of Gaseous Electronics,
U. Cal. P., Berkeley (1955)
75. Loeb, L. B.,
Phys. Rev., 113, p. 7 (1959)
76. Loeb, L. B.,
Electrical Corona, U. Cal. P., Berkeley (1965)
77. Loeb, L. B., Kip, A. F., Hudson, G. G. and Bennett, W. H.
Phys. Rev., 60, p. 717 (1941)
78. Loeb, L. B., and Meek, J. M.
The Mechanism of Electrical Spark, Stan. U. P.,
Stanford (1941)
79. Loeb, L. B., Parker, J. H., Dodd, E. E., and English, W. N.
Rev. Sci. Inst., 21, p. 47 (1950)
80. Loeb, L. B., Westberg, R. G. and Huang, H. C.
Phys. Rev. 123, p. 43 (1961)
81. Loeb, L. B., and Wijsman, R. A.
J. Appl. Phys., 19, p. 797 (1948)
82. Mair-Leibnitz, H.
Z. Physik, 95, p. 499 (1935)
83. Makin, B., and Keck, J. C.
Phys. Rev., 100, p. 729 (1955)
84. Malters, L.
Phys. Rev., 49, p. 879 (1936)
85. Mandle, F.
A. E. R. E., Rept., T/R 1006, H. M. S. O., London (1952)

86. Marr, G. V.
Photo-ionization Processes in Gases,
Academic Press, New York (1967)
87. Masch, K.
Arch. Elektrotechn. 26, p. 587 (1932)
88. Massey, H. S. W., and Burhap, E. H. S.
Electronic and Ionic Impact Phenomena,
Clarendon Press, Oxford (1952)
89. Meek, J. M.
Phys. Rev., 57, p. 722 (1940)
90. Meek, J. M., and Cragg, J. D.
Electrical Breakdown of Gases, Clarendon
Press, Oxford (1953)
91. Meek, J. M. and Saxe, R. F.
Proc. I.E.E., 102, p. 221 (1955)
92. Menes, M.
Phys. Rev., 116, p. 481 (1959)
93. Menes, M., and Fisher, L. H.
Phys. Rev., 94, p. 1 (1954)
94. Merrill, F. H. and von Hippel, A.
J. Appl. Phys., 10, p. 873 (1939)
95. Millikan, R. A.
Phys. Rev., 7, p. 355 (1916)
96. Millikan, R. A.
Phys. Rev., 39, p. 397 (1932)
97. Miyoshi, Y.
Phys. Rev. 103, p. 1609 (1956)
98. Miyoshi, Y.
Phys. Rev. 117, p. 355 (1960)

99. Nasser, E.
Dielectrics, 1, p.110 (1963)
100. Nasser, E., and Loeb, L. B.
J.Appl.Phys., 34, p.3340 (1963)
101. Nerbut, P., Berg, D., Works, C. N., and Dakin, T. W.
Trans.A.I.E.E., 78-III, p.545 (1959)
102. Nielson, R. A., and Bradbury N.E.
Phys.Rev., 51, p.69 (1937)
103. Paetow, H.
Z.Physik, 111, p.770 (1939)
104. Papoular, R.
Electrical Phenomena in Gases, Iliffe, London (1965)
105. Penning, F. M.
Phil.Mag., 11, p.961 (1931)
106. Petropoulos, G. M.
Phys.Rev., 78, p.250 (1950)
107. Pfaue, J.
Z.Angew Phys., 16, p.15 (1963)
108. Pfaue, J., and Raether, H.
Z.Physik, 153, p.523 (1959)
109. Raether, H.
Z.Physik, 110, p.611 (1938)
110. Raether, H.
Z.Physik, 112, p.464 (1939)
111. Raether, H.
Arch.Elektrotech. 34, p.49 (1940)
112. Raether, H.
Z.Physik, 117, p.375 (1941)
113. Raether, H.
Erg.d.e. Naturwiss, 22, p.73 (1949)

114. Raether, H.
Z. Angew. Phys., 5, p. 211 (1953)
115. Raether, H.
Erg. d. e. Naturwiss, 33, p. 175 (1961)
116. Raether, H.
Electron Avalanches and Breakdown in Gases,
Butterworth, London (1964)
117. Reed, R. I.
Ion Production by Electron Impact, Academic
Press, London (1962)
118. Rogowski, W.
Arch. Elektrotech., 16, p. 496 (1926)
119. Schlumbohm, H.
Z. Angew. Phys., 11, p. 156 (1959)
120. Schlumbohm, H.
Z. Physik, 159, p. 212 (1960)
121. Schlumbohm, H.
Z. Naturforsch, 16A, p. 510 (1961)
122. Schlumbohm, H.
Z. Physik, 170, p. 233 (1962)
123. Schmidt-Tiedeman, K. J.
Z. Physik, 150, p. 299 (1958)
124. Schonland, B. F., and Collen, H.
Proc. Roy. Soc. 143, p. 654 (1934)
125. Schröder, G. A.
Z. Angew. Phys., 13, p. 367 (1961)
126. Schulz, G. J., and Fox, R. E.
Phys. Rev., 106, p. 1179 (1957)
127. Strigel, R.
Electrical Impulse Strength, Springer, Berlin (1955)

128. Strigel, R., and Gaenger, Z.
Elektrotechnik, 39, p. 516 (1949)
129. Tholl, H.
Z. Naturforsch, 18A, p. 587 (1963)
130. Thomson, J. J.
Phil. Mag., 47, p. 337 (1924)
131. Townsend, J. S.
Electricity in Gases, Clarendon Press, Oxford (1915)
132. Townsend, J. S.
Motion of Electrons in Gases, Clarendon Press,
Oxford (1925)
133. Townsend, J. S., and Bailey, V. A.
Phil. Mag., 42, p. 873 (1921)
134. Townsend, J. S., and Tizard, H. T.
Proc. Roy. Soc., A88, p. 336 (1913)
135. Trichel, G. W.
Phys. Rev., 55, p. 382 (1939)
136. Varney, R. N.
Phys. Rev., 93, p. 1156 (1954)
137. Vogel, L.
Z. Physik, 148, p. 335 (1957)
138. Waidmann, G.
Dielectrics, 1, p. 81 (1963)
139. Waters, R. T., and Jones, R. E.
Phil. Tr. Roy. Soc., 256, p. 185 (1964)
140. Wijsman, R. A.
Phys. Rev., 75, p. 833 (1949)

CHAPTER 3

LIQUID DIELECTRICS

3.1 Introduction

Liquid dielectrics, particularly hydrocarbon groups, have received a considerable measure of attention during the present century on account of their technical importance in electrical engineering.

The liquids are mainly used as impregnants for high-voltage cables and capacitors, and as filling compounds for transformers, circuit breakers, and terminals.

In some applications, the liquid has additional important functions, for example, as a heat transfer agent in transformers or as an arc quencher in circuit breakers.

A first appraisal would suggest that liquid dielectrics should prove extremely useful, in fact more so than either gaseous or solid dielectrics.

They should be of more use than gases because of their much higher densities and more convenient than solids because they will fill a space to be insulated more easily. Moreover, they will tend to be self-healing should a discharge occur in them. Finally, they could be circulated to dissipate any heat generated in the system.

However, in spite of these advantages, liquid insulants are used less frequently than either solids or gases and then usually only as impregnating media, a role in which they are called upon to withstand relatively low stresses. Thus, the insulating potentialities of liquid dielectrics are hardly being exploited at the present time.

The study of the electric strength of liquid dielectrics has been the subject of careful investigation for many years, but attempts to correlate the experimental results with theories of breakdown process are made more difficult by the fact that

there has been a considerable disparity in the results obtained by any one worker.

The gap in the information available is in the actual breakdown mechanism, the main difficulty being the very short time involved, which is of the order of microseconds.

In a liquid dielectric, electrically stressed for a wide time range (fraction of a microsecond to some days), three distinct ranges of breakdown can be seen. A first stage with long-lasting stressing and low breakdown values is followed by a middle stage from a few microseconds to a few milliseconds with increasing breakdown voltages, as intermediate to the third stage of impulse breakdown, with the duration of stressing becoming shorter.

Whereas in the first stage of breakdown, impurities such as fibres and surface laminae on the electrodes are a decisive influence on the level of the breakdown voltage, in the third stage, the breakdown is suggested to be electrical in type and based on streamer propagation similar to that in the gaseous dielectric.

The major line of investigation by many workers has been concentrated upon measurements of quantities external to the liquid under observation, e. g. voltage level and delay time of breakdown.

A better insight into the mechanism of breakdown in liquids is obtained by placing an electro-magnetic radiation-sensitive film in the electrode gap region. On application of an impulse voltage of sufficient magnitude, a discharge pattern is formed on the film which is sensitive to polarity, level and duration of potential and the position of the film.

The study of growth and structure of discharge in the form of streamers from the point-electrode provides a better insight into the mechanism of breakdown in liquid dielectrics.

3.2 Literature Survey

3.2.1 Introduction

The behaviour of dielectric liquids exposed to electric stress has been the subject of comprehensive reviews by Gemant¹⁷, Whitehead⁷⁶, Nikuradse⁵¹, Koppelman³⁴, Macfadyen⁴⁵, Vick⁶⁷, Lewis⁴¹, Sharbaugh and Watson⁶⁰.

Pioneering work on the electrical breakdown of liquid dielectrics was mainly concerned with the conditions prevailing in electrical apparatus. These were, basically, breakdown due to the secondary effects such as the presence of fibres, chemical impurities, water particles and electrode effects.

The recent investigations are largely associated with the breakdown due to the physical and chemical properties of liquids. To achieve this aim there has been tremendous progress in experimental techniques.

To have a clear understanding of the physical nature of dielectrics, liquids with a simple molecular structure are used and the secondary effects in most cases have been abolished.

An understanding of the experimental work is needed before theories of breakdown can be explained.

Attempts to correlate the experimental results with theories of breakdown process are made more difficult by the fact that, in general, there has been considerable disparity in the results obtained by any one worker, even when extreme care is taken to remove the disturbing factors.

Factors influencing the breakdown process are explained and an attempt is made to outline the possible mechanism of breakdown in organic liquids.

Measurements of ion mobility have been made under controlled conditions and of particular interest in this respect are studies on

liquid helium. The use of liquified gases in breakdown studies has made possible the investigation of hitherto unobserved electrode phenomena.

3.2.2 Pre-Breakdown Conduction

Investigations of the electrical conduction process in insulating liquids is fraught with difficulties and reliable information on the processes involved is difficult to acquire.

Measurements of ion mobilities provide important data on the nature of charge carriers in dielectric liquids. The conduction could be due to the presence of ionic impurity, to solid particles of sub-micron size which become charged and, at high field, due to electrons injected from the negative electrode.

An additional factor to be considered is the liquid motion due to the induced motion of charge carriers of various sorts¹⁶.

3.2.2.1 Low Field Conduction

At low fields (< 1 KV/cm), resistivities of 10^{15} to 10^{20} ohm-cm are obtainable for hydrocarbons. Hart and Mungall²³ have made a thorough and systematic study of several of the phenomena associated with low field conduction. Very high values of resistivity are obtained for liquified gases^{13, 63, 65} even at high field intensities.

Because the natural conductivity of pure liquids is small and rather erratic, many workers^{3, 4, 13, 36, 50, 65, 78} have induced charge carriers into the liquid in a controlled manner and studied the enhanced current produced. By inducing current, it is possible to obtain more information about the basic processes occurring but there are difficulties when the stress is increased towards breakdown values.

By switching the inducing agent on or off, it is possible to measure the transit of charge carriers between the electrodes

and thus to determine their mobilities under a variety of conditions.

For hydrocarbon liquids, of which hexane is typical, the mobilities of positive and negative ions are found by Le Blanc³⁶ to be in the range $10^{-4} - 10^{-3} \text{ cm}^2/\text{V-sec}$. The positive ion is rather less mobile than the negative one. As shown in Fig. (3.1), the drift mobility is found to change with the absolute temperature θ according to the relation:

$$\mu = \mu_0 \exp\left(\frac{-E}{k\theta}\right) \quad (3.1)$$

where $E = 0.14 - 0.02 \text{ eV}$ and $\mu_0 = 0.3 - 0.2 \text{ cm}^2/\text{V-sec}$

The product of mobility and liquid viscosity changes with temperature (see Fig. 3.1) indicating a violation of Walden's rule.

3.2.2.2 High Field Conduction

Until recently the d. c. measurements, suffering from polarization, chemical effects and erratic current at elevated field, were restricted to fields less than 25 per cent of breakdown values but Green^{19, 20}, House²⁷ and Sletton^{61, 62} have succeeded in extending their d. c. current measurements above 1 MV/cm.

High field current bursts have been ascribed to a variety of causes including (1) gas removal from surface layers in the form of bubbles, (2) sporadic removal of oxygen to expose sites of low work functions, (3) impurities moving into the high field region on the test gap, (4) the particle coming to rest upon the cathode, (5) formation of polymer layers on the electrodes to produce more stable surface conditioning.

The use of pulsed voltages has minimized the troubles encountered with direct current, and readily permits the measurement of pre-breakdown current at fields near breakdown^{48, 73}.

Watson and Sharbaugh⁷³ made a comparison of conduction current obtained by d. c. and pulsed fields. The results (see

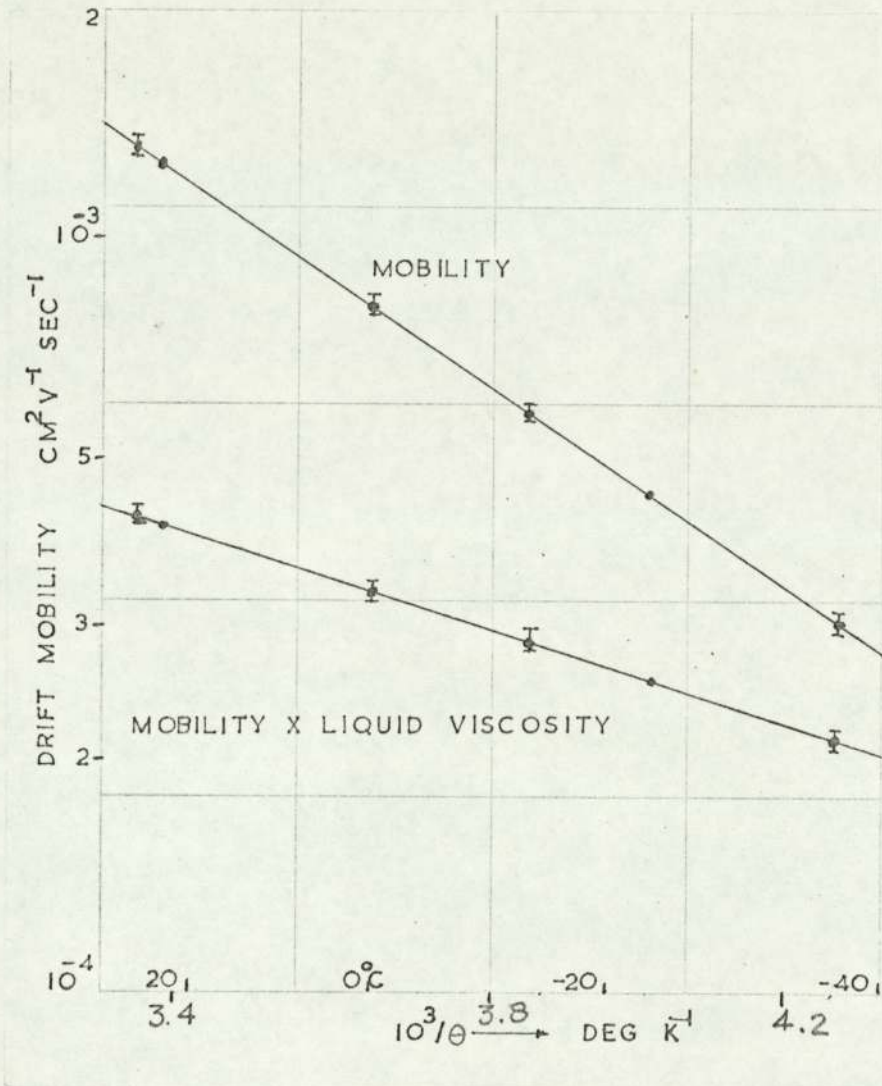


Fig. 3.1. THE DEPENDANCE OF THE DRIFT MOBILITY OF ELECTRONS IN HEXANE UPON TEMPERATURE.

(After Le Blanc 36).

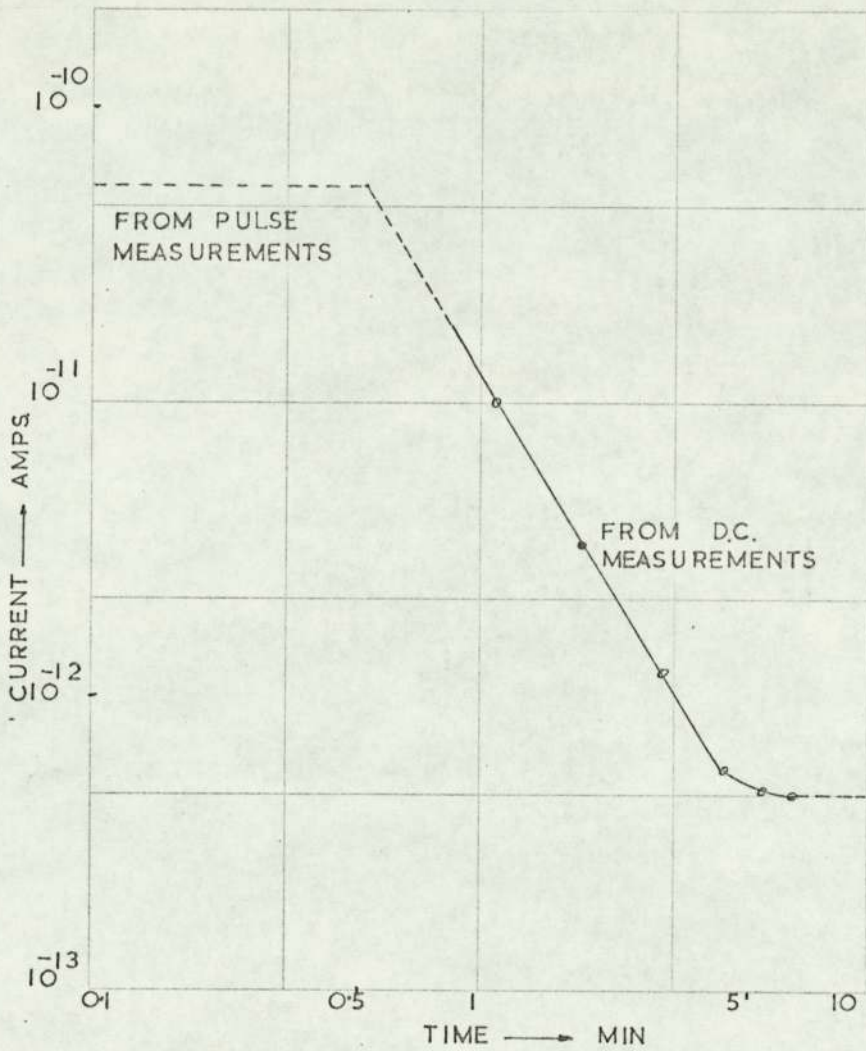


Fig. 3.2. A COMPARISON OF THE MAGNITUDE OF CONDUCTION CURRENTS IN n-HEXANE UNDER d.c. AND PULSE CONDITIONS.

(After Watson and Sharbaugh 73)

$E = 59\text{KV/cm}$; $d = 254$ microns; stainless steel electrodes

Fig. 3.2) show a greater magnitude of current under pulsed field. The drop in conduction current with time is suggested by Kao and Calderwood²⁸ to be associated with the decrease of conduction and drift velocity of charge carriers.

One of the most controversial points in the interpretation of conduction in liquids concerns the presence (or absence) of an electron multiplication process. Watson and Sharbaugh⁷³ found no evidence for α -process at fields up to 1.2 MV/cm, but observed marginal indication of the beginning of the process at 1.3 MV/cm as shown in Fig. 3.3

3.2.3. Electrode Effect

The influence of the nature of the electrode metal and particularly that of the cathode upon the breakdown of liquid dielectrics has been studied by many investigators^{13, 18, 37, 49, 53, 80}. However, the sensitivity of the electron emission characteristics of a metal to the physical and chemical condition of its surface make it very difficult to obtain reproducible results.

According to Hirano²⁶, the breakdown voltage varies with electrode materials. The breakdown voltage varies according to the surface conditions of the electrode owing to the existence of absorbed gas. The electrode material itself and its conductivity have little effect on the breakdown voltage if there is no absorbed gas.

Salvage⁵³ observed a distinct cathode effect on the electric strength of hydrocarbon liquids. The electric strength using Al, Cr, Ag, Ni, and Pt cathodes increases regularly in the order shown, which is also the order of increase of the vacuum work function. This result indicates that the space-charge mechanism suggested by von Hippel and Alger⁶⁹ for cathode effects in alkali halides has its counterpart in liquid studies, and that a negative space charge is formed by electron emission from the cathode.

Lewis^{38, 39} presents an explanation for the apparent disagreement among various observers as to the existence of a cathode

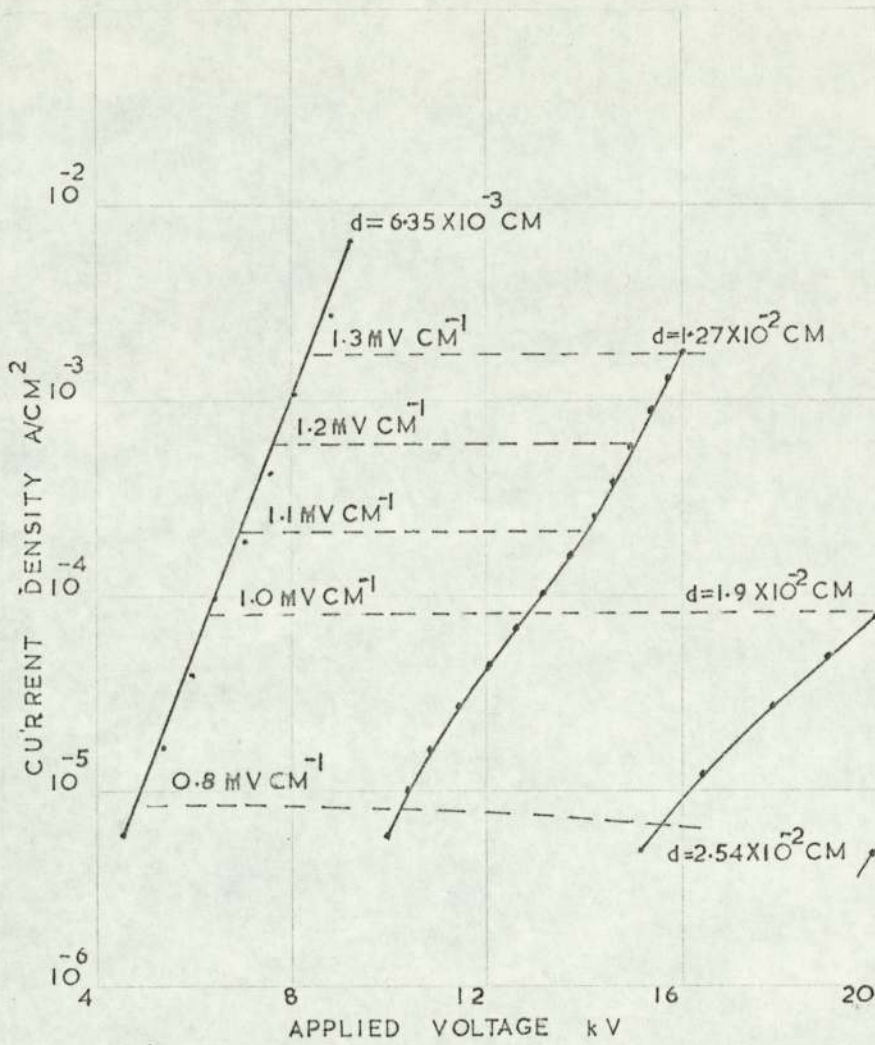


Fig. 3.3. THE DEPENDANCE OF CONDUCTION CURRENT DENSITY IN n-HEXANE UPON VOLTAGE AT DIFFERENT ELECTRODE SEPARATIONS.

(After Matson and Sharbaugh 73)

Lines of constant field strength are shown as dashed line.

dependence of the electric strength of liquids. He points out that the electric strength measured for a particular electrode-dielectric system depends solely on the liquid characteristics if, at the requisite breakdown voltage, the cathode field is sufficiently high to produce copious electron emission. On the other hand, if the field necessary to produce avalanche in the liquid is too low to provide adequate field emission, then the breakdown of the system will be primarily determined by the electron emission characteristics of the cathode. He supports this argument by experimental measurements on n-hexane with point-to-plane electrodes composed of metals having different work functions.

A recent tendency has been the use of highly polished electrode surface. Kao and Higham²⁹ have shown that polishing electrodes increases the electric strength. An unpolished cathode had the same effect in reducing the strength as both electrodes being unpolished. He suggests that a rough cathode surface may increase field emission due to field enhancement caused by the physical irregularities.

The use of mercury as the cathode has been suggested by Sharbaugh, Bragg and Crowe⁵⁶. Such an electrode provides a smooth surface and is easy to prepare. Nevertheless, they substituted a stainless steel cathode for a mercury cathode in their later work¹² so eliminating a troublesome correction caused by the deformation of the mercury under electrostatic stress.

Sharbaugh, Cox, Crowe and Auer⁵⁸, using highly polished steel hemisphere electrodes have found a relation between the breakdown field and the logarithm of the area of electrode. Similar work by Kao and Higham²⁹ shows an increase in electric strength by increase of area. The statistical study of the electrode area effect in the breakdown of transformer oil by Weber and Endicott^{74, 75} causes one to speculate as to what degree complex emission effect may be involved, as well as other factors, in the breakdown mechanism.

If there is a disparity in the sizes of the asperities on the electrode surface and the most prominent of these initiates breakdown, then an increase in the area of the electrode will lead to a greater probability of breakdown.

The dependence of electric strength on gap length is taken as evidence of an electron multiplication process in liquid dielectrics¹⁸.

Kao and Higham²⁹ show that for a gap length greater than a certain value the electric-strength is practically independent of the gap length, but below this value the electric strength increases rapidly with decreasing gap length. This phenomenon, they suggest, is in agreement with the collision ionization theory.

When flat electrodes are used, the electric strength of hydrocarbon liquids is nearly independent of the spacing of the electrodes. Thus, the effect of volume of liquid under stress is small, if it exists at all.

More often, breakdown studies are made with spherical electrodes rather than flat ones. In this case, a strong dependence upon electrode spacing is normally observed, especially in the small gap range 5-100 microns. Watson and Sharbaugh⁷³ have shown that, for this geometry, the area under high stress is proportional to the product of the radius and the spacing, and it is shown that such a dependence is primarily an electrode area effect. They suggest that, before the importance of this effect was recognised, the gap dependence was erroneously cited as evidence for collision ionization in liquids.

The liquified gases, such as argon and helium, do not produce any solid deposits as the result of a discharge and are thus ideal for a detailed examination of electrode effects. By allowing the electrode surfaces to oxidise in dry air after polishing, Swan and Lewis^{64, 65} have shown that it is possible to alter the static electric strength of liquid argon in a regular way (see Fig. 3.4). The form of variation depends on the metal and it is particularly interesting

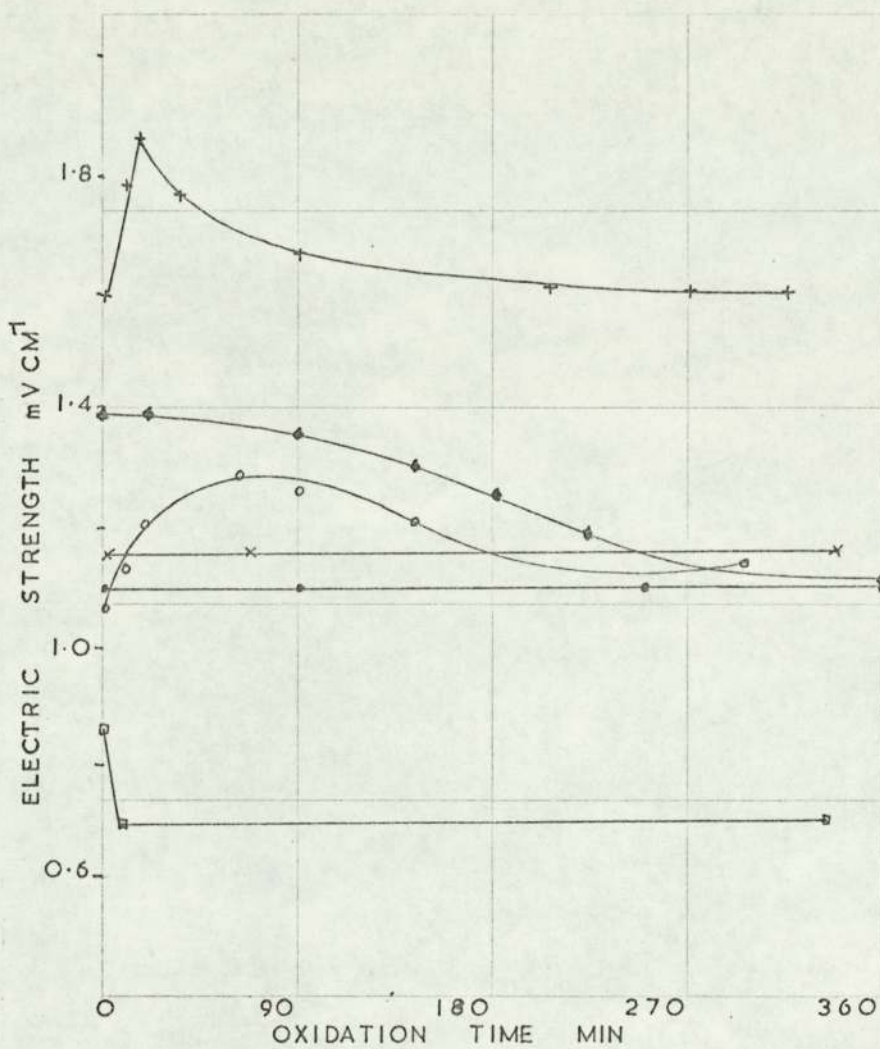


Fig. 3.4. INFLUENCE OF ELECTRODE OXIDATION ON THE d.c. BREAKDOWN OF LIQUID ARGON.

(After Savm and Lewis⁶⁵)

+ Stainless steel

◆ Copper

o Brass

x Gold

● Platinum

□ Aluminium

in the case of stainless steel. They showed that it is possible to obtain the effects of cathode and anode separately by keeping the oxidation of one electrode at a fixed level as in Fig. 3.5. It will be seen that the degree of anode oxidation affects the strength, one of the few situations in which the anode has other than a passive role in determining the strength of an insulent.

The anode effect may be removed either by taking out the traces of oxygen from the argon liquid or by using pulses rather than steady voltages. On the other hand, cathode effects remain when the oxygen is removed and are certainly important when pulse voltages are used.

All these effects together suggest most strongly that, with oxygen present, negative ions are formed by oxygen-trapping of electrons; these move to the anode and can be blocked from being neutralised there by the presence of oxide layers. The negative space charge set up then leads to a lower electric strength. If short pulses of voltages are employed, there is no time for the effective transport of negative ions to the anode, and hence it does not control the strength.

Although a definite dependence on anode conditions is not found with the hydrocarbons, it would not be true to say that the anode does not influence the strength of these liquids. In fact, it is most probable that the anode is always strongly blocking for hydrocarbon liquids containing dissolved oxygen, whatever the particular condition of the metal surface.

3.2.4 Impurities Effect

It has been found that any type of impurity in a liquid dielectric has a severe effect on its electric strength. The presence of minute solid particles and of dissolved water and air either facilitate the more basic process of rupture by locally concentrating the electric field, or introduce an entirely new kind of breakdown, perhaps by

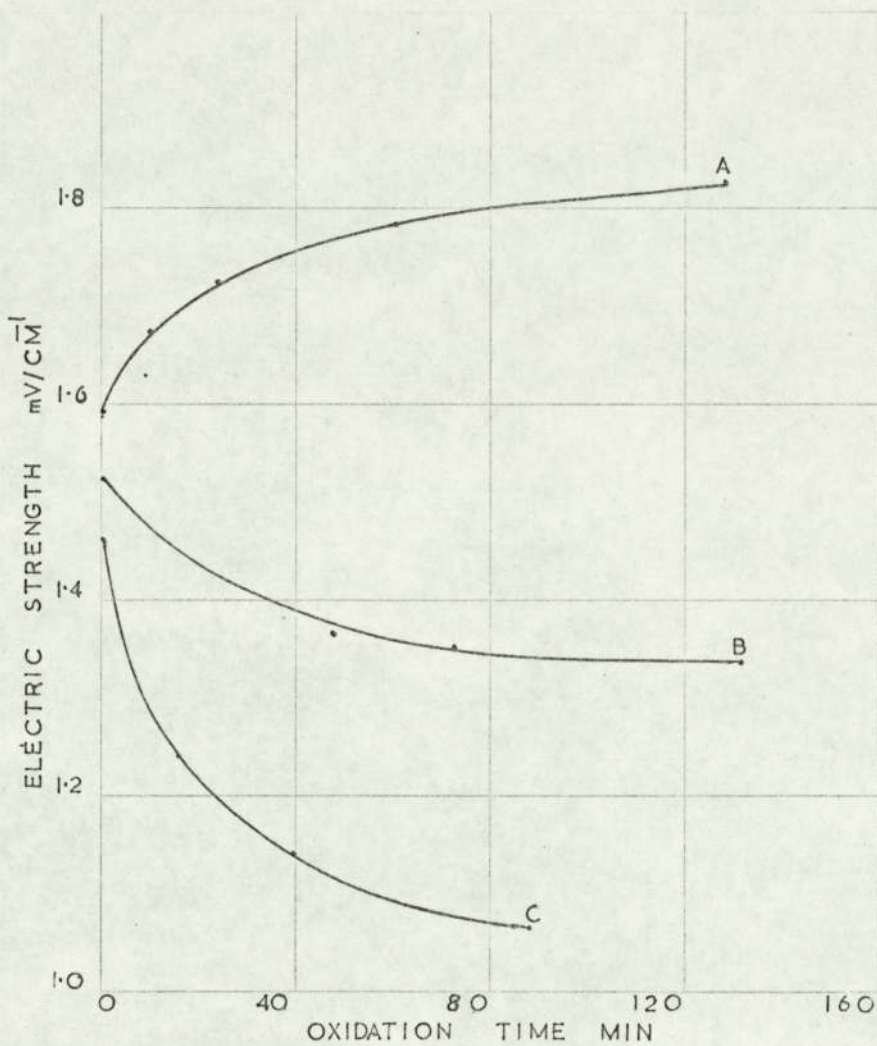


Fig. 3.5. CONDITIONING EFFECTS OF ANODE AND CATHODE ON THE ELECTRIC STRENGTH OF LIQUID ARGON.

(After Sawm and Lewis 65)

- a, Stainless steel electrodes; various oxidation of cathode
- b, Stainless steel electrodes; 24 hours oxidation of cathode; various oxidation of anode.
- c, Gold cathode, stainless steel anode; various oxidation of electrodes.

bubble formation, or the building of conducting bridges across the inter-electrode gap.

Fine drops of water in a strong electric field join up between the electrodes forming a conducting filament in the liquid dielectric as suggested by Gemant¹⁷. The severe fall in the electric strength of a liquid dielectric by the addition of a small volume of water is observed by Zein-El-Dine and Tropper⁸⁰. Matsijenski and Tropper⁴⁹ have reported a 100% increase in the d. c. electric strength of hexane by passing the liquid over a drying agent.

The effect of small particles and fibres on the electric strength of liquid dielectrics has been investigated by many workers^{14, 15, 27, 32}. The idea has developed that the particles cause distortion of field across the gap. Kok and Corbey³² have observed a bridge forming at the gap, formed by contaminants of high dielectric constant which flow toward the maximum field stress. Similar observation is made by Hakim and Higham²² using a Toepler Schlieren method of photography.

The accepted method of cleaning the liquid from particles of more than a few microns in size is by circulating the liquid through cycles of distillation and filtration.

Edward¹⁵ has reported exceedingly high values of electric strength for pure organic liquids. He found the maximum electric strength to be some 20-100% higher than the highest values previously reported in literature. Edward attributed these changes to the elimination of minute particles from the breakdown gap. He suggests that particles as small as one micron may give rise to the lower but reproducible values of electric strength found in his earlier work¹⁴ and by other investigators.

3. 2. 5 Temperature Effect

A dependence of the electric strength upon temperature has been observed in liquids for both d. c. and pulsed voltages. There is a rather slow change centred around room temperature,

terminating in a rapid decrease near the boiling point. Below room temperature, a considerable rise in strength occurs. The effect is not one of density alone, for the results show the same general character after a correction has been made for the density change.

A temperature dependence is complicated by possible changes in cathode emission, gas content and viscosity.

While investigating the pressure characteristic of breakdown voltage, Hirano²⁵ observed that the dissolved gas in the liquid affects the characteristics at temperatures above 30^o C. He suggests that the variation of breakdown voltage caused by variation of temperature of oil at atmospheric pressure depends on water content, the absorbed gas on the electrodes, and gas emulsion.

Salvage⁵³ using direct voltage, found that the electric strength of n-hexane decreased with increasing temperature, the rate of decrease becoming greater as boiling point was reached. He attributed this effect to bubble formation from the absorbed gas layer on the electrode.

The dependence of the electric strength of aliphatic hydrocarbons on temperature is accounted for by the change in density due to thermal expansion according to Crowe, Sharbaugh and Bragg¹².

Figure 3.6 from the work by Goodwin and Macfadyen¹⁸ shows that, while normal breakdown strength E increases with the number of carbon atoms in the chain, it decreases uniformly with rising temperature. But working on the same line, Lewis^{37, 40} has found a distinct break in the electric strength versus temperature characteristics (see Fig. 3.7), even when density changes are accounted for. These breaks occur at temperatures which are in very good agreement with similar breaks in the characteristics of other properties such as density, viscosity, and heat capacity.

Lewis^{37, 40} has shown that these variations are consistent with changes in thermal molecular motion which influence the

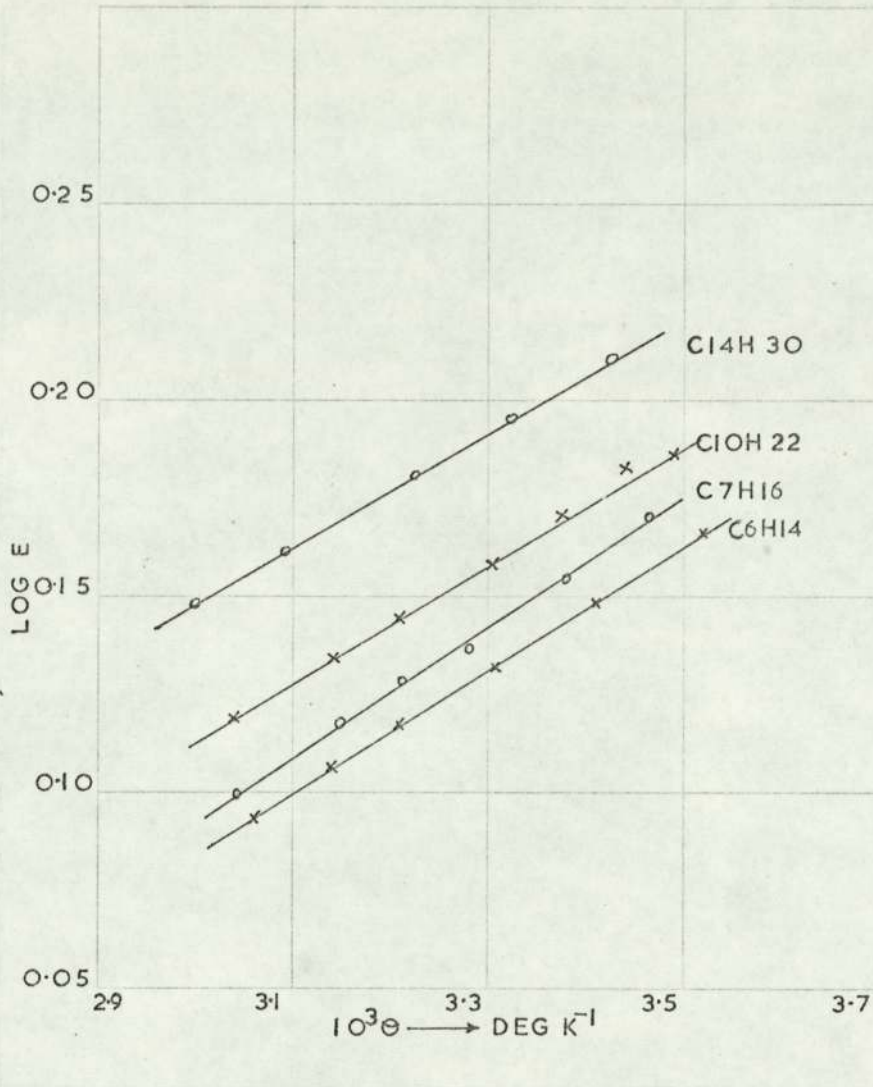


Fig. 3.6. VARIATION OF ELECTRIC BREAKDOWN STRENGTH OF n-PARAFFINS WITH TEMPERATURE.

(After Goodwin and Macfadyen, 18).

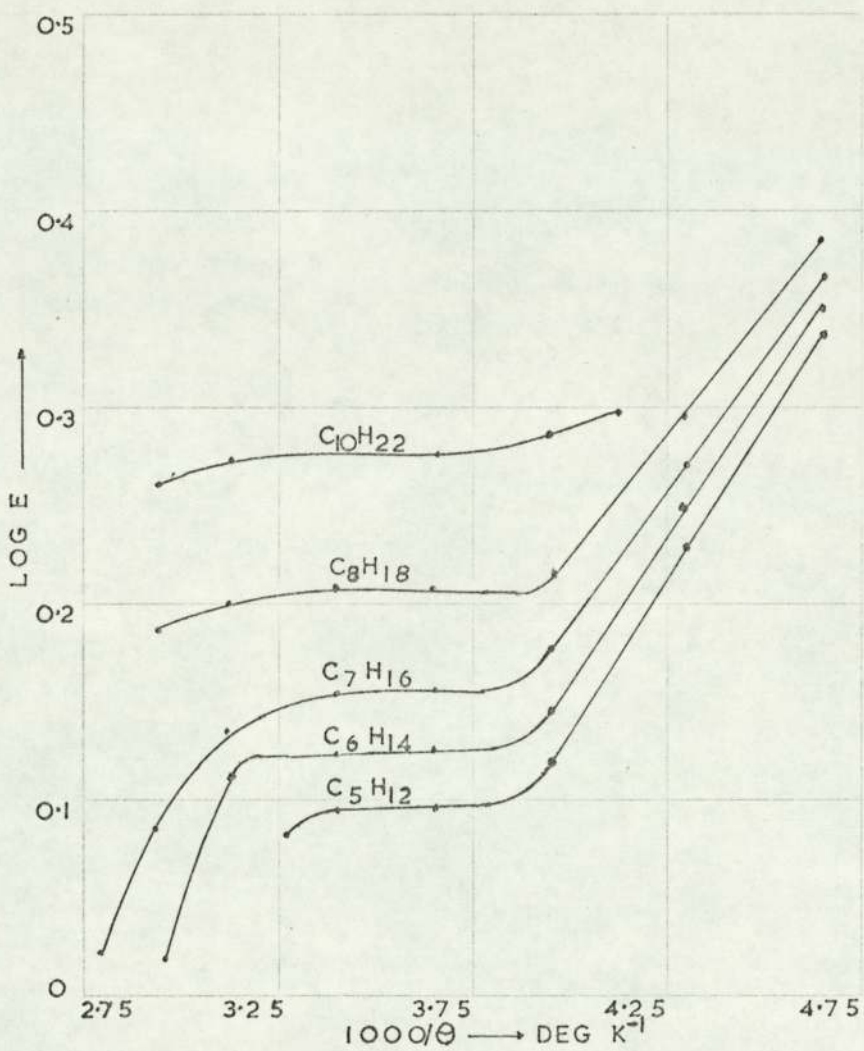


Fig. 3.7. ELECTRIC STRENGTH OF n-PARAFFINS AS A FUNCTION OF TEMPERATURE.

(After Lewis 40).

d = 762 microns

electronic mean free path, but Kao and Higham²⁹ interpret the results in an entirely different way. They propose that breakdown occurs in a vapour bubble formed in the liquid and that the temperature variations of surface tension and vapour pressure influence the development of the bubble.

3.2.6 Pressure Effect

The density increase of a liquid due to normal applied hydrostatic pressure is so small that no change in electric strength arising from it would be expected. However, depending on the experimental conditions, the observed breakdown strengths usually exhibit, to a greater or lesser extent, some kind of dependence on pressure. For example, the results may depend upon the gas content of the liquid, the amount of gas absorbed on the electrodes, or the state of equilibrium of the liquid with the gas above it in the cell.

One of the first to suggest the effect of pressure on electric strength of liquid dielectrics was Kock³⁰. He found that the electric strength of pure liquids such as benzene increases with increasing pressure.

The effect of absorbed gas on the breakdown of liquid insulations was investigated by Hirano^{24, 25}. Experimental results led to the conclusion that the change of dielectric strength of liquid insulation with the change of atmospheric pressure depends on the absorbed gas on the electrode and is quite independent of the gas absorbed in the liquid; the larger the quantity of absorbed gas, the lower the dielectric strength.

Basseches and Barnes¹ in their study of liquid dielectrics under stress found that, once gas evolution was started, it could be controlled under certain conditions. Increasing the pressure of gas above the surface of the liquid could be used as a means of suppressing further evolution. It is suggested that the initiation of gas evolution is dependent upon a species of gas nuclei present in an

undissolved state in the liquid.

Edward¹⁴, using rectangular pulse voltage shows an increase in electric strength of some hydrocarbons with pressure which is independent of the gas used to apply the pressure.

Clark⁶ found no pressure dependence using impulse voltages, but with a d. c. and a. c. supply the electric strength of transformer oil decreased with decrease in pressure. This dependence disappeared, however, when the oil was thoroughly degassed. He attributed the pressure dependence to the role played by gas bubbles in the electric breakdown mechanism.

Watson and Higham⁷² have investigated the effect of hydrostatic pressure on transformer oil at pressures up to 33 atmospheres and have shown that the electric strength is pressure-dependent, particularly in the range immediately above atmospheric pressure.

This possibility draws attention to the hydrostatic pressure

$$p = \frac{(\epsilon - 1)(\epsilon + 2)}{24} E^2 \quad (3.2)$$

existing in a liquid of dielectric constant ϵ when exposed to a field intensity E , as shown by Hakim and Higham²¹. With approaching breakdown, this pressure may reach one atmosphere.

Kao and Higham²⁹ have investigated the effects of hydrostatic pressure on various polar and non-polar liquids. A marked increase in breakdown strength was exhibited with increasing applied hydrostatic pressure. Some of the results obtained on degassed liquids in a 200 micron gap are shown in Fig. 3.8.

Kao and Higham²⁹ suggest that it is unlikely that the pressure dependence of electric strength is due only to the change of liquid density or viscosity without cavity formation. They propose the following possibilities for the cavity formation:

(a) Gas cavities may originally exist between the liquid and solid phases in the pores and cracks of solid impurities or

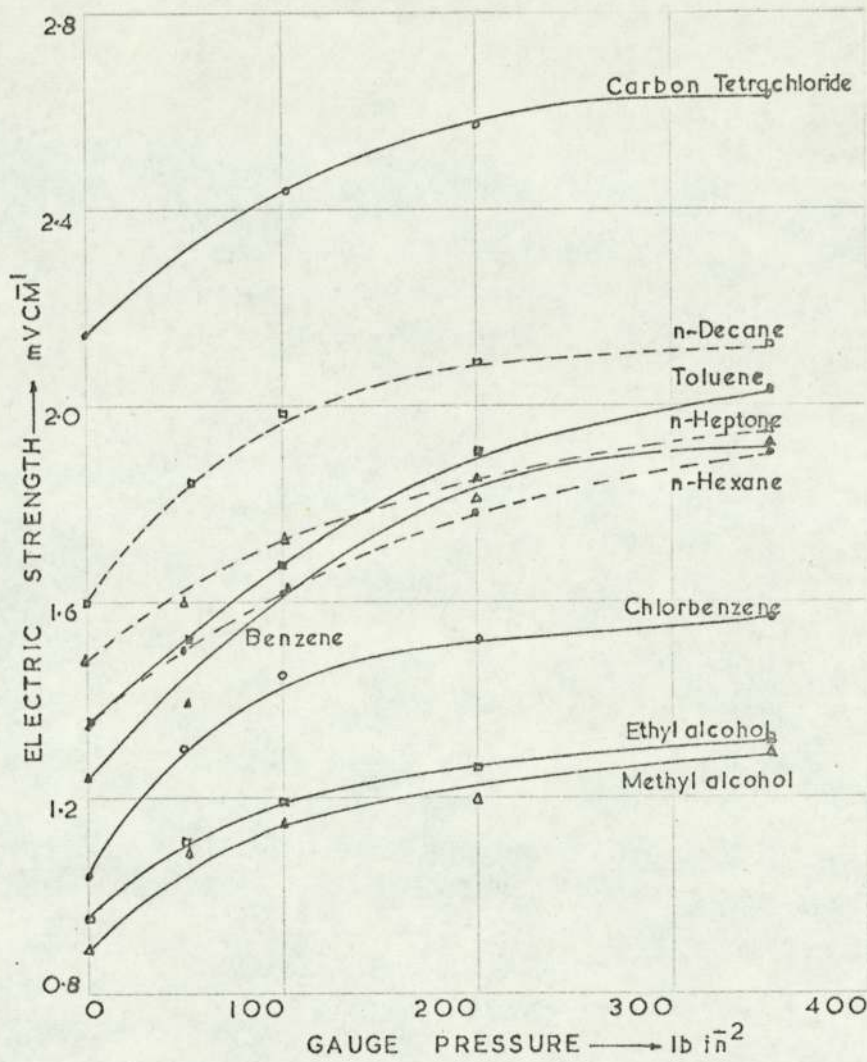


Fig. 3.8. THE DEPENDANCE OF THE IMPULSE ELECTRIC STRENGTH OF SOME ORGANIC LIQUIDS UPON APPLIED PRESSURE.

(After Kao and Higham 29).

$d = 200$ microns; stainless steel electrodes, 6.35 mm diameter; pulse length, 4.5 sec.

in the valleys of electrode surface.

(b) Electrostatic repulsion between clusters of space charges may overcome the surface tension of the liquid and form cavities.

(c) Chemical dissociation in the liquid by electron bombardment may produce gases which may form cavities if their densities can locally reach a certain value.

(d) If the liquid contains conducting impurities and the duration of applied voltage is long, a cavity may form at the junction of impurities, presumably due to the thermal effect, and the cavity may be filled with gas or vapour.

3.2.7 Density Effect

Discussion by Crowe, Bragg and Sharbaugh⁹ shows that the strength should depend linearly on the density of hydrocarbons, to a first approximation, provided that the mechanism is electric and the process is dominated by the behaviour of slow electrons.

The electric strengths of members of three different homologous series of liquids are studied by Sharbaugh, Crowe and Cox⁵⁹. The results (see Fig. 3.9) show that the strength increases regularly for the alkanes and silicones but is constant for the alkyl benzenes. It is clear that the density alone is not the controlling factor because of the large variation in the electric strength of alkyl benzenes. Branching of the hydrocarbon molecules leads to a lowering of the electric strength.

Lewis^{37, 40} observed that the electric strengths measured for the alkane series, pentane through decane, increases with chain length (see Fig. 3.7). He attributed this effect to the energy lost to the orientation of the dipole molecules under an applied field.

The density effect has also been observed by Goodwin and Macfadyen¹⁸ (see Fig. 3.6) and Salvage⁵³.

Paschen's similarity law for breakdown in gases is known to fail at high pressure - high density⁶⁸, presumably because of a change in the way in which electrons dissipate their energy to

gas molecules.

Crow, Bragg and Sharbaugh¹⁰ have discussed the basis for Paschen's Law and present evidence that a new similarity law exists for the condensed phase.

3.2.8 Time Effect

Macfadyen and Edward^{46, 47}, using short rectangular pulses of 0.25-20 microseconds duration have found that the breakdown strength of organic liquids increases as the duration of the voltage pulse diminishes for intervals below 20 microseconds. As the pulse duration is reduced below a certain value called the "limiting breakdown time", the electric strength of liquid rises above the value for sufficiently long pulses. (see Fig. 3.10). Once started, the breakdown is complete within a few nanoseconds.

The work of Edward¹⁴ has indicated that the time lag is approximately constant for a variety of liquids, and therefore is relatively insensitive to structure and composition of the liquid. He suggests that the time lag is occupied with the development of electron avalanches across the gap.

However, Goodwin and Macfadyen¹⁸ have presented evidence that there is a definite correlation between time lag and the molecular weight - or density - of a liquid hydrocarbon. More especially, they found that it was directly proportional to the time required for positive ions, produced by ionizing collision between electrons and molecules, to cross the gap. On this basis, the time lag for a 50 micron gap varied from about one microsecond for n-hexane to about twelve microsecond for n-tetradecane. These observations were taken as evidence that mobility of positive ions plays a major role in the mechanism of electrical breakdown in liquids.

Crow, Sharbaugh and Bragg^{11, 12}, using n-hexane and n-nonane two liquids of widely different molecular weight and viscosity, and electrode separation of 51 microns, have shown

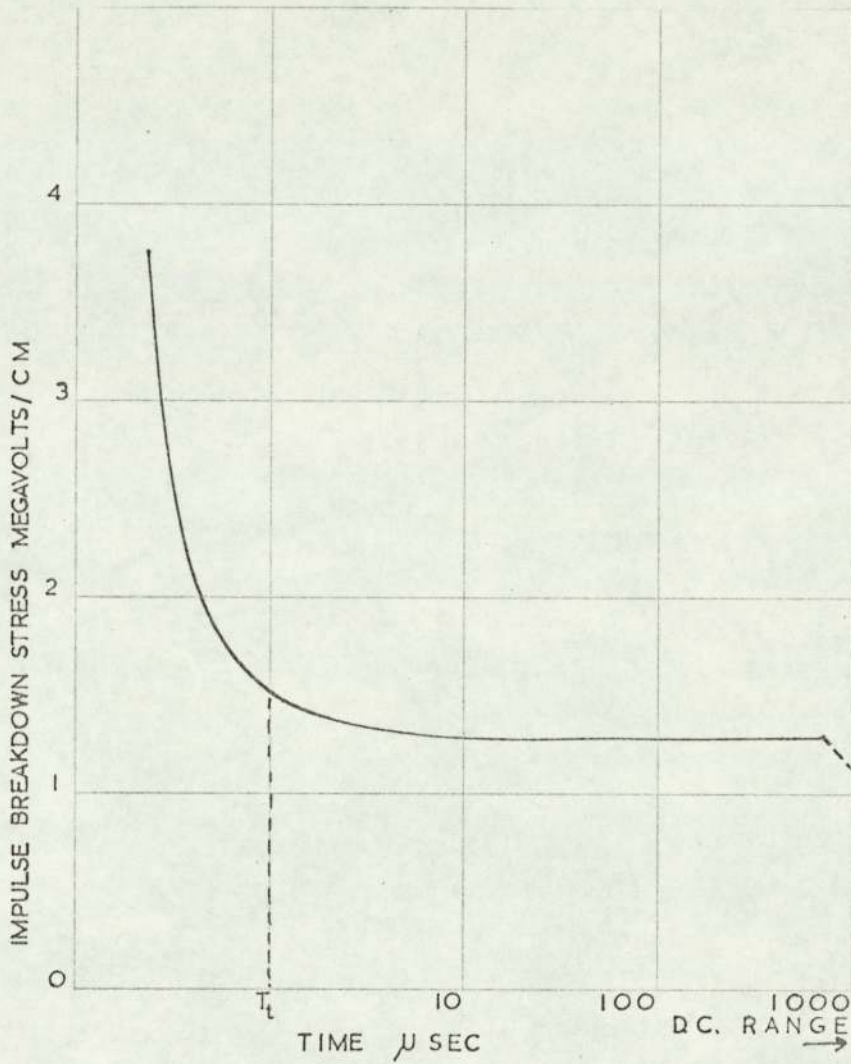


Fig. 3.10. BREAKDOWN STRENGTH OF LIQUIDS AS A FUNCTION OF APPLIED PULSE LENGTH

that the electric strength is independent of time when the applied pulse is longer than about one microsecond (see Fig. 3.11) but rises sharply for shorter pulses. The formative time lag for breakdown of both liquids was about 1.4 microseconds, a result in contradiction with measurements of Goodwin and Macfadyen¹⁸. They showed that any formative time lag which occurs in a microsecond, and is independent of molecular structure and viscosity of the liquid, could not involve the transit time of positive ions formed in the electron avalanches, as proposed by Goodwin and Macfadyen¹⁸.

Crowe⁷ has measured the formative time lag for a group of straight-chain hydrocarbon liquids for gaps of the order of 100 microns with a view to settling areas of agreements and differences with Edward¹⁴ and also with Goodwin and Macfadyen¹⁸. Results (see Fig. 3.12) establish the fact that the formative time lag increases in a regular manner with increasing gap length. The issue of some time past is whether the time lag is related to molecular structure or not. Goodwin and Macfadyen¹⁸ found a regular variation with molecular structure while Edward¹⁴ and Crowe and co-workers⁹⁻¹¹ have reported otherwise.

The work by Crowe⁸ further supports the argument that formative time lag is insensitive to molecular structure in the liquids.

From the experimental data, it is estimated that the mobility of the species of charge particle involved is $9.1 \times 10^{-3} \text{ cm}^2/\text{Volt sec}$. This seems to be too fast for positive ions, but could possibly indicate electrons that have suffered retardation due to trapping or attachment processes.

The interpretation of d. c. breakdown measurements is simplified to some extent by the absence of any time variation in the individual processes. Sletton^{61, 62} has shown that this advantage is lost by the formation of space charges and by the influence of solid impurities.

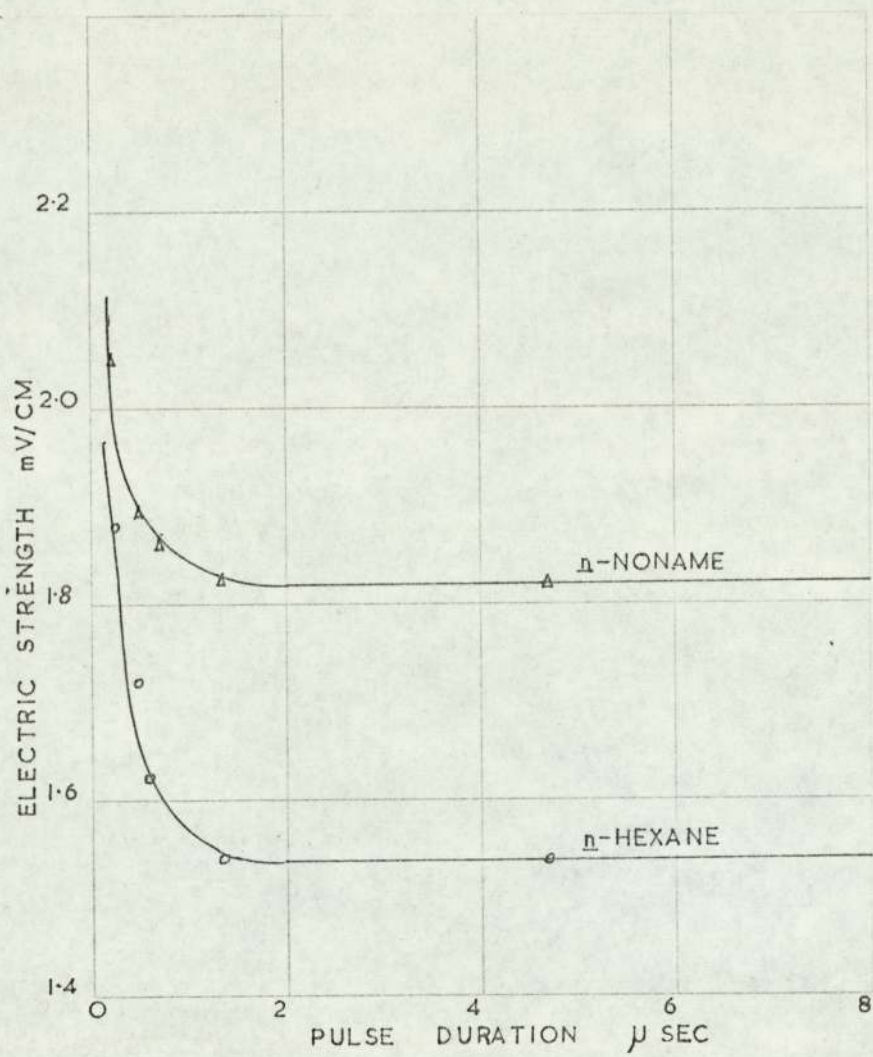


Fig. 3.11. THE TIME DEPENDANCE OF ELECTRICAL BREAKDOWN IN LIQUID HYDROCARBONS.

(After Crow, Sharbaugh and Braggs 12).

Stainless steel electrodes, $d = 50$ microns.

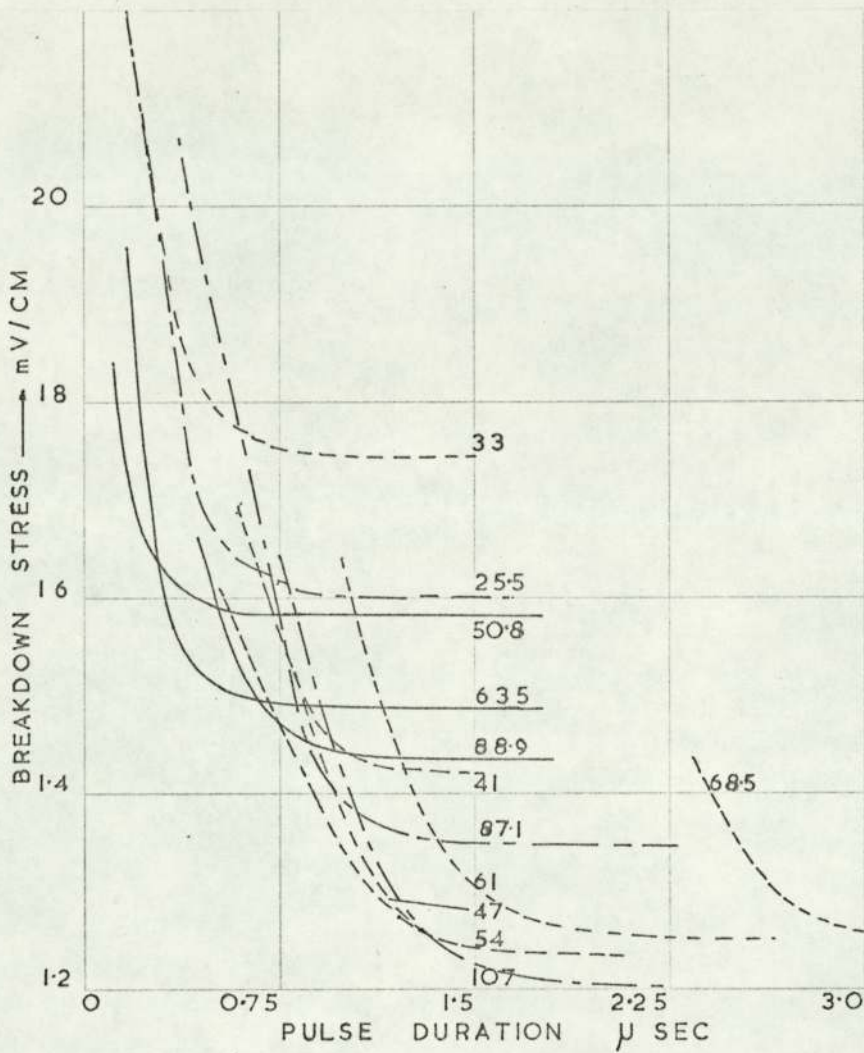


Fig.3.12. RELATIONSHIP BETWEEN TIME LAG, GAP LENGTH, AND ELECTRIC STRENGTH FOR n-HEXANE.

Gap length in microns indicated on each curve.

- Crowe⁸; Steel electrodes.
- Goodwin and Macgadyen¹⁸; Phosphur-bronze electrodes
- · - Edwards¹⁴; Phosphur-bronze electrodes

With microseconds and submicrosecond impulse voltages, however, the movement of ions and impurities is curtailed to a large extent but the temporal variations of the breakdown processes become significant.

These results suggest that only the formative time lag is involved. However, Ward and Lewis⁷⁰ have reported statistical time lags at 1.8 MV/cm in n-hexane. They have shown that the increase of strength for pulse durations less than T_c (Fig. 3.10) is a result of statistical availability of electrons and is therefore dependent on electrode material and surface condition. For pulses greater than T_c the probability that each electron produces a breakdown becomes significant, and the strength depends more on liquid properties.

3.2.9 Mechanism of Breakdown

The improved experimental techniques have enabled a measure of unanimity to be reached as to the general trends of the dependence of breakdown strength on a number of variables, although exceptions exist and agreement upon absolute values is not satisfactory.

Modern interpretation of the mechanism of breakdown^{29,45} in purified hydrocarbon liquids involve four primary processes. These are electron emission from the cathode, electron interaction with the bulk of liquid resulting in energy loss, cavity formation and elongation and electron multiplication by the process of ionization producing ultimately avalanches and complete breakdown. All of these primary processes will be strongly dependent on the field and the actual breakdown dependent on the electric field strength will be determined by a suitable combination of these mechanisms. Certain secondary processes may also arise such as those due to residual impurities.

Salvage⁵³ performed a very extensive series of measurements on hydrocarbons, mostly hexane, with steady and pulsed field and

showed a distinct cathode effect on the electric strength. He suggests space-charge mechanism for cathode effect formed by electron emission.

The hypothesis that the body of the liquid requires to be exposed to a certain field strength to cause rupture is presented by Crowe, Bragg and Sharbaugh^{9, 12}. Electron emission from the cathode is assumed and, as a result of the finite mobility of electrons in the liquids, a negative space charge accumulates, intensifying the field near the anode until a hypothetical "breakdown intensity" is reached. If cathode emission is low, this condition may be reached without field distortion. They have developed the theory in some detail and obtained experimental confirmation from breakdown measurements employing an aqueous solution of lithium chloride - an ionic salt - the concentration of which can be varied at will so that the emission of negative ions is under control.

Toriyama and Sakamoto⁶⁶ made a spectroscopic study of breakdown of liquid dielectrics. Their studies on the corona discharge in liquid dielectrics led to the conclusion that, in general, the first step is a dissociation of the liquid to molecules or atoms, and that these dissociated molecules or atoms became electrically charged. In his later work, Sakamoto⁵² studied the current-voltage characteristics of liquid insulations when stressed with both uniform and non-uniform fields. He concluded that the rapid increase in current observed with high electric fields was due to electron emission from the cathode and subsequent ionization of absorbed gases, rather than to collision ionization of liquid molecules. On the other hand, Hirano²⁴ attributes the breakdown of liquid insulations to ionization by collision.

Studies of conduction and breakdown in pure organic liquids by Goodwin and Macfadyen¹⁸ employing rectangular pulse technique leads to a theory of breakdown. Their conduction measurements support the view that strong fields produce conduction by emission from the cathode, together with ionization by electron collision with the liquid molecules. Accepting this interpretation of the pre-break-

down conduction currents, they show that a state of instability may arise from the combined effects of cathode emission and field distortion by ionic space charge. The theory accounts for the dependence of electric strength on electrode separation, cathode metal, pulse duration, and constitution of the liquid

Yamanaka and Suita⁷⁹ have applied their techniques for measuring electron avalanche distribution to liquids. They conclude that the electron avalanche formation is the decisive cause of the electric breakdown in liquids and that the critical avalanche size in liquid is about a hundred times smaller (10^5 electrons) than that in solids (10^7 electrons).

From the observed pressure effects on the breakdown of transformer oil, Watson and Higham⁷² conclude that a breakdown mechanism involving cavitation is possible under certain circumstances. Watson⁷¹ with further studies suggests that the breakdown can result from a number of mechanisms: an ionic mechanism in the pure transformer oil occurring with voltage impulse of microsecond duration; a second region - millisecond time range - where cavitation takes place; and finally, a region where particle impurities take effect owing to long duration of applied voltage.

The thermal breakdown of Watson and Sharbaugh⁷³ is based upon the energy, ΔH , needed to boil the liquid, that is:

$$\Delta H = m \left[C_p (\theta_b - \theta_o) + l_b \right] \quad (3.3)$$

where m is the amount of liquid evaporated, C_p is the average specific heat of the liquid at constant pressure over the range from the ambient temperature θ_o to the boiling point θ_b and l_b is the latent heat of vaporization at the boiling point.

In order to put the model on a quantitative basis, the local energy input is related to the applied field by:

$$\Delta H = AE^n T_r \quad (3.4)$$

where T_r is the residence time of the liquid in the high field

region near an asperity and may well be equal to the critical time lag T_c (see Fig. 3.10). In most cases, $n = \frac{3}{2}$ gives the closest approximation as shown in Fig. 3.8.

Krasucki³⁵ suggests that the breakdown results from the formation and growth in liquid of a bubble of vapour which is initiated by development of a point of zero pressure. He assumes that the particles of impurities, sub-micron in size, result in low pressure regions in the liquid at high electric field.

The condition for the onset of an avalanche in its simplest form in liquid can be expressed by von Hippel's⁶⁸ energy-balance criterion:

$$Ee\lambda = kh\nu \quad (3.5)$$

The left-hand side where E is the applied field and λ is the electron mean free path gives the energy gained by an electron from the field between collisions - that is, in travelling a distance λ . If $h\nu$ is the minimum quantum of energy required for excitation of the first vibrational level and k is a factor somewhat larger than unity (taking into account the fact that several levels may be involved), then the right-hand side represents the energy lost by an electron on collision.

The criterion has been applied to liquids by many authors^{10, 37, 57, 59, 70} and has been re-examined in great detail by Lewis⁴². He shows that in application to liquid alkanes ν is associated with vibrational modes of the carbon-hydrogen bonds. The breakdown field strength may be written as:

$$E = KN \left(\sum n_i Q_i \right)_{\max} \quad (3.6)$$

where Q_i and n_i are the maximum value of the cross section and the density of Group CH_i ($i = 1, 2, 3,$) contained in the molecules. The value of K depends on experimental conditions such as electrode configuration and material, voltage waveform and also on the frequency of the vibrational modes.

In the normal alkanes only CH_3 and CH_2 groups are present so that a plot of $E n_{\text{CH}_3}^{-1}$ against $n_{\text{CH}_2} \cdot n_{\text{CH}_3}^{-1}$ should give a straight line with an intercept of $k n_{\text{CH}_3}$ and a slope of $K Q_{\text{CH}_2}$. Such is indeed found to be true⁴², as shown in Fig. 3.13, where data are given for both d. c. and microsecond pulse applied voltages.

Berg and Kraitchman² offer support for the theory by Lewis³⁹. This concept may be applied to results such as those of Sharbaugh, Crowe and Cox⁵⁹ on the substituted aromatic compounds.

Kao and Higham²⁹ suggest a theory on breakdown, which is a combination of the hypotheses put forward by other experimenters, and their interesting work on cavities. They find good agreement between theoretical calculations of electric strength under various conditions and experimental results, and conclude that the electric breakdown mechanism consists of three main processes: electrical emission from the cathode, impact ionization and space charge formation in the liquid, cavity formation and elongation leading to a total breakdown.

A critical cavity size of 0.5 micron for n-hexane is suggested. Cavities below this size will collapse while larger cavities elongate under a field strength of about 2 MV/cm under normal conditions. Such an elongation may reach a critical value, then the cavity itself may break down and trigger the total breakdown of the liquid.

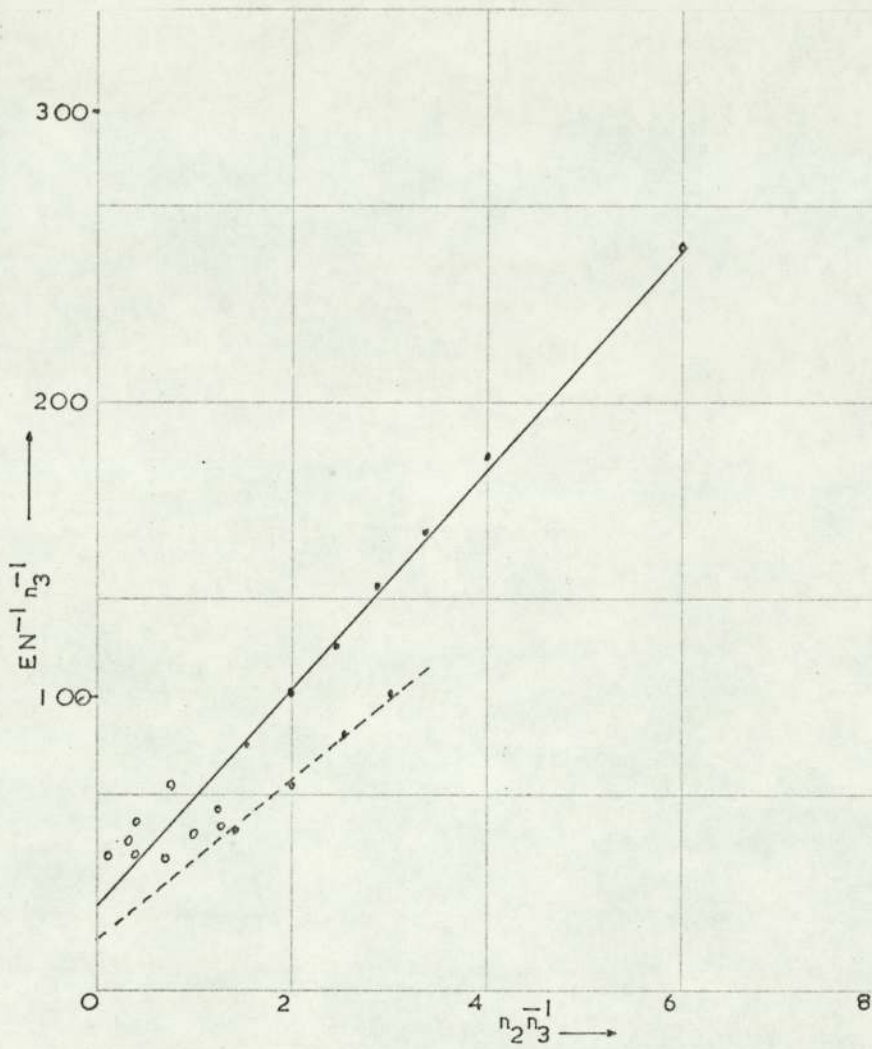


Fig.3.13. TEST PLOT OF ELECTRIC STRENGTH AS A FUNCTION OF MOLECULAR STRUCTURE FOR THE LIQUID ALKANES. (After Lewis 42).

— Pulse voltage --- Direct voltage
 o Branched alkanes ● Normal alkanes

3.3 Instrumentation

Similar instrumentation techniques to those used in the studies of gaseous dielectrics (see Section 2.3.) are employed. Pulse duration limiter triggering circuit (see Section 2.3.1.1.3) in conjunction with the chopping gap (see Section 2.3.1.1.6) are utilised throughout the experiments.

The test cell (see Fig. 3.14) comprises a glass cell with metallic electrodes of point-plane geometry arranged such that it provides sufficient surface area externally thus reducing the risk of tracking in air.

The electrode gap is made adjustable up to a distance of 4.5 cm by the operation of an externally mounted screw set specially sealed. A simple adjustable cassette supports the film within the test cell.

Both single and double emulsion film are used in a similar manner as in Section 2.3.2.2 except that they are washed in solvents to remove any trace of hydrocarbon liquids prior to development.

Transformer oil is selected as the liquid suitable for investigation. This is a relatively complex liquid but readily available. Its behaviour under high voltage electric surges is of special interest to power engineers.

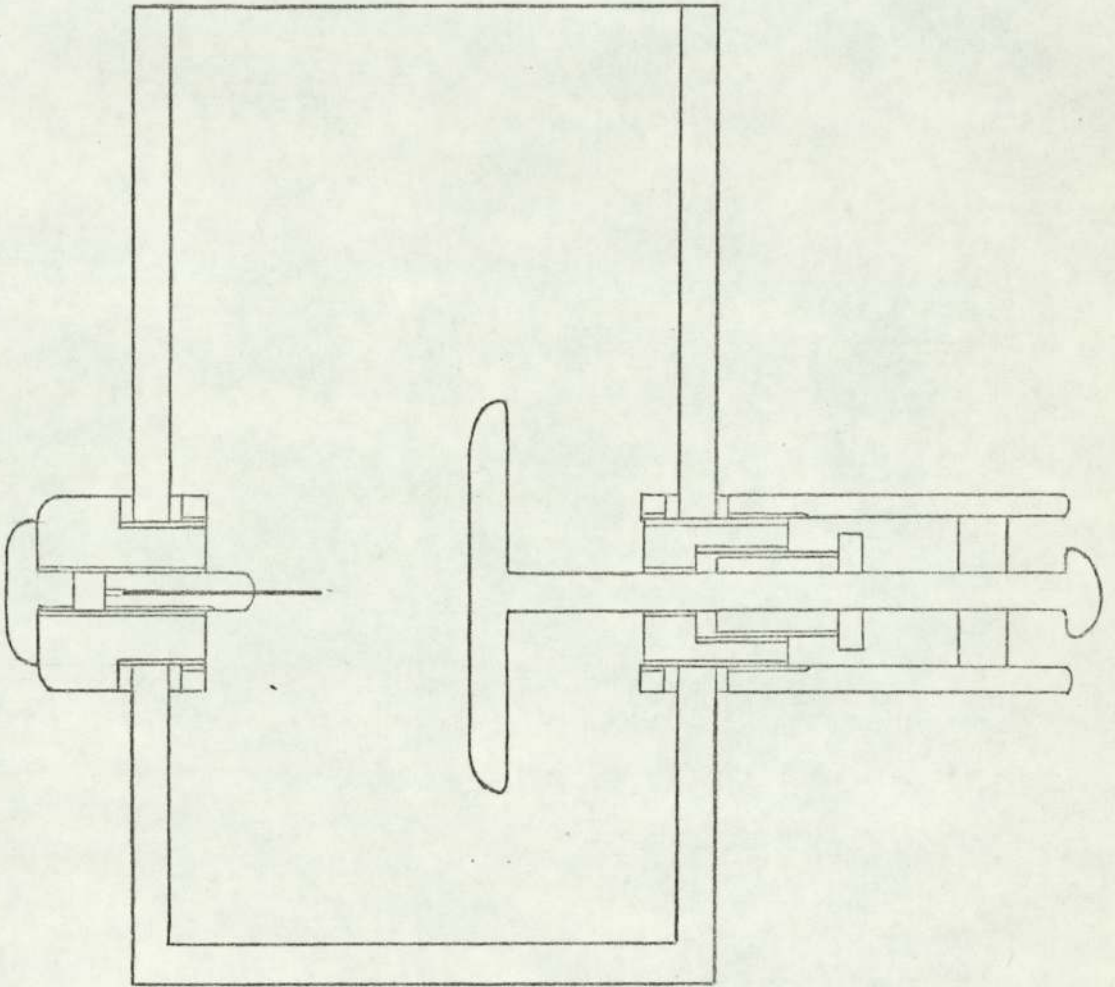


Fig. 3.14 The Test Cell Scale 1:1

3.4 Experimental Results

3.4.1 Streamer Range at Voltages Below Breakdown

Radiation-sensitive films are placed transverse to the field and a certain distance from the point-electrode. By increasing the impulse level in steps, the voltage at which the streamers reach the film is recorded. With repetition of the same procedure at several planes in the electrode inter-space, the streamer propagation range as a function of impulse level is found for both positive and negative streamers.

The streamer range for an electrode gap of 2.5 cm is shown in Fig. 3.15 and for a gap of 4.0 cm in Fig. 3.16. The radius of curvature of the point-electrode is kept unchanged at 100 microns.

The extent of photo-ionization and primary streamers is found to be so negligible that practically all the results are those of secondary streamers. This is confirmed by the occurrence of breakdown when the streamers propagate beyond the half-way gap length.

3.4.2 Streamer Spatial-temporal Build-up

The streamer growth at voltages above breakdown is investigated with the aid of chopped impulse wave. At different potential levels above the breakdown value, the impulse duration is increased in steps and the reach of the streamer propagation is measured. This process results in the spatial-temporal build-up of the secondary streamers as shown in Fig. 3.17 for point-cathode and in Fig. 3.18 for point-anode. The impulse potential level varies in the range 75 - 200 kV. The electrode gap is 2.5 cm and the radius of curvature of the point-electrode is 100 microns.

TABLE 3.1 Variation in Streamer Range with applied potential in transformer oil at N. T. P.

Point-plane electrode; radius of curvature of point, C , = 100 microns
 $1/50 \mu s$ impulse wave.

(a) Electrode gap length, G , = 2.5 cm

Streamer range, L_s , mm		2	5	10	15	20	25
Impulse Wave kV	Point-Cathode	39	57	70	76	81	81
	Point-Anode	35	39	50	55	58	58

(b) Electrode gap length, G , = 4.0 cm

Streamer range, L_s , mm		2	5	10	15	20	25	30	40
Impulse Wave kV	Point-Cathode	50	65	75	85	90	97	100	100
	Point-Anode	35	45	60	70	75	77	79	79

FIG. 3.15 Secondary Streamer Range as a Function of Impulse Voltage in Transformer Oil at N.T.P.

POINT-PLANE ELECTRODE
 RADIUS OF CURVATURE OF POINT, $C=100$ microns
 ELECTRODE GAP LENGTH, $g=2.5$ cm.
 $1/50 \mu s$ IMPULSE WAVE

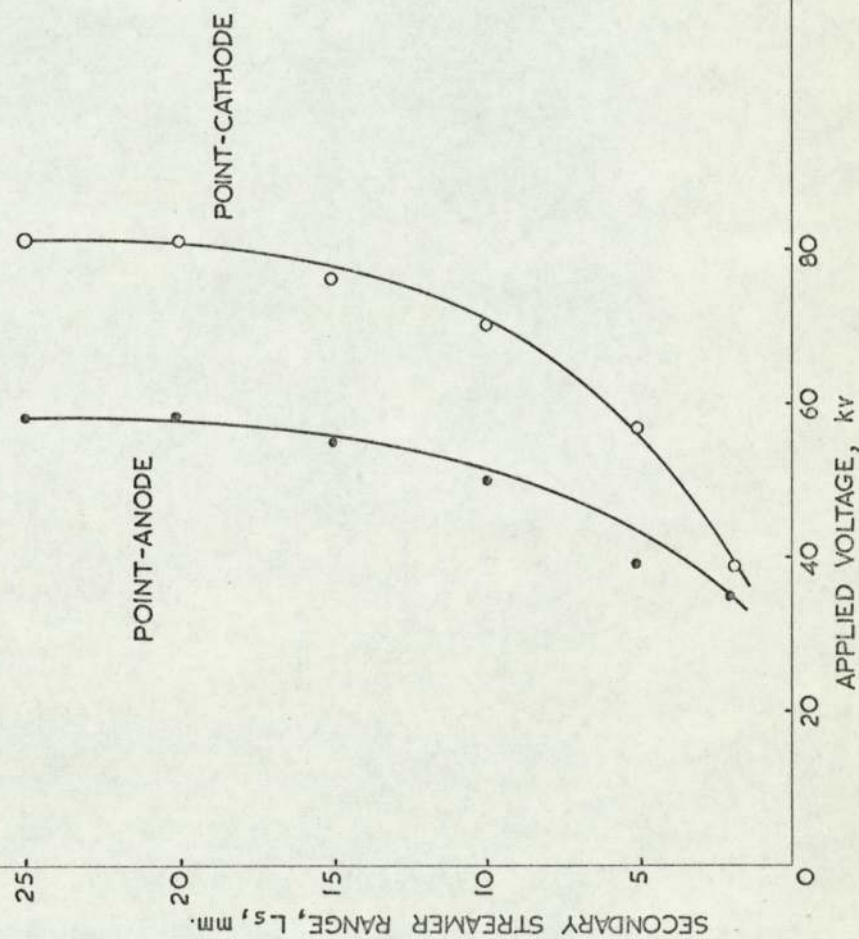


FIG. 3.16 Secondary Streamer Range as a Function of Applied Voltage in Transformer Oil at N.T.P.

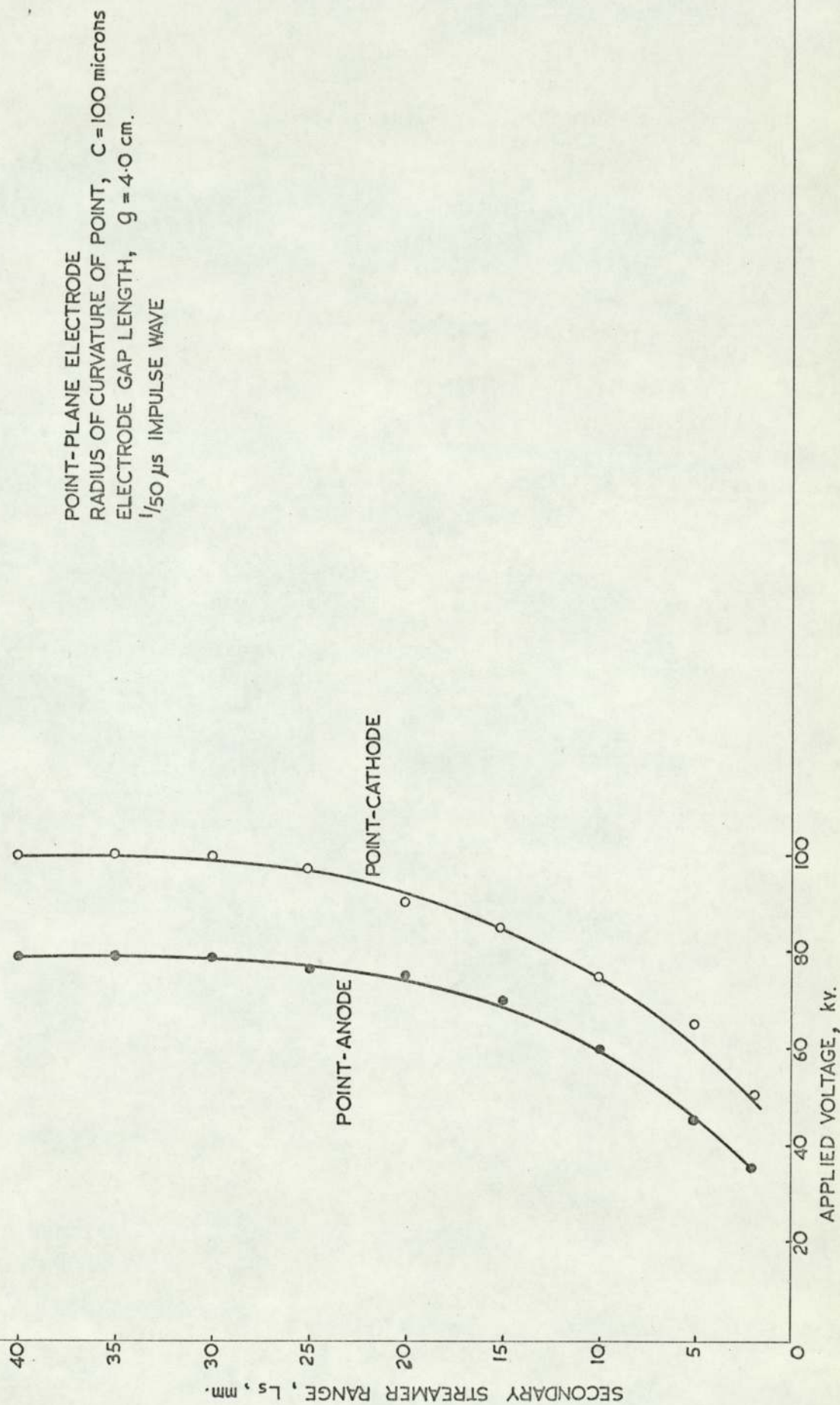


TABLE 3.2 Secondary negative-streamer range, L , in transformer oil at N. T. P. Point-plane electrode; point-cathode; $1/50 \mu s$ chopped wave; radius of curvature of point, C , = 100 microns; electrode gap length, G , = 2.5 cm.

		75 kV Pulse Width μs								
L_{mm}		2	5	10	15	20	25	30	35	50
2		✓								
	0	✓	✓	✓						
	0	✓	✓	✓						
	0	0	0	0						
5										
	0		✓	✓	✓					
	0		✓	✓	✓					
	0	0	0	0	✓					
10										
	0				✓	✓				
	0				✓	✓				
	0				0	✓				
15										
	0					✓	✓			
	0					0	✓			
	0					0	0			
20										
	0						✓	✓		
	0						0	✓		
	0						0	0		
25										
	0							✓	✓	
	0							0	✓	
	0							0	0	

		100 kV Pulse Width μs							
L_{mm}		2	5	10	15	20	25	30	35
2		✓							
	0	✓	✓						
	0	✓	✓						
	0	0	✓						
5									
	0		✓	✓					
	0		✓	✓					
	0	0	0	✓					
10									
	0			✓	✓				
	0			✓	✓				
	0			0	0				
15									
	0				✓	✓			
	0				0	✓			
	0				0	0			
20									
	0					✓	✓	✓	
	0					0	✓	✓	
	0					0	0	✓	
25									
	0						✓	✓	✓
	0						0	✓	✓
	0						0	0	✓

		150 kV Pulse Width μs						
L_{mm}		2	6	10	14	18	22	26
2		✓						
	0	✓						
	0	✓						
	0	0						
5								
	0		✓					
	0		✓					
	0	0	✓					
10								
	0		0	✓				
	0		0	✓				
	0		0	0				
15								
	0			✓	✓	✓		
	0			0	0	✓		
	0			0	0	0		
20								
	0				✓	✓	✓	
	0				0	0	✓	
	0				0	0	0	
25								
	0					✓	✓	✓
	0					0	0	✓
	0					0	0	0

		200 kV Pulse Width μs					
L_{mm}		1	2	3	4	5	6
2		✓					
	0	✓					
	0	✓					
	0	0					
5							
	0		✓				
	0		✓				
	0	0	✓				
10							
	0		✓	✓	✓		
	0		0	0	✓		
	0		0	0	0		
15							
	0		0	✓	✓		
	0		0	0	✓		
	0		0	0	0		
20							
	0			✓	✓	✓	
	0			0	0	✓	
	0			0	0	0	
25							
	0				✓	✓	✓
	0				0	0	✓
	0				0	0	0

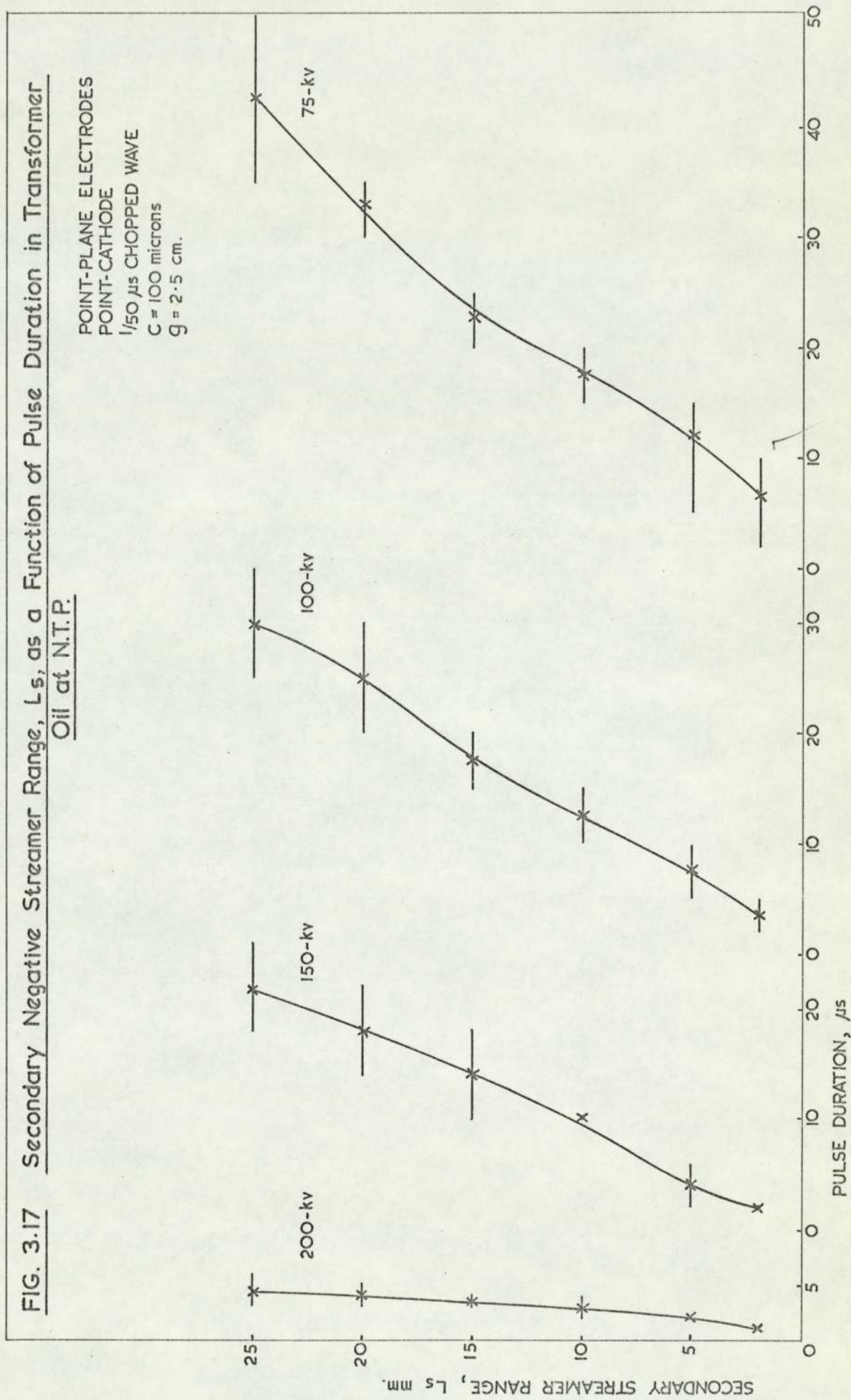


TABLE 3.3 Secondary positive-streamer range, L , in transformer oil at N.T.P. Point-plane electrode; point-anode; $1/50 \mu s$ chopped wave; radius of curvature of point, C , = 100 microns; electrode gap length, G , = 2.5 cm.

75 kV
Pulse Width μs

L_{mm}	2	4	8	12	16	20
2	✓ 0 0 0 0	✓ ✓ 0 0	✓ ✓ 0 0			
5		0 0 0 0	✓ ✓ 0 0	✓ ✓ 0 0		
10			✓ 0 0 0	✓ 0 0		
15			✓ 0 0 0	✓ ✓ ✓ ✓		
20				✓ 0 0 0	✓ ✓ ✓ 0	
25					✓ ✓ 0 0	✓ ✓ ✓ ✓

100 kV
Pulse Width μs

L_{mm}	2	4	6	8	10	12	14	16
2	✓ 0 0 0 0	✓ ✓ 0 0	✓ ✓ ✓ 0					
5		0 0 0 0	✓ ✓ 0 0	✓ ✓ ✓ ✓				
10			0 0 0	✓ ✓ 0	✓ ✓ 0			
15					✓ 0 0 0	✓ ✓ 0 0	✓ ✓ 0 0	
20						✓ 0 0 0	✓ ✓ 0 0	
25						✓ ✓ 0 0	✓ ✓ ✓ ✓	✓ ✓ ✓ ✓

150 kV
Pulse Width μs

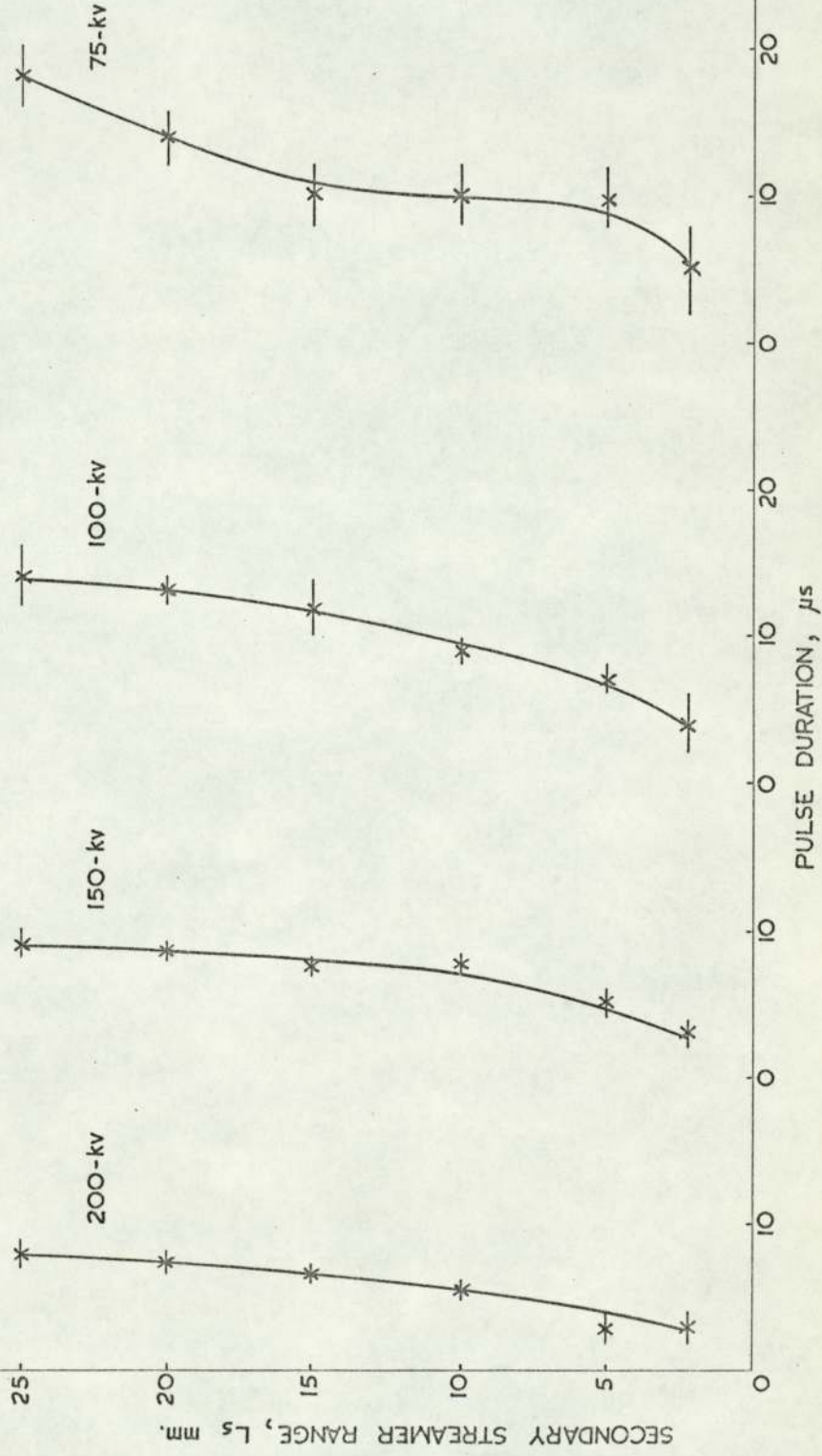
L_{mm}	2	4	5	6	7	8	9	10
2	✓ ✓ 0 0	✓ ✓ 0						
5		✓ 0 0	✓ ✓ 0	✓ ✓ 0				
10					✓ ✓ 0	✓ ✓ 0		
15					✓ 0 0	✓ ✓ 0		
20						✓ 0 0	✓ ✓ 0	
25						✓ 0 0 0	✓ ✓ 0 0	✓ ✓ ✓ ✓

200 kV
Pulse Width μs

L_{mm}	2	4	5	6	7	8	9
2	✓ ✓ 0 0	✓ ✓ ✓ 0					
5		✓ 0 0 0	✓ ✓ ✓ 0				
10			✓ 0 0 0	✓ ✓ 0			
15				✓ 0 0	✓ ✓ 0		
20					✓ ✓ 0	✓ ✓ ✓	
25					✓ ✓ 0 0	✓ ✓ ✓ 0	✓ ✓ ✓ ✓

FIG. 3.18 Secondary Positive Streamer Range, L_s , as a Function of Pulse Duration in Transformer Oil
at N.T.P.

POINT-PLANE ELECTRODES.
POINT-ANODE
1/50 CHOPPED WAVE
C = 100 microns
g = 2.5 cm.



3.4.3 Streamer Velocity

To make a reasonable evaluation of the extensive volume of measurements on the streamer spatial-temporal build-up, a new method of presentation is employed. The results are shown in percentage value in Fig. 3.19 for different potential levels and polarities. The number on each line represents the pulse duration.

From the graphs of streamer range as a function of pulse duration, the velocity of streamers are deduced. The secondary positive and negative streamers velocity for both 100% and 50% values are shown in Fig. 3.20 for the voltage range 75 - 200 kV.

3.4.4 Time-integrated Streamer Pattern

The time-integrated traces of secondary streamers are shown in Fig. 3.21 for point-cathode and in Fig. 3.22 for point-anode arrangements. Extensive branching of the discharge is recorded irrespective of the polarity of the impulse voltage. The branching increases with the range of streamers across the gap.

FIG. 3.19 Secondary Streamer Range as a Function of Pulse Duration in Transformer Oil at N.T.P.

POINT-PLANE ELECTRODE
 C = 100 microns
 g = 2.5 cm.
 1/50 μs CHOPPED WAVE

Numbers on Graphs Correspond to Pulse Duration.

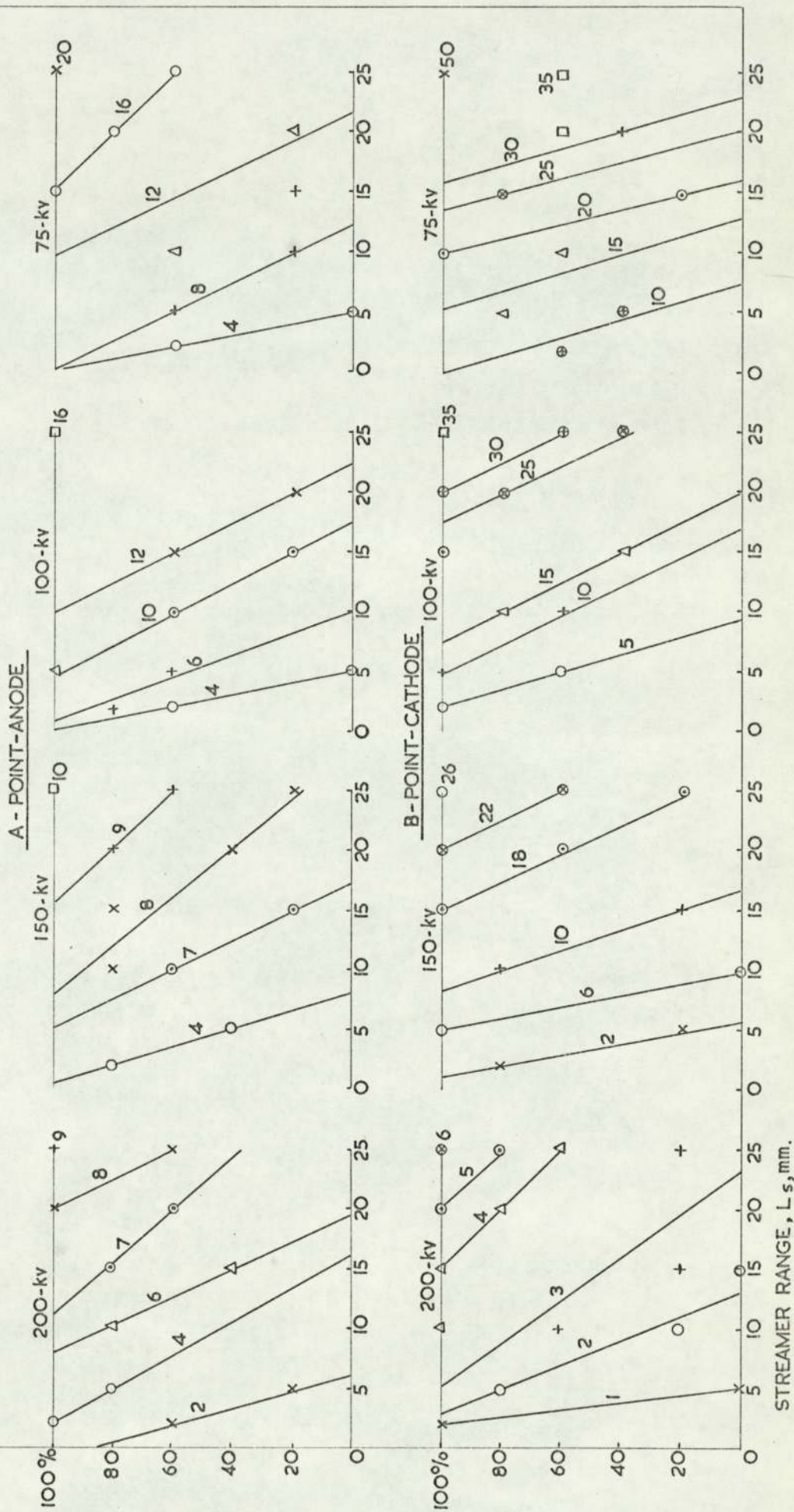


TABLE 3.4 Secondary Streamer Velocity in Transformer Oil at N. T. P.

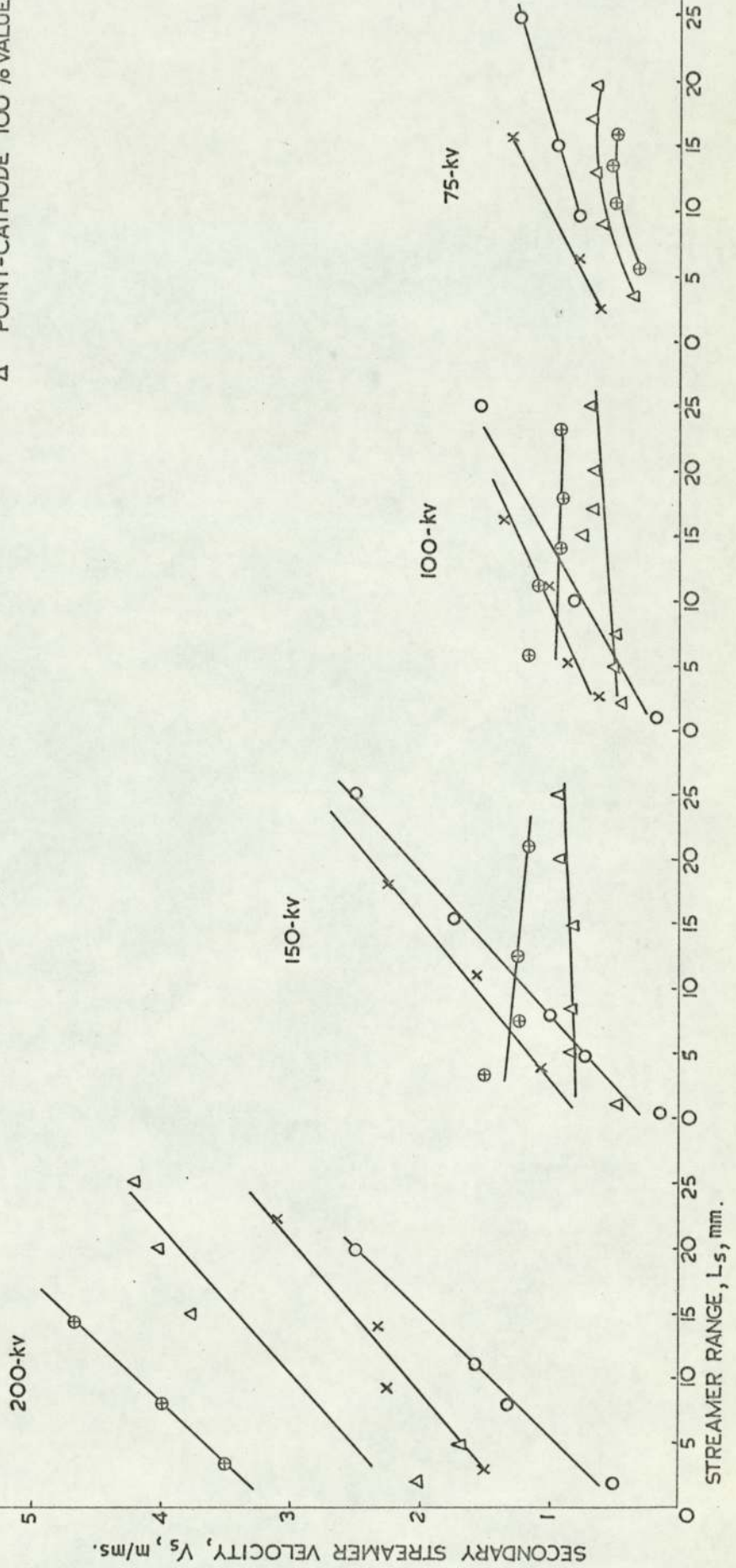
Point-plane electrode; $1/50 \mu\text{s}$ chopped wave; radius of curvature of point, $C = 100$ microns
 electrode gap length, $G = 2.5$, cm

Potential level	200 kv		150 kv		100 kv		75 kv							
Streamer parameters	L_s mm	T μs	V_s m/ms	L_s mm	T μs	V_s m/ms	L_s mm	T μs	V_s m/ms					
Point-Anode	50% value	3	2	1.5	4.3	4	1.08	2.5	4	0.63	2.5	4	0.63	
		9	4	2.25	11	7	1.58	5.3	6	0.88	6.3	8	0.79	
	100% value	13.8	6	2.3	18	8	2.25		11	10	1.1	15.6	12	1.3
		22	7	3.1				16.3	12	1.36				
	50% value	2	4	0.5	0.5	4	0.125		1	6	0.17	9.5	12	0.79
		8	6	1.3	5	7	0.72		5	10	0.5	15	16	0.94
	100% value	11	7	1.6	7.8	8	0.98		10	12	0.83	25	20	1.25
		20	8	2.5	15.4	9	1.73		25	16	1.56			
	50% value	25	9	2	25	10	2.5							
		3.5	1	3.5	3.5	2	1.75		5.8	5	1.16	5.3	15	0.34
100% value	8	2	4	7.5	6	1.23		11	10	1.1	10	20	0.5	
	14	3	4.63	12.5	10	1.25		13.8	15	0.92	13.5	25	0.54	
100% value	2	1	2	21	18	1.16		18	20	0.9	16	30	0.53	
				23.3	25	0.93		23.3	25	0.93				
100% value	2	1	2	1	2	0.5		2	5	0.4	3.5	10	0.35	
				5	6	0.83		5	10	0.5	9	15	0.6	
100% value	3	1.5	8.3	7.5	15	0.83		7.5	15	0.5	13	20	0.65	
				15	18	0.83		15	20	0.75	17	25	0.68	
100% value	15	3.75	20	20	22	0.91		17	25	0.68	19.5	30	0.65	
				25	26	0.96		20	30	0.67	25	35	0.71	
100% value	25	4.18	25	25	26	0.96		25	30	0.67	25	35	0.71	
				25	26	0.96		25	30	0.67	25	35	0.71	

FIG. 3.20 Secondary Streamer Velocity in Transformer Oil at Electric Field Strength Beyond Breakdown

POINT-PLANE ELECTRODES
 $C = 100$ microns
 $g = 2.5$ mm.
 $1/50 \mu s$ CHOPPED WAVE

X POINT-ANODE 50% VALUES
 O POINT-ANODE 100% VALUES
 ⊕ POINT-CATHODE 50% VALUES
 Δ POINT-CATHODE 100% VALUES



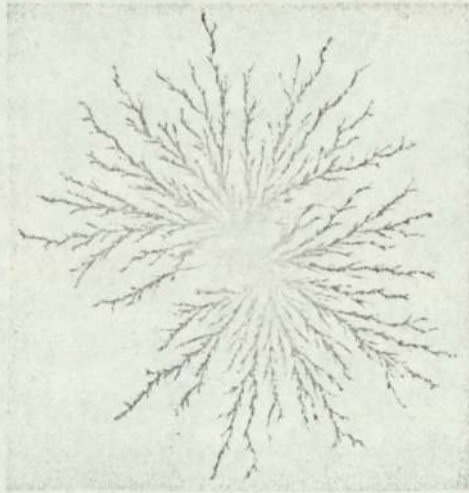


Fig. 3.21 Negative Secondary Streamer Pattern when film is placed against the point-electrode transverse to the main electric field axis in oil.

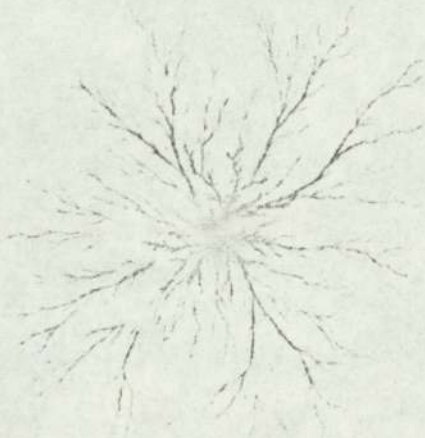


Fig. 3.22 Positive Secondary Streamer Pattern when film is placed against the point-electrode transverse to the main electric field axis in oil.

3.5 Discussion

The experimental evidence provides a clear picture of the behaviour of transformer oil under electric field strength at pre- and post-breakdown values. With the increase in the magnitude of applied voltage, avalanches accumulate at the converging field near the point-electrode and set up streamers. Below breakdown field strength, the growth of the streamers reaches a limit in size which does not change with increase in voltage duration.

The streamers develop in the form of numerous branches which propagate until the earthed electrode is reached. They can span half-way across the gap within two microseconds.

A secondary streamer may penetrate to over half the gap length without causing breakdown, but once the propagation reaches beyond the range, the breakdown is normally assured.

The streamers grow with increase in voltage and time. They have been recorded at a field strength as low as half the breakdown field for the electrode gap lengths of 2.5 and 4.0 cm.

Above a certain field strength, if enough time is allowed, the secondary streamers bridge the gap and the breakdown occurs. This explains the increase in breakdown voltage with reduction of its duration and also explains the contradiction which exists between groups of investigators^(29, 37), particularly in a point-plane geometry.

The formative time lag in the lower voltage range is about twice as long in the case of point-cathode as compared with the point-anode. This gap narrows down with the increase in voltage and, at very high over-voltage, the reverse situation arises. As much as 90% of the formative time lag may be required for the streamers to propagate only half-way across the gap.

The velocity of negative secondary streamers at low values of over-voltage is nearly constant at about 10^5 cm/sec, across the gap. At higher over-voltages, the growth of negative secondary streamers

is accelerated across the gap, reaching a value of about 5×10^5 cm/sec. near the plane anode.

The positive secondary streamer velocity, which is of the same magnitude as the negative one near the point-electrode, increases with the progress across the gap. Near the plane-cathode, the increase in velocity is nearly twofold.

3.6 Bibliography

1. Basseches, H., and Barnes, M. W.
Ann.Rept. Conf. on Elec.Ins. (1956)
2. Bergs, D., and Kraitchman, J.
Ann.Rept. Conf. on Elec.Ins. (1956)
3. Blanc, D., Gron, G., Mathieu, J., Ponsan, M. and Pujol, T.
C.R. Acad.Sci., Paris, 249, p. 2546 (1959)
4. Blanc, D., and Mathieu, J.
J.Phys.Radium 21, p. 675 (1960)
5. Bragg, J. K., Sharbaugh, A. H., and Crowe, R. W.
J.Appl.Phys., 25, p. 383 (1954)
6. Clark, F. M.
J.Franklin Inst., 215, p. 39 (1933)
7. Crowe, R. W.
Ann.Rept. Conf. on Elec.Ins. (1954)
8. Crowe, R. W.
J.Appl.Phys., 104, p. 572 (1956)
9. Crowe, R. W., Bragg, J. K., and Sharbaugh, A. H.
Ann.Rept. Conf. on Elec.Ins. (1952)
10. Crowe, R. W., Bragg, J. K. and Sharbaugh, A. H.,
J.Appl.Phys., 25, p. 392 (1954)
11. Crowe, R. W., Sharbaugh, A. H., and Bragg, J. K.
Ann.Rept. Conf. on Elec.Ins. (1953)
12. Crowe, R. W., Sharbaugh, A. H., and Bragg, J. K.
J.Appl.Phys., 25, p. 1480 (1954)
13. Dornte, R. W.
Indust.Engrg.Checm., 32, p. 1529 (1940)

14. Edward, W. D.
Canada, *J. Phys.*, 29, p. 310 (1951)
15. Edward, W. D.
J. Chem. Phys., 20, p. 753 (1952)
16. Essex, V., and Secker, P. E.
Brit. J. Appl. Phys. (J. Phys. D.), 1, p. 63 (1968)
17. Gemant, A.
Zeits. Phys., 33, p. 789 (1925)
18. Goodwin, D. W., and Macfadyen, K. A.
Proc. Phys. Soc. (London), B66, p. 85 (1953)
19. Green, W. B.
J. Appl. Phys., 26, p. 1257 (1955)
20. Green, W. B.
J. Appl. Phys., 27, p. 921 (1956)
21. Hakim, S. S. and Higham, J. B.
Nature, London, 189, p. 996 (1961)
22. Hakim, S. S. and Higham, J. B.
Proc. Phys. Soc. (London), 80, pt. 1, p. 190 (1962)
23. Hart, J., and Mungall, A. G.
Trans. A. I. E. E., Pt. 3, p. 1295 (1958)
24. Hirano, S.
J. Inst. Elec. Eng. Japan, 63, p. 463, (1943)
25. Hirano, S.
J. Inst. Elec. Eng. Japan, 65, p. 271 (1944)
26. Hirano, S.
J. Inst. Elec. Eng. Japan, 65, p. 359 (1945)
27. House, H.
Proc. Phys. Soc. (London), B70, p. 913 (1957)
28. Kao, K. C. and Calderwood, J. H.
Proc. I. E. E., 112, p. 597 (1965)

29. Kao, K. C. and Higham, J. B.
J. Electrochem. Soc., 108, p. 522 (1961)
30. Kock, G.
Elektrot. Zeits., 36, p. 85 (1915)
31. Kok, J. A.
Electrical Breakdown of Insulating Liquids, Phillips
Technical Library, Holland (1961)
32. Kok, J. A., and Corbey, M. M. G.
Appl. Sci. Res., 4B, p. 474 (1955)
33. Komelkov, V. S.
Acad. Sci, U. S. S. R., 47, p. 268 (1945)
34. Koppelman, F.
Z. Tech. Phys., 16, p. 126 (1935)
35. Krasucki, Z.
E. R. A. Rept. 5157 (1966)
36. Le Blanc, O. H.
J. Chem. Phys., 30, p. 1443 (1959)
37. Lewis, T. J.
Proc. I. E. E., pt. IIA, 100, p. 141 (1953)
38. Lewis, T. J.
Proc. Phys. Soc. (London), B66, p. 425 (1953)
39. Lewis T. J.
J. Appl. Phys., 27, p. 645 (1956)
40. Lewis, T. J.
J. Appl. Phys., 28, p. 503 (1957)
41. Lewis, T. J.
Progress in Dielectrics, Vol 1, Heywood, London (1959)
42. Lewis, T. J.
J. Electrochem. Soc., 107, p. 185 (1960)

43. Lewis, T. J.
Advancement of Science, p. 501 (1964)
44. Liao, T. W., and Anderson, J. G.
Trans. A. I. E. E., pt. 1, 72, p. 641 (1953)
45. Macfadyen, K. A.
Brit. J. Appl. Phys., 6, p. 1, (1955)
46. Macfadyen, K. A., and Edwards, E. D.
Nature, London, p. 163 (1949)
47. Macfadyen, K. A., and Edwards, E. D.
Proc. Phys. Soc. (London), B66, p. 665 (1953)
48. Macfadyen, K. A. and Helliwell, G. C.
J. Electrochem. Soc., 106, p. 1022 (1959)
49. Maksiejewski, J. L., and Tropper, H.
Proc. I. E. E., pt. II, 101, p. 183 (1954)
50. Morant, M. J.
Nature, London, 187, p. 48 (1960)
51. Nikuradse, A.
Das Flussige Dielektrum, Springer, Berlin (1934)
52. Sakamoto, S.
J. Inst. Elec. Eng. Japan, 73, p. 722 (1953)
53. Salvage, B.
Proc. I. E. E., pt. II, 98, p. 227 (1951)
54. Sharbaugh, A. H., Bragg, J. K., and Crowe, R. W.
Ann. Rept. Conf. on Elec. Ins. (1952)
55. Sharbaugh, A. H., Bragg, J. K., and Crowe, R. W.
J. Appl. Phys., 24, p. 16 (1953)
56. Sharbaugh, A. H., Bragg, J. K., and Crowe, R. W.
J. Appl. Phys., 24, p. 814 (1953)
57. Sharbaugh, A. H., Bragg, J. K., and Crowe, R. W.
J. Appl. Phys., 26, p. 434 (1955)

58. Sharbaugh, A. H., Cox, E. B., Crowe, R. W., and Auer, P. L.
Ann. Rept. Conf. on Elec. Ins. (1955)
59. Sharbaugh, A. H., Crowe, R. W., and Cox, E. B.
J. Appl. Phys., 27, p. 806 (1956)
60. Sharbaugh, A. H., and Watson, P. K.
Progress in Dielectrics, Vol. 4, Heywood, London (1962)
61. Sletton, A. M.
Nature, London, 187, p. 48 (1960)
62. Sletton, A. M.
Ann. Rept. Conf. on Elec. Ins. (1961)
63. Swan, D. W., and Lewis, T. J.
Proc. Phys. Soc., London, 76, p. 36 (1960)
64. Swan, D. W.
J. Electrochem. Soc., 107, p. 180 (1960)
65. Swan, D. W., and Lewis, T. J.
Proc. Phys. Soc., London, 78, p. 448 (1961)
66. Toriyama, Y, and Sakamoto, S.
J. Inst. Elec. Eng., Japan, 64, p. 271 (1944)
67. Vick, F. A.,
Sci. Prog., 43, p. 267 (1955)
68. von Hippel, A.,
J. Appl. Phys., 8, p. 815 (1937)
69. von Hippel, A., and Alger, R. S.
Phys. Rev., 76, p. 126 (1949)
70. Ward, B. W., and Lewis, T. J.
Ann. Rept. Conf. on Elec. Ins. (1963)
71. Watson, P. K.
Ann. Rept. Conf. on Elec. Ins. (1955)

72. Watson, P. K., and Higham, J. B.
Proc.I.E.E., pt. IIA, 100, p. 168 (1953)
73. Watson, P. K., and Sharbaugh, A. H.
J.Electrochem.Soc. 107, p. 516 (1960)
74. Weber, K. H., and Endicott, H. S.
Ann.Rept.Conf. on Elec.Ins. (1955)
75. Weber, K. H., and Endicott, H. S.
Trans.A.I.E.E., (P.A.S.), 24, p. 371 (1956)
76. Whitehead, S.
Dielectric Phenomena, Vol. 2, Benn, London, (1928)
77. Williams, R. L.
Canada. J.Phys., 35, p. 134 (1957)
78. Williams, R. L., and Stacey, F. D.
Canada. J.Phys., 35, p. 928 (1957)
79. Yamanka, C., and Suita, T.
J.Phys.Soc.Japan, 8, p. 277 (1953)
80. Zein El-Dine, M. E., and Tropper, H.
Proc.I.E.E., pt. II, 102, p. 1355 (1955)

CHAPTER 4

SOLID DIELECTRICS

4.1 Introduction

The first period of extensive studies of an electrical breakdown in solid dielectrics started over forty years ago, and has been on inorganic groups of materials, especially those possessing high stability and crystalline structure.

The second period covers the last decade when organic solid dielectrics, especially the group of polymers, came to the forefront due to their ever-increasing role in all branches of the electrical industry.

When breakdown strength of solids is referred to, without qualification, it usually means the value obtained by placing a plane slab of the material between electrodes, and raising the voltage over a certain period of time until failure occurs.

It has gradually become evident that results so obtained do not represent any single property of the material tested. Even homogeneous materials, free from faults and leakage currents causing excessive heating, give results which conflict with the idea of a single strength characteristic of the material in the following manner:-

- (a) if good contact is secured between the electrodes and the material, failure occurs outside the electrode area, where the stress in the material is relatively low, and at a distance from the electrode which precludes explanation in terms of the electrostatic stress - concentration at the edges;
- (b) the withstand voltage is not proportional to thickness but more nearly to the square root of thickness;
- (c) immersion media play an important part and by increasing their conductivity the strength can be greatly increased;
- (d) the breakdown voltage is time-dependent.

About 1925, it became apparent that tests of this kind

measured the response of the material to some degradation process occurring at the interface between the material and its immersion medium. It was soon established that, in homogenous, low-loss, materials, the secondary failure was caused by discharges in the ambient medium, although their role was not elucidated in detail until 1955.

The effects of discharges explain all the anomalies mentioned earlier. In tests by the "plane slab" method: (a) if the electrodes make good contact, the discharge can only impinge ^{OUTSIDE} ~~outside~~ the electrodes where the failure occurs; (b) where discharge impinges on the material, the stress concentration becomes a function of discharge diameter/specimen thickness ratio resulting in the special strength-thickness relationship; (c) high conductivity reduces the stress in the medium, and so postpones the onset of discharges to a higher applied voltage; (d) either in a "short time" by a few high stress acting discharges, or in a "longer time" by many more acting at lower stress ~~the breakdown may occur.~~

The spatial structure of the breakdown channels and their development with time as a function of voltage level, waveform and duration in polymethylmethacrylate (PMMA) were studied. This material possesses desirable mechanical and optical properties (see Appendix 7.10) and can be readily polished.

It has been possible, by taking suitable precautions, to limit the amount of energy converted in the breakdown channels and to distinguish the spatial progress of streamers produced during the disruptive phase.

The occurrence of discrete discharge channels in the solid dielectric implies that the electric field has become inhomogeneous at the beginning of the disruptive phase. It therefore seems reasonable to study the development of the streamers in an electric field which is originally non-uniform. An added advantage is that, for the same applied voltage level, a larger

electrode gap can be utilised.

Due to the absence of dielectric recovery in solids, the discharge channels provide a permanent record of breakdown phenomena. By employing transparent solid dielectrics, advantage is taken of these undesirable channels which are measured by optical means.

4.2 Literature Survey

4.2.1 Introduction

Prior to the studies of von Hippel³⁶, who measured the intrinsic electric strength of a series of alkali halides, the literature on the electric strength of solid dielectrics consisted to a large extent of compendia of unrelated observations.

Early knowledge of breakdown processes is extensively summarised by Whitehead⁸² for the period up to 1932. The same author⁸³ in 1951 deals in detail with the concept of intrinsic strength of solids. There has been numerous surveys of the progress in this field by many authors^{14, 15, 25, 50, 54, 58, 67, 71, 84}.

Theories relating to the failure of solid dielectrics are shown in a chart form in table (4.1). These can be divided into two main groups: (a) failures due to "primary effects" which are generally of "short duration", and (b) failures due to "secondary effects" which are of "long duration".

In most engineering applications of solid dielectrics, it is the secondary effects which lead to system failures. This has resulted in tremendous scientific interest and effort being concentrated in understanding the failure mechanism of this type. However, it is the study of primary effects, especially those of a microscopic nature, which bring about the deepest insight into material behaviour and usually leads into new and improved material discovery.

4.2.2 Electrode Effect

Speculation about the influence of the cathode on electric strength was stimulated by the work of von Hippel and Alger⁴⁰, who used specimens of unannealed potassium bromide with cathodes of saturated aqueous potassium bromide solution, mercury and evaporated gold. The mean electric strength in the former case was 0.84 MV/cm but with metal cathodes it was only about 0.55 MV/cm.

THEORIES OF BREAKDOWN

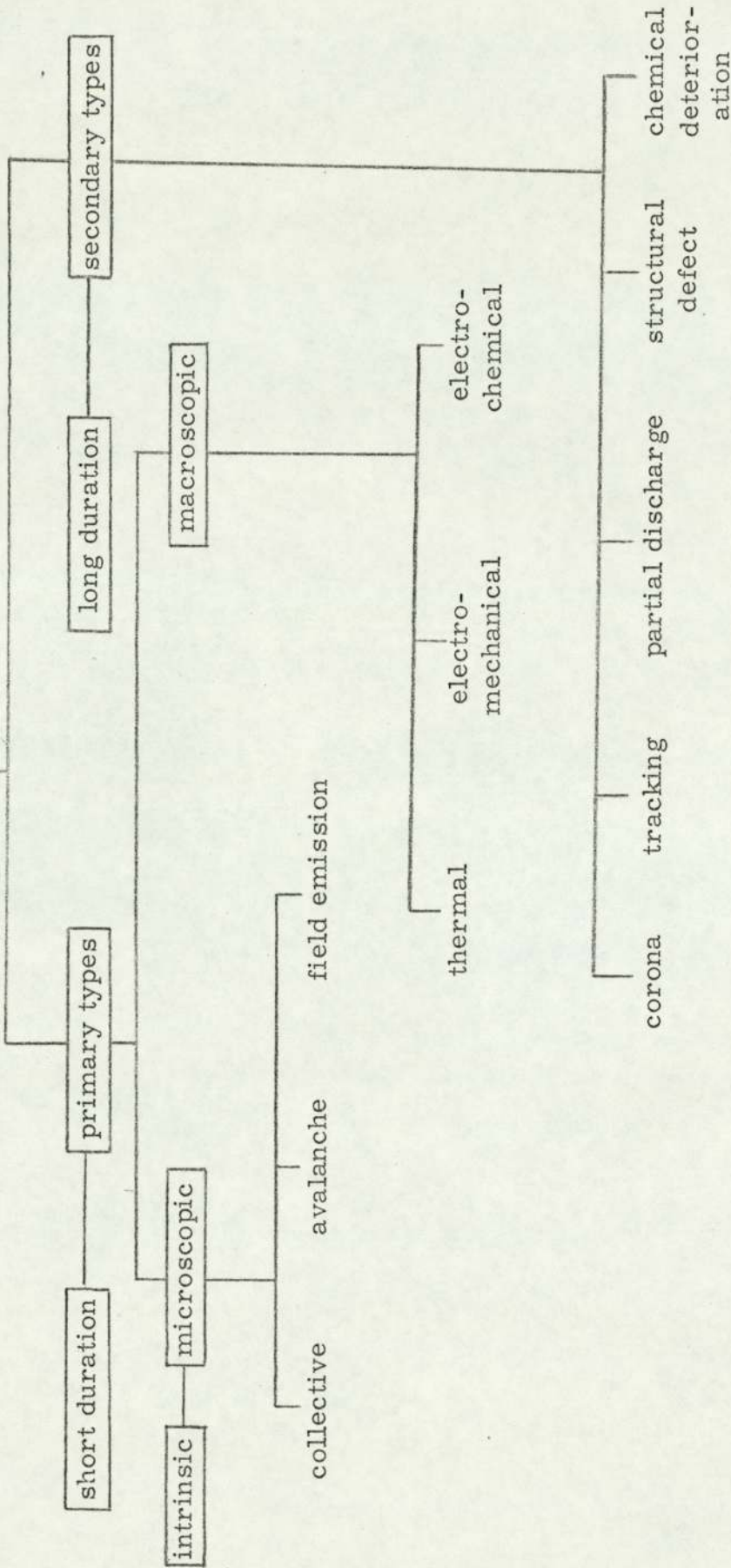


TABLE 4.1 Theories of Breakdown of Solid Dielectrics

Vorob'yev⁷⁸ has obtained results which indicate that the mean electric strength of sodium chloride with electrolytic cathode is about 70% greater than with graphite cathode, but Kostrygin⁴⁵ has stated that the electric strength obtained in these two circumstances is the same.

Cooper and Grossart¹⁷ observed no differences in the mean electric strength of potassium bromide with cathodes of graphite, gold and electrolyte, but Calderwood, Cooper and Wallace¹¹ obtained a difference of about 20% between the electric strength of potassium chloride with electrolytic and graphite cathode.

The difference can be explained by structural differences, influence of annealing and the scatter in experimental results.

Oakes^{55, 56} reported mean electric strength of 5.9, 6.9 and 7.6 MV/cm, for specimens of polyethylene having silver electrodes, graphite electrodes, and graphite anodes and mercury cathodes, respectively. Cooper, Rowson and Watson¹⁹ reported mean values of 4.9 and 4.4 MV/cm with cathodes of colloidal graphite and evaporated aluminium respectively, employing impulse voltages.

Vermeer^{76, 77}, who used electrodes of evaporated silver, mercury and electrolytic solutions, concluded that the intrinsic electric strength of glass was independent of the electrode substance.

There is evidence that the electric strength depends on specimen thickness in the range 1 - 1000 microns. Vorob'yev et al claim that the electric strength of sodium chloride, potassium chloride, potassium bromide, polymethyl metacrylate and celluloid decrease slowly with thickness. Cooper's¹⁵ study on potassium bromide confirms this view (see Fig. 4.1). Cooper and Smith²⁰ established a high negative correlation coefficient between minimum values of electric strength and thickness for strain-free sodium chloride single crystals in the range 100 - 700 microns. The value at 20°C decreased from 0.85 to 0.70 MV/cm. Kostrygin⁴⁵ found that the

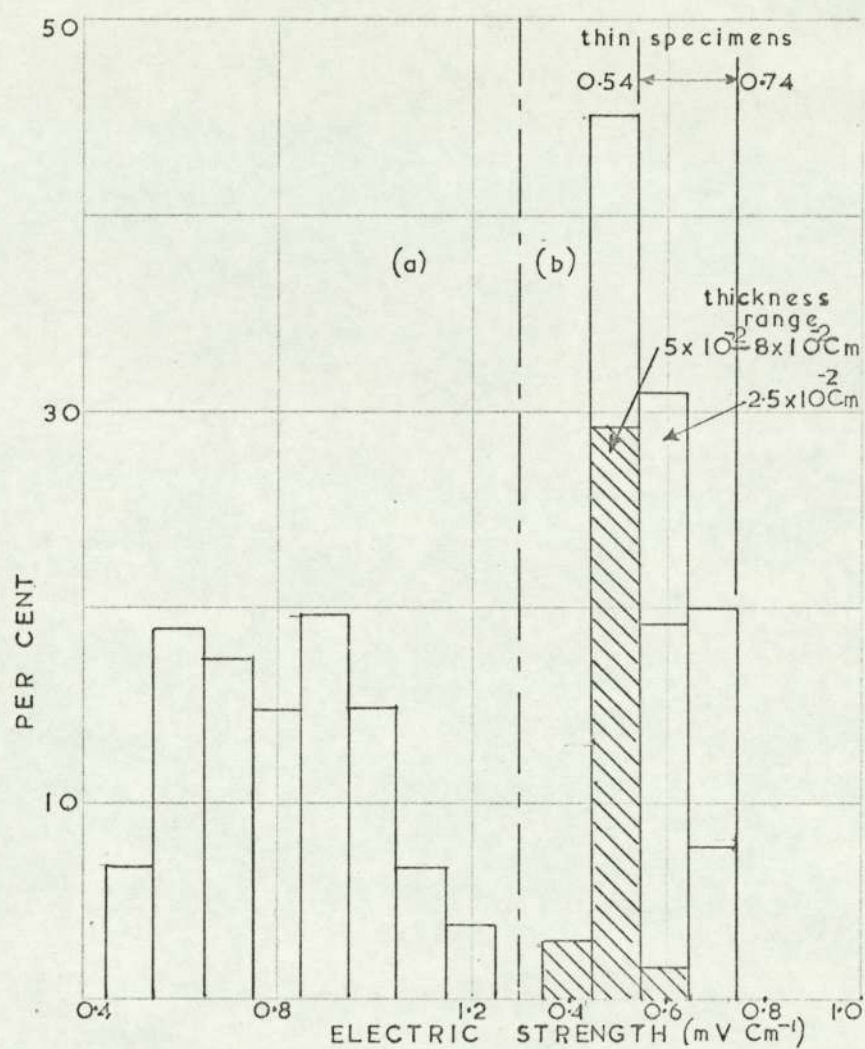


Fig. 4.1 THE INFLUENCE OF ANNEALING AND THICKNESS OF POTASSIUM BROMIDE ON ELECTRIC STRENGTH.

(After Cooper 15)

Temperature 20°C

a, 63 Specimens

b, 73 Annealed specimens

electric strength of sodium chloride single crystals decreased from 7.5 to 2.6 MV/cm in the thickness range 3-16 microns. Ryu and Kawamura⁶² have claimed that the strength of potassium chloride is constant in the range 10-110 microns, but this claim, for statistical reasons, is of doubtful validity.

Vermeer's^{76,77} work appears to show that the electric strength of glass is independent of specimen thickness. Cooper et al.¹⁹ have shown that the electric strength of polythene measured under pulse voltages is given by:

$$E_b = 12.8 - 3 \log L \quad (4.1)$$

where L is the thickness in mil. and E_b is in MV/ins. These investigators re-examined measurements made by Oakes⁵⁵ employing d. c. field which have been considered to show independence of electric strength with thickness. They concluded that a statistically significant decrease from 7.0 to 6.4 MV/cm occurred as the thickness increased from about 1 - 10 mils.

Many electrical breakdown experiments have been performed using evaporated dielectric films^(6, 9, 24, 41, 62, 72). This technique provides specimens covering a wide thickness range. However, it is by no means certain that such films possess structures which are independent of the film thickness.

4.2.3 Immersion Medium Effect

Grunewald³⁴ made a substantial advance in the studies of electrical strength of inorganic dielectrics by using a semi-conducting immersion medium. He achieved a field strength in excess of 3 MV/cm for mica without failure.

Von Hippel³⁶ used nitrogen at a pressure of 100 atmospheres as an immersion medium, and obtained the intrinsic strength of alkali halides in the range of 1 MV/cm. He abandoned this technique due to its unsuitability at higher stresses and replaced it by a solid semi-conducting immersion medium. Employing this method, von Hippel³⁸ obtained what is now thought to be the true intrinsic

strength for muscovite mica at 10 MV/cm.

Thomas^{74, 75}, independently of von Hippel, used both conducting liquids and non-conducting liquids under high pressure as immersion media and achieved 8 MV/cm for mica.

Hackett and Thomas³⁵ improved the conducting liquid technique by introducing barriers to limit the current through the medium and confirmed von Hippel's value of 10 MV/cm for mica. At the same time, the recessed specimen technique was introduced and results agreeing with those from liquid immersion were obtained. The recessed specimen technique replaced the immersion method, being easier and more reliable, and was applied to a considerable number of plastic materials and to inorganic materials such as glass, silicon, quartz and alkali halides (see Fig. 4.2).

McKeown⁵³ devised the solid immersion technique known by his name and for polyethylene obtained an electric strength of 8 MV/cm against 7 MV/cm by the recessed specimen method. The latter is currently under suspicion as suffering from errors.

4.2.4 Temperature Effect

4.2.4.1 Crystalline Solids

4.2.4.1.1 Polar Crystals

The ease of growth of single crystals has made the alkali halides particularly attractive compounds for study. Several groups of workers^(3, 10, 16, 40, 44, 46) have measured the breakdown strength of the two alkali halides, potassium bromide and sodium chloride, over a range of temperatures. Cooper¹⁴ gives the collected results (see Fig. 4.3) of eleven investigations. From these data, it is usually concluded that the breakdown strength increases with increasing temperature. The large spread in values between different investigations, amounting to as much as 100 per cent, indicates that, even in these simple systems, uncontrolled variables still exist. It has been suggested that lattice deformation and orientation with respect to field may be partially responsible.

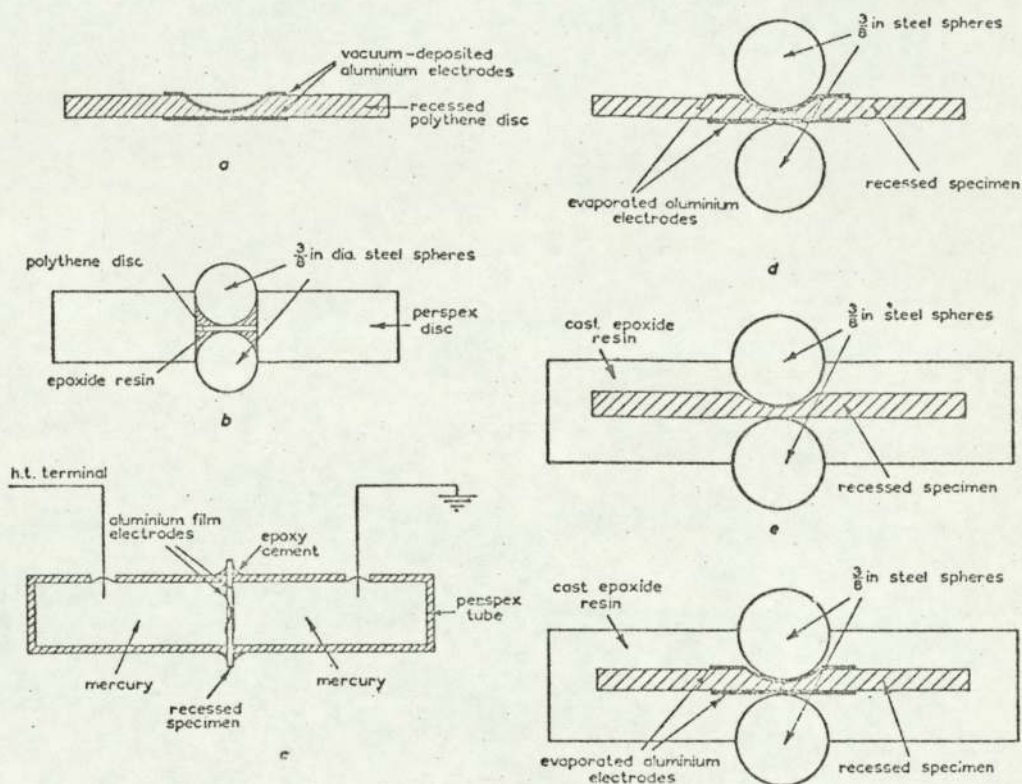


Fig. 4.2 TYPES OF SPECIMENS EMPLOYED IN ELECTRIC STRENGTH MEASUREMENTS

- a, Recessed specimen
- b, McKewon specimen 53
- c, Test cell for recessed specimen using a mercury heat sink
- d, Recessed specimen with aluminium electrode and $\frac{3}{8}$ " steel heat sink
- e, Encapsulated recessed specimen without aluminium electrode
- f, Encapsulated recessed specimen with aluminium electrodes

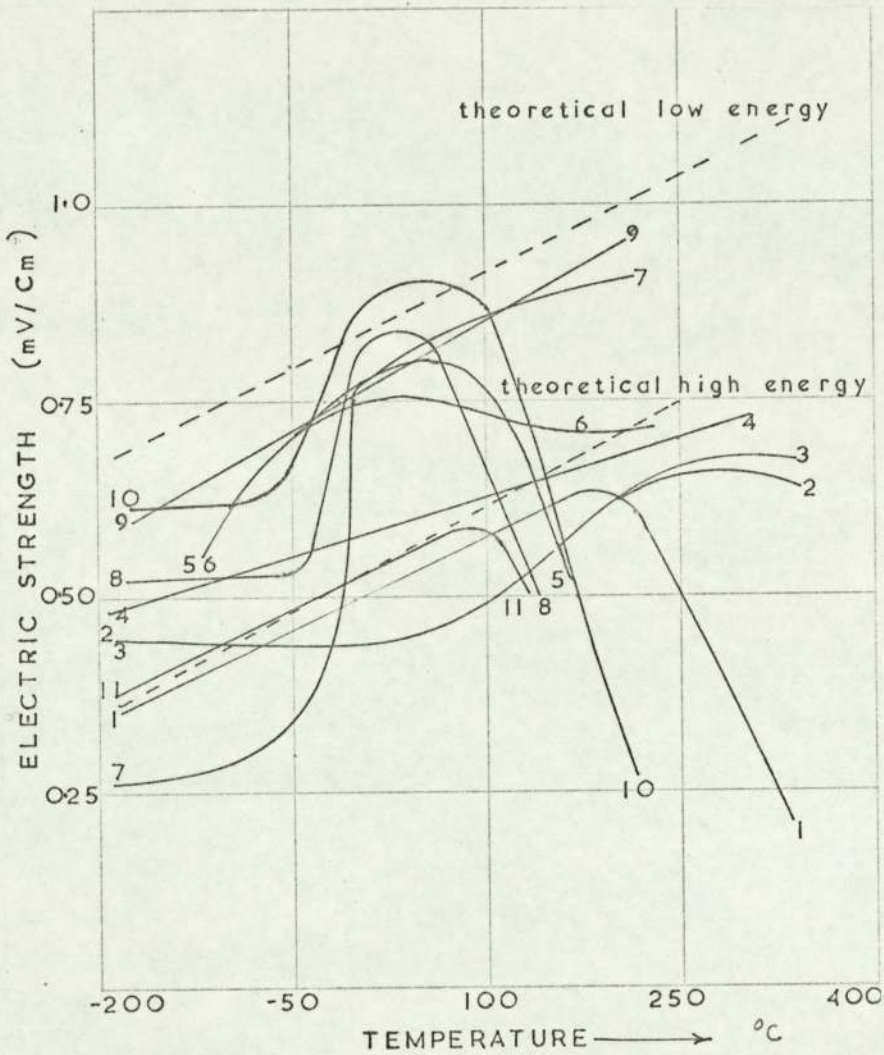


Fig. 4.3 ELECTRIC STRENGTH OF POTASSIUM BROMIDE AS A FUNCTION OF TEMPERATURE.

1. von Hippel and Alger⁴⁰; d.c.
2. von Hippel and Alger⁴⁰; 1 m.sec pulse.
3. von Hippel and Alger⁴⁰; 0.1 m.sec pulse.
4. von Hippel and Alger⁴⁰; 1 μ sec pulse.
5. Kuchin⁴⁶; d.c.
6. Kuchin⁴⁶; 1 μ sec pulse.
7. Austen and Whitehead³; d.c.
8. Buehl and von Hippel¹⁰; d.c.
9. Konorova and Scrokina⁴⁴; 1 μ sec Pulse.
10. Konorova and Scrokina⁴⁴; d.c.
11. Cooper and Farnandez¹⁴; 1/8000 μ sec pulse.

4.2.4.1.2 Non-polar crystals

Mica has been the subject of a number of investigations^{3, 35, 41, 62}. At low temperature regions, there is even smaller temperature dependence of strength (see Fig. 4.4) than was observed for alkali halides. Above room temperature, the strength drops by an order of magnitude of up to 600°C. These data were obtained with clear muscovite mica with d.c. voltage, although good agreement is found with impulse at low temperature.

4.2.4.2 Amorphous and partially Crystalline Solids

O'Dwyer⁵⁷ shows that the electric strength of glass at low temperature is about 9 MV/cm and is independent of temperature for pulse voltages (see Fig. 4.5). For a given stress time, there is a transition above which there is a sharp decrease in strength. This temperature increases with decreasing stress time.

The breakdown strengths of a variety of polymers have been measured and good agreement is found among different investigators^{2, 5, 48, 56}. As with glass, there is a good evidence of relatively constant and high strength at low temperature, with a rapidly decreasing strength at higher temperature as shown in Fig. 4.6. Some recent studies by McKeown⁵³, which are confirmed by Parkman et al.⁶¹, suggest that the sudden drop in strength with increase in temperature is due to the expansion and distortion of the sample at elevated temperature. McKeown⁵³ and Lawson⁴⁷ have shown that, by rigid containment of the specimen, high electric strength results (see Fig. 4.7).

4.2.5 Intrinsic or Electronic Breakdown

4.2.5.1 Introduction

There is no direct experimental way of knowing whether or not observed breakdown is intrinsic, so the concept necessarily remains an ideal one, to be identified in practice only as the highest value - for a given material - obtainable after all known secondary effects seem to have been eliminated. The intended meaning is the field

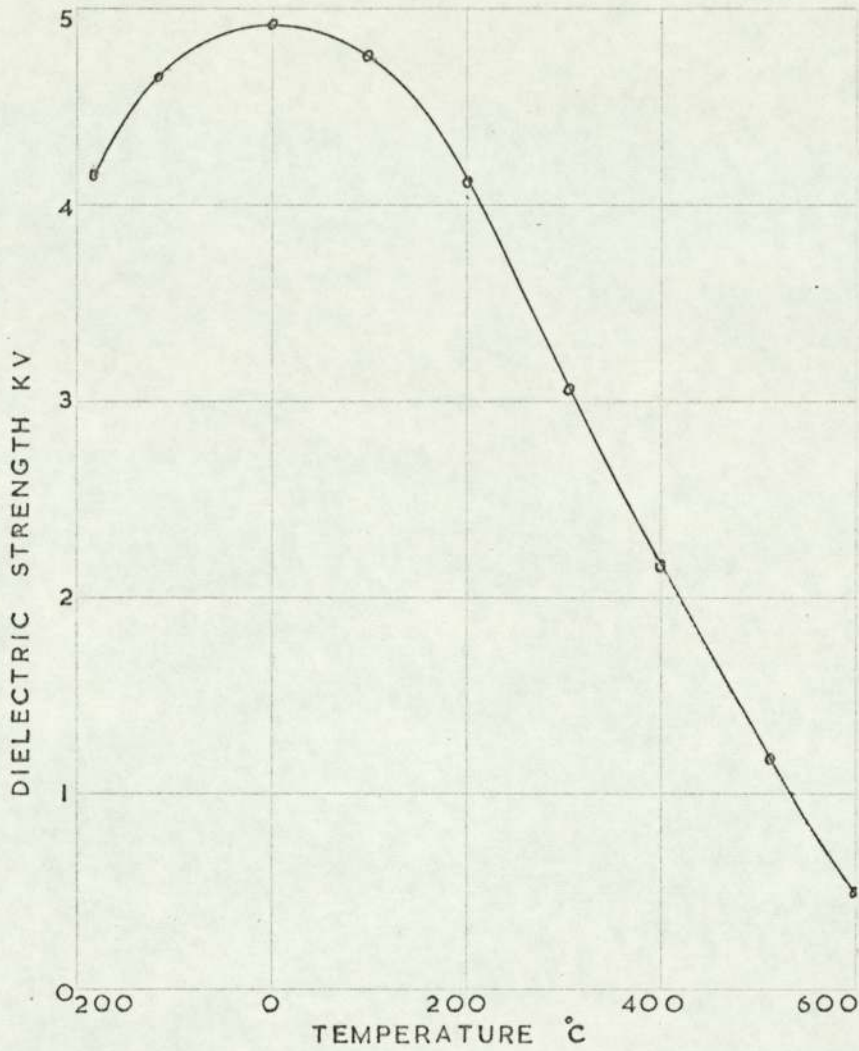


Fig. 4.4 THE ELECTRIC STRENGTH OF MUSCOVITE RUBY CLEAR MICA AS AFFECTED BY THE TEMPERATURE.

(After Hacket and Thomas³⁵)

d = 5 microns

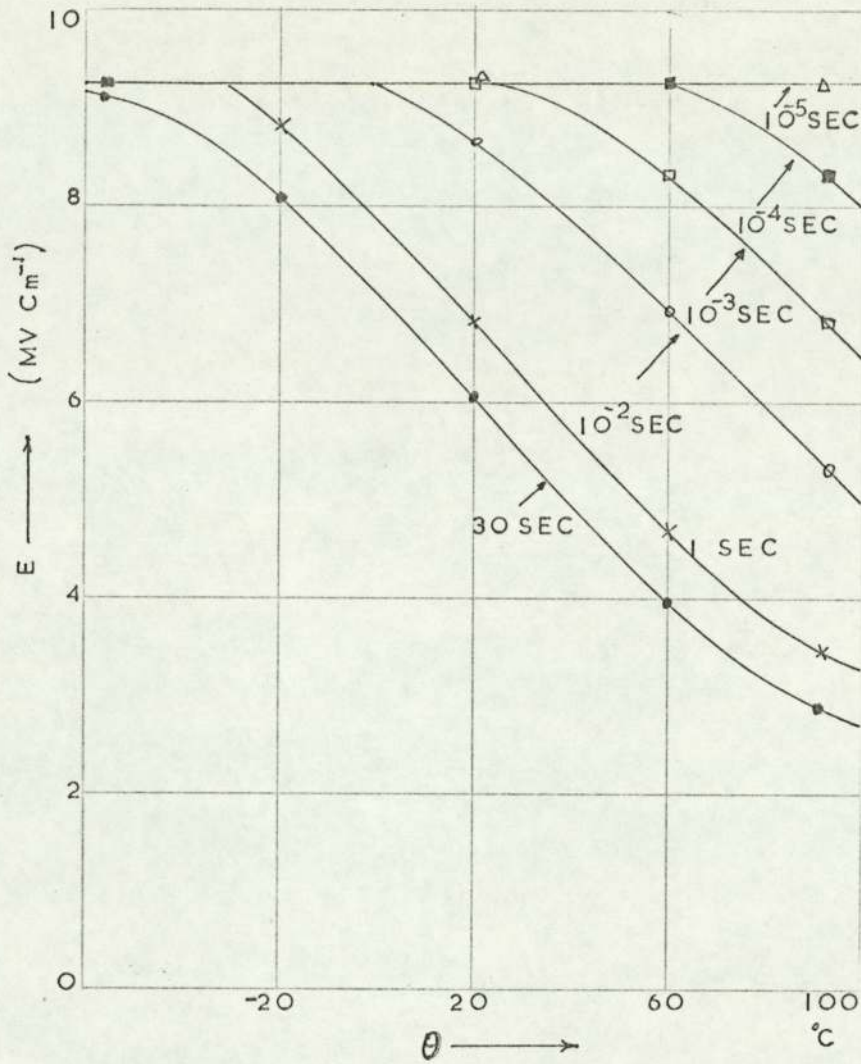


Fig. 4.5 THE EFFECT OF TEMPERATURE ON THE BREAKDOWN STRENGTH OF A BOROSILICATE FOR DIFFERENT VOLTAGE RISE TIMES USING LIQUID ELECTRODES (COPPER SULPHATE AND CALCIUM CHLORIDE). (After Vermeer⁷⁶)

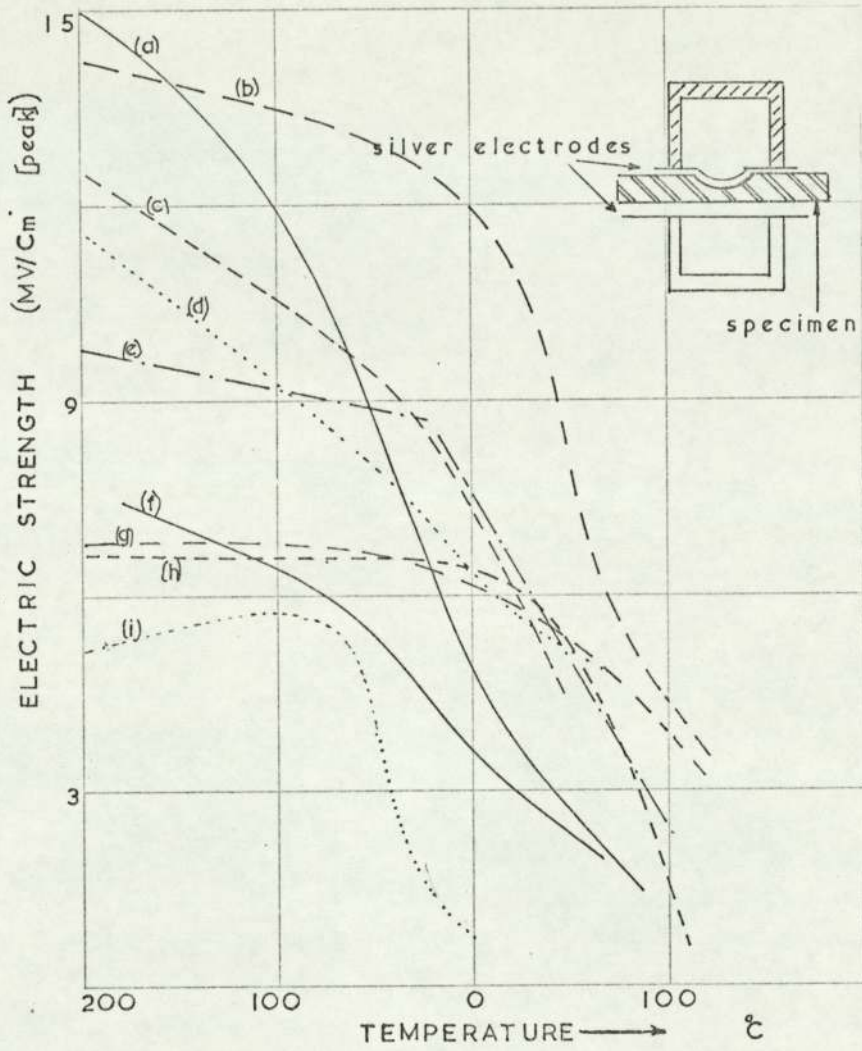


Fig. 4.6 ELECTRIC STRENGTH OF POLYMERS AS A FUNCTION OF TEMPERATURE.

(After Ball 5 and Oakes 55,56)

- | | | |
|--|---|-----------|
| (a) Polyvinyl alcohol |) | |
| (b) Polymethyl methacrylate |) | |
| (c) Polyvinyl chloride-acetate |) | Polar |
| (d) Chlorinated polythene (55% chlorine) |) | |
| (e) Chlorinated polythene (8% chlorine) |) | |
| (f) Clear baking oil-varnish |) | |
| (g) Polystyrene |) | |
| (h) Polythene |) | Non-polar |
| (i) Polyisobutylene |) | |

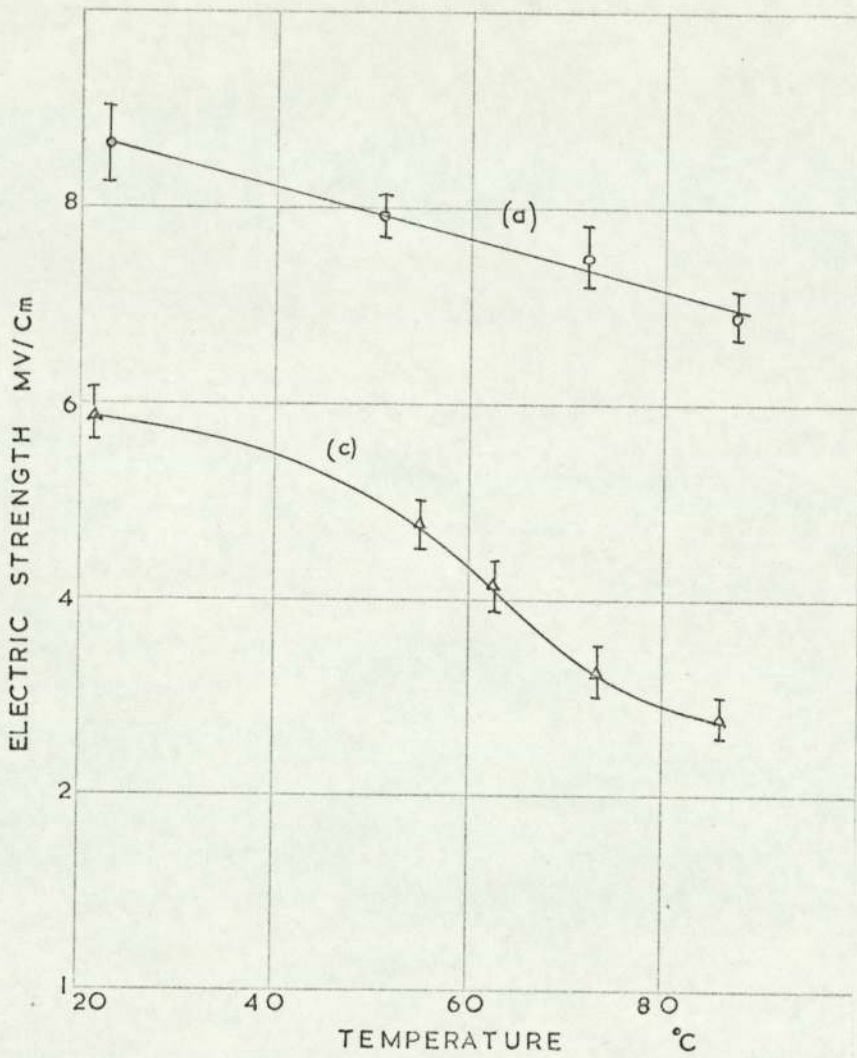


Fig. 4.7 THE VARIATION OF ELECTRIC STRENGTH OF POLYETHYLENE WITH TEMPERATURE

o, McKeown 53; McKeown specimen
 Δ, Lawson 47; Recessed specimen

intensity at which free electrons in the material are accelerated without limit by the direct electrostatic action of the field. Whether the concept is really valid in this form is dubious. It seems likely that any catastrophic acceleration of electrons must be preceded by an unlimited increase in the conductivity of the material - the so-called stress-enhanced conductivity.

Experimental evidence near the breakdown stress is still lacking, owing to the difficulty of detecting small conduction currents in the presence of high voltages. This results in the intrinsic breakdown being indistinguishable from thermal instability, although the numerical difference may be small, if the final rise of conduction occurs over a narrow enough range of voltage. Experimental evidence indicates that for many materials the range of uncertainty is in fact a narrow one.

Intrinsic strength has meaning only for a limited range of substances. The material must be homogeneous, so that breakdown cannot occur through interstices. It must be mechanically strong enough to withstand the large forces set up by the field which may exceed 100 kg/cm^2 . Its conductivity must be sufficiently low that suitable conditions of temperature and frequency can be chosen to eliminate thermal instability at fields below the intrinsic value.

4.2.5.2 Boltzmann's Transport Equation

The application of an electric field to solid dielectrics disturbs the distribution of charge carriers. The energy of the electron changes, the density of states between energy W and $W + dW$ remains the same, but $p(W)$, the probability of occupation of a state of energy W , changes to a new value $p'(W)$. The distribution of charge carriers is therefore obtained by $p(W)$. If the applied field is removed, $p'(W)$ reverts to $p(W)$.

The rate at which the field distribution reverts due to scattering by interaction with imperfection or lattice vibrations is given by:-

$$\left. \frac{dW}{dt} \right|_{\text{scattering}} = \frac{p'(W) - p(W)}{\tau} \quad (4.2)$$

where τ is the relaxation time characteristic of the system, which is a function of the scattering mechanism, bringing the system back to equilibrium. The charge carriers (electrons) in presence of both electric field and temperature will accelerate. Hence, in one dimension,

$$\left. \frac{dW}{dt} \right|_{\text{drift}} = - \frac{qE_x}{m^*} \frac{dW}{dV_x} + V_x \frac{dW}{dx} \quad (4.3)$$

where V_x , m^* , and q are the drift velocity in x-axis, the effective mass, and the charge of an electron respectively.

Extending to three dimensions,

$$\left. \frac{dW}{dt} \right|_{\text{drift}} = - \left(\frac{qE}{m^*} \right) \cdot \nabla_v W + V \cdot \nabla_r W \quad (4.4)$$

During its drift, the electron is scattered by interaction with imperfections or lattice vibrations. The scattering processes tend to restore equilibrium.

In equilibrium or steady state,

$$\left. \frac{dW}{dt} \right|_{\text{drift}} + \left. \frac{dW}{dt} \right|_{\text{scattering}} = 0 \quad (4.5)$$

and the new probability function in the absence of magnetic field is given by Boltzmann's transport equation,

$$P' = p + \tau \left(\frac{qE}{m^*} \cdot \nabla_v W - V \cdot \nabla_r W \right) \quad (4.6)$$

The theories of intrinsic breakdown are the solution of Boltzmann's transport equation which in general form is given by:-

$$\frac{\partial f(p)}{\partial t} = \left. \frac{\partial f(p)}{\partial t} \right|_d + \left. \frac{\partial f(p)}{\partial t} \right|_s + \left. \frac{\partial f(p)}{\partial t} \right|_e + \left. \frac{\partial f(p)}{\partial t} \right|_i \quad (4.7)$$

The terms with suffixes d, s, e and i denote the rate of change of electron distribution $f(p)$ in momentum space due to (a) the applied field, (b) the scattering mechanism, (c) interelectronic collision, and (d) ionization and recombination. The effect of

diffusion, involving concentration gradients is neglected.

In the stationary state:-

$$\frac{\partial f(P)}{\partial t} = 0$$

In practice, the solution of Boltzmann's equation requires that some approximation be made. These take different forms in the theories of collective and avalanche breakdown.

Typical curves for the rate of gain of energy from the field for a particular field strength and the rate of energy loss to the lattice are shown in Fig. 4.8 for polar and non-polar crystals. It will be observed that only for points A, B, C and D are the two rates equal and the steady-state equation valid. It may be further noted that two of these points, B and D, represent points of unstable equilibrium. Thus, electrons having energy corresponding to these points continue to gain energy until either the stable point, C, is reached, or until some other energy barrier, such as ionization, is encountered.

In non-polar crystals, only the acoustical modes can be excited by electron collisions. In polar crystals, however, an additional strong interaction with the optical modes is possible (see Fig. 4.8b) with its peak at low energy in the vicinity of $k_0\theta$, where k_0 is Boltzmann's constant and θ is the characteristic temperature. These interactions have been examined in various approximations by von Hippel³⁶⁻³⁹, Fröhlich²⁶⁻³¹, Mott and Gurney⁵⁴, Seeger and Teller^{63, 64}, Callen¹², and Seitz^{65, 66}.

4.2.5.3 Collective Breakdown Theory

In collective breakdown, it is assumed that the initial density of free electrons is sufficiently great for collisions between electrons to determine the distribution of electrons in energy. This distribution is Maxwellian with an electron temperature which can be determined as a function of electric field, E . If the applied field is greater than a critical field, E_c , the electron temperature θ_e - as distinct from the lattice temperature, θ - increases without limit.

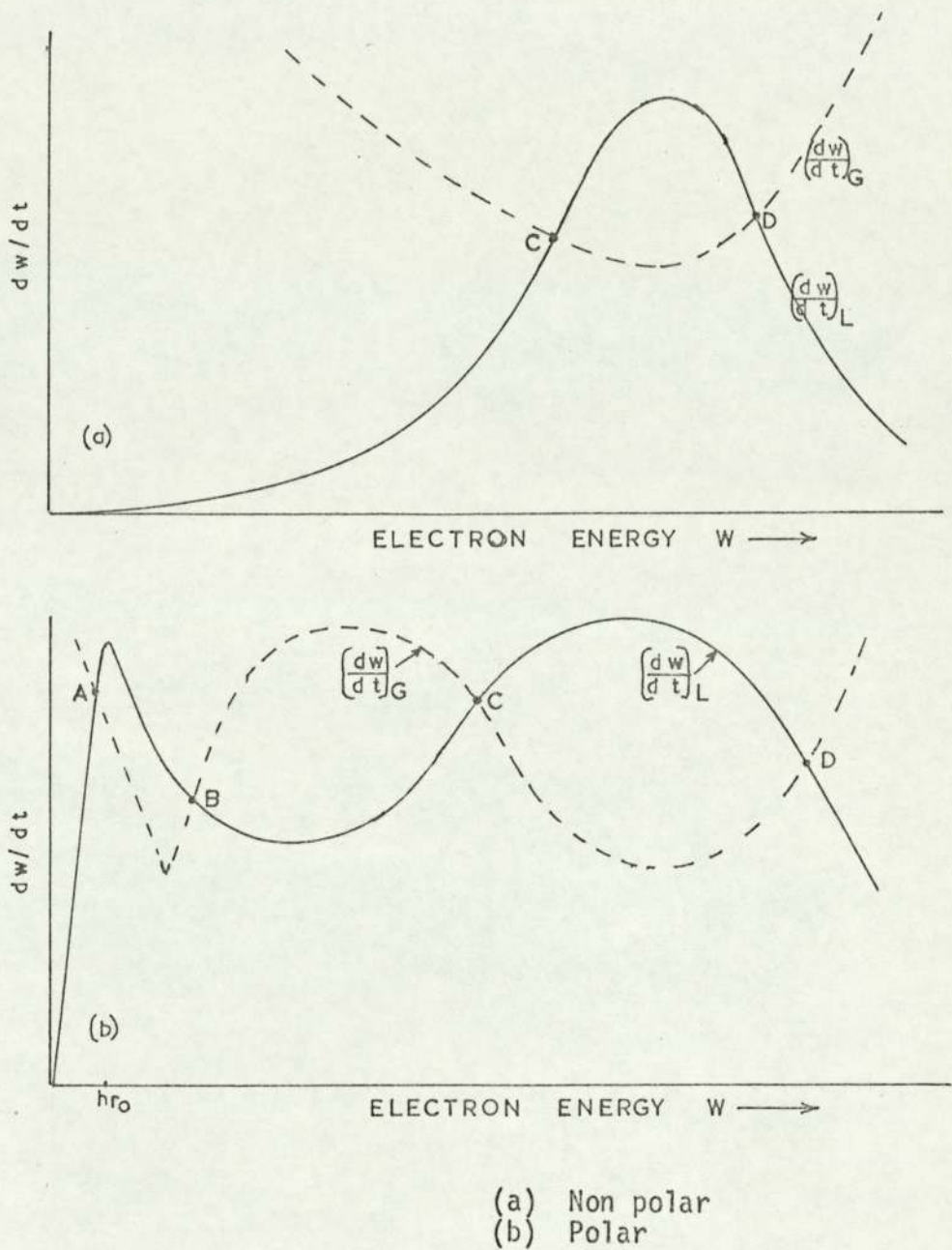


Fig. 4.8 RATES OF GAIN AND LOSS OF ENERGY TO CRYSTAL LATTICE.
(After Seitz 49)

(a) Non-polar crystal, (b) Polar crystal.

———— Rate of energy loss
----- Rate of energy gain

The first theory was proposed by von Hippel³⁶⁻³⁹ and was placed on a quantitative basis by Seeger and Teller^{63,64} and the second was advanced by Fröhlich²⁶⁻²⁹ and later modified by Fröhlich and Paranjape³². von Hippel calculated the electric field necessary to render the normal distribution of electron energies unstable, so that a 'thermal' electron might be indefinitely accelerated in the field. This is referred to as the 'low energy' criterion, since an electron of low energy may be accelerated. Fröhlich and co-workers^{26,32,33} maintained, and it is now generally accepted, that the von Hippel criterion leads to too high a breakdown field, on the grounds that electrons of more than average energy (i. e. those in the tail of the Maxwell-Boltzmann distribution) are more easily accelerated and are always present in sufficient numbers as to cause instability. Both theories refer to polar crystals and consider losses to optical modes of lattice only. The curves of Fig. 4.8b are therefore re-drawn to include energy losses to optical modes only and energy gain curves for several applied fields, $E_1 < E_2 < E_3 < E_4$ (see Fig. 4.9).

von Hippel assumed that all electrons thermally excited to the conduction band have the same energy, corresponding to the point A for a given applied field. The system would then be stable for all fields less than E_4 . Above E_4 , electrons would gain energy faster than they would lose it, so that their energy would increase to a value of W_i , the ionization energy. This field was assumed to be the breakdown field. It was possible to calculate the electric strengths of the alkali halides and the values so obtained agreed reasonably well with measured breakdown fields. It should be noted that this theory predicts that there will be no measurable pre-breakdown current, and that the ionization coefficient, α will be discontinuous, rising from zero to a very large value at E_4 .

The breakdown criterion proposed by Fröhlich²⁶ was somewhat less stringent. He allowed firstly for the fact that the conduction electrons will have a distribution of energy, and that a few would have very high energies. Thus, even at a field below breakdown

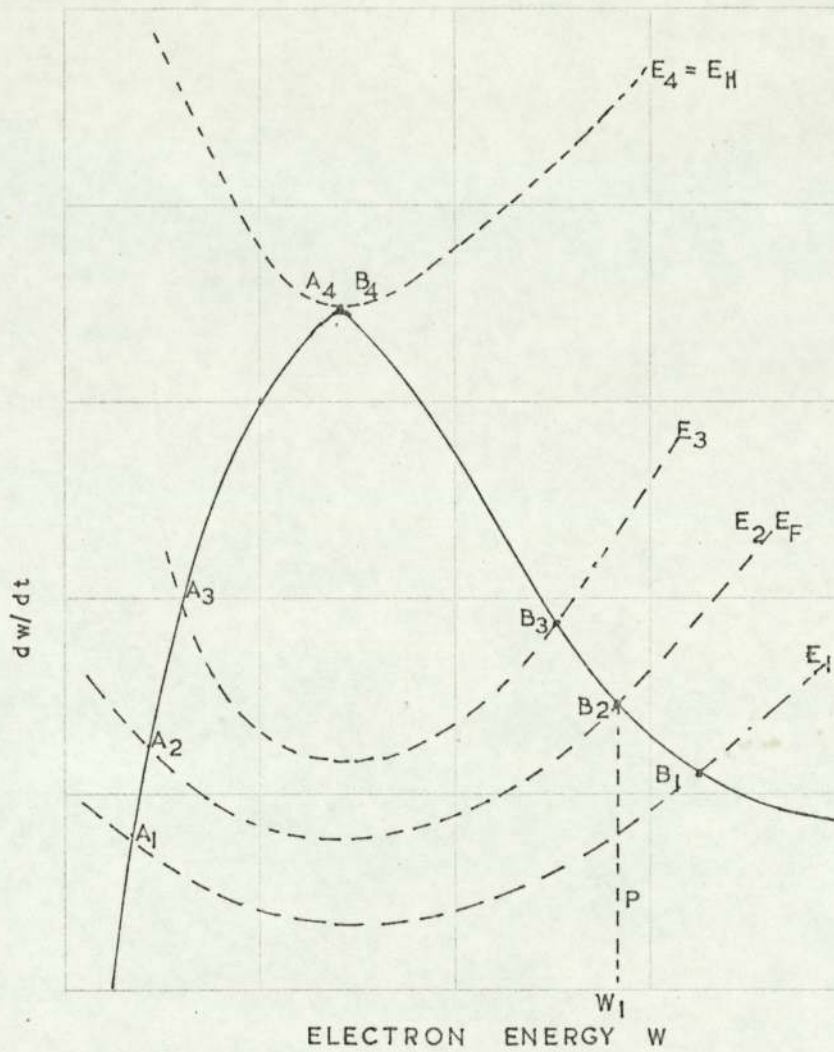


Fig. 4.9 RATES OF GAIN AND LOSS OF ENERGY TO CRYSTAL LATTICE IN THE OPTICAL MODE

——, Rate of energy loss

-----, Rate of energy gain

$E_1 < E_2 < E_3 < E_4$

(say E_1 in Fig. 4.9), occasional electrons would gain enough energy to cause ionization, producing new electrons and leaving charged holes in the lattice.

The electrons produced by occasional ionization at an applied field E_1 will gain energies up to approximately W_i (point P) while attempting to recombine, at which point they are still losing energy faster than they can gain it. They will thus, on the average, recombine and there will be very little net gain in the number of electrons by ionization.

At an electric field E_3 , electrons gaining energy W_i during attempted recombination now gain energy faster than they lose it, so that they do not recombine. Thus, the occasional ionization by electrons on the high-energy tail of distribution function leads to an ever-increasing number of electrons and, finally, to breakdown. The minimum field at which this can occur is E_2 , and this is defined by Fröhlich as the breakdown field. Like the theory of von Hippel, the Fröhlich theory predicts essentially no pre-breakdown current and a discontinuity in α at the breakdown threshold.

With reference to Fig. 4.9, it is evident why the von Hippel theory is sometimes referred to as having a low-energy criterion while that of Fröhlich has a high-energy criterion. It may be noted that the Fröhlich theory predicts a lower value for the breakdown field than does that of von Hippel. The reason that one often finds values calculated by the two theories to be in essential agreement arises from the different lattice parameters which are used in the calculations. However, when the excitation of the acoustical modes is included in the treatment, these differences may be only of academic interest.

Seitz⁶⁶ has shown that while interaction with acoustical modes of vibration was dominant in non-polar crystals, it must also be included in the treatment of polar crystals. This inclusion in the theory causes the electric strength calculated according

to Fröhlich criterion to shift to higher values more nearly equal to those predicted by von Hippel criterion.

In Fig. 4.10, E_F denotes the field at which $\left. \frac{dW}{dt} \right|_L$ and $\left. \frac{dW}{dt} \right|_G$ intersect at the ionization energy W_i , and breakdown would occur at this applied field according to the original Fröhlich criterion. However, when the acoustical modes are included, the corresponding intersection of the energy gain and loss curves occurs at much higher values of $\frac{dW}{dt}$ and the newly predicted breakdown field is given by E'_F . The calculated value of the breakdown field using the von Hippel criterion E_H remains unchanged when the acoustical modes are included in the losses.

Using the refined treatment, the breakdown fields predicted according to Fröhlich and von Hippel theories are considerably higher than those measured experimentally.

In the treatments so far, assumptions are made, (a) that the electrons either occupy the energetically stable valence band or are free in the conduction band, and (b) that the only important collisions are between electrons and the lattice. While these assumptions are valid in relatively perfect crystals at low temperatures, they do not represent the facts at higher temperatures. This is particularly so in crystals containing impurities or imperfections, or in amorphous or partly amorphous materials. Even highly purified crystals at higher temperatures develop lattice defects which may serve as electron traps. The energy levels for such defects and those due to impurity atoms usually lie rather close to the conduction band. Consequently, electrons so trapped are rather easily raised thermally to the conduction band which, as a result, becomes relatively highly populated. In this case, it is no longer feasible to ignore collision between electrons in the conduction band; in fact, in the temperature range of interest to this theory, such collisions by far predominate over those involving the lattice. The free electrons now gain energy from the field and rapidly share it with one another as well as with those in imper-

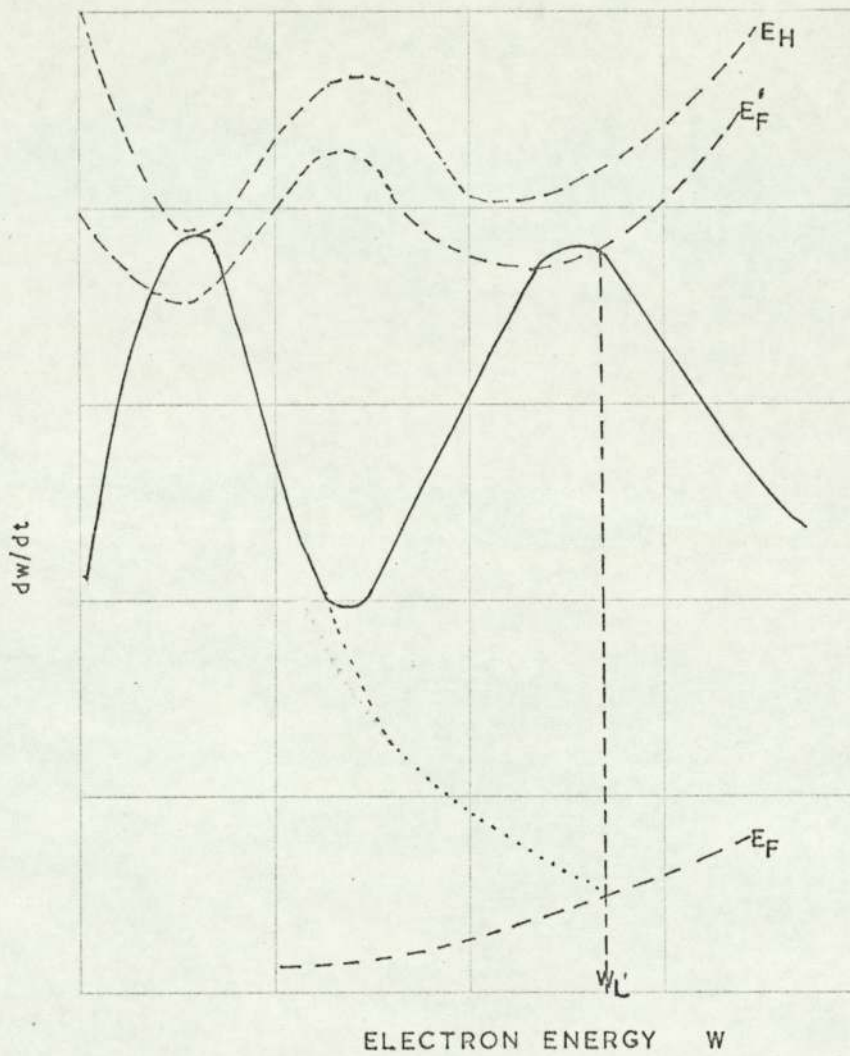


Fig. 4.10 RATES OF ENERGY GAIN AND LOSS TO CRYSTAL LATTICE IN OPTICAL AND ACOUSTICAL MODES.

- ____, Rate of energy loss in optical and acoustical modes
- , Rate of energy gain in optical and acoustical modes
-, Rate of energy loss in optical mode

fection levels, thus reaching an electron temperature, θ_e , considerably higher than that of the lattice.

Since the electrons in the conduction band, N_c , are essentially in thermal equilibrium with those in the imperfection and impurity level, N_i , at a temperature θ_e , hence:

$$\frac{N_c}{N_i} = R \exp \left(- \frac{\Delta V}{k \theta_e} \right) \quad (4.8)$$

where ΔV is the average energy between trap levels of the conduction band and R is the ratio of the number of energy levels in the interval $k\theta_e$ of the conduction band to the number of excited impurity level.

Usually $N_c \ll N_i$, so that as θ_e increases, N_c increases rapidly, while N_i remains relatively constant. Since energy loss to the lattice occurs largely via the trapped electrons, a large increase with electron temperature would not be expected. Actually, the rate of loss is a function of the difference, $\theta_e - \theta_o$, where θ_o is the lattice temperature. Thus, as the lattice temperature is increased for a given value of θ_e , the rate of loss is decreased, becoming zero at $\theta_e = \theta_o$.

Curves for the rate of energy gain from the field and the rate of loss to the lattice are drawn in Fig. 4.11 as a function of θ_e for several values of applied field and one value of θ_o . With an applied field E_1 , the electrons will reach the stable electron temperature given by A_1 . When the field is E_3 , the energy gain is always larger than the loss and the breakdown will occur. The maximum field at which a stable electron temperature is possible is E_2 , for which the gain and loss curves are tangential at A_2 . Obviously, as the lattice temperature is raised and the curve for the rate energy loss is lowered, the breakdown field is also lowered.

The high-temperature theory of Fröhlich^{30, 31} thus predicts a temperature dependence for the electric strength which is

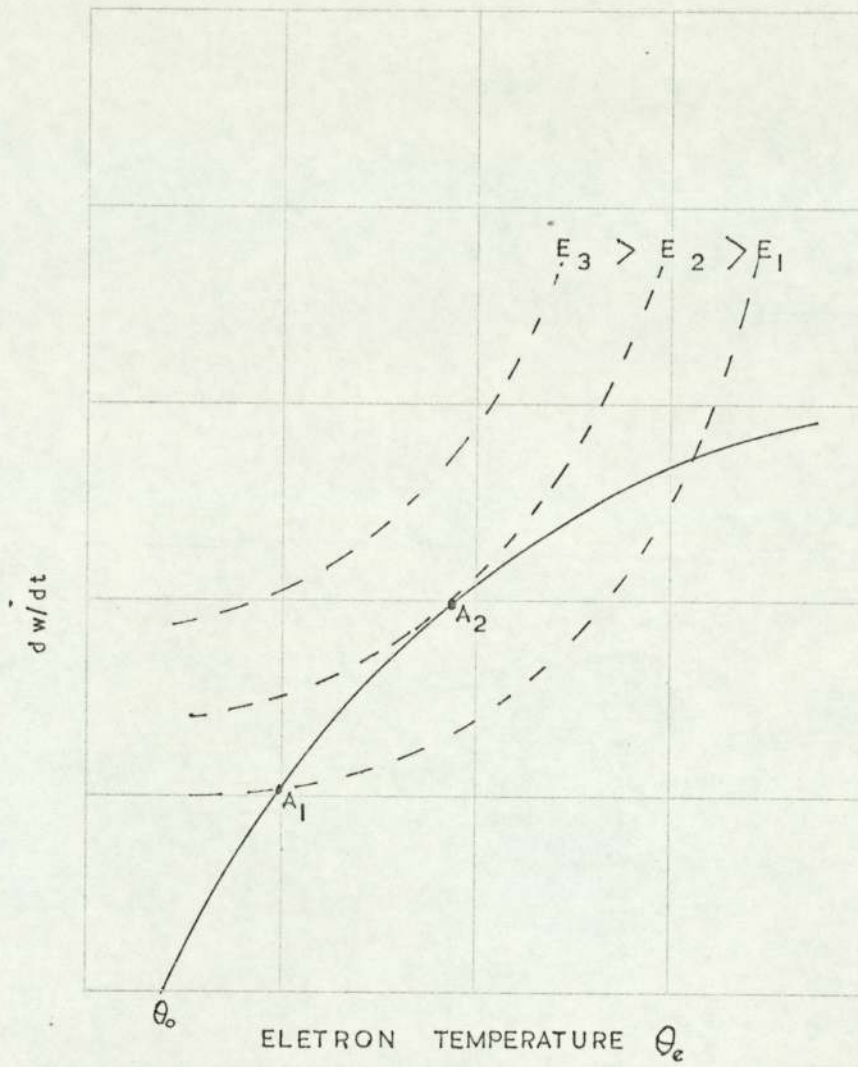


Fig. 4.11 RATES OF ENERGY GAIN AND LOSS AS A FUNCTION OF ELECTRON TEMPERATURE,

- , Rate of energy loss
 ----, Rate of energy gain

opposite in sign to that predicted by the low temperature theories. The temperature for the transition from the low temperature to the high temperature theory should decrease with increasing concentrations of impurities and imperfections in crystals. The sharp drop in electric strength of polyethylene near the glass-rubber transition temperature (see Fig. 4.6) has been attributed to the increase in the number of trapping centres.

In associating a drop in electric strength with increasing temperature with the Fröhlich theory, care must be taken to eliminate the possibility of ordinary thermal mechanisms which show a similar temperature dependence.

Lawson⁴⁷, while using McKeown technique in the study of electrical breakdown of polyethylene, found a reasonable agreement with Fröhlich's high temperature theory (see Fig. 4.12). He calculated the constants in Fröhlich's "hot electron" criterion for breakdown field strength,

$$E = C(T) \exp\left(\frac{\Delta V}{2k\theta_0}\right) \quad (4.9)$$

to be $\Delta V = 0.06 \text{ eV}$ and $C(T) = 2.66 \text{ MV/cm}$.

4.2.5.4 Avalanche Theory

Theories of avalanche breakdown of solid dielectrics^{25, 85, 86} have envisaged situations in which a destructive current is generated by the mechanism of electron collision ionization multiplication. At an electrical field beyond a critical value the electrons achieve energies high enough to liberate electrons bound to lattice atoms in a process similar to breakdown in gases. Avalanche theories become involved with the mechanics of individual collisions, and although extensive mathematical work has been done, the parameters are not well enough known to lead to numerical predictions which can be checked by experiment,

Franz²⁵ has calculated the impact ionization for high energy electrons in a very complicated form involving many approximations.

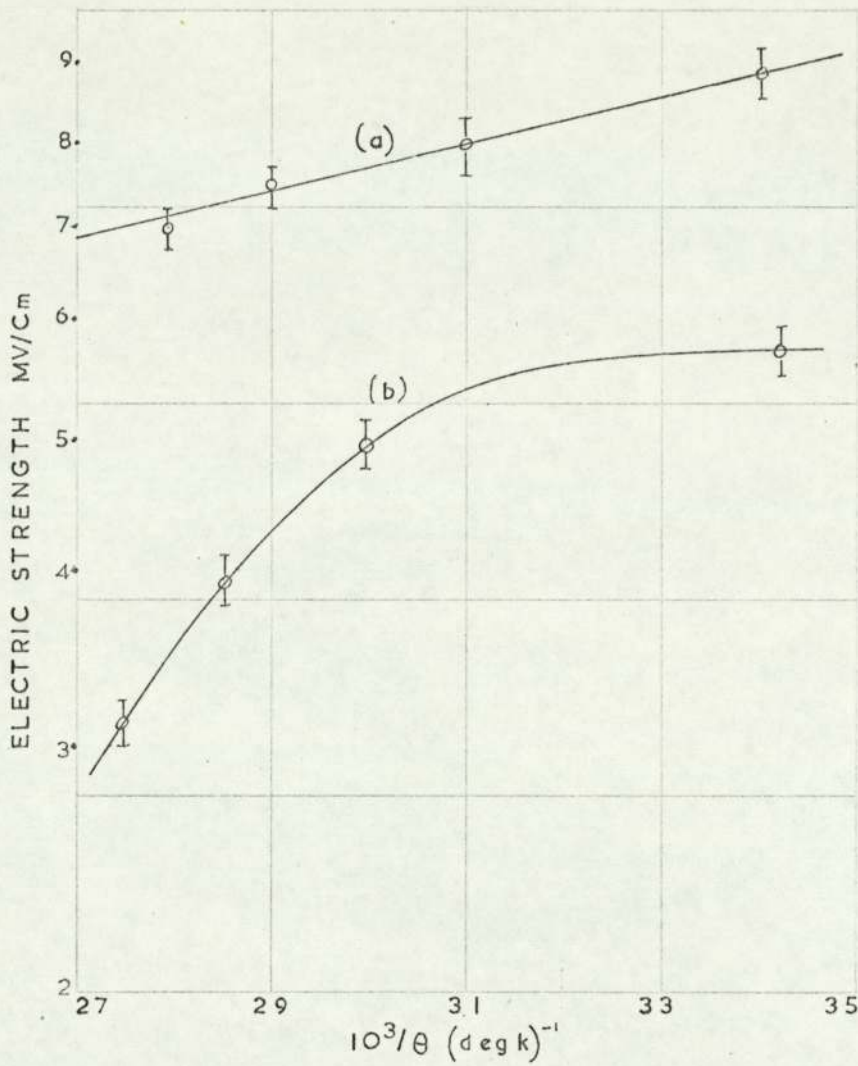


Fig. 4.12 THE ELECTRIC STRENGTH OF POLYETHYLENE VERSUS THE INVERSE OF ABSOLUTE TEMPERATURE

(After Lawson 47)

The plotted points are means for 6-10 specimens, and 95% confidence limits of the mean are shown

- a, McKeown specimens
- b, Recessed specimens

He neglects inter-electronic collisions but considers the effect of $\frac{\partial f(p)}{\partial t}$ in Boltzmann's Eqn. 4.7. The mean rate of ionization per unit time, ω , as a function of electric field is given by Franz as:

$$\omega = \frac{S(W_2)}{\int_0^I \rho(W) dW} \quad (4.10)$$

where the number of electrons per unit volume, $\rho(W) dW$, whose energy is in the range W to $W + dW$ is given by⁹¹:

$$\rho(W) = \frac{3 m S(W_2)}{2 q^2 W E^2} \int_W^I \frac{dW'}{1 + \frac{3 \mathcal{Z}' B'_\infty}{2 W' A'}} \exp\left(\int_W^{W'} \frac{\Phi''}{W''} dW''\right) \quad (4.11)$$

where $S(W_2)$ is the number of electrons passing through the energy surface W_2 in momentum space per unit time due to the action of the applied field and electron-phonon collision.

Franz's assumption that the maximum value of $\Phi(W)$ occurs at a value of (W) well below (I) applies to polar optical vibration. Wolff⁸⁵ has calculated ω for covalent crystals considering only non-polar vibrational modes and using essentially the same method as Franz but assuming that $\Phi(W)$ will not have a maximum at an energy less than (I) . He also assumes that $\rho(W) = 0$ if $W \gg I$ and effectively takes $S(W)$ as constant.

Yamashita⁸⁶ has extended Wolff's calculation by removing the restriction that $\rho(W) = 0$ for $W \gg I$ and considers the effect of diffusion in solving Boltzmann's equation. However, he derives the value of W on the assumption that diffusion can be neglected.

O'Dwyer⁵⁸ has shown that, on fairly simple theoretical grounds, a reasonable relation for the collision ionization rate per unit length as a function of field strength is:

$$\alpha(E) = \frac{1}{\lambda} \exp\left(-\frac{H}{E}\right) \quad (4.12)$$

where H is the field strength characteristic of the dielectrics and

λ is a length given by:-

$$\lambda = \frac{\bar{\mu}}{q} (2 m I)^{\frac{1}{2}} \quad (4.13)$$

where I is the threshold energy for collision and $\bar{\mu}$ is the mean mobility. On the basis of the collision ionization function (Eqn. 4.12), different approaches have been made to the problem of finding a critical field strength.

Seitz⁶⁶ considered the possibility that, even at fields below those at which energy instabilities like those of von Hippel and Fröhlich could occur, electron avalanches of sufficient size might develop to cause thermal or mechanical rupture of the crystal. He adopted as a criterion for breakdown the condition that every lattice atom in the volume of one avalanche should gain, on the average, 10 eV of energy. Such a condition would certainly lead to a conducting path in the crystal and consequent breakdown. He found that fulfilment of this criterion required that the initial electron makes 40 multiplications in crossing the gap.

Then
$$\alpha(E) d = 40 \quad (4.14)$$

where d is the thickness of the dielectric. Substituting Eqn. (4.14) in (4.12) gives the critical field strength as:

$$E_c = \frac{H}{\ln\left(\frac{d}{40\lambda}\right)} \quad (4.15)$$

4.2.5.5 Field Emission Theory - Zener Effect

Above a certain critical electric field strength applied to solid dielectrics, the electrons in the valence band can 'tunnel' through the potential barrier, corresponding to the gap of forbidden energy levels, into the conduction band without changing their energy.

Zener⁸⁸ was one of the first exponents of theoretical development concerning breakdown phenomena. He proposed that breakdown occurs when the electrostatic field becomes sufficiently strong to ionize the atoms of the insulator by a process akin to

field emission. The electrons in the bands act somewhat like travelling waves and can be described by a wave function.

The probability that an electron is at a certain position in the crystal is proportional to the square of the magnitude of its wave function. In the forbidden band, the travel of the wave is damped exponentially as the forbidden region is penetrated. If the forbidden band is narrow enough or if the field is strong enough, there is some probability that an electron will tunnel through to the conduction band. The energy of an electron is conserved as it moves under the influence of a field E , and its energy, measured from a band edge, changes with time and with its position in the crystal. These effects were investigated subsequently by Franz²⁵ and Houston^{40a}. These investigators found that the transition probability per unit time when the field intensity is E is given by:

$$P = \frac{2 \pi q E d}{h} \left[\frac{\exp(-\alpha)}{\{1 - \exp(-\alpha)\}^2} \right] \quad (4.16)$$

$$\text{where} \quad \alpha = \frac{m d W_g^2}{q E h^2} \quad (4.17)$$

and W_g is the energy gap between filled and empty band, d is the lattice spacing, h is Planck's constant and q and m are the electron charge and mass. Franz²⁵ has shown that this leads to a current of the order of 1 amp/cm² when E takes the value

$$E = 0.33 \times 10^6 W_g^2 \text{ V/cm} \quad (4.18)$$

The lattice spacing is assumed to be 3×10^{-8} cm.

4.2.6 Thermal Breakdown

There are several processes which cause heat to be generated in a dielectric specimen under electric stress: (a) the flow of ionic current, (b) interaction of electronic currents with the lattice, and (c) the displacement of bound ions or dipoles in an a. c. field. The quantity of heat generated by one or more of

these mechanisms increases with the applied voltage, and if a specimen cannot dissipate this self-generated heat at a rate equal to its formation rate, then the temperature will rise spontaneously. Breakdown may then take place through an electronic mechanism when the intrinsic strength falls as a result of temperature increase or when the sample simply melts, decomposes, or becomes a dissociated electrolyte.

Power generated in solid dielectrics is given by:

$$P = \sigma E^2 \quad (4.19)$$

for d. c. field, and

$$P = \epsilon_r \epsilon_0 f E^2 \tan \delta \quad (4.20)$$

for a. c. field, where σ is the conductivity, ϵ_r is the relative permittivity, δ is the loss angle and f is the field frequency.

There are two very general equations which apply to thermal breakdown and which serve as the starting point for all theoretical treatment of the subject. The first is the so-called "equation of continuity of heat", which states that heat input to an element of volume must be completely accounted for either by raising the temperature of the sample, or by heat flow out of the volume element. Thermal breakdown field for a dielectric specimen of arbitrary shape involves the solution of the differential equation:

$$\sigma E^2 = C_v \frac{d\theta}{dt} + \text{div} (k \text{ grad } \theta) \quad (4.21)$$

where C_v is the heat capacity and k is the thermal conductivity. The first term on the right-hand side can be ignored when the dielectric sample is subjected to a d. c. field and the second term can be neglected when pulse field is applied.

The second general equation expresses the "continuity of current flow" through the sample and, in the absence of collisional ionization, states that all the current flowing into the element must come out. This is expressed as:

$$\text{div } J = \text{div} (\omega C_0 \epsilon E) = 0 \quad (4.22)$$

where C_0 is the vacuum capacitance of the system.

In Eqns. (4.21) and (4.22), C_v , σ , k , and E are functions of temperature and σ may also be a function of E . With the use of the two continuity equations, Whitehead⁸³ and Franz²⁵ provided solutions from which several useful generalisations can be made concerning long-duration or ordinary thermal breakdown.

The breakdown occurs when the temperature of the hottest part of the sample reaches the decomposition or critical temperature θ_c but a state of instability can also occur at a temperature θ_m which is less than θ_c (see Fig. 4.13a). The difference between these two temperatures is shown in Fig. 4.13b, where the steady state rate of heat generation, $P(\theta, E) E^2$, and the rate of heat dissipation, $H(\theta, \theta_a)$, are plotted as a function of temperature θ . The ambient temperature is assumed to be θ_a .

The rate of generation for a constant electric field is a convex curve to the temperature axis, since the electrical conductivity is usually given as:

$$\sigma = \sigma_0 \exp\left(-\frac{Wg}{2k\theta}\right) \quad (4.23)$$

This relationship is confirmed for various glasses (see Fig. 4.14) by Taylor⁷³ and for alkali halides (see Fig. 4.15) by Cooper¹⁴.

With increased values of applied field, the family of curves P_1 , P_2 and P_3 are drawn. Curves are shown for two materials having different critical temperatures, θ_{c1} and θ_{c2} . For P_1 watt/cc input to sample 1, the temperature will rise to θ_1 where a stable condition is attained. Thermal breakdown will occur for this sample at an applied field corresponding to the P_2 curve. For sample 2, the thermal run-away temperature θ_m is below the critical temperature θ_{c2} . At P_3 watt/cc heat input, it is only necessary to wait for temperature to rise spontaneously until the sample reaches the temperature θ_m .

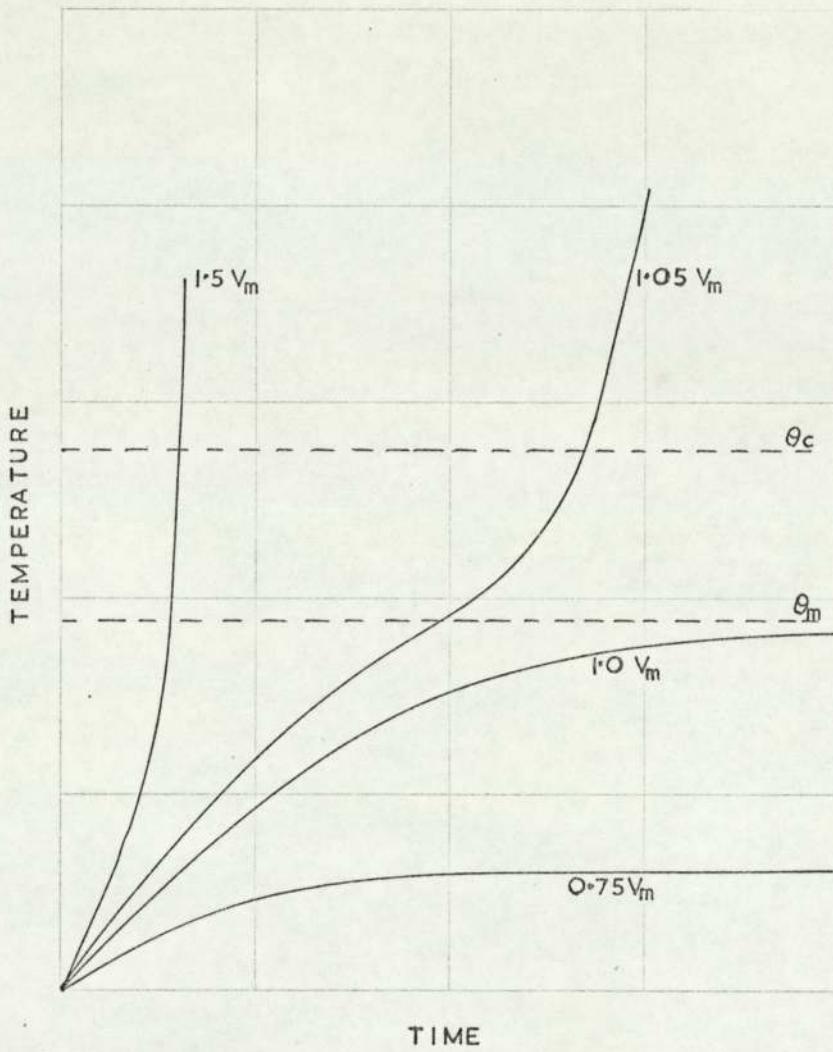


Fig. 4.13 SCHEMATIC CONSTRUCTION OF THE CRITICAL FIELD STRENGTH FOR THERMAL BREAKDOWN.

(a) DEPENDANCE OF TEMPERATURE UPON TIME FOR SEVERAL VALUES OF APPLIED VOLTAGE

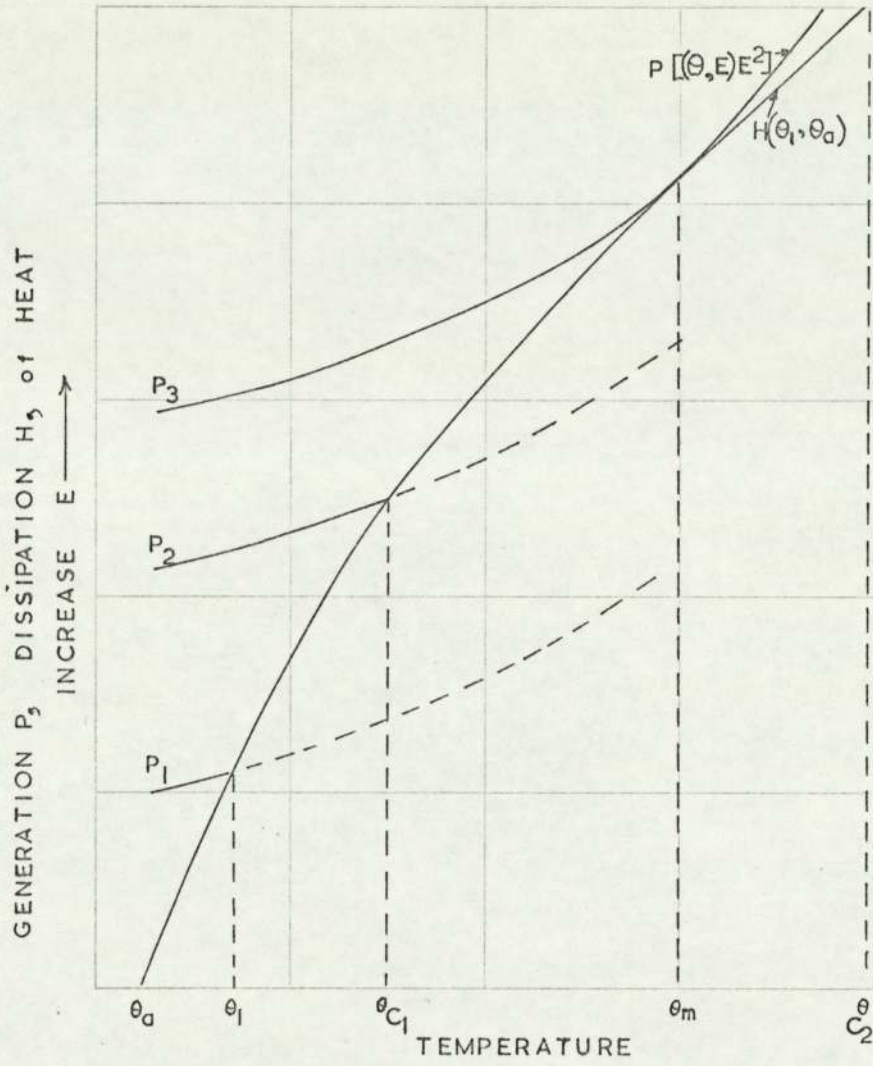


Fig. 4.13 (b) RATE OF GENERATION AND LOSS OF HEAT AS A FUNCTION OF TEMPERATURE

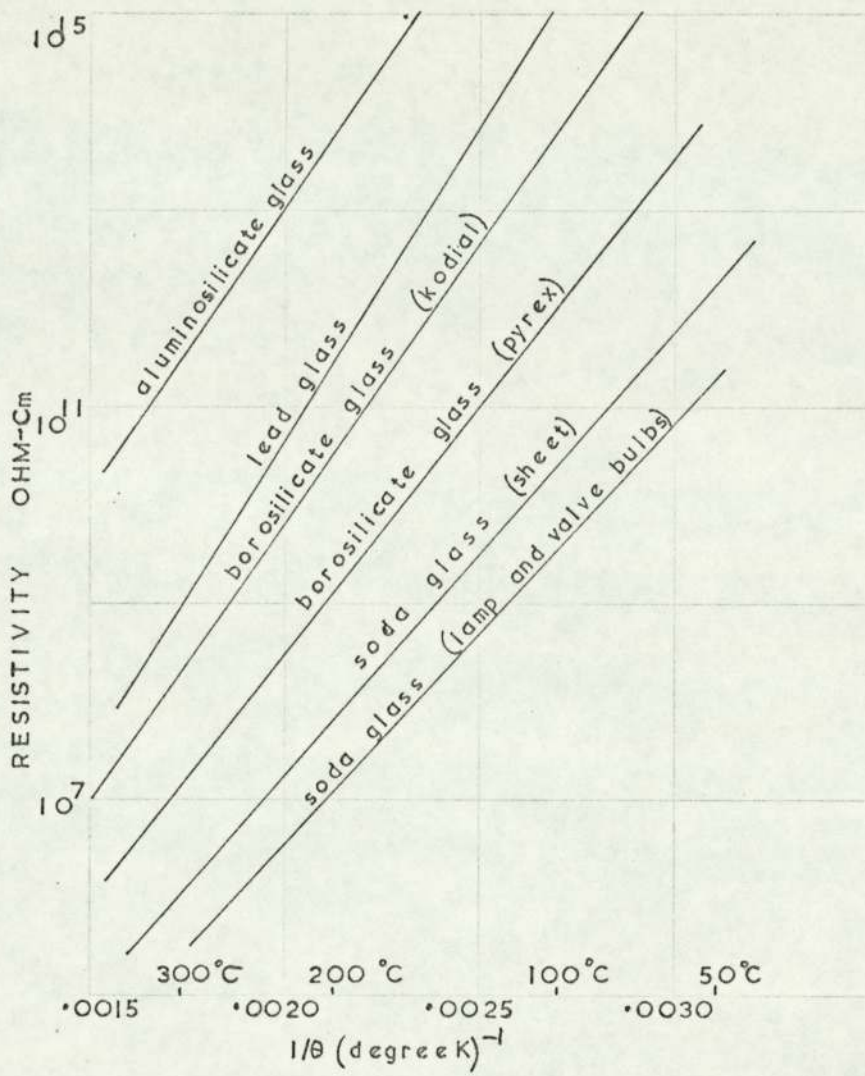


Fig. 4.14 EFFECT OF TEMPERATURE ON INSULATION RESISTANCE OF VARIOUS GLASSES
(After Taylor 73)

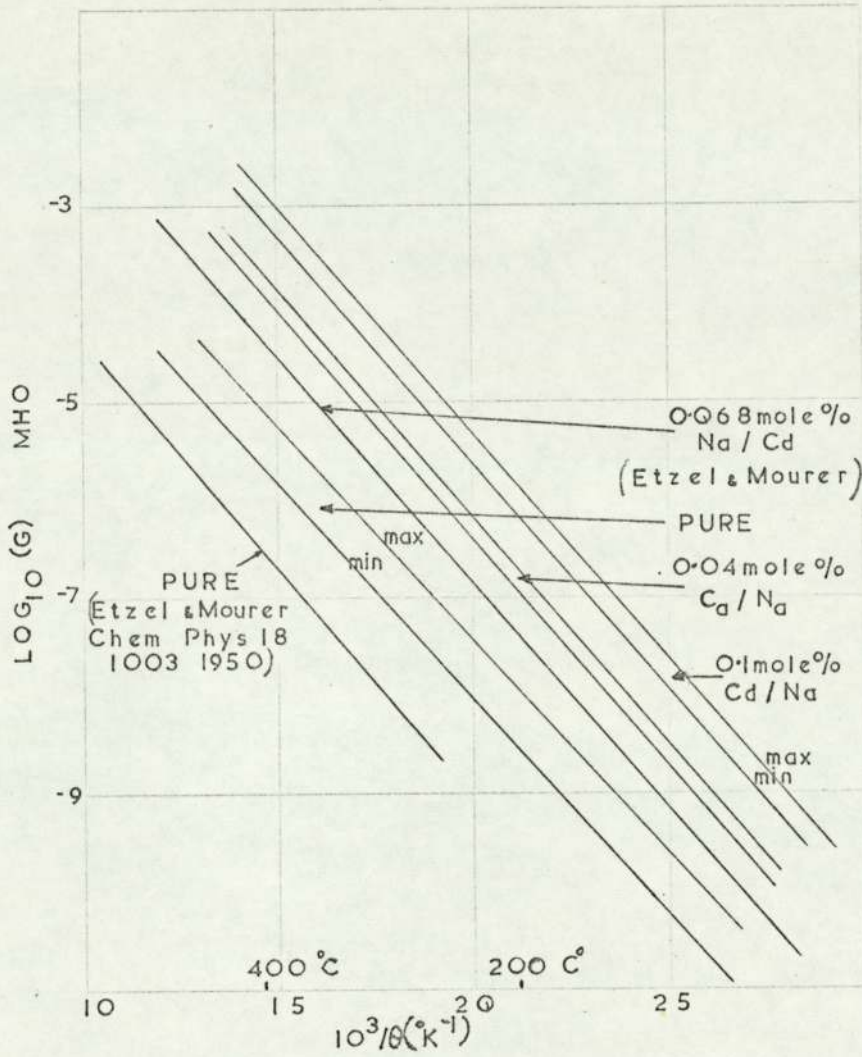


Fig. 4.15 IONIC CONDUCTIONS OF SODIUM CHLORIDE-CADMIUM CHLORIDE MIXED CRYSTALS. THE LINES REPRESENT THE EXTREMES FROM GROUPS OF ABOUT 10 SIMILAR SPECIMENS.
(After Cooper 14)

when the breakdown will occur. Thermal breakdown voltage is the applied voltage for which the equation $P = H$ fails to have a real solution.

A similar set of curves $\frac{dW}{dt}/G$ and $\frac{dW}{dt}/L$, rather than P and H was discussed in connection with the Fröhlich³⁰ high temperature theory of electronic breakdown. In that case, θ_m would rise to θ_c in a "short time" of order of microsecond or less, while seconds or even hours are required in the case of ordinary thermal breakdown.

4.2.7 Gas-Discharge Breakdown

Electrical breakdown of solids can be initiated by gas discharges occurring either in voids in the solid or in the vicinity of electrodes on the surface⁴⁹. Such discharges chemically degrade the solid and result either in a gradual erosion until the intrinsic strength is exceeded in some spot, or in the production of species which raise the electrical losses to the point where thermal runaway is possible.

Often, if mechanical forces are present, electrical failure may occur as a result of the degradation of mechanical properties of the material by discharges. For example, in many polymers, cross-linking reactions may cause embrittlement, with ultimate failure due to cracking. Material under mechanical strain may undergo 'stress cracking' or 'ozone-cutting' owing to scission of polymer chains by the discharges or their products.

4.2.8 Electrochemical Breakdown

Electrochemical breakdown is of great engineering importance especially in the case of capacitors and cables⁴⁹. Weakly dissociated impurities in the impregnant give rise to d.c. leakage currents which form decomposition products by electrode reactions. One of the products most frequently produced is nascent hydrogen which may react with the impregnant to give strongly dissociated compounds. Examples of the latter would be hydrochloric acid in

chlorine-substituted impregnants, or organic acids in an epoxy resin system. Such processes are auto-catalytic and a thermal run-away condition is produced. Increased temperature aggravates the situation resulting in more dissociation. The increase in voltage increases the leakage current.

While this kind of deterioration is more common in direct current systems, it also occurs in alternating current systems to a lesser extent. Asymmetrical electrode systems in a.c. field result in rectification action which is necessary for electrochemical processes to occur.

4.2.9 Electromechanical Breakdown

Applying a potential V across a plane slab of dielectric of initial thickness d_0 and dielectric constant ϵ_r , laterally unconstrained, with electrodes free to follow the material, the electromechanical stress produced is related to the compressed thickness, d , by the equilibrium formula:

$$\frac{1}{2} \epsilon_r \epsilon_0 \left(\frac{V}{d} \right)^2 = Y \ln \left(\frac{d_0}{d} \right) \quad (4.24)$$

where Y is Young's modulus for the dielectric.

Since the equation

$$V = 1.5 \times 10^5 d \left[\frac{Y}{\epsilon_r} \ln \left(\frac{d_0}{d} \right) \right]^{\frac{1}{2}} \quad (4.25)$$

has a maximum value at $\frac{d}{d_0} = 0.6$, no real value of V can produce a stable value of $d < 0.6 d_0$. An intrinsic electrical failure as described, for example, by the Fröhlich high temperature theory may occur prior to the state of mechanical instability. In the absence of electrical failure, further increase in potential makes the thickness unstable and the sample will collapse.

The electric strength at the point of collapse is:

$$E_c = \frac{V}{d} = \left(\frac{Y}{\epsilon_r \epsilon_0} \right)^{\frac{1}{2}} \quad (4.26)$$

while the apparent electric strength of the specimen is

$$E_a = \frac{V}{d_o} = \left(\frac{Y}{e \epsilon_r \epsilon_o} \right)^{\frac{1}{2}} \quad (4.27)$$

Stark and Garton⁶⁸ have found a reasonable similarity between their results on electrical strengths of polyisobutylene and polyethylene with variation of mechanical strength with temperature (see Fig. 4.16). Mechanical failure of polyethylene is not expected at room temperature where the theory, based on value of 3×10^9 dyne/cm² for Young's modulus¹³ gives 40 MV/cm for the onset of mechanical instability.

Fava²³, using an optical lever system, has shown that the true compressive strain in recessed specimens of polyethylene are masked by lateral expansion in the compressed samples.

4.2.10 Highly Divergent Field Breakdown - Treeing

If a high-voltage gradient is applied to an insulating material and a dielectric puncture results, the failure sometimes occurs progressively rather than instantaneously. By using a sharp pointed electrode, the electric stress adjacent to it becomes comparatively high in relation to the rest of the stressed insulation. Dielectric failure begins at this point and progresses to the other electrode in a tree-shape fashion^{4, 8, 42, 43, 48, 51, 52, 59, 60}.

Mason⁴⁸, while investigating the problem of partial discharge, noted that a second breakdown mechanism, referred to as treeing, appears to operate when eroded cavities develop a shape which can concentrate the stress at the advancing tip of the cavity. Kitchen and Pratt^{42, 43} have observed tree-like partial discharge channels in various stages of development in polythene cable insulations which had been taken out of service. These "trees" develop at inclusions or voids. Olyphant⁵⁹ has found evidence of breakdown by treeing in resin castings of high-voltage components and suggests that earlier observations of the phenomenon may have been prevented by the opaque nature of most insulators.

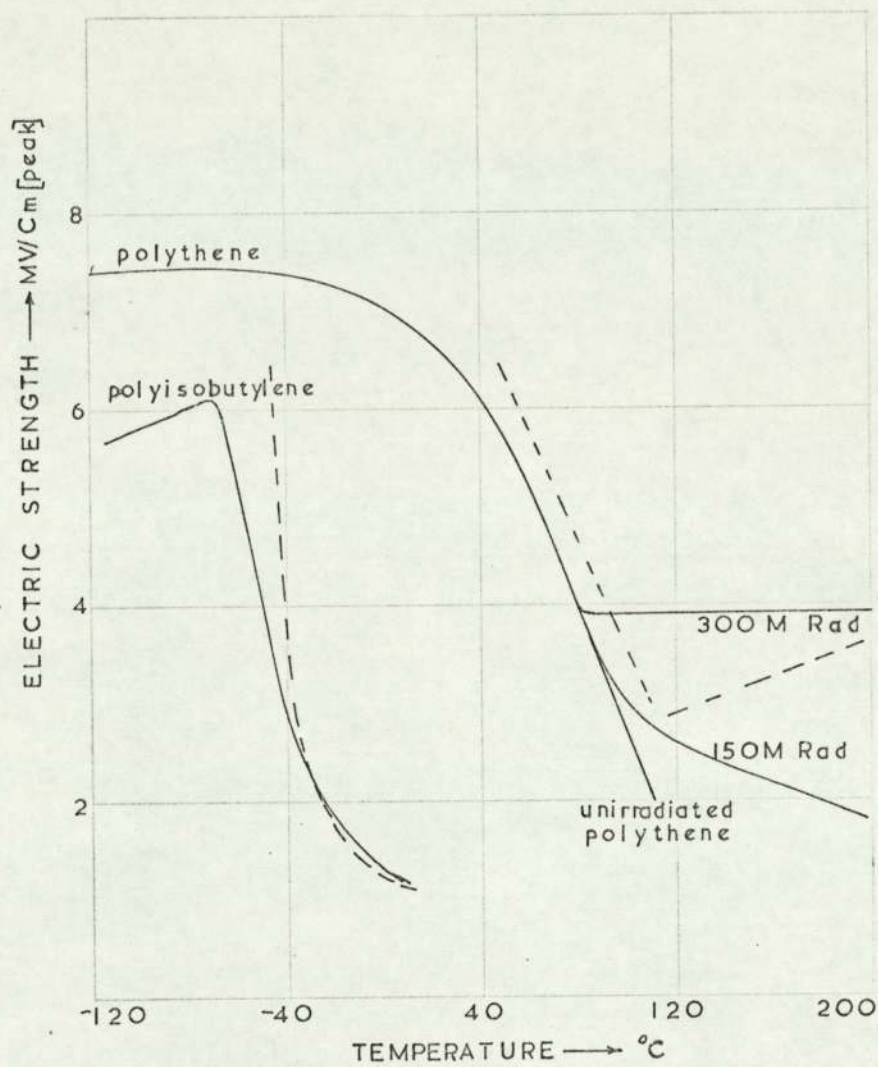


Fig. 4.16 ELECTRIC STRENGTH OF POLYTHENE AND POLYISOBUTYLENE LIMITED BY MECHANICAL FAILURE.

—, Stark and Garton 68

-----, Calculated from Eqn 4.25.

Mason's studies of breakdown in a point to plane electrode configuration of polyethylene, despite considerable scatter of results, suggest that (a) average electric stress, E_{av} , decreases with increase in temperature (see Fig. 4.17), (b) the breakdown stress for a given electrode configuration at room temperature is 25% greater if the point is negative than if it is positive, (c) E_{av} decreases with increasing electrode separation, and (d) E_{av} increases with radius of the curvature of the point electrode (see Fig. 4.18). Mason accounted for his results by assuming that the conductivity of polythene depends on the electric field in the manner predicted by Fröhlich's high temperature theory³⁰.

Bolton, Cooper and Gupta⁸ have pointed out that a polarity effect can be expected with Seitz's single avalanche criterion, since a destructive avalanche can be generated with a lower voltage when the electrons move into the region of high field.

Olyphant and Johnson⁶⁰ established that "tree" channels in epoxy resins and PMMA are hollow, non-conducting tubules except at the most advanced stage when some carbonization occurs. They assert that tree propagation breakdown mechanism is almost certainly by the action of single, separate discharges. These in turn become extinguished by the gas pressure which is a by-product of decomposition of the solid. These views have been reaffirmed by Bolton et al.⁸.

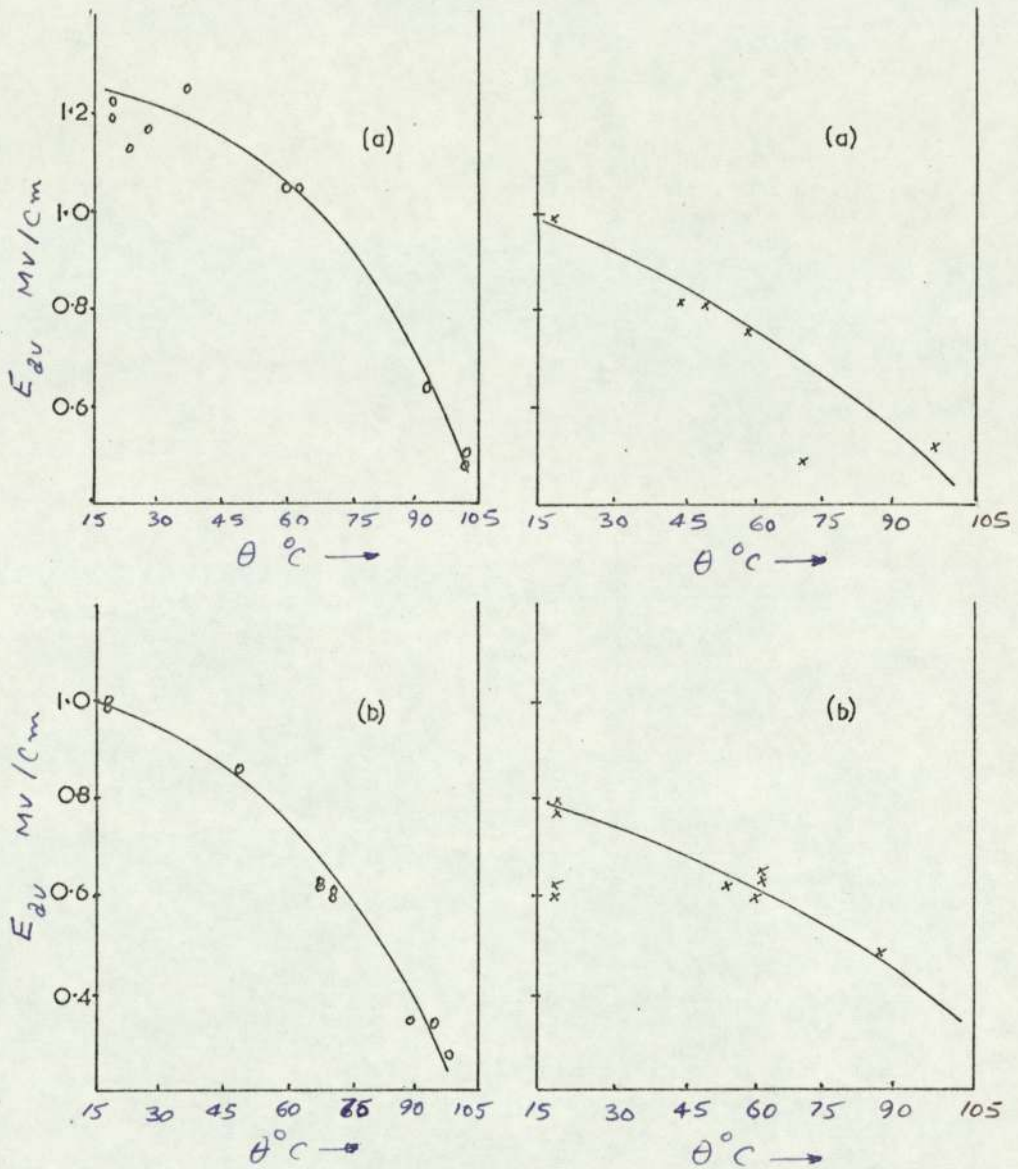


Fig. 4.17 THE VARIATION OF AVERAGE ELECTRIC STRENGTH OF POLYETHYLENE WITH TEMPERATURE IN A DIVERGENT FIELD.

(After Mason 48)

Point-electrode radius of curvature range 1.5-7.5 microns

(a) 250-350 microns electrode gap

(b) 450-600 microns electrode gap

o, point - cathode

x, point - anode

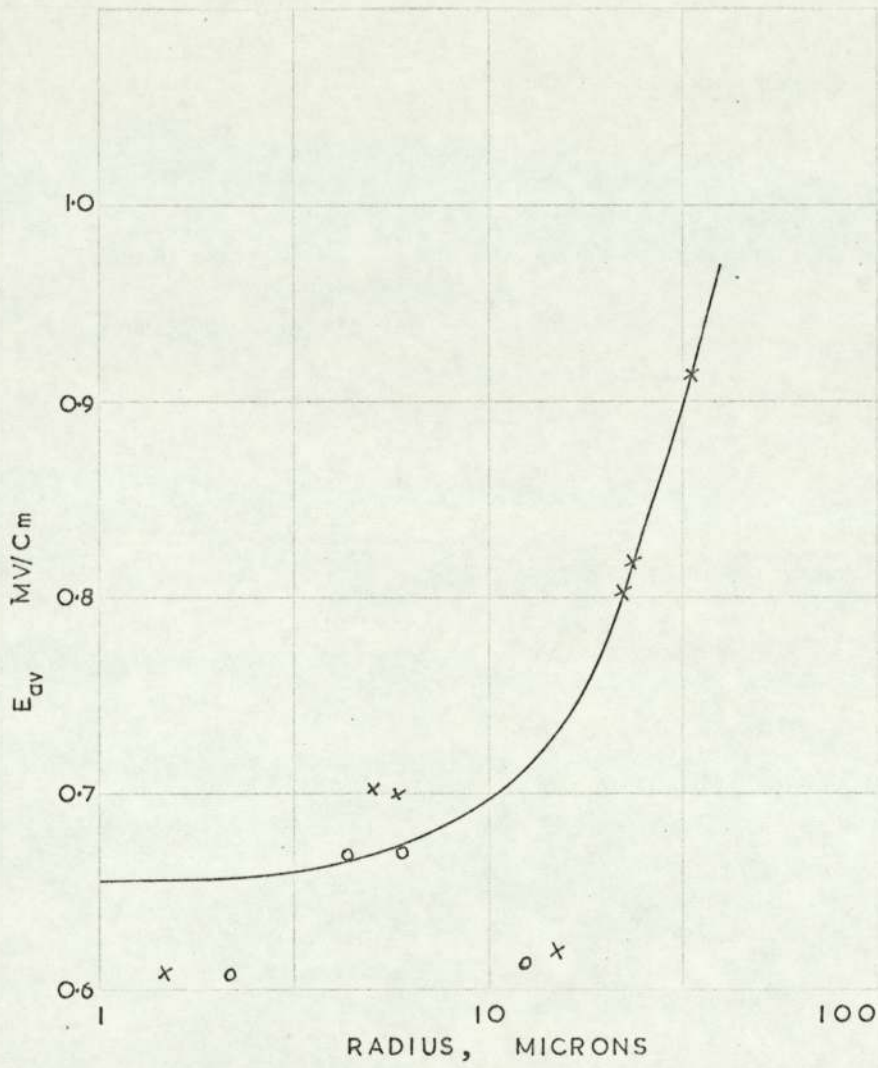


Fig. 4.18 THE VARIATION OF DIVERGENT-FIELD ELECTRIC STRENGTH WITH RADIUS OF CURVATURE OF THE POINT.

(After Mason 48)

Temperature, 60°C ; electrode gap, 500 microns.

o, point - cathode

x, point - anode

4.3 Instrumentation

To make a detailed study of discharge propagation in solid dielectrics, similar instrumentation techniques to those used in the case of gaseous dielectrics (see Section 2.3) are employed.

Visual examination of streamers is made with a microscope. By continuous adjustment of the focal length, a detailed spatial picture of streamer propagation is provided. Photographs are taken with the aid of a Nikon profile projector with exposures made in the direction transverse to the electric field.

4.3.1 Test Sample Design

A special mould is designed to provide a large number of samples easily, cheaply and of high mechanical, chemical and optical quality. The mould as shown in Figs. 4.19 and 4.20 is suitable for injection moulding of polymers and, being symmetrically fed, provides two identical samples in each operation, with appropriate electrodes at a desired gap setting. The two opposite surfaces on the mould facing the electrode gap are highly polished. With the application of transparent polymers, a detailed optical observation of the inter-electrode space is made possible. The moulding geometry is so designed as to reduce the possibility of surface tracking of the material. With the needles well embedded in the material, the mechanical stresses on the stem of the needle are relieved.

Steel sewing needles, no. 2 demi-longues, are employed as point-electrodes. The type chosen provides a mechanically strong electrode to withstand the load shock of the injection moulding. The needles are chemically washed for the removal of dust particles and surface contamination prior to mould insertion. It is possible to make Corona free electrical connection to the electrodes without application of heat.

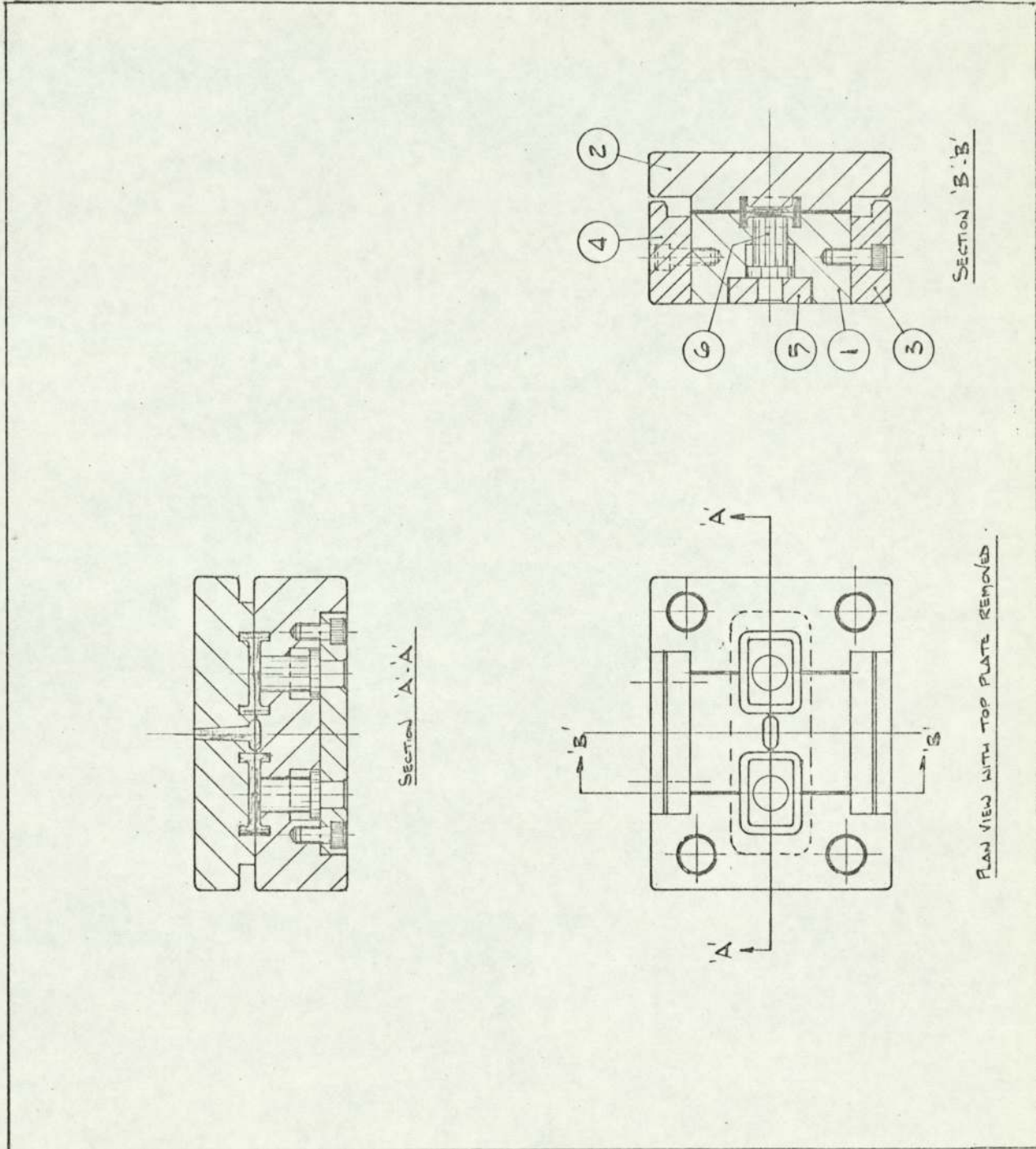


Fig. 4.19a Balanced-fed mould designed for injection moulding of polymers

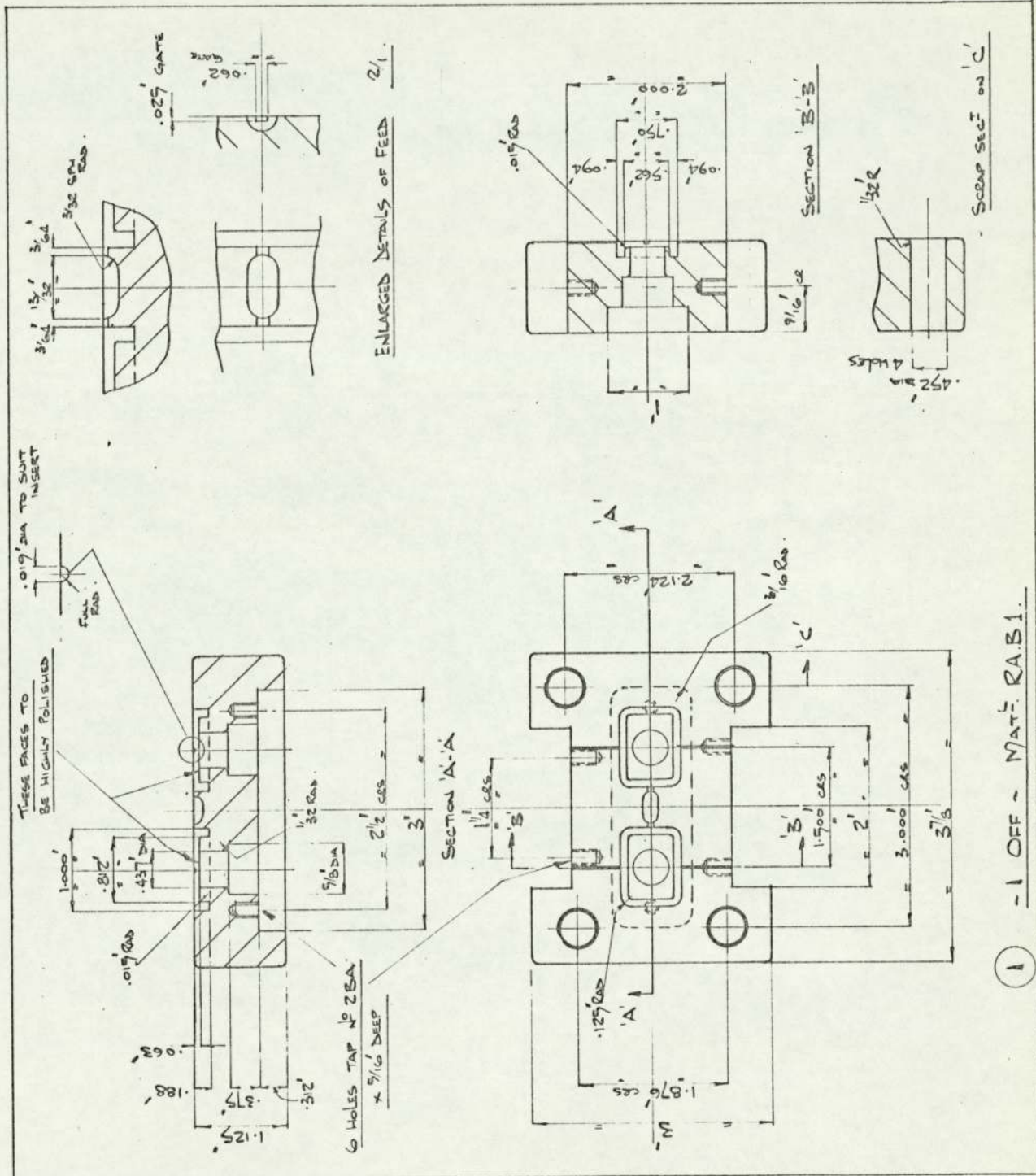


Fig. 4.19b Balanced-fed mould designed for injection moulding of polymers

Plane electrodes were provided in two ways:-

- a) Small gap setting - a plane electrode is made from a steel ball bearing grinded to a semi-sphere. The semi-spherical electrode is brazed to the needle shank and the plane face is rounded on the edge.
- b) Large gap setting - the sample with one point-electrode is cut at a desired gap length and a silver emulsion paint is applied to the plane side. This is then utilised as the plane-electrode after drying.

4.4 Experimental Results

4.4.1 Streamer Inception and Breakdown Voltages

Samples of PMMA are subjected to a series of impulse waves of varying magnitude in a point-plane electrode system. After each impulse application samples are examined under the microscope and the voltage level at which streamer channels become visible are recorded.

The test voltage level is increased until breakdown occurs. The two potential levels provide the streamer inception and breakdown voltages of the material as a function of the electrode gap length.

The electrode gap lengths selected are 1, 3 and 5 mm. The radius of curvature of the point-electrode is kept at 13 microns. The sample temperature is in the range $20^{\circ} \pm 5^{\circ}$ C.

The inception and breakdown voltages for the positive streamers in PMMA are shown in Fig. 4.21(a) and for the negative streamers in Fig. 4.21(b).

4.4.2 Streamer Propagation

The streamer range, the length L of the farthest channel in the main field, increases with the rise in impulse level. The range for three gap settings of 1, 3 and 5 mm for both polarities at the point are shown in Figs. 4.22 to 4.24.

Lower streamer penetration depth in the scatter region at a certain gap length and impulse wave generally correspond to the side movement of the streamer away from the main field axis.

The average values of streamer range for different gap length, impulse level and polarity are shown in Fig. 4.25.

TABLE 4.2 Streamer Inception and Breakdown Voltage in PMMA for different gap lengths at room temperature

Point-plane electrodes; $1/50 \mu s$ impulse wave;

C = 13 microns.

Polarity	Point-anode			Point-cathode		
	1	3	5	1	3	5
gap length, mm						
Inception voltage kV	23	22	30	25	26	30
	25	24	32	27	28	32
	27	26	36	29	30	36
	29	28	38		32	38
			30		34	40
			32			
Breakdown voltage kV		34				
		35				
	31	69	98	55	108	145
	33	73	106	57	113	150
	35	75	108	59	115	155
		77	110	61	117	160
	79		63	119		
				121		

FIG. 4.21 Streamer Inception and Breakdown Voltages in PMMA for Different Gap Length.

POINT-PLANE ELECTRODES
 $1/50 \mu\text{s}$ IMPULSE WAVE
 $C = 13$ microns

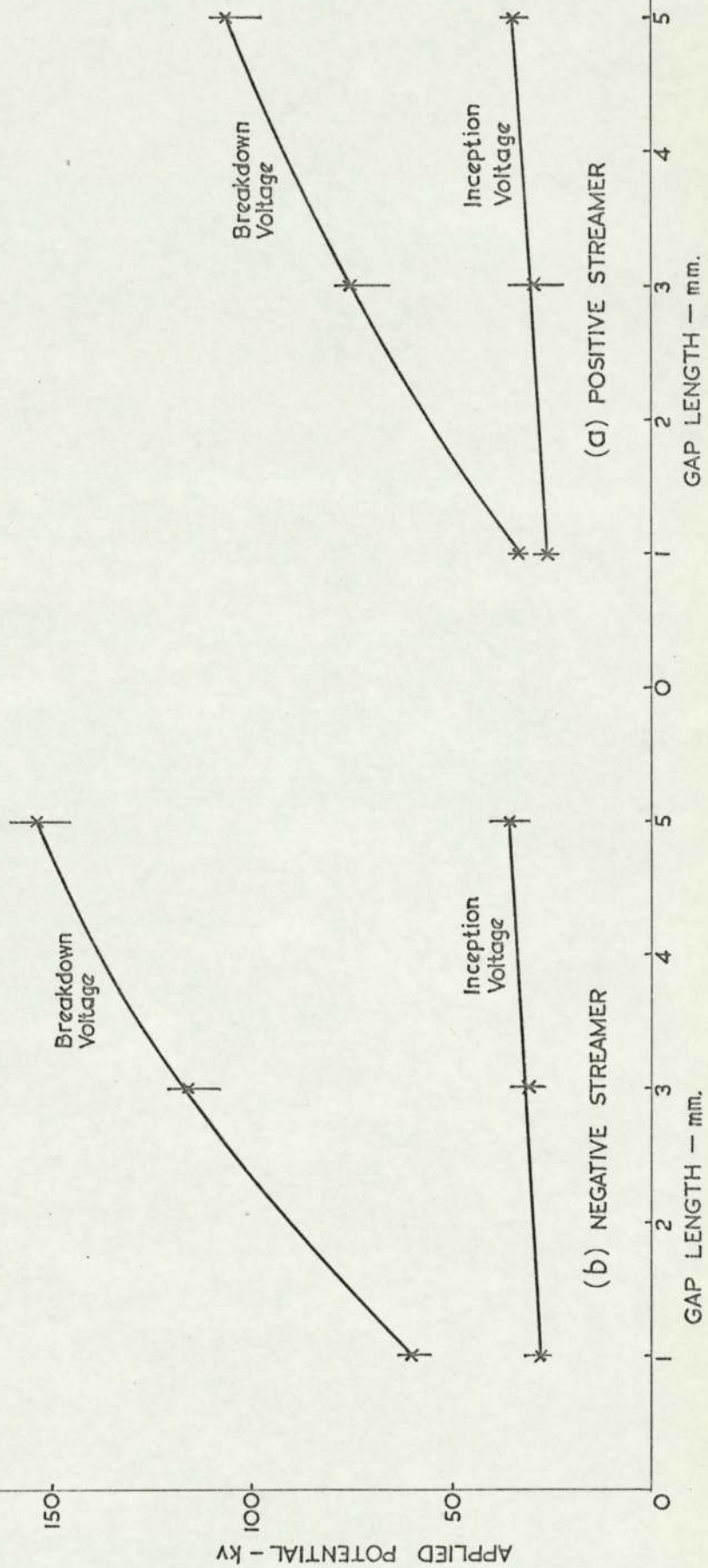


TABLE 4.3 Streamer Range Variation in PMMA at an electrode gap length of 1.0 mm with changes of applied voltage.

Point-plane electrodes; $1/50 \mu\text{s}$ impulse wave;
 $c = 13$ microns.

(a) Point-cathode

Impulse voltage kV	25	30	40	50	60	70
Streamer range mm	0	0	0.10	0.27	0.51	BD
	0	0	0.15	0.28	0.63	BD
	0	0	0.18	0.31	0.72	BD
	0	0	0.20	0.32	0.77	BD
	0	0	0.25	0.38	0.89	BD
	0	0.08	0.26	0.41	BD	BD
	0	0.12	0.27	0.43	BD	BD
	0	0.15	0.32	0.53	BD	BD

(b) Point-anode

Impulse voltage kV	25	27	29	31	33	35	37
Streamer range mm	0	0	0	0.32	0.57	0.71	BD
	0	0	0	0.34	0.61	0.78	BD
	0	0	0.06	0.39	0.62	0.81	BD
	0	0	0.11	0.41	0.67	0.86	BD
	0	0.04	0.15	0.43	0.70	0.91	BD
	0	0.07	0.20	0.50	0.74	BD	BD
	0	0.12	0.27	0.54	0.83	BD	BD
	0	0.12	0.38	0.63	BD	BD	BD

FIG. 4.22 Streamer Range in PMMA as a Function of Applied Voltage for a 1.0mm. Gap Length

POINT-PLANE ELECTRODES
1/50 μs IMPULSE WAVE
C = 13 microns

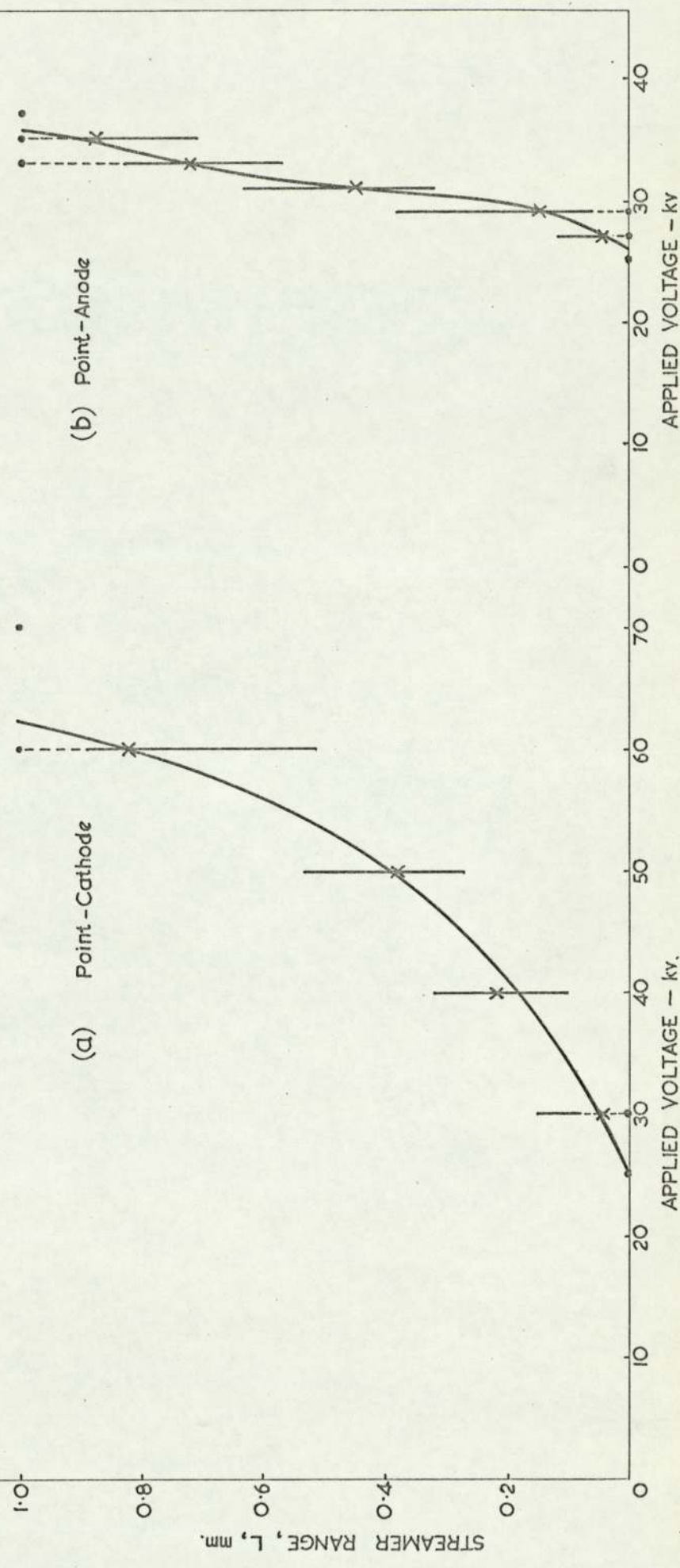


TABLE 4.4 Streamer Range Variation in PMMA at an electrode gap length of 3.0 mm with changes of applied voltage

Point-plane electrodes; $1/50 \mu\text{s}$ impulse wave; $c = 13$ microns

(a) Point-cathode

		<u>V, kV</u>									
		30	40	50	60	70	80	90	100	110	120
L_1 mm	0	0.04	0.20	0.29	0.41	0.43	0.66	0.86	1.4	BD	
	0	0.10	0.21	0.30	0.42	0.48	0.68	0.91	1.68	BD	
	0	0.13	0.22	0.33	0.42	0.52	0.69	0.93	1.72	BD	
	0	0.18	0.25	0.34	0.43	0.54	0.71	0.97	2.2	BD	
	0	0.21	0.27	0.37	0.45	0.63	0.71	1.04	BD	BD	
	0	0.22	0.27	0.39	0.49	0.71	0.73	1.05	BD	BD	
	0	0.26	0.29	0.40	0.50	0.77	0.74	1.17	BD	BD	
	0	0.28	0.31	0.42	0.52	0.79	0.78	1.28	BD	BD	

(b) Point-anode

		<u>V, kV</u>											
		25	30	35	40	45	50	55	60	65	70	75	80
L_1 mm	0	0	0	0.61	1.26	1.38	1.52	1.91	2.01	2.27	2.48	BD	
	0	0	0	0.65	1.28	1.39	1.55	1.93	2.07	2.35	2.61	BD	
	0	0	0	0.73	1.32	1.41	1.62	1.94	2.12	2.42	2.68	BD	
	0	0	0.09	0.73	1.37	1.41	1.62	2.00	2.14	2.51	BD	BD	
	0	0	0.41	0.85	1.38	1.45	1.68	2.03	2.25	2.81	BD	BD	
	0	0	0.56	0.92	1.43	1.46	1.71	2.08	2.57	BD	BD	BD	
	0	0	0.71	1.01	1.51	1.53	1.77	2.11	2.37	BD	BD	BD	
	0	0.1	0.82	1.10	1.57	1.61	1.81	2.21	2.76	BD	BD	BD	

FIG. 4.23 Streamer Range in PMMA as a Function of Applied Voltage for a 3.0mm. Gap Length

POINT-PLANE ELECTRODES

$1/50\mu\text{s}$ IMPULSE WAVE

$C=13$ microns

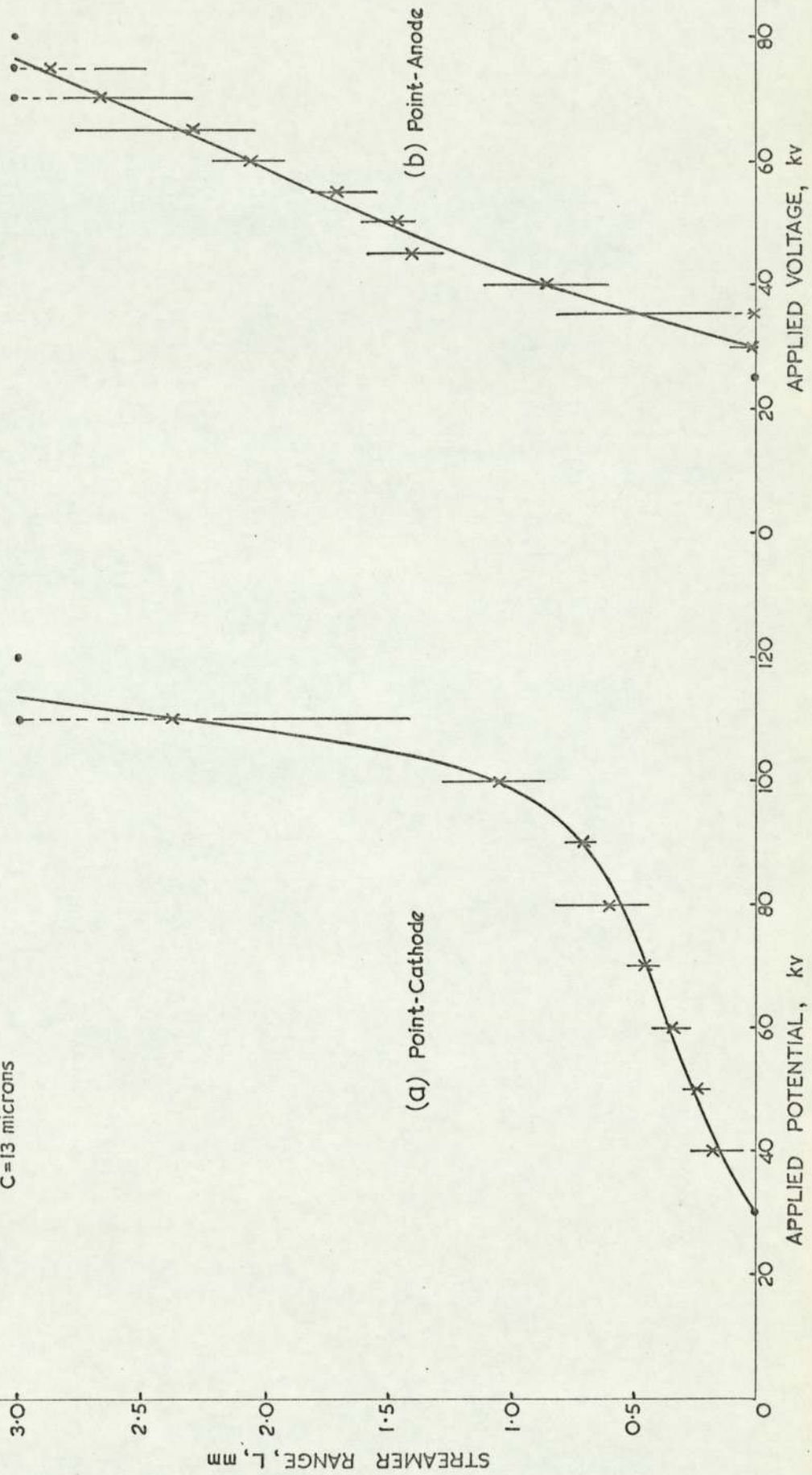


TABLE 4.5 Streamer Range Variation in PMMA at an electrode gap length of 5.0 mm with changes of applied voltage

Point-plane electrodes; $1/50 \mu\text{s}$ impulse wave; $c = 13$ microns

(a) Point-cathode

Voltage, kV	35	40	50	60	70	80	90	100	110	120	130	140	150	160
L_1 mm	0	0	0.03	0.17	0.28	0.32	0.52	0.56	0.68	1.02	1.25	1.95	2.74	BD
	0	0	0.09	0.18	0.29	0.37	0.54	0.71	0.75	1.16	1.40	2.07	3.36	BD
	0	0	0.15	0.21	0.30	0.40	0.61	0.75	0.78	1.37	1.73	2.11	3.82	BD
	0	0	0.16	0.21	0.33	0.43	0.63	0.76	0.92	1.41	1.78	2.47	BD	BD
	0	0	0.19	0.25	0.34	0.49	0.63	0.79	0.98	1.65	1.92	2.58	BD	BD
	0	0.04	0.23	0.26	0.37	0.51	0.68	0.81	1.07	1.72	2.03	2.93	BD	BD
	0	0.11	0.29	0.28	0.37	0.53	0.70	0.81	1.16	1.76	2.19	3.02	BD	BD
	0	0.18	0.32	0.29	0.41	0.57	0.71	0.83	1.18	1.91	2.34	3.11	BD	BD

(b) Point anode

Voltage, kV	30	35	40	50	60	70	80	90	100	110
L_1 mm	0	0	0.50	0.81	1.31	1.63	2.00	2.08	2.51	BD
	0	0	0.64	0.90	1.42	1.68	2.06	2.24	2.67	BD
	0	0	0.67	0.93	1.48	1.70	2.09	2.41	3.83	BD
	0	0	0.68	0.97	1.51	1.76	2.10	2.57	2.98	BD
	0	0	0.72	1.02	1.55	1.81	2.17	2.64	3.13	BD
	0	0.32	0.79	1.07	1.57	1.83	2.21	2.70	3.25	BD
	0	0.38	0.83	1.08	1.60	1.89	2.23	2.73	3.71	BD
	0	0.47	0.85	1.12	1.62	1.92	2.28	2.81	BD	BD

FIG. 4.24 Streamer Range in PMMA as a Function of Applied Voltage for a 5.0 mm. Gap Length

POINT-PLANE ELECTRODES
 $1/50 \mu\text{s}$ IMPULSE WAVE
 $C = 13$ microns

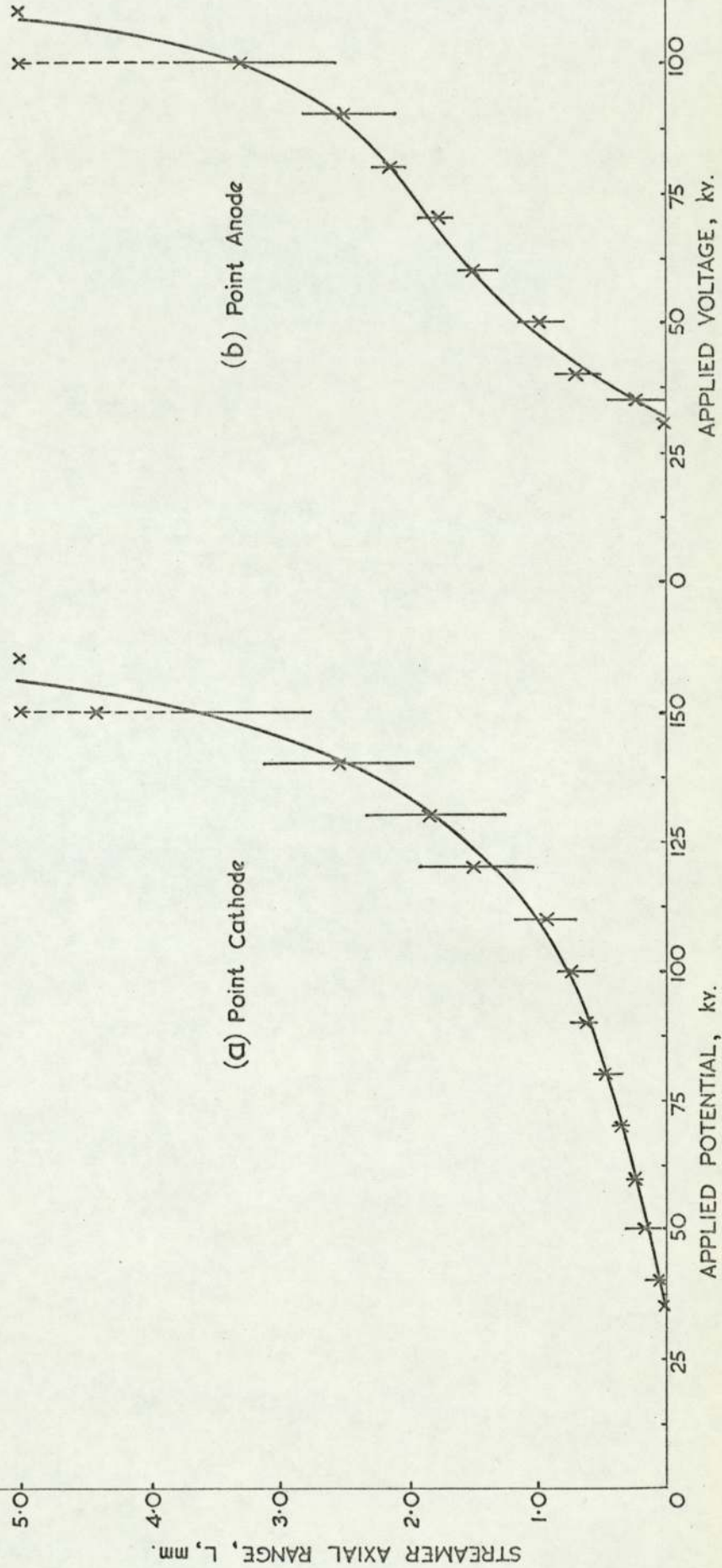
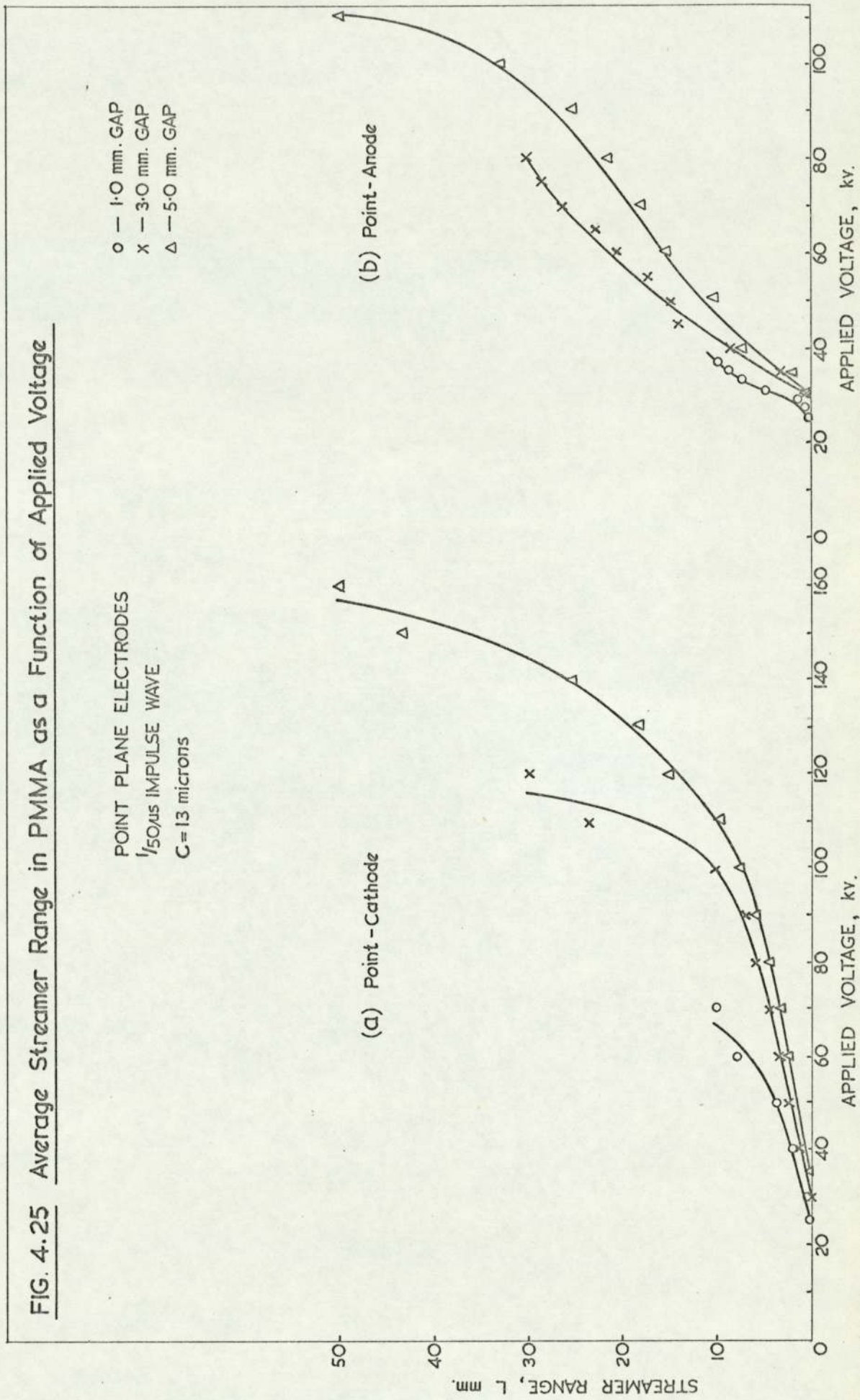


FIG. 4.25 Average Streamer Range in PMMA as a Function of Applied Voltage



4.4.3 Spatial Build-up of Streamers

The spatial build-up of the positive and negative streamers is shown in Figs. 4.26 and 4.27. The extensive fine branching of the positive streamers stands in contrast to the thicker stems and shorter branches of the negative streamers.

The observation shows that breakdown always occurs if a streamer tip reaches the plane electrode. Determination of the scatter region of the streamer penetration would also give the scatter region of the impulse breakdown voltage.

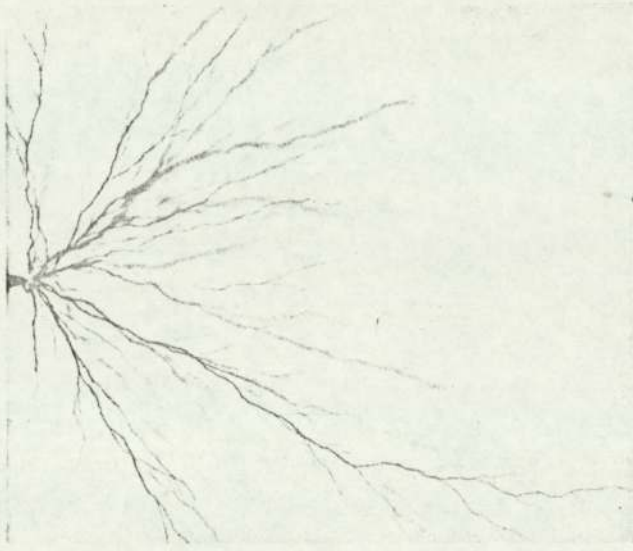


Fig. 4.26 Positive Streamer Pattern in PMMA

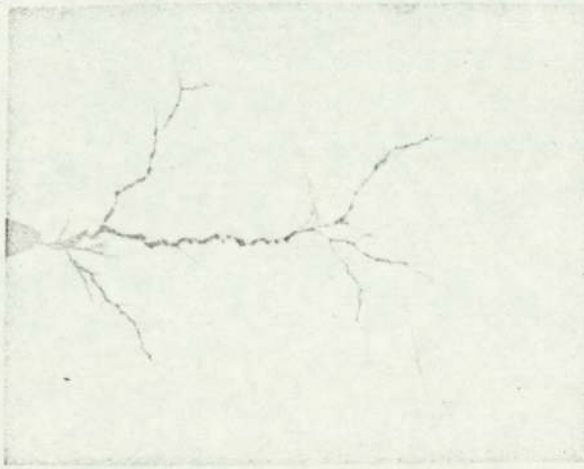


Fig. 4.27 Negative Streamer Pattern in PMMA

4.5 Discussion

The subject of electrical breakdown of solid dielectrics is one in which an unusual number of difficulties conspire to frustrate any satisfactory comparison of theory with experiment. Considering only the simplest theory and the simplest ionic crystal, i. e. Fröhlich's criterion for the critical field strength:

$$E = \frac{K (\epsilon - n_o^2) q \nu (m h \nu)^{\frac{1}{2}}}{a h \nu_o} \log^{\frac{1}{2}} \frac{h \nu_o}{m a^2 \nu^2} \coth^{\frac{1}{2}} \frac{\theta_D}{2\theta} \quad (4.28)$$

where K = a constant of order of unity provided the electrical units are in e. s. u., and the others in c. g. s.

$(\epsilon - n_o^2)$ = the contribution to dielectric constant from the infra-red spectrum.

q = electronic charge

m = electronic mass

a = lattice spacing

ν_o = frequency of the u.-v. absorption limit

ν = the lowest frequency in the infra-red spectrum.

$\theta_D = \frac{h\nu}{k}$ = Debye characteristic temperature

θ = absolute temperature

h = Planck's constant

k = Boltzmann's constant

This theoretical expression requires six constants of the crystals, namely ϵ , n_o , a , ν , ν_o and θ_D . These are rarely available with any accuracy.

On the experimental side, ionic crystals are mechanically weak, and it is established that some of them are subject to work-hardening under the compressive force of the field so that they increase in electric strength during the measurement. This, even when the crystals are initially annealed, leads to a spread of strength of $\pm 25\%$ at room temperature. The effect at other

temperatures is not well established but, from the great variation of results from different investigators, it is thought to be large.

There is inadequate information in the published data about the treatment of the results. Before the work-hardening effect was discovered by Cooper¹⁴, it appeared reasonable to accept the highest results as necessarily nearest to the true strength. Cooper and Fernandez¹⁶ have quoted the minimum values while Konorova and Sorokina⁴⁴ are believed to have employed the "90%" failure level.

The variation of strength with temperature is less uncertain on the theoretical side, since in the simple theory it involves only one constant, θ_D . Experimentally, however, the results vary considerably between different investigators. Taking potassium bromide as an example, with a Debye temperature low enough to give appreciable variation of intrinsic strength before the thermal instability supervenes, Cooper¹⁴ gives a survey of collected results (see Fig. 4.3). It will be seen that some curves rise linearly with temperature, as required by theory, while others show a sharp transition around a temperature of -20°C . This unknown variation is not correlated to duration of the stress, the conductivity of the specimen or with any one investigator. This behaviour may be connected with ratio between the field required for failure, and the field required to cause work-hardening.

Considering that the theory contains no disposable constants, the agreement in absolute value is good confirmation and the agreement in general of the observed rise toward high temperature with the predicted increase is also significant, since all other forms of breakdown have the opposite dependence.

Results on muscovite mica³⁵ agree in magnitude with the results of the simple theory, although this is not strictly applicable to so complex a crystal. The predicted increase with temperature is too small to observe with any certainty (see Fig. 4.4).

Fröhlich has given a theory, in general terms, for amorphous materials but the data required for insertion into the expression are not available for such complex structures, and all that can be said is that one expects, and finds, a strength about one order of magnitude higher than in ionic crystals. Most of the amorphous materials tested, even when as different as glass and polyethylene, show a nearly constant electrical strength in the range 5 - 15 MV/cm below some temperature at which thermal instability or electro-mechanical failure supervenes, and the apparent strength falls.

Results accumulated over the past three decades show that the intrinsic strengths of solid dielectrics range from just below 1 MV/cm for some alkali halides to a record value of 15 MV/cm for polyvinyl alcohol at -196° C. The electric strength of the great majority lie in the range 5 to 10 MV/cm. It is interesting to compare these values with the highest working stress in industrial applications of solid dielectrics, about 200 kv/cm. There are many practical considerations which at present justify this wide discrepancy, but further development work directed at its reduction would undoubtedly be well repaid.

The problems associated with experimental techniques already developed are as follows:-

1. Surface Tracking - Discharge along the surface of the solid specimen takes place during the build-up of the electric field both in gaseous and liquid environments.
2. Cracks - Very fine cracks appear in the solid sample when a needle is inserted providing an electrically weak path.
3. Gas or Void Inclusion - Due to poor surface adhesion, fine gas bubbles between the metallic electrode and the solid dielectric are trapped. In the case of needles, heated prior to insertion, when cooling occurs, small voids appear in the metal-dielectric inter-phase. Both gaseous inclusion and voids with low discharge inception voltage will dominate the breakdown mechanism.

4. Gap Setting - The likelihood of providing the same electrode geometry at a required gap setting is extremely difficult.
5. Cost - Unfortunately cost is usually the main deciding factor in adapting a measurement technique. The main problems mentioned above result in a high rejection ratio for the samples, raising the overall cost.

An endeavour has been made to overcome problems experienced by previous investigators by the use of a suitable design of samples made by injection moulding.

Electrical breakdown studies of PMMA show that the streamer inception voltage increases slightly with gap length and is generally lower for point-anode than point-cathode.

The breakdown voltage increases sharply with the increase of gap length. For any gap setting, the breakdown is lower for point-anode than point-cathode. It is observed that, once the streamer crosses the inter-electrode space, the breakdown immediately follows. This sequence of events suggests that the streamers are of secondary type similar to those observed in liquid.

4.6 Bibliography

1. Amakakawa, K., Yoshida, T., Moriuchi, T., and Inuishi, Y.
Elec. Eng. Japan, 84, p. 50 (1964)
2. Artbauer, J., and Griač, J.
Proc. I.E.E., 112, p. 818 (1965)
3. Austen, A. E., and Whitehead, S.
Proc. Roy. Soc., A176, p. 33 (1940)
4. Baker, W. P.
Nature, 177, p. 886 (1956)
5. Ball, I. D. L.
Proc. I.E.E., 98, p. 84 (1951)
6. Bashara, N. M.
I.E.E.E. Trans. (Compt. Part) CP10-12, p. 4 (1963-65)
7. Bird, D. W., and Pelzer, H.
J.I.E.E., 96, pt. 1, p. 44 (1949)
8. Bolton, B., Cooper, R., and Gupta, K. G.
Proc. I.E.E., 112, p. 1215 (1965)
9. Bradley, A.
Insulation, 10, p. 31 (1964)
10. Buehl, R. C., and von Hippel, A.
Phys. Rev., 56, p. 941 (1939)
11. Calderwood, J. H., Cooper R., and Wallace, A. A.
Proc. I.E.E., 100, p. 105 (1953)
12. Callen, H. B.
Phys. Rev., 76, p. 1394 (1949)
13. Charlesby, A., and Hancock, N. H.
Proc. Roy. Soc., A218, p. 245 (1953)

14. Cooper, R.
 'Progress in Dielectrics, Vol 5, Heywood, London (1963)
15. Cooper, R.
 Brit. J. Appl. Phys., 17, p. 149 (1966)
16. Cooper, R., and Fernandez, A.
 Proc. Phys. Soc. Lond., B71, p. 688 (1958)
17. Cooper, R., and Grossart, E. T.
 Proc. Phys. Soc. Lond., B66, p. 716 (1953)
18. Cooper, R., Grossart, E. T., and Wallace, A. A.
 Proc. Phys. Soc. Lond., B70, p. 172 (1957)
19. Cooper, R., Rowson, C. A., and Watson, D.
 Nature, 197, p. 663 (1963)
20. Cooper, R., and Smith, W. A.
 Proc. Phys. Soc. Lond., B78, p. 734 (1961)
21. Cooper, R., and Wallace, A. A.
 Proc. Phys. Soc. Lond., B66, p. 1113 (1953)
22. Cooper, R., and Wallace, A. A.
 Proc. Phys. Soc. Lond., B69, p. 1287 (1956)
23. Fava, R. A.
 Proc. I.E.E., 112, p. 819 (1965)
24. Feldman, C.
 Nature, 203, p. 964 (1964)
25. Franz, W.
 Encyclopedia of Physics, Springer, Berlin (1956)
26. Fröhlich, H.
 Proc. Roy. Soc., A160, p. 230 (1937)
27. Fröhlich, H.
 Proc. Roy. Soc., A172, p. 94 (1939)
28. Fröhlich, H.
 Proc. Roy. Soc., A178, p. 493 (1941)

29. Fröhlich, H.
Phys.Rev., 61, p. 200 (1942)
30. Fröhlich, H.
Proc.Roy.Soc., A188, p. 521 (1947)
31. Fröhlich, H.
Proc.Roy.Soc., A188, p. 532 (1947)
32. Fröhlich, H., and Paranjape, B. V.
Proc.Phys.Soc.Lond., B69, p. 21 (1956)
33. Fröhlich, H., and Mott, N. F.
Proc.Roy.Soc., A141, p. 446 (1939)
34. Grunewald, F.
Arch.für Elekt., 12, p. 79 (1923)
35. Hackett W., and Thomas, A. M.
J.I.E.E., 88, Pt. 1, p. 295 (1941)
36. von Hippel, A.
Zeit. für Physik, 67, p. 707 (1931)
37. von Hippel, A.
Zeit. für Physik, 68, p. 309 (1932)
38. von Hippel, A.
Ergeb.d.exakt.Nature., 14, p. 79 (1935)
39. von Hippel, A.
J.Appl.Phys., 8, p. 815 (1937)
40. von Hippel, A., and Alger, R. S.
Phys.Rev., 76, p. 127 (1949)
- 40a Houston, W. V.
Phys.Rev., 57, p. 184 (1940)
41. Kawamura, H., Ohkura, H., and Kikuchi, T.
J.Phys.Soc.Japan, 9, p. 541 (1954)

42. Kitchen, D. W., and Pratt, O. S.
A. I. E. E. Trans. Pt. III (P. A. S.), 77, p. 180 (1958)
43. Kitchen, D. W., and Pratt, O. S.
A. I. E. E. Trans. Pt. III (P. A. S.), 81, p. 112 (1962)
44. Konorova, E. A., and Sorokina, L. A.
Soviet Phys., F. E. T. P., 5, p. 143 (1957)
45. Kostrygin, V. A.
Soviet Physics - Solid State, 2, p. 1664 (1960)
46. Kuchin, V. D.
Soviet Physics - Solid State, 1, p. 406 (1959)
47. Lawson, W. G.
Proc. I. E. E., 113, p. 197 (1966)
48. Mason J. H.
Proc. I. E. E., 113, p. 197 (1966)
49. Mason, J. H.
Progress in Dielectrics, Vol. 1, Heywood, London (1959)
50. Mason, J. H.
Proc. I. E. E., 112, p. 1407 (1965)
51. McMahan, E. J., and Perkins, J. R.
I. E. E. E. Trans. (P. A. S.), 69, p. 1106 (1963)
52. McMahan, E. J., and Perkins, J. R.
I. E. E. E. Trans. (P. A. S.), 70, p. 1253 (1964)
53. McKeown, J. J.
Proc. I. E. E., 112, p. 824, (1965)
54. Matt, N. F., and Gurney, R. W.
Electronic Progress in Ionic Crystals, O. U. P., New York (1940)
55. Oakes, W. G.
Proc. I. E. E., Pt. 1, 95, p. 36 (1948)
56. Oakes, W. G.
Prof. I. E. E., Pt. 1, 96, p. 37 (1949)

57. O'Dwyer, J. J.
Adv. in Phys., 7, p. 349 (1958)
58. O'Dwyer, J. J.
Theory of Dielectric Breakdown in Solids, Clarendon
Press, Oxford (1964)
59. Olyphant, M. Jr.
I.E.E.E. Trans (P.A.S.), 69, p. 1128 (1963)
60. Olyphant, M. Jr., and Johnson, R. A.
Ann.Rept. Conf. on Elec. Inst. (1961)
61. Parkman, N., Goldspink, A. F., and Lawson, W. G.
Electronic Letters, 1, p. 98 (1965)
62. Ryu, I., and Kawamura, H.
J. Phys. Soc. Japan, 9, p. 438 (1954)
63. Seeger, R. J., and Teller, E.
Phys.Rev., 54, p. 515 (1938)
64. Seeger, R. J., and Teller, E.
Phys.Rev., 56, p. 352 (1939)
65. Seitz, F.
The Modern Theory of Solid, McGraw-Hill (1940)
66. Seitz, F.
Phys.Rev., 76, p. 1376 (1949)
67. Seitz, F., and Turnbull, D.
Solid State Physics, Academic (1955)
68. Stark, K. H., and Garton, C. G.
Nature, 176, p. 1225 (1955)
69. Stratton, R.
Proc.Roy.Soc., A242, p. 355 (1957)
70. Stratton, R.
Proc.Roy.Soc., A246, p. 406 (1958)

- 254
71. Stratton, R.
Progress in Dielectrics, Vol. 3, Heywood, London (1961)
 72. Tanaka, T., and Inuishi, Y.
Elec. Eng. Japan, 86, p. 1 (1966)
 73. Taylor, H. E.
J. Soc. Glass Technol., 39, p. 193 (1955)
 74. Thomas
World Power, 24, p. 85 (1935)
 75. Thomas
World Power, 24, p. 125 (1935)
 76. Vermeer, J.
Physica, 20, p. 313 (1954)
 77. Vermeer, J.
Physica, 22, p. 1257 (1956)
 78. Vorob'yev, A. A.
Soviet Physics - J.E.T.P., 3, p. 225 (1956)
 79. Vorob'yev, A. A., Vorob'yev, G. A., and Kostygin, V. A.
Izv. Akad. Nauk S. S. S. R., 2, p. 62 (1961)
 80. Vorob'yev, G. A.
Fiz. Tverdogo Tela, 6, p. 3494 (1964)
 81. Watson, D. B., Heyes, W. Kao, K. C. and Calderwood, J. H.
I.E.E.E. Trans. E.I - 1, 2, p. 20 (1965)
 82. Whitehead, S.
Dielectric Phenomena, III: Breakdown of Solid Dielectric,
Ernest Benn, London (1932)
 83. Whitehead, S.
Dielectric Breakdown of Solid, Clarendon Press,
Oxford (1951)

84. Whitehead, S.
The Insulation of Electrical Equipments, John Wiley
& Sons, New York (1954)
85. Wolff, P. A.
Phys.Rev., 95, p. 1415 (1954)
86. Yamashiti, J.
Progs.Theor.Phys., Osaka, 2, p. 95 (1956)
87. Yasui, T.
Sum.Elec.Tech.Rev., 10, p. 49 (1967)
88. Zener, C. M.
Proc.Roy.Soc., 145, p. 523 (1934)

CHAPTER 5

CONCLUSION

5. CONCLUSION.

It is relatively easy to discover a relationship between the breakdown strength of dielectric materials and some physical property such as density or temperature, but it is much more difficult to ascertain the significant process which gives rise to this relationship.

The studies in point-plane electrode geometry have established the presence of primary streamers in air for a large range of impulse potentials both below and above the value for which the streamers cross the gap. As the point potential increases the streamers move further into the gap showing strong radial branching.

The primary streamers are not only present in the immediate vicinity of the main axis but they also possess considerable lateral extension up to the plane electrode.

In the low field region, the imposing force due to the electric field on the primary streamers is negligible. Its main effect is generally to guide the streamer tip along the field lines. A theory of primary streamer propagation in this region is suggested which is in accord with the experimental results.

The conductivity of the streamer tail is of major significance in long streamers. As the primary streamer crosses a gap, the flow of electrons in the main trunks and the feeding branches results in higher conductivity of the channels near the point-electrode.

The high conductivity near the point-electrode initiates the secondary streamers. These are identified with the bright filaments which have been observed to grow from the point-electrode even before the primary streamer tips reach the plane-electrode. A theory to cater for secondary streamer propagation suggests that the axial range of secondary streams is proportional to the applied voltage.

The secondary streamers may eventually reach the plane electrode especially if the return streamers are active near the plane.

There is remarkable similarity between the experimental results and the mechanism of natural lightning. Both phenomena appear

to start with electron avalanches near the virtual point charge leading to streamers which propagate towards the plane-electrode. The visible stepped-leader in the case of lightning can be identified with the secondary streamers and the return stroke with the return streamers.

The design of the test cells and their associated measurement techniques fulfils the requirements that include simplicity, ease of operation and high sensitivity. They also have the added advantage of relative cheapness considering the number of results required.

In the case of solid dielectrics the yield of suitable samples made by injection moulding increases dramatically to over 95% compared to that of other investigators (<50%).

By selecting a film of appropriate sensitivity, the photon radiation, primary streamer, return streamer, secondary streamer and breakdown channels are recorded.

The sequence of events in the high-pressure breakdown of air, depicted schematically by the diagram in Fig. 5.1., takes the following course

I - Primary Streamer

When the positive potential of the point-electrode reaches an "adequate" value called primary streamer inception voltage in air at atmospheric pressure, a single avalanche, or a group of intense smaller converging avalanches, will create sufficient space charge distortion together with adequate photoionization in the gas so as to launch a primary streamer.

II - Primary streamer propagation

Once the primary streamers are launched they propagate in all directions along the field lines providing an extensive spatial pattern. The streamer head contains high density electrons and positive ions and the tail is of low conductivity neutral plasma. The primary streamers are invisible and may cross the whole of electrode gap.

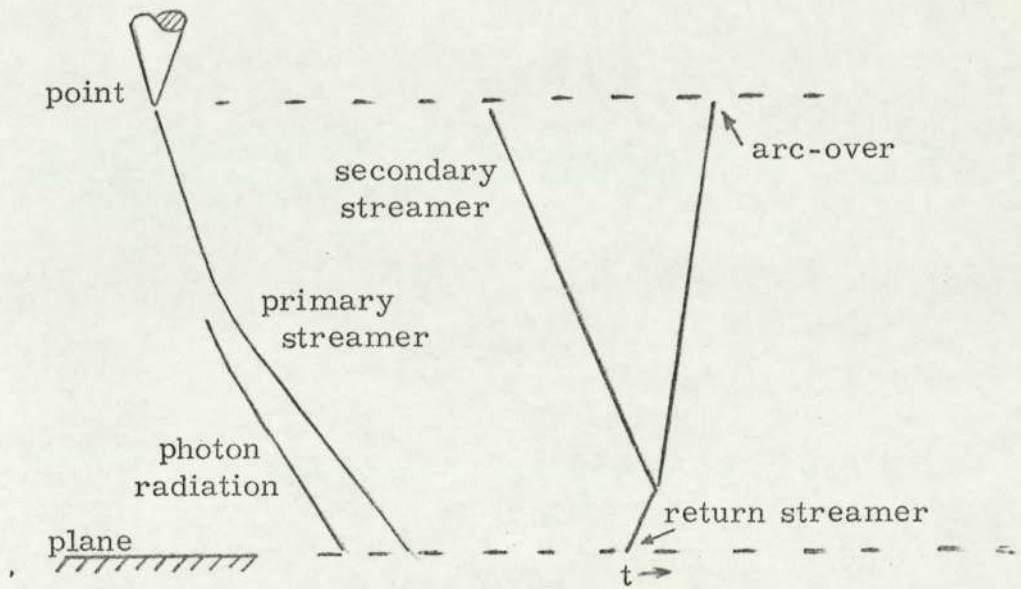


FIG. 5. 1. Schematic diagram indicating the sequence of events leading to breakdown in air at N. T. P.

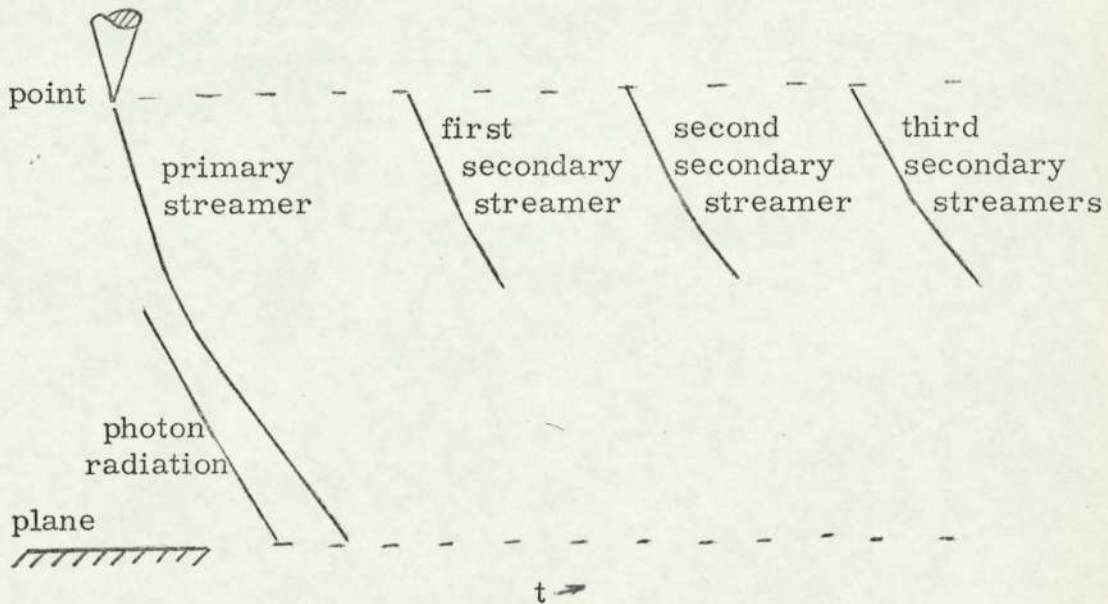


FIG. 5. 2. Schematic diagram indicating the sequence of events leading to Corona in air at N. T. P.

III - Space Charge Effect.

The positive space charge near the point-electrode modifies the electric field such that further streamer initiation is suppressed.

IV - Secondary Streamer

If a higher potential threshold called secondary streamer inception voltage is reached at the point-anode, the primary streamers are followed by secondary streamers. These are the well known "visible corona" generally emitting visible electro-magnetic waves from their main branches. The secondary streamers contain highly conducting plasma tails.

V - Return Streamers.

Intensive photons generated at the streamer tip travel ahead of secondary streamers and on reaching the plane-cathode start avalanches leading to anode-directed negative streamers called return streamers.

VI - Breakdown

Once a single secondary streamer and a return streamer meet near the plane-cathode, a highly conducting low impedance plasma is produced between the two electrodes. Subject to energy availability of the external source the arc-over results.

If the secondary streamer propagation is halted within the half-way gap length, the probability of breakdown is diminished and the sequence of events follows the pattern shown in Fig. 5.2. This is the phenomenon normally referred to as corona discharge where the first and the subsequent secondary streamers are visible filamentary discharge with the associated shock waves.

CHAPTER 6

SUGGESTION FOR FURTHER STUDIES

6. SUGGESTION FOR FURTHER STUDIES.

Future studies are expected to be carried out in two distinct phases. The first one is an extension of the present investigation utilising the same instrumentation techniques, test cells and materials. More emphasis should be given to the application of sub-microsecond voltage pulses to air in divergent field as this mode was found to be most fruitful.

Presence and progress of streamers now established in all three media can be studied more clearly in large electrode gaps.

The electromagnetic radiation sensitive film technique can be applied to solid dielectrics in a sandwich form. This is expected to provide some evidence of photon radiation and primary streamers. Opaque solid dielectrics could also be investigated by this technique.

The second phase should cover changes both in instrumentation and materials. In order to carry out further long term research on this project the most valuable piece of equipment required is an ultra high speed camera which possesses a writing speed in excess of a million frame per second. This would record the sequence of events occurring in the liquids and solids from the moment of electric field application. A clearer picture of streamers and the rate of their growth with time and voltage could thus be obtained. The ultra high speed camera would also be of use in problems of post-breakdown mechanism.

In the early stages of discharge the intensity of any emitted light is extremely low. An ultra high speed image converter in streak or framing modes could well be a suitable tool due to its high image intensifying property.

Where there exists a complete absence of emitted light in the discharge life cycle, as for example with primary streamers, direct photography will bear no fruit.

The application of electrical stress to a dielectric medium results in setting of mechanical force. In a divergent electric field, localised stresses would occur resulting in change of refractive index within the homogeneous material.

For the study of primary streamers, a Schlieren method of photography, which renders visible on a screen or photographic plate areas of different refractive index, is recommended. This could incorporate a laser light source and an ultra high speed camera.

Schlieren technique, which can readily be modified to shadow-graph method of photography, offers an added benefit in that it is able to outline the shock wave phenomenon occurring in all electrical discharges.

The chemical analysis of discharge products in gaseous dielectrics, and the decomposition products in liquid and solid dielectrics, is a strong tool which is not yet fully utilised. This type of investigation may indicate the possible reactions taking place in the material subjected to high electric field stress. The relative measure of the different discharge products may also underline the dominating reaction. One important point to be considered in this aspect is that the life cycle of some of the products, especially those in the excited state, is extremely short.

Choice of suitable material should at first be limited to those of simple atomic or molecular structure. It is proposed to select helium, n-hexane and polyethylene as the next group of material for electrical breakdown studies. A large volume of information is now available on fundamental properties of these materials.

The work presented is only an opening into a most fascinating field. It is hoped that future studies incorporating electrical, optical and chemical instrumentation will eventually provide a possible explanation of electrical breakdown in dielectrics under all conditions.

CHAPTER 7

APPENDICES

7. Appendices

7.1 Electric Field in a Point-Plane Electrode System

Representing a point-plane electrode system by a charged hyperboloid in prolate spheroidal co-ordinates (see Section 2.5.1.4) leads to the determination of the electric field in the electrode gap given by:

$$E = \frac{V (\sinh^2 \eta + \sin^2 \theta)^{-\frac{1}{2}}}{a \left(\ln \cot \frac{\theta_0}{2} \right) \sin \theta} \quad (\text{A.1.1})$$

A hyperboloid is a hyperbola

$$\frac{z^2}{d^2} - \frac{x^2}{b^2} = 1 \quad (\text{A.1.2})$$

rotated about z-axis.

Radius of curvature is given by:

$$C = \left[1 + \left(\frac{dz}{dx} \right)^2 \right]^{\frac{3}{2}} \left[\frac{d^2 z}{dx^2} \right]^{-1} \quad (\text{A.1.3})$$

At the tip of the hyperboloid when $Z =$ gap length, G

$$\frac{dz}{dx} = 0$$

$$\therefore C = \left(\frac{d^2 z}{dx^2} \right)^{-1} \quad (\text{A.1.4})$$

Differentiating equation A.1.2:

$$\frac{2z}{d^2} \frac{d^2 z}{dx^2} + \frac{2}{d^2} \left(\frac{dz}{dx} \right)^2 = \frac{2}{b^2} \quad (\text{A.1.5})$$

when $Z = G$, equation simplifies to

$$\frac{d^2 z}{dx^2} = \frac{d^2}{b^2 G} \quad (\text{A.1.6})$$

From equations A.1.4. and A.1.6:

$$\frac{C}{G} = \frac{b^2}{d^2} \quad (\text{A.1.7})$$

$$\begin{aligned} \text{But } b &= a \sin \theta_o \\ d &= a \cos \theta_o \\ \therefore \theta_o &= \arctan \left(\frac{C}{G} \right)^{\frac{1}{2}} \quad (\text{A.1.8}) \end{aligned}$$

$$\begin{aligned} \text{Also at the point } Z &= G \\ G &= a \cos \theta_o \\ \text{i.e. } a &= \frac{G}{\cos \theta_o} \quad (\text{A.1.9}) \end{aligned}$$

If the electrode gap, G , and the radius of curvature of point-electrode are given, then equations A.1.8 and A.1.9 define a and θ_o in equation A.1.1.

The electric field in per unit value is given by

$$\frac{E}{E_{av}} = \frac{\cos \left\{ \arctan \left[\left(\frac{C}{G} \right)^{\frac{1}{2}} \right] \right\} (\sinh^2 \eta + \sin^2 \theta)^{-\frac{1}{2}}}{\sin \theta \left\{ \ln \cot \left[\frac{1}{2} \left(\arctan \left(\frac{C}{G} \right)^{\frac{1}{2}} \right) \right] \right\}} \quad (\text{A.1.10})$$

A computer program is designed for the solution of per unit value of electric field given by Eqn. A.1.10, in terms of radius of curvature of point electrode, C , and the electrode gap, G . A flow diagram of the required program is depicted in Fig. A.1 and a specimen digital program is given in Fig. A.2.

7.2 Diffusion Coefficient, D .

The diffusion coefficient can be expressed in terms of the rate of change of mean square of distance of electrons from any point. Let the distance be symmetrical about the centre O . This condition holds as far as radial motion from O is concerned. The electron density n is then a function of the radial distance r . The number of electrons included between spheres of radii r and $r + dr$ is $4\pi r^2 n dr$ and the mean square of their distance from O is:

C FIELD ABOUT A CHARGED HYPERBOLOID IN PROLATE
 C SPHEROIDAL COORDINATES.
 C

```

REAL M
10 READ(3,100)C
100 FORMAT(F10.0)
    IF(C.LT.0.0) STOP
    READ(3,100)DELTA,P
    WRITE(2,101)C,DELTA,P
    THETA0=ATAN(SQRT(C))
    A=COS(THETA0)
    B=A*LOG(COS(THETA0/2.0)/SIN(THETA0/2.0))
    THETA0=THETA0*57.29578
11 THETA=THETA0
    READ(3,100)EAV
    IF(EAV.LT.0.0)GOTO 10
    WRITE(2,103)EAV
1 THETA1=THETA
    THETA=THETA/57.29578
    ER=A/(B*SIN(THETA)**2)
    M=COS(THETA)/A
    E=ER*EAV
    Y=E/P
    WRITE(2,102)THETA1,ER,M,E,Y
    IF(THETA1-THETA0)2,3,2
3 THETA=THETA1+1.0
    THETA=AIN(THETA)
    ALPHA=THETA
    GOTO1
2 IF(THETA1.EQ.90.0)GOTO11
    IF(THETA1-ALPHA-5.0)4,4,5
4 THETA=THETA1+DELTA
    GOTO1
5 IF(THETA1-90.0)6,6,7
6 THETA=THETA1+5.0
    GOTO1
7 THETA=90.0
    GOTO1
101 FORMAT(7H C/G = ,F7.5,7X,12H INCREMENT = ,F7.5,5X,4HP = ,F6.
1 3X,5H THETA,7X,5HE/EAV,10X,1HM,8X,1HE,9X,3HE/P)
102 FORMAT(F9.2,F13.5,F13.4,F7.1,F12.1)
103 FORMAT(///7H EAV = ,F5.1/)
    STOP
    END

```

Fig. A. 2. Specimen digital program for electric field strength
 in a point-plane electrode geometry.

$$R^2 = \frac{\int_0^{r'} 4\pi n r^4 dr}{\int_0^{r'} 4\pi n r^2 dr} \quad (\text{A. 2. 1})$$

The upper limit r' is taken very large, so that

$$n = 0 \text{ and } \frac{dn}{dr} = 0 \text{ when } r = r' \quad (\text{A. 2. 2})$$

The total number of particles is constant; hence, when differentiated with regard to time, Eqn. A. 2. 1 becomes:

$$\int_0^{r'} r^4 \frac{dn}{dt} dr = \frac{d(R^2)}{dt} \int_0^{r'} nr^2 dr \quad (\text{A. 2. 3})$$

The rate of increase of the number of particles in the included space is equal to the difference between the rates at which electrons flow across the two surfaces. Thus, representing the radial velocity of transport by U_r :

$$4\pi r^2 \frac{dn}{dt} dr = 4\pi r^2 (n U_r) - \left[4\pi r^2 (n U_r) + \frac{d}{dr} (4\pi r^2 n U_r) dr \right]$$

or $r^2 \frac{dn}{dt} = - \frac{d}{dr} r^2 n U_r = \frac{d}{dr} (r^2 D \frac{dn}{dr}) \quad (\text{A. 2. 4})$

From Eqns. A. 2. 3 and A. 2. 4,

$$\int_0^{r'} r^2 \frac{d}{dr} (r^2 D \frac{dn}{dr}) dr = \frac{d(R^2)}{dt} \int_0^{r'} nr^2 dr \quad (\text{A. 2. 5})$$

Integrating by parts and making use of the conditions in Eqn. A. 2. 2, it is simply shown that

$$\frac{d(R^2)}{dt} \int_0^{r'} nr^2 dr = 2D \int_0^{r'} r^3 \frac{dn}{dr} dr = 6D \int_0^{r'} nr^2 dr$$

$$\text{or } \frac{d(R^2)}{dt} = 6D \quad (\text{A. 2. 6})$$

7.3 Diffusion Equation

Considering diffusion into a semi-infinite slab of a homogeneous, isotropic material which is given by the equation:

$$\nabla^2 \eta = \frac{1}{D} \frac{\partial \eta}{\partial t} \quad (\text{A. 3. 1})$$

where source-sink term is zero and D is the diffusion coefficient assumed constant.

Let initial condition be

$$\eta(x, 0) = 0 \quad (\text{A. 3. 2})$$

and the boundary conditions

$$\eta(0, t) = K, \quad t > 0 \quad (\text{A. 3. 3})$$

$$\lim_{x \rightarrow \infty} \eta(x, t) = 0$$

Assuming η is not a function of z and y , Eqn. A. 3. 1 becomes:

$$\frac{\partial^2 \eta}{\partial x^2} = \frac{1}{D_c} \frac{\partial \eta}{\partial t} \quad (\text{A. 3. 4})$$

Taking the Laplace transform of each side of Eqn. A. 3. 4 yields:

$$\frac{d^2 N(x, s)}{dx^2} = \frac{S}{D_c} N(x, s) - \eta(x, 0) \quad (\text{A. 3. 5})$$

The initial condition specified by Eqn. A. 3. 2 eliminates the initial condition introduced by the Laplace transform of the derivative $\frac{\partial \eta}{\partial t}$.

$$\therefore \frac{d^2 N(x, s)}{dx^2} = \frac{S}{D_c} N(x, s) \quad (\text{A. 3. 6})$$

where $N(x, s)$ is the Laplace transform of $\eta(x, t)$.

The solutions to Eqn. A. 3. 6 are of the form:

$$N(x, s) = F_1(s) \exp\left(\sqrt{\frac{S}{D_c}} x\right) + F_2(s) \exp\left(-\sqrt{\frac{S}{D_c}} x\right) \quad (\text{A. 3. 7})$$

where, $F_1(s)$ and $F_2(s)$ are arbitrary functions of s to be determined from the boundary conditions A.3.3. In order to apply these boundary conditions, they can first be transformed.

$$\therefore \mathcal{L}[\eta(0, t) = K] = N(0, s) = \frac{K}{S} \quad (\text{A.3.8})$$

and

$$\mathcal{L}\left[\lim_{x \rightarrow \infty} \eta(x, t) = 0\right] = \lim_{x \rightarrow \infty} N(x, s) = 0 \quad (\text{A.3.9})$$

Application of the boundary condition specified by Eqn. A.3.7 to Eqn. A.3.9 indicates that

$$F_1(s) = 0 \quad (\text{A.3.10})$$

From Eqns. A.3.7, A.3.8, A.3.10,

$$F_2(s) = \frac{K}{S} \quad (\text{A.3.11})$$

$$\therefore N(x, s) = \frac{K}{S} \exp\left(-\sqrt{\frac{S}{D_c}} x\right) \quad (\text{A.3.12})$$

Equation A.3.12 is the Laplace transform of the solution to the diffusion equation A.3.4 with the initial and boundary conditions given by Eqns. A.3.2 and A.3.3.

The inverse transform of Eqn. A.3.12 is

$$\eta(x, t) = \mathcal{L}^{-1}\left[\frac{K}{S} \exp\left(-\sqrt{\frac{S}{D_c}} x\right)\right] = K \operatorname{erfc} \frac{x}{2\sqrt{D_c t}} \quad (\text{A.3.13})$$

Equation A.3.13 can also be written as:

$$\eta(x, t) = K \left(1 - \operatorname{erf} \frac{x}{2\sqrt{D_c t}}\right) \quad (\text{A.3.14})$$

$$\text{as } \operatorname{erfc} Y = 1 - \operatorname{erf} Y \quad (\text{A.3.15})$$

$$\text{where } \operatorname{erf} Y = \frac{2}{\sqrt{\pi}} \int_0^Y \exp(-U^2) dU \quad (\text{A.3.16})$$

7.4 Secondary Streamer Tail Parameters

$$\text{Current in the streamer } i = \pi r_s^2 (n_i - n_{e2}) q U_r \quad (\text{A.4.1})$$

but from Appendix 7.7, $n_i U = n_{e2} U_r = n_{e2} (U + U_e)$

$$\therefore n_i - n_{e2} = n_{e2} \frac{U_e}{U} \quad (\text{A.4.2})$$

and if the electron drift velocity $U_e = \rho E$ (A.4.3)

$$\therefore i = \pi r_s^2 n_{e2} \rho q E \frac{U_r}{U} \quad (\text{A.4.4})$$

Resistance per unit length

$$R = \frac{1}{\pi r_s^2 n_{e2} \rho q} \frac{U}{U_r} \quad (\text{A.4.5})$$

from Appendix 7.5

$$\therefore R = \frac{4 n_{es}}{n_{e2} r_s U_r} \quad (\text{A.4.6})$$

Assuming $\epsilon_r = 1$ for the medium, capacitance per unit length, making simplified electrode geometry, is:

$$C = \frac{1}{2 \ln \left(\frac{r_\infty}{r_s} \right)} \quad (\text{A.4.7})$$

7.5 Electrical Potential and Field Strength of the Secondary Streamer

The potential difference between a point $r = 0$ in the streamer head and the plane-electrode, assumed $r = \infty$, is given by

$$V = \int_{r=0}^{r=\infty} E dr \quad (\text{A.5.1})$$

If the streamer tip radius is r_s , then two distinct regions of r can be considered, $0 < r < r_s$ and $r_s < r < r_\infty$

Region $0 < r < r_s$

In the streamer itself the field will essentially be one-dimensional. In this region, Poisson's equation may be written as:

$$\frac{dE}{dr} = 4\pi q (n_i - n'_e) \quad (\text{A. 5. 2})$$

From Appendix 7.7

$$\frac{dE}{dr} = 4\pi q n'_e \frac{U_e}{U} \quad (\text{A. 5. 3})$$

and assuming $U_e = \rho E$ (A. 5. 4)

$$\frac{dE}{dr} = \frac{4\pi q \rho}{U} n'_e E \quad (\text{A. 5. 5})$$

From Eqn. A. 5. 12

$$\frac{dE}{dr} = \frac{n'_e}{n_{e_s}} \frac{E}{r_s} \quad (\text{A. 5. 6})$$

From Appendix 7.9:

$$E = E_s \exp\left(\frac{n'_e}{n_{e_s}} \frac{r - r_s}{r_s}\right) \quad (\text{A. 5. 7})$$

$$\therefore V_1 = \int_0^{r_s} E dr = \frac{n_{e_s}}{n'_e} E_s r_s \left[1 - \exp\left(-\frac{n'_e}{n_{e_s}}\right)\right] \quad (\text{A. 5. 8})$$

Region $r_s < r < r_\infty$

Beyond the streamer tip which has a radius of r_s the electric field may be represented by:-

$$\frac{1}{r} \frac{d}{dr} (rE) = 4\pi q (n_i - n_e) \quad (\text{A. 5. 9})$$

From Appendix 7.7

$$\frac{d}{dr} (rE) = 4\pi q n_e \frac{U_e}{U} r \quad (\text{A. 5. 10})$$

If the electron drift velocity is given by

$$U_e = \rho E$$

$$\therefore \frac{d}{dr} (rE) = \frac{4\pi q \rho n_e}{U} r E \quad (\text{A. 5. 11})$$

At the streamer tip $r = r_s$; $\frac{dE}{dr} = 0$

$$\therefore 4\pi Q n_{e_s} r_s / \rho = U \quad (\text{A. 5. 12})$$

Equation A. 5. 11 becomes:

$$\frac{d}{dr} (rE) = \frac{n_e}{n_{e_s}} \frac{rE}{r_s} \quad (\text{A. 5. 13})$$

From Appendix 7.9 $rE = r_s E_s \exp\left(\frac{1}{\alpha r_s} + \frac{n_e}{n_{e_s}}\right)$

$$\quad (\text{A. 5. 14})$$

$$\therefore V_2 = \int_{r_s}^{r_\infty} E dr = r_s E_s \exp\left(\frac{1}{\alpha r_s} + \frac{n_e}{n_{e_s}}\right) \ln\left(\frac{r_\infty}{r_s}\right)$$

$$\quad (\text{A. 5. 15})$$

From Eqns. A. 5. 8 and A. 5. 15:

$$V = V_1 + V_2 = \int_{r=0}^{r=\infty} E dr = \int_{r_0}^{r_s} E dr + \int_{r_s}^{r_\infty} E dr$$

$$= r_s E_s \left\{ \exp\left(\frac{1}{\alpha r_s} + \frac{n_e}{n_{e_s}}\right) \ln\left(\frac{r_\infty}{r_s}\right) + \frac{n_{e_s}}{n_{e_s}} \left[1 - \exp\left(-\frac{n_{e_s}}{n_{e_s}}\right) \right] \right\}$$

$$\quad (\text{A. 5. 16})$$

Simplification

As αr_s is of the order of 10^2 and $\frac{n_e}{n_{e_s}} \ll 1$

$$\exp\left(\frac{1}{\alpha r_s} + \frac{n_e}{n_{e_s}}\right) \rightarrow 1 \quad (\text{A. 5. 17})$$

i.e. the effect of space charge is negligible in the field integral.

$$\text{As } \frac{n_{e_s}}{n_{e_s}} \gg 1, \quad \exp\left(-\frac{n_{e_s}}{n_{e_s}}\right) \rightarrow 0 \quad (\text{A. 5. 18})$$

$$\therefore V = r_s E_s \left[\ln\left(\frac{r_\infty}{r_s}\right) + \frac{n_{e_s}}{n_{e_s}} \right] \quad (\text{A. 5. 19})$$

$$\text{As } \ln\left(\frac{r_\infty}{r_s}\right) \gg 1,$$

$$\frac{n_{e_s}}{n'_e} \ll \ln \frac{r_\infty}{r_s} \quad (\text{A. 5. 20})$$

$$\therefore V = r_s E_s \ln \frac{r_\infty}{r_s} \quad (\text{A. 5. 21})$$

7. 6 Gas Ionization and Photon Production

The production of electrons and photons are strongly localised to the region of maximum electric field at the tip of the streamer. In the gaseous air, the photo-ionization of oxygen molecule with ionization potential of 12.15 eV may be caused by the line radiation from upper energy level to the ground state of nitrogen molecule, ionization potential being 15.58 eV.

From an increase in electron density, δn_e across the streamer tip, photons are produced at a rate given by:

$$\text{rate of photon production} = K_g \pi r_s^2 M U_r \delta n_e \quad (\text{A. 6. 1})$$

where relative velocity of the streamer tip $U_r = U + U_e$

K_g = a constant relating the cross-section for ionization in oxygen to photon-production in nitrogen by electron impact

M = nitrogen to oxygen mole ratio

U = streamer tip propagation speed

U_e = electron drift velocity.

Within the volume of a disc of thickness δr and radius r_s , a distance r ahead of the streamer, the photon absorption is given by:

$$\text{photon absorption} = \frac{1}{2} K_a \left(1 - \frac{r}{\sqrt{r_s^2 + r^2}} \right) \exp(-K_a r) \delta r \quad (\text{A. 6. 2})$$

where K_a = photon absorption coefficient.

If a fraction k of the absorbed photon produces a photo-

electron, then

$$\pi r_s^2 n_e U_r = \frac{k}{2} K_a K_g \pi r_s^2 M U_r \delta n_e \int_0^{\infty} \left(1 - \frac{r}{\sqrt{r_s^2 + r^2}}\right) \exp(-K_a r) dr \quad (\text{A.6.3})$$

where n_e = electron density outside the streamer tip

n'_e = electron density inside the streamer tip

$$\delta n_e = n'_e - n_e$$

$$\therefore n'_e = n_e \left(1 + \frac{1}{\Delta}\right) \quad (\text{A.6.4})$$

where $\Delta = k K_g M f(K_a r_s)$

$$f(K_a r_s) = \frac{1}{2} K_a r_s \int_0^{\infty} \left(1 - \frac{\psi}{\sqrt{1 + \psi^2}}\right) \exp(-K_a r_s \psi) d\psi$$

$$\psi = \frac{r}{r_s}$$

7.7 Ions and Electrons Movement

On the assumption that electrons and ions move essentially one dimensionally, the equations of continuity for the motion of ions and electrons relative to a frame of reference, advancing at the same speed U as the streamer tip, become:

$$\frac{d}{dr} (n_e U_r) + \frac{k}{2} K_a K_g M U_r \delta n_e \left(1 + \frac{r}{\sqrt{r_s^2 + r^2}}\right) \exp(-K_a r) + n_e U_e \alpha = 0 \quad (\text{A.7.1})$$

$$\frac{d}{dr} (n_i U) + \frac{k}{2} K_a K_g M U_r \delta n_e \left(1 + \frac{r}{\sqrt{r_s^2 + r^2}}\right) \exp(-K_a r) + n_e U_e \alpha = 0 \quad (\text{A.7.2})$$

where

the first term \equiv electrons or ions production rate

the second term \equiv photo-ionization rate

the third term \equiv Townsend's electron multiplication rate.

From Eqns. A. 7. 1 and A. 7. 2

$$\eta_i U = \eta_e U_r = \eta_e (U + U_e) \quad (\text{A. 7. 3})$$

7. 8 Electric Field Strength ahead of the Secondary Streamer

Outside the streamer tip the electric field strength is given from Appendix 75 by:

$$\frac{d}{dr} (rE) + A (rE) = 0 \quad (\text{A. 8. 1})$$

where $A = - \frac{\eta_e}{\eta_{e_s} r_s}$

$$\therefore E + r \frac{dE}{dr} + ArE = 0$$

$$\frac{dE}{dr} + \left(\frac{Ar + 1}{r} \right) E = 0 \quad (\text{A. 8. 2})$$

The solution to Eqn. A. 8. 2 is given by:

$$E = K \exp \left[- \int \frac{Ar + 1}{r} dr \right]$$

$$E = K \exp \left[- Ar - \ln r \right]$$

$$E = \frac{K}{r} \exp (- Ar) \quad (\text{A. 8. 3})$$

Initial condition gives $r = r_s, E = E_s$

$$\therefore K = r_s E_s \exp \left(- \frac{\eta_e}{\eta_{e_s}} \right)$$

$$\therefore rE = r_s E_s \exp \left(\frac{\eta_e}{\eta_{e_s}} \cdot \frac{r - r_s}{r_s} \right) \quad (\text{A. 8. 4})$$

The space charge is composed of a high density electron region decaying in a distance of the order $\frac{1}{\alpha}$ and a low density, photo-ionization part decaying in a distance of the order $\frac{1}{K_a}$.

$$(a) \quad \text{range} \quad r_s < r < r_s + \frac{1}{\alpha}$$

In this range $n_e \doteq n_{e_s}$ and the equation A.8.4 gives

$$rE = r_s E_s \exp\left(\frac{r - r_s}{r_s}\right) \quad (\text{A.8.5})$$

In this region, rE changes from $rE = r_s E_s$ at $r = r_s$
to $rE = r_s E_s \exp\left(\frac{1}{\alpha r_s}\right)$ (A.8.6)
at $r = r_s + \frac{1}{\alpha}$

$$(b) \quad \text{range} \quad r_s + \frac{1}{\alpha} < r < 2r_s$$

In this range, the space charge effect is overestimated such that $\frac{1}{K_a} \doteq r_s$.

From Eqns. A.8.4 and A.8.6

$$rE = r_s E_s \exp\left(\frac{1}{\alpha r_s}\right) \exp\left(\frac{n_e}{n_{e_s}} \frac{r - r_s}{r_s}\right) \quad (\text{A.8.7})$$

In this region, rE changes from $rE = r_s E_s \exp\left(\frac{1}{\alpha r_s}\right)$
at $r = r_s + \frac{1}{\alpha}$ (A.8.8)
to $rE = r_s E_s \exp\left(\frac{1}{\alpha r_s}\right) \exp\left(\frac{n_e}{n_{e_s}}\right)$
at $r = 2r_s$

Taking an overestimate in the region $r_s < r < r_\infty$

$$rE = r_s E_s \exp\left(\frac{1}{\alpha r_s} + \frac{n_e}{n_{e_s}}\right) \quad (\text{A.8.9})$$

7.9 Electric Field Strength inside the Secondary Streamer Tip

The electric field strength inside a streamer tip is given from Appendix 7.5 by:

$$\frac{dE}{dr} + AE = 0 \quad (\text{A.9.1})$$

$$\text{where } A = - \frac{\eta_e'}{\eta_e r_s}$$

The solution to Eqn. A.9.1 is given by:

$$\begin{aligned} E &= K \exp \left(- \int A dr \right) \\ E &= K \exp (-Ar) \end{aligned} \quad (\text{A.9.2})$$

At the tip surface where $r = r_s$, $E = E_s$

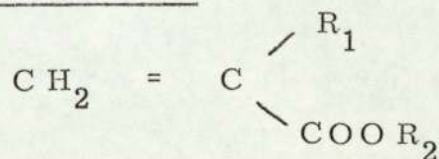
$$K = E_s \exp \left(- \frac{\eta_e'}{\eta_e r_s} \right) \quad (\text{A.9.3})$$

From Eqns. A.9.2 and A.9.3

$$E = E_s \exp \left(\frac{\eta_e'}{\eta_e r_s} \cdot \frac{r - r_s}{r_s} \right) \quad (\text{A.9.4})$$

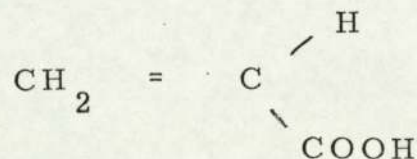
7.10 Polymethylmethacrylate (P.M.M.A.)

(a) Basic Acrylic Formula

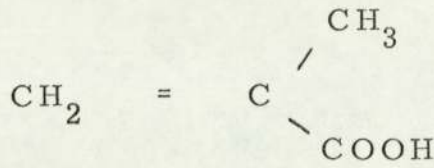


Replacement of R_1 or R_2 , or both, by hydrogen, or an aliphatic group such as methyl (CH_3) or ethyl (C_2H_5) yields a wide range of acrylic monomers.

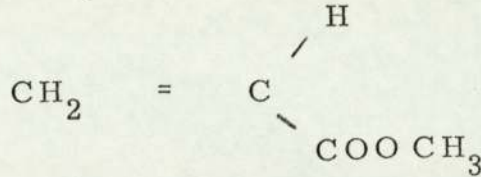
R_1 or R_2 replaced by hydrogen \longrightarrow acrylic acid



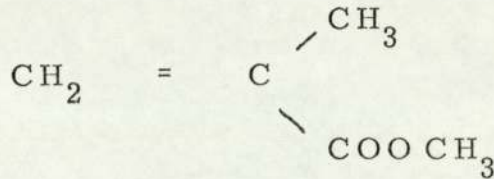
R_1 by methyl, R_2 by hydrogen \longrightarrow methacrylic acid

(b) Esters of two above Acids

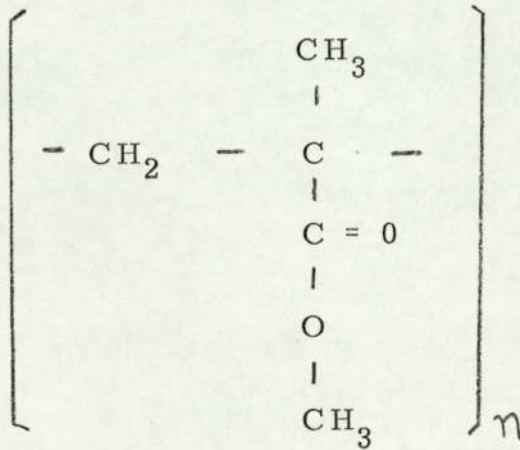
e.g. methyl esters



methyl acrylate



methyl methacrylate

(c) Polymerization(d) Properties of Moulded P. M. M. A.

specific gravity	1.17 - 1.20
refractive index	1.49
tensile strength	7,000 - 11,000 lb/in ²
modulus of elasticity	4.5 x 10 ⁵ lb/in ²
impact strength	0.3 - 0.5 ft. lb/in. notch
hardness	85 - 105 Rockwell scale M